# The role of mitochondria in collective cell migration of *Xenopus laevis* mesendoderm

Gustavo G Pacheco

Bethesda, Maryland

Bachelor of Science, University of Chicago, 2017

A Dissertation presented to the Graduate Faculty of the

University of Virginia in Candidacy for the

Degree of Doctor of Philosophy

Department of Cell Biology

University of Virginia

December, 2024

**Abstract**

Cell migration is the directed movement of cells from one location to another often in response to chemical or physical signals in their environment and is essential in various biological phenomena such as wound healing, immune responses, cancer metastasis, and morphogenesis. Furthermore, it is an energetically costly process requiring significant stores of cellular energy in the form of adenosine triphosphate (ATP) to fuel processes such as actin cycling, actomyosin contractility, and phosphorylation of cell adhesion signaling proteins. The major forms of cell migration are single and collective. In single cell migration, individual cells move independently to position themselves within tissues and interstitial spaces. In contrast, collective migration involves groups of cells that remain interconnected, coordinating their movements as a unit. Twenty-first century advancements in tools for manipulating and assaying bioenergetics in live samples support initial investigations into the regulation of metabolism in single cell migration, but studies in collective cell migration remain limited. The mechanical coordination of cell-extracellular matrix (ECM) and cell-cell adhesions underlie efficient collective migration. However, the mechanistic links between cell biomechanics and bioenergetics in the energetically costly process of collective cell migration remain elusive.

In Chapter 2 we report an increase in mitochondrial activity along the leading row of motile *Xenopus laevis* gastrula-stage mesendoderm cells at sites where fibronectin-**α**5β1 integrin substrate traction stresses are greatest. Real-time metabolic analyses demonstrate that **α**5β1 integrin dependent increases in oxidative phosphorylation occur in mesendoderm cells on fibronectin substrates. This elevation in metabolic activity is

reduced following pharmacologic inhibition of focal adhesion kinase (FAK) signaling. The integrin-linked mitochondrial oxidative phosphorylation via FAK signaling is conserved in cells from various human tissues. Attachment of mesendoderm cells to fibronectin-Glutathione-S-Transferase (GST) fusion protein fragments that support differing $\alpha 5\beta 1$ integrin conformational and ligand-binding affinity states, leads to an increase in mitochondrial activity when both the Arg-Gly-Asp (RGD) and Pro-Pro-Ser-Arg-Asn (PPSRN) synergy sites of fibronectin are engaged by the receptor. Stretching single mesendoderm cells on deformable fibronectin substrates also results in a FAK-dependent increase in mitochondrial membrane potential. Inhibition of mitochondrial membrane potential or mitochondrial ATP synthase activity slows collective cell migration velocity in vivo, further suggesting that integrin-dependent adhesion and signaling contribute to ATP production.

In Chapter 3, I delved into the connections between mitochondrial metabolism and cell adhesion. I demonstrated that aconitase, a citric acid cycle enzyme, function is critical for collective mesendoderm migration in the intact embryo. Based on comparisons of mesendoderm cells on fibronectin-GST fusion proteins, we found that integrin activation fails to affect rates of mitochondrial biogenesis or degradation within the timescale of gastrulation. I observed that mesendoderm treated with manganese to produce integrin activation presented with high mitochondrial membrane potential. Examinations of mesendoderm cell clusters presented mitochondria with a high degree of clustering and high membrane potential near protrusion regions. This is in addition to clustering of mitochondria near the leading edges of mesendoderm cells in the migratory

tissue. This was in addition into our observation of accumulations of mitochondria close to C-Cadherin adhesions in dissociated cells.

Finally, in Chapter 4 I aimed to further examine the role of metabolism in adhesive processes during gastrulation. I presented the preliminary metabolomics studies on *Xenopus laevis* gastrulae in the presence or absence of a fibronectin morpholino. Notably, metabolites related to pyrimidine and aromatic amino acid processes showed the greatest changes due to the knockdown. The potential significance of these processes in the developmental processes of gastrulation and future studies are discussed. In sum, this dissertation highlights an underexplored link between ECM-integrin adhesion and mitochondrial metabolism in early embryonic cell migration. We propose that fibronectin-integrin engagement provides an important signal for shaping the metabolic landscape of collectively migrating cells. Continued study of the interplay between adhesive processes and metabolism will inform our approaches for targeting dysregulated cell migration in pathological contexts.

**Acknowledgments**

First and foremost, I want to express my deepest gratitude to my advisor, Douglas W DeSimone, for your unwavering guidance, patience, and support throughout my doctoral journey. Your expertise, encouragement, and mentorship have been invaluable to my academic and personal growth.

I extend my heartfelt thanks to the members of my dissertation committee, Ann E Sutherland, David F Kashatus, and Raymond E Keller, for their insightful feedback, constructive criticism, and commitment to fostering the quality of my research.

To my lab members, past and present, thank you for creating a collaborative and supportive environment that made long hours in the lab both productive and enjoyable. A special thanks to Bette J Dzamba, Tien Comlekoglu, Benjamin C Edwards, Wakako Endo, Minah Khan, Kara Davidson, Keri Quasey, and David R Shook for their camaraderie, technical support, and for being a constant source of inspiration.

I am also grateful to the funding agencies and institutions that made this research possible, including the National Institutes of Health (National Institute of General Medical Sciences, National Institute of Child Health and Human Development, and National Heart, Lung, and Blood Institute), the University of Virginia Office of Citizen Scholar Development, the Korean Society for Molecular and Cellular Biology, and Cell Press. Their financial support enabled me to pursue my research with focus and dedication.

On a personal note, I want to thank my family and friends for their unconditional love, patience, and understanding during this challenging yet rewarding journey. To my parents, Gustavo and Sara, thank you for instilling in me the value of education and

perseverance. To my sister and brother-in-law, Adelina-Romina and Conor, thank you for your endless encouragement and for being a pillar of support throughout this journey.

Finally, I would like to acknowledge the broader scientific community, whose contributions and collaborations continue to inspire and challenge us all in the pursuit of knowledge. This dissertation is a culmination of the collective efforts of many, and I am profoundly grateful for each person who has played a part in this journey.

Gustavo G Pacheco

**Table of contents**

**List of abbreviations**

| | |
|---|---|
| AAA | Aromatic amino acids |
| Akt | Protein kinase B |
| ADP | Adenosine diphosphate |
| AMP | Adenosine monophosphate |
| AMPK | Adenosine monophosphate kinase |
| ANOVA | Analysis of variance |
| ATP | Adenosine triphosphate |
| BC | Bent-Closed |
| $BH_4$ | Tetrahydrobiopterin |
| BMP | Bone morphogenetic protein |
| BSA | Bovine serum albumin |
| C-Cadherin-FC | C-Cadherin fragment protein |
| CI | Complex I |
| CII | Complex II |
| CMF-MBS | $Ca^{2+}$/$Mg^{2+}$-free MBS |
| COMO | Control morpholino |
| CoQ | Coenzyme Q |
| CPSII | Carbamoyl phosphate sythetase II |
| CS-MS | Cysteine shotgun mass spectrometry |
| CMP | Cytidine monophosphate |
| $CO_2$ | Carbon dioxide |
| CTP | Cytidine triphosphate |

| | |
|---|---|
| DAHP | D-arabino-heptulosonate-7-phosphate |
| DC | Dendritic cell |
| DFA | Danichick's for amy (media) |
| DHODH | Dihydroorotate dehydrogenase |
| DMZ | Dorsal marginal zone |
| Drp1 | Dynamin related protein 1 |
| dUMP | Deoxyuridine monophosphate |
| dTMP | deoxythymidine monophosphate |
| ECM | Extracellular matrix |
| EDTA | Ethylenediaminetetraacetic acid |
| EGTA | Ethylene glycol-bis(β-aminoethyl ether)-N,N,N′,N′-tetraacetic acid |
| EMT | Epithelial-to-mesenchymal transition |
| ETC | Electron transport chain |
| EC | Extended-closed |
| EO | Extended-open |
| ERK | Extracellular signal-regulated kinase (ERK |
| ESC | Embryonic Stem Cell |
| FAK | Focal adhesion kinase |
| FCCP | Carbonyl cyanide-p-trifluoromethoxyphenylhydrazone |
| FDG-PET | Fluorodeoxyglucose positron emission tomography |
| FGF | Fibroblast Growth Factor |
| FN | Fibronectin |
| FNMO | Fibronectin morpholino |

| | |
|---|---|
| FTIR | Fourier Transform Infrared |
| GFP | Green fluorescent protein |
| GST | Glutathione-s-transferase |
| GTP | Guanosine triphosphate |
| HIF-1α | Hypoxia-inducible factor 1-alpha |
| HPLC | High-performance liquid chromatography |
| $H_2O_2$ | Hydrogen peroxide |
| IF | Intermediate filament |
| ILK | Integrin Linked Kinase |
| iMAC | Immortalized macrophage |
| IDO | Indoleamine 2,3-dioxygenase |
| KEGG | Kyoto Encyclopedia of Genes and Genomes |
| LC | Liquid chromatography |
| LC-MS/MS | Liquid chromatography tandem mass spectrometry |
| LC3 | Microtubule-associated proteins 1A/1B light chain 3B |
| LKB1 | Liver kinase B1 |
| MAPK | Mitogen-activated protein kinase |
| MBS | Modified barth's saline |
| MMP | Mitochondrial membrane potential |
| MMPs | Matrix metalloproteinases |
| Mfn1 | Mitofusin 1 |
| MIDAS | Metal ion-dependent adhesion site |
| Miro1 | Mitochondrial rho 1 |

| | |
|---|---|
| MS | Mass spectrometry |
| MS1 | Tandem mass spectrometry stage 1 |
| MS2 | Tandem mass spectrometry stage 2 |
| MTG | Mitotracker green |
| mTOR | Mechanistic target of rapamycin |
| MO | Morpholino |
| $NAD^+$ | Nicotinamide adenine dinucleotide |
| $NADP^+$ | Nicotinamide adenine dinucleotide phosphate |
| NMR | Nuclear magnetic resonance |
| NRF1 | Nuclear respiratory factor 1 |
| NOX2 | NADPH oxidase 2 |
| Opa1 | Optical atrophy 1 |
| OCR | Oxygen consumption rate |
| PAK1 | p21 activated kinase 1 |
| PCA | Principal component analysis |
| PDMS | Polydimethylsiloxane |
| PFK-1 | Phosphofructokinase-1 |
| PGC-1α | Peroxisome proliferator-activated receptor gamma coactivator 1-alpha |
| PINK1 | PTEN-induced kinase 1 |
| PI3K | Phosphatidylinositol 3-kinase |
| PLL | Poly-l-lysine |
| PMSF | Phenylmethylsulfonyl fluoride |

| | |
|---|---|
| PPSRN | Proline-Proline-Serine-Arginine-Asparagine |
| Pyk2 | Proline-rich tyrosine kinase 2 |
| p62 | Sequestosome 1 |
| Pre-Tx | Pre-treatment |
| Rac1 | Rac family small GTPase 1 |
| RCF | Relative centrifugal force |
| RGD | Arginine-glycine-aspartic acid |
| RhoA | Ras homolog family member A |
| ROS | Reactive oxygen species |
| RFU | Relative fluorescence units |
| SDS-PAGE | Sodium dodecyl-sulfate polyacrylamide gel electrophoresis |
| SERT | Serotonin transporters |
| Sirt1 | Sirtuin 1 |
| STAT3 | Signal transducer and activator of transcription 3 |
| TAARs | Ttrace amine-associated receptors |
| TAZ | Transcriptional coactivator with PDZ-binding motif |
| TBS | Tris-buffered saline |
| TBST | TBS with 0.1% tween20 detergent |
| TDO | Tryptophan 2,3-dioxygenase |
| TFAM | Mitochondrial transcription factor A |
| TGF-β | Transforming growth factor-beta |
| TMRE | Tetramethylrhodamine, ethyl ester |
| TRIM21 | Tripartite motif containing 21 |

| | |
|---|---|
| TOMM20 | Translocase of outer mitochondrial membrane 20 |
| T3 | triiodothyronine |
| T4 | thyroxine |
| UDP | Uridine diphosphate |
| UMP | Uridine monophosphate |
| UTP | Uridine triphosphate |
| UHPLC-MS/MS | ultra-high performance liquid chromatography–tandem mass spectrometry |
| US | United States |
| Vdac1 | Voltage dependent anion channel 1 |
| VEGF | Vascular endothelial growth factor |
| Wnt | Wingless-related integration site |
| YP | Yolk Platelet |
| 3D | Three-dimensional |
| 2-NBDG | 2-[N-(7-nitrobenz-2-oxa-1,3-diazol-4-yl) amino]-2-deoxy-D-glucose |

**List of figures**

# Chapter 1

## Introduction

## Cell migration

Coordination of cell migration is essential for homeostatic processes of multicellular life, such as morphogenesis and immune surveillance, while dysregulated cell migration underlies pathological processes, including aberrant wound healing and cancer metastasis (Li et al., 2013; Trepat et al., 2012). Single and collective cell migration are the two principal modes of motility that underlie cell and tissue movements (Friedl and Gilmour, 2009; Rørth, 2009). Single cell migration supports the independent positioning of cells in tissues and interstitial spaces, while in collective migration cells remain connected and movements coordinated (Friedl, 2004; Ridley et al., 2003).

## Single cell migration

Single cell migration is the process by which individual cells move from one location to another (Alberts et al., 2015). The cell begins by polarizing in its direction of movement which involves reorganization of the cytoskeleton and concentration of signaling molecules towards the front of the cell (Dow and Humbert, 2007; Etienne-Manneville, 2008). Actin polymerizes at the cell's leading edge to form protrusions of broad, sheet-like extensions (i.e. lamellipodia) or thin, spike-like extensions (i.e. filopodia) that extend toward the direction of movement (Le Clainche and Carlier, 2008; Xue et al., 2010). The cell then forms new adhesions with the extracellular matrix (ECM) through structures called focal adhesions, which connect the ECM to the cytoskeleton thereby anchoring the protrusions (Horwitz and Parsons, 1999; Mostafavi-Pour et al., 2003). Myosin motor proteins interact with actin filaments in the rear of the cell to generate contractile forces thereby pulling the cell body forward (Horwitz and Webb,

2003; Sheetz, 1994). Finally, the adhesions at the rear are released which allows the cell to fully retract its trailing edge and move forward (Cramer, 2013; Hetmanski et al., 2019).

The resulting primary types of single cell migration are mesenchymal, ameboid, and lobopodial (Wells and Parsons, 2011). Mesenchymal migration is an adhesive and highly directed form of movement in which the cells (e.g. fibroblasts, endothelial cells, and some cancer cells) are elongated and form strong adhesions with the ECM (Innocenti, 2018; Yamada and Sixt, 2019). Mesenchymal migration can also involve ECM degradation by enzymes like matrix metalloproteinases (MMPs) (Chen and Parks, 2009; Koshikawa et al., 2000). By contrast, amoeboid migration is a less adhesive and flexible form of movement that relies on the ability of cells (e.g. immune and some cancer cells) to squeeze through gaps in the ECM rather than degrading with less ECM attachment and more shape-shifting through actin-driven protrusions (Friedl et al., 2001; Wolf et al., 2003). Lobopodial migration is a distinctive form of cell movement, especially in three dimensional (3D) environments, involving blunt, rounded protrusions called lobopodia that are driven by Ras homolog family member A (RhoA)-mediated actomyosin contractility, hydrostatic pressure, and minimal ECM degradation thereby allowing cells to move effectively through dense 3D tissues (Petrie et al., 2014; Yamada and Sixt, 2019).

While a variety of mechanisms underlie the phenomenon of single cell migration, a few are highlighted here. Actin cytoskeleton dynamics are critical as actin filaments are essential for generating protrusions at the cell front with actin polymerization at the leading edge pushing the membrane outward to form lamellipodia or filopodia (Blanchoin et al., 2014; Mitchison and Cramer, 1996). Myosin motor proteins, such as

Myosin II, interact with actin filaments to generate contractile forces, allowing the cell to pull itself forward which is especially important in the rear of the cell for facilitating retraction (Garrido-Casado et al., 2021; Vicente-Manzanares et al., 2009). Within the focal adhesion protein complexes that link the cell's cytoskeleton to the ECM, proteins like integrins, talin, vinculin, and focal adhesion kinase (FAK) help the cell adhere to and exert traction on the ECM (Cox et al., 2006; Nagano et al., 2012). At the same time, signaling pathways through various signaling molecules regulate cytoskeletal dynamics and cell polarity, including the Rho Guanosine triphosphate (GTP)ases Rac, Rho, and Cdc42 (Raftopoulou and Hall, 2004; Ridley, 2001). Rac promotes actin polymerization at the leading edge, while Rho promotes actomyosin contraction at the rear (Lawson and Burridge, 2014; Pankov et al., 2005). Lastly, MMPs are important for mesenchymal migration as they are secreted to degrade ECM components to create a path for cell movement through the tissue (Legrand et al., 1999; Nabeshima et al., 2002).

In addition to these mechanisms, cell migration is often guided by external cues that can influence direction, speed, and pattern of migration. In the case of chemotaxis, cells move toward or away from a chemical gradient (Keller and Segel, 1971; Roussos et al., 2011). For example, immune cells are attracted to sites of infection by chemoattractants, or chemical signals (Inoue et al., 2012; Mañes et al., 2005). Cells undergoing haptotaxis, such as mesenchymal cells strongly attached to the ECM, move along gradients of adhesive molecules in the ECM (Aznavoorian et al., 1990; Carter, 1967). During durotaxis cells move toward stiffer regions of the ECM, including during cancer and fibrosis where cells migrate toward stiffer tissue (DuChez et al., 2019; Sunyer and Trepat, 2020). Finally, in electrotaxis cells can respond to electric fields by moving

toward or away from the electrical stimulus, as evidenced in wound healing contexts (Cortese et al., 2014; Zhao, 2009).

**Collective cell migration**

Collective cell migration refers to the coordinated movement of a group of cells that maintains cell-cell adhesion while moving as a cohesive unit (Ilina and Friedl, 2009; Rørth, 2009). Unlike single cell migration, where cells move independently, collective migration involves cells moving together in groups, maintaining communication and coordination with their neighbors (Trepat et al., 2012; Vicente-Manzanares and Horwitz, 2011). A key aspect is the influence of cell-cell adhesion as cells in collective migration remain connected through cell-cell junctions, such as adherens junctions and tight junctions, to enable their communication, sharing of signaling molecules, and movement as a unit (Collins and Nelson, 2015; Friedl and Mayor, 2017). The organization into leader and follower cells is critical as in many cases, certain cells at the front of the group, known as leader cells, guide the direction and path of migration with follower cells remaining connected to leader cells thereby ensuring coordinated movement (Qin et al., 2021; Theveneau and Linker, 2017). Furthermore, the group must maintain mechanical cohesion to allow force transmission across the collective to pull cells forward, even when some cells lag behind (De Pascalis and Etienne-Manneville, 2017; Kabla, 2012) This is in addition to polarity as collective migration requires front-rear polarity at the group level with leader cells usually establishing this polarity, extending protrusions toward the direction of migration, and follower cells maintaining this orientation within the group (Capuana et al., 2020; Reffay et al., 2011).

Interactions between the cytoskeleton, cell adhesion molecules, and signaling pathways are coordinated by some key mechanisms. Cytoskeletal dynamics are regulated as actin polymerization in leader cells forms protrusions at the migration front, while actomyosin contractility helps follower cells maintain tension and cohesiveness (Lucas et al., 2013; Pandya et al., 2017). Notably, cell-cell adhesion plays a critical role as proteins, such as cadherins, form junctions between cells to allow mechanical and chemical signaling across the group (Peglion et al., 2014; Theveneau and Mayor, 2012). Focal adhesions are also essential as integrin proteins in these cell-matrix adhesions anchor cells to the ECM and transmit traction forces from the leading edge to follower cells (Friedl and Gilmour, 2009; Friedl et al., 2004). Various signaling pathways regulate cytoskeletal organization, adhesion dynamics, and cell polarity, including Rho GTPase, Phosphatidylinositol 3-kinase (PI3K)/Protein kinase B (Akt), and wingless-related integration site (Wnt) signaling (VanderVorst et al., 2019; Yamaguchi et al., 2015). In particular, the Rho GTPases Rac and Rho help establish front-rear polarity by modulating actin and myosin activity (Pandya et al., 2017; Zegers and Friedl, 2014). Guidance cues and gradients have also been shown to play a role in collective migration as chemotactic, durotactic, or topographical cues from the environment help orient the collective towards specific locations, such as wound sites or high ECM stiffness area (Rørth, 2007; Sunyer et al., 2016). One unique type of guidance cue observed in collective migration is cohesotaxis, a mechanism in which migrating cells in a tissue are coordinated mechanically to produce directed polarized protrusive activity at the leading edge of the tissue in the direction of migration where cells remain in contact with their neighbors (Comlekoglu et al., 2024; Weber et al., 2012). Similar to single cell migration,

chemotactic signals have also been found to play a role in collective migration. For example, binding of the chemokine receptor, CXCR4, to its ligand, CXCL12/SDF-1 in immune and cancer cells creates a chemotactic gradient that directs the migration of cell clusters towards higher concentrations of SDF-1 to facilitate organized movement (Kabashima et al., 2007; Theveneau and Linker, 2017).

Depending on the tissue type, cell type, and physiological context a few major types of collective cell migration are observed (Rørth, 2009). As is often observed in the contexts of epithelial wound healing or tissue repair, during sheet migration cells move as a flat sheet, maintaining cell-cell junctions and coordinated movements (Etienne-Manneville, 2014; Vitorino et al., 2011). In developing tissues and in neural crest cell migration, cells can move in single-file strands or chains (i.e. strand or chain migration) (Friedl, 2004; Méhes and Vicsek, 2014). In some cancer metastases cluster migration is observed with clusters of cells migrating together when cancer cells break off and invade other tissues in groups (Debets et al., 2021; Yamamoto et al., 2023). Finally, in angiogenesis or vessel sprouting endothelial cells collectively migrate to form new blood vessels which is critical for both development and tumor growth (Arima et al., 2011; Costa et al., 2016).

In sum, single and collective cell migration differ in some key points, in particular that collective migration involves coordinating movements among multiple cells. Furthermore, in collective migration intercellular communication is critical as cells communicate mechanically and chemically within the group through adhesion molecules and junctions. In addition, pathfinding for collective differs from single as leader cells in the front must sense environmental cues and guide the entire group, which helps the

collective respond to directional signals more efficiently. Finally, in collective migration mechanical cohesion is critical as collective migration requires force transmission across cells thereby enabling them to overcome environmental obstacles collectively.

**Collective cell migration in morphogenesis**

Morphogenesis is the biological process through which an organism's shape, structure, and form are developed during embryonic growth and tissue organization (Gilbert, 2013; Wolpert et al., 2023). It involves the coordination of cellular processes such as cell differentiation, proliferation, migration, adhesion, and apoptosis to create tissues, organs, and overall body structure (Gumbiner, 1996; Lecuit and Lenne, 2007). During morphogenesis, groups of cells may be brought together to introduce new inductive interactions that support the formation of complex, three dimensional structures and organs (eg. hearts, limbs, lungs, and eyes) from simple epithelial sheets and mesenchymal cell masses (Hogan, 1999; Turing, 1990). Our understanding of collective cell motility has been enhanced by studies of morphogenetic developmental processes, such as movement of the lateral line primordium in zebrafish or border cells in *Drosophila* (Aman and Piotrowski, 2009; Montell, 2003; Weijer, 2009). *Xenopus* morphogenetic movements during gastrulation, including the migration of the mesendoderm along the blastocoel roof have also enhanced our understanding of collective migration in development (Figure 1.1) (Huang and Winklbauer, 2018; Scarpa and Mayor, 2016). However, our understanding of the molecular processes that regulate organized movements of cell clusters remains largely incomplete. For example, how do

multipolar single cells integrate mechanical and chemical signals from the extracellular matrix (ECM) and neighboring cells to produce a polarized migrating stream of cells?

The need to understand and target dysregulated collective movements is further illustrated by congenital abnormalities and metastatic neoplasms rising to the leading causes of mortality in the twenty-first century within infants and all age groups, respectively (US Centers for Disease Control, 2020). In fact, while child infant mortality rates have declined throughout the 21st century, congenital malformations continue to be the leading cause of death in United States (US) infants (Ely and Driscoll, 2020; Murphy et al., 2021). Of the four most common congenital malformations, three arise from dysregulated embryonic morphogenesis (heart defects, cleft lip and/or palate, spina bifida) (Mai et al., 2019). Our understanding of the defects in morphogenesis that underlie malformations in the human embryo remain limited (Ferrer-Vaquer and Hadjantonakis, 2013; Moris et al., 2021). Increased understanding of embryonic morphogenesis is critical to reduce suffering from congenital malformations.

The mesendoderm of the *Xenopus* gastrula offers a useful system for studying the molecular mechanisms of collective migration within the context of embryo morphogenesis (Davidson et al., 2004; DeSimone et al., 2005; Keller et al., 2003). *Xenopus* embryos are amenable to high resolution live imaging, straightforward ex vivo culture, and tractable physical manipulations (Chien et al., 2018; Dzamba et al., 2009). Furthermore, the characterized biochemical processes and morphogenic fate maps in the developing *Xenopus* embryo make this system an ideal model for approaching mechanisms of migration (Dworkin and Dworkin-Rastl, 1991; Keller, 1975; Keller, 1976). We seek to understand the molecular processes regulating cell cluster movements.

**Mesendoderm morphogenetic migration in gastrulation**

Lewis Wolpert famously postulated, “It is not birth, marriage, or death, but gastrulation which is truly the most important time in your life” (Wolpert and Vicente, 2015). Understanding how early developing animals undergo gastrulation; a period of coordinated, rapid tissue shape changes and movements, has long perplexed humans (Leptin, 2005; Wallingford, 2019). The principal aims of gastrulation are to properly position the three germ layers (ectoderm, mesoderm, and endoderm) via complex movements of tissues (Huang and Winklbauer, 2018). Understanding how mechanical and chemical inputs direct organized tissue movements during gastrulation is an area of active investigation (Ichikawa et al., 2020; Loose and Patient, 2004; Weber et al., 2012).

The mechanosensitive drivers of mesendoderm migration belong to the integrin and cadherin protein families. Integrins mechanically link the actin and intermediate filament cytoskeleton to the ECM through protein adaptors (eg. talin, paxillin, and FAK) (Harburger and Calderwood, 2009; Hynes, 2002). The integrin family of transmembrane receptors mediates the transmission of extracellular mechanical signals at focal adhesions which strengthen cytoskeletal connections that help cells endure the significant traction forces generated during migration (Galbraith et al., 2002; Gardel et al., 2010). Their role in cell migration is covered more extensively in Chapter 2.

In contrast to integrins, type I and II cadherins represent a family of cell adhesion proteins that play a crucial role in maintaining the structural integrity of tissues by mediating cell-to-cell adhesion (Takeichi, 1988; Takeichi, 1991). These transmembrane proteins are primarily found on the surface of epithelial and other tissue cells, where they

help cells adhere to each other in a calcium-dependent manner (Häussinger et al., 2002; Kim et al., 2011). Cadherins are essential for the formation and maintenance of adherens junctions, which are specialized cell junctions that link the actin cytoskeleton of one cell to that of its neighboring cells (Oda and Takeichi, 2011; Yap et al., 1997). Cadherins are linked to the actin and intermediate filament cytoskeleton through downstream catenin proteins (e.g. α-catenin, β-catenin, plakoglobin) (Stemmler, 2008). This connection to the cytoskeleton helps cells maintain shape, respond to mechanical forces, and communicate signaling cues important for development, tissue maintenance, and wound healing (Halbleib and Nelson, 2006; Lansdown, 2002). Each cadherin molecule on the surface of a cell binds specifically to cadherins on adjacent cells through their extracellular domains, forming mostly homophilic (same-type) interactions (Harrison et al., 2011; Niessen et al., 2011). This interaction requires calcium ions ($Ca^{2+}$), which stabilize the structure of cadherins and are necessary for their adhesive function (Meng and Takeichi, 2009; O'Keefe et al., 1987). While still poorly understood, the complex mechanical and biochemical crosstalk between cadherins and integrins are thought to underlie morphogenetic processes in gastrulation (Weber et al., 2011).

During *Xenopus* gastrulation, mesendoderm cells migrate collectively across a fibronectin substrate assembled by blastocoel roof cells (Figure 1.2) (Boucaut and Darribere, 1983; Dumortier et al., 2012). While cells efficiently migrating in a cohort must establish cell-ECM mechanical interactions via integrins, they also require coordination of cell-cell mechanical contacts via cadherins (Friedl and Gilmour, 2009; Weber et al., 2012). Integrin α5ß1 adhesions are essential to establish physical connections with the fibronectin matrix and engage forward cell movement (Davidson et

al., 2002; Winklbauer and Nagel, 1991). In turn, C-cadherin adhesions are critical for maintaining cell cohesiveness and influencing the extension of monopolar protrusions (Davidson et al., 2002; Winklbauer and Nagel, 1991). Tugging forces on C-cadherin adhesions in the rear of mesendoderm cells recruit keratin 8 intermediate filaments and plakoglobin to sites of stressed adhesions (Weber et al., 2012).

Traction stress maps of mesendoderm explants on fibronectin show that the protrusive edge of leader row cells generates high traction stress in the direction of migration with follower row cells exerting transient low traction stresses in multiple directions (Sonavane et al., 2017). Due to these adhesive forces, leading edge mesendoderm cells maintain monopolar protrusive activity that enhances collective migration (Davidson et al., 2002; Sonavane et al., 2017; Weber et al., 2012). Subsequently, the axial mesoderm involutes and elongates in the anterior-posterior direction as cells orient mediolaterally and intercalate to promote convergence and extension of the tissue (Keller, 2002).

**Mitochondrial dynamics in cell migration and adhesion**

Regulated localization of mitochondria in migratory cells was first suggested following the identification of mitochondria trafficking along neuronal axons to energetically expensive growth cones (Hollenbeck and Saxton, 2005; Morris and Hollenbeck, 1993). It is currently thought that cell migration requires dynamic repositioning of mitochondria to address cellular energetic needs (Majumdar et al., 2019). Microtubule-based mitochondrial transport to the leading edge of migratory cells is dependent on the mitochondrial adaptor GTPase, Mitochondrial rho 1 (Miro1) (Desai et

al., 2013). During single cancer cell migration, mitochondria are most commonly redistributed to the nucleus and leading cell edge (Majumdar et al., 2019; Seetharaman and Etienne-Manneville, 2020).

Mitochondria are highly dynamic organelles that undergo cycles of fusion, the union of separate mitochondrial segments, and fission, or the division of the mitochondrial network into smaller components (Chan, 2006b; Detmer and Chan, 2007). The key regulators of fusion dynamics are the outer mitochondrial membrane GTPases Mitofusin 1 (Mfn1) and Mfn2 and the inner mitochondrial membrane GTPase Optical atrophy (Opa1) (Ishihara et al., 2009; Liesa and Shirihai, 2013). Fission dynamics are controlled by the GTPase dynamin-related protein (Drp1) at the outer mitochondrial membrane (Detmer and Chan, 2007; Mozdy et al., 2000).

The relationship between mitochondrial fission and fusion dynamics, cell migration, and epithelial-to-mesenchymal transitions (EMT) have highlighted the potential regulation of mitochondrial dynamics by cell adhesion. Lamellipodial protrusions are enriched in integrin-focal adhesion complexes during mesenchymal migration (Seetharaman and Etienne-Manneville, 2020). These complexes transmit high mechanical stress during cell migration (Majumdar et al., 2019; Zhao et al., 2013). Disruption of mitochondrial fission following knockdown of Drp1 reduces both mitochondrial localization to lamellipodia and cell velocity, whereas inhibition of mitochondrial fusion via inhibition of Mfn1 and Mfn2 increases mitochondria redistribution to lamellipodia and cell migration (Seo et al., 2018; Zhao et al., 2013). The oncogenic transcription factor Myc directly binds to the promoters of Drp1 and the mitochondria-microtubule motor adaptor proteins, Miro1, Miro2, and Milton to promote

mitochondrial fission and cell migration (Agarwal et al., 2019; Scheid et al., 2021). Cumulatively, such findings suggest a link between integrin-focal adhesion complex formation and a localized increase in mitochondrial fission. Downregulation of E-cadherin is a conserved step in cells undergoing EMT during development, wound healing, and cancer (Rogers et al., 2013; Thiery et al., 2009). Induction of EMT is associated with reduced mitochondrial fusion and Mfn1 activity resulting in increased mitochondrial fission, glycolysis, and migration in cancer cells (Sessions and Kashatus, 2021; Zhang et al., 2020). Thus, it is hypothesized that classical cadherin signaling, such as from E-cadherin or C-cadherin, is associated with increased mitochondrial fusion. Additional investigations into cancer progression and treatment resistance have highlighted the role of mechanical cues from the ECM on intracellular metabolic processes with greater ECM stiffness promoting mitochondrial fission for the facilitation of redox homeostasis which enabled cancer cells to survive oxidative stress and resist chemotherapy (Romani et al., 2022).

**Metabolism in cell migration and adhesion**

The connection between adhesion-dependent signaling and metabolism was initially proposed more than 20 years ago. The late Zena Werb first demonstrated that activation of the α5β1 integrin-Rac family small GTPase 1 (Rac1) pathway generated reactive oxygen species (ROS) derived from mitochondria (Kheradmand et al., 1998; Werner and Werb, 2002). The influence of tissue stiffness on dendritic cell (DC) metabolism and immune function has shown that increased mechanical stiffness enhances DC activation, proliferation, and glucose metabolism via the Hippo signaling pathway

molecule Transcriptional coactivator with PDZ-binding motif (TAZ), thereby supporting priming of immune system responses (Chakraborty et al., 2021). The effect of a tissue's ECM density has also been found to affect the bioenergetics of micratory cells with only highly motile cancer cells, not the entire cell population, showing metabolic changes in their ATP:ADP ratios in response to collagen density (Zanotelli et al., 2022). An optimal collagen density resulted in reduced energy expenditure and enhanced movement (Zanotelli et al., 2022). Therefore, ECM mechanics plays a critical role in dictating the energy costs associated with cell migration and determining the energetic strategies of cancer cells during migration (Zanotelli et al., 2022).

The control of cellular metabolism by other integrins, such as αvβ3 integrin, has been an active area of investigation (Davis et al., 2016; Freeberg et al., 2020). It is now well-established that thyroid hormone exerts a wide array of post-transcriptional effects via αvβ3 integrin activation (Cody et al., 2007; Hoffman et al., 2002; Lin et al., 2011a; Lin et al., 2011b). One associated process includes the calorigenic effect, or the dramatic stimulation of cellular respiration in the presence of thyroid hormone (Padron et al., 2014; Yehuda-Shnaidman et al., 2014). However, the potential for thyroid hormone to bind to both mitochondrial membranes and αvβ3 integrin has made it difficult to distinguish the contributions of integrin activation from direct mitochondria binding in engaging cellular respiration (Davis et al., 2016; Goglia et al., 1994). Taken together, these studies suggest that integrin signaling may be associated with rises in mitochondrial respiration.

Studies of EMT have also informed our understanding of the link between cell adhesion and metabolism. Notably, expression of the snail family transcriptional

repressor 1-Euchromatic histone lysine N methyltransferase 2-DNA methyltransferase 1 (Snai1-G9a-Dnmt1) complex, the key regulator of E-cadherin promoter methylation, results in a downregulation of E-cadherin and fructose-1,6-bisphosphatase with an increase in glycolysis (Dong et al., 2013; Sousa et al., 2019). Furthermore, application of mechanical force to E-cadherin via an electromagnetically controlled bead stimulates Liver kinase B1 (LKB1) (Bays et al., 2017). The stimulation of LKB1 recruits Adenosine monophosphate (AMP)-activated protein kinase to the E-cadherin mechanotransduction complex resulting in increased glucose uptake and ATP production (Bays et al., 2017; Evers et al., 2021). Such changes are consistent with increased glycolytic flux (Herzig and Shaw, 2018). Ultimately, cadherin-dependent signaling may be linked to an increase in glycolytic flux. Studying the relationship between EMT and glucose metabolism in promotion of triple negative breast cancer cell migration has found that glycolysis supports single-cell migration in confined environments (Schwager et al., 2022). However, faster and slower populations of migratory cells exhibited differences in sensitivities to the inhibition of glycolysis or oxidative phosphorylation with more mesenchymal, highly migratory cells predominantly utilizing glycolysis, while more epithelial, less migratory cells relying on mitochondrial respiration (Schwager et al., 2022). Furthermore, these metabolic and migratory phenotypes were plastic as manipulating glucose metabolism or EMT was able to shift cells between these states, thereby affecting their glycolytic and migratory characteristics(Schwager et al., 2022).

**Warburg effect**

The Warburg effect is a phenomenon whereby cancer cells preferentially utilize glycolysis for energy production even when in the presence of sufficient oxygen to support normal mitochondrial oxidative phosphorylation (Liberti and Locasale, 2016; Vander Heiden et al., 2009). A key feature of the Warburg effect is aerobic glycolysis with cancer cells having an abnormally high rate of glucose uptake and conversion of most of it to lactate through glycolysis despite the abundance of oxygen (Gatenby and Gillies, 2004; Lunt and Vander Heiden, 2011). In addition, mitochondrial oxidative phosphorylation is suppressed in cancer cells resulting in a reduced reliance on the more energy-efficient process (Sica et al., 2020; Zheng, 2012). As the end product of aerobic glycolysis in cancer cells is often lactate, this contributes to the production of an acidic tumor microenvironment that can support invasion and immune evasion (Apostolova and Pearce, 2022; Parks et al., 2020).

The Warburg effect is particularly effective for driving cancer progression. Glycolysis is faster than oxidative phosphorylation (Chaudhry and Varacallo, 2024; Zheng, 2012). Therefore glycolysis from the Warburg effect can provide quick ATP generation for the rapidly dividing cancer cells (Sholl-Franco et al., 2010; Strahl and Hamoen, 2010). The intermediates of glycolysis serve as biosynthetic precursors for nucleotides, amino acids, and lipids critical for cell proliferation (Hosios et al., 2016; Lane and Fan, 2015). As many tumors develop hypoxic regions due to inadequate blood supply, glycolysis allows cancer cells to still thrive in these conditions (Hockel, 2001; Höckel and Vaupel, 2001). Mutations in oncogenes (e.g. MYC and PI3K) and loss of tumor suppressors (e.g. p53) have been shown to enhance glycolytic metabolism (Dang et al., 1997; Levine and Puzio-Kuter, 2010). In addition, the transcription factor Hypoxia-

inducible factor 1-alpha (HIF-1α) upregulates glycolytic enzymes and glucose transporters in response to low oxygen conditions (Denko, 2008; Yeung et al., 2008). In addition, mitochondrial dysfunction in cancer cells due to mutations or alterations in mitochondrial function also contribute to the reduced oxidative phosphorylation of the Warburg effect (Potter et al., 2016; Vaupel and Multhoff, 2021).

Notably, the Warburg effect has impacts on cancer care (Chen et al., 2007). The Warburg effect serves as the basis for fluorodeoxyglucose positron emission tomography (FDG-PET) (Miles and Williams, 2008). This imaging modality detects increased glucose uptake in tissues, thereby allowing for the identification of tumors (Kostakoglu et al., 2003). In addition, drugs targeting glycolysis, lactate production, or glucose transporters are being explored in clinical trials (Pelicano et al., 2006; Tilekar et al., 2020). This is in addition to the introduction of combination therapies which combine metabolic inhibitors with traditional therapies (e.g. chemotherapy and radiation) to enhance efficacy (Kery and Papandreou, 2020; Luo et al., 2023). Recent studies have shown that the Warburg effect is not universal for all cancers with some tumors relying on oxidative phosphorylation or mixed metabolic pathways (Danhier et al., 2017; Gentric et al., 2017). Therfore, understanding the metabolic preferences of specific cancers is crucial for advancing personalized medicine (Jacob et al., 2019; Nielsen, 2017).

**Warburg effect in embryogenesis**

An appreciation for similarities in the adaptations embryonic and cancer cells undergo to overcome challenges common to embryogenesis and tumorigenesis, such as cell division and differentiation, has highlighted the use of the Warburg effect in early

embryonic contexts (Krisher and Prather, 2012; Ma et al., 2010). May of the key features of the Warburg effect in cancer are conserved in the early embryo (Shyh-Chang et al., 2013). Early embryonic cells rely heavily on glycolysis, despite being in the presence of oxygen and lacking defects in oxidative phorphorylation, to support rapid proliferation (Milman and Yurowitzki, 1967; Redel et al., 2012). These early embryonic cells prioritize biosynthesis over energy efficiency by shunting glycolytic intermediates into anabolic pathways which can supply precursors for nucleotides, amino acids, and lipids required for cell growth and differentiation (Krisher and Prather, 2012; Tennessen et al., 2014). The inefficiencies in ATP production from glycolysis are offset by its ability to meet biosynthetic and redox demands (Sattler and Mueller-Klieser, 2009; Vazquez et al., 2010). In addition, early embryonic environments are often in hypoxic-like states due to low oxygen before vascularization (Dunwoodie, 2009; Webster and Abela, 2007). HIF-1α is thus often upregulated, which drives glycolytic enzyme expression and promotes the Warburg-like metabolism (Kierans and Taylor, 2021; Marin-Hernandez et al., 2009). Notably, mitochondrial oxidative phosphorylation is downregulated in many early embryonic cells to minimize ROS production as they could damage DNA and cell structures (Srinivas et al., 2019; Stark, 2005).

The Warburg effect has been involved in a variety of embryonic contexts. During mammalian blastocyst formation, cells exhibit high glycolytic flux to support rapid cell division and differentiation (Gardner and Harvey, 2015; Watson and Barcroft, 2001). The inner cell mass, which gives rise to the embryo proper, exhibits particularly high glycolytic activity (Hewitson and Leese, 1993; Houghton, 2006). In the context of stem cell maintenance and differentiation, embryonic stem cells (ESCs) exhibit a

glycolysis-dominant metabolism (Gu et al., 2016; Moussaieff et al., 2015). As ESCs differentiate, they undergo a metabolic switch toward oxidative phosphorylation (Funes et al., 2007; Mandal et al., 2011). Within neural tube development, neural progenitor cells have also been shown to exhibit Warburg-like metabolism to support neurogenesis in early development (Lees et al., 2018; Zheng et al., 2016). Insights into embryonic metabolism may inform our understanding of cancer and provide new approaches for regenerative medicine or stem cell therapy (Harland, 2018; Intlekofer and Finley, 2019).

**Nutrition during embryogenesis**

A stable nutritional source is critical to provide the necessary biosynthetic precursors for the various metabolic programs active during embryonic development (Gardner et al., 2000; Reynolds et al., 2022). While matrotrophic species (e.g. *Homo sapiens* and *Mus musculus*) have evolved maternal nutrition via placenta for post-implantation development, lecithotrophic species (e.g. *Xenopu laevis*, *Danio rerio*, *Drosophila melanogaster*) derive their nutrition primarily from yolk within the egg for their development (Levin and Bridges, 2020; Trexler and DeAngelis, 2003). As the work contained in this thesis is primarily focused on *Xenopus laevis* embryogenesis, it is critical to review the current understanding of the dense, membrane-bound specialized organelles called yolk platelets (YPs) that store and supply nutrients during embryonic development of amphibians, sea urchins, and *Caenorhabditis elegans* (Jorgensen, 2008). However, there are many outstanding reviews of placental nutrition and metabolism that should be considered in the context of mammalian embryogenesis (Brett et al., 2014;

Cetin and Alvino, 2009; Godfrey, 2002; Lager and Powell, 2012; Sferruzzi-Perri and Camm, 2016).

During embryogenesis YPs vary in size and number across different regions of the embryo, being more concentrated in the vegetal hemisphere, a yolk-rich region (Danilchik and Gerhart, 1987). The YPs are distributed to all embryonic cells, which consume the yolk intracellularly over the course of embryogenesis (Jorgensen et al., 2009). YPs are formed in the oocyte during oogenesis and originate from vitellogenin, a precursor protein synthesized in the maternal liver and transported to the oocyte via the bloodstream (Li and Zhang, 2017; Wiley and Wallace, 1981). Proteins are the primary component of YPs and include phosvitin and lipovitellin, which are derived from vitellogenin (Bergink and Wallace, 1974; Finn, 2007). Lipids in the YPs (stored as triglycerides and phospholipids) serve as an energy source and are used for membrane biosynthesis (Kuksis, 1992). While YPs contain only a small amount of carbohydrates, they are usually in the form of glycogen to support immediate energy needs(Robertson, 1979).

YPs play a number of roles in the developing embryo. Most notably, they serve as a reservoir by storing nutrients that are metabolized to support embryonic growth and differentiation until external feeding is possible (Juneja and Kim, 2018). However, as YPs are more abundant in the vegetal hemisphere during the early cleavage stages, this differential distribution of YPs influences cleavage patterns with the vegetal pole dividing more slowly compared to the animal pole due to the physical barrier posed by the yolk (Shimogama et al., 2021). This significantly impacts morphogenesis during gastrulation and organogenesis, as YP-rich cells in the vegetal pole move inward to contribute to the

formation of the endoderm and other internal structures (Arendt and Nübler-Jung, 1999). There is also extensive metabolism of the YP components with enzyme proteases, such as cathepsins, breaking down the proteins in YPs into amino acids (Britton and Murray, 2004; Mallya et al., 1992). Lipases also hydrolyze the stored lipids into fatty acids and glycerol for energy and structural function (Speake et al., 1998). As development progresses, yolk platelets are gradually broken down and absorbed (Romano et al., 2004). By the time of hatching, the yolk reserves are nearly depleted, coinciding with the transition to external feeding (Komazaki et al., 2002).

**Summary and dissertation outline**

Collective cell migration relies on the physical coordination of integrin-dependent cell-ECM and cadherin-dependent cell-cell adhesions. This form of cell migration is central to the morphogenetic movement of the mesendoderm in gastrulation. The regulation of the energy metabolism that fuels these energy-intensive processes remains poorly understood. In this dissertation, I further characterize the role cell adhesion plays in regulating and organizing the bioenergetics of collective cell migration. The work contained in Chapter 2 identifies $\alpha5\beta1$ integrin activation and signalling via FAK as critical to producing the mitochondrial activity needed for collective mesendoderm migration, and is the primary focus of this thesis. From examining the generalizability of integrin-FAK mitochondrial metabolism in other tissues to considering the potential contributions of integrin activation to differences in mitochondrial content, the studies in Chapter 3 seek to expand the central findings from Chapter 2 in a a few directions. We evaluated the spatial distribution of mitochondrial activity and clustering in groups of mesendoderm cells or motile tissue while also testing the contribution of exogenous

integrin activation to mitochondrial activity. Finally, Chapter 4 is a summary of the work from these two chapters and introduces preliminary metabolomic analyses from *Xenopus laevis* gastrulae with or without a fibronectin expression knockdown. This allows for a discussion of both future experimental approaches and the significance of this work. Together, this dissertation is an overview of the influence of adhesive processes on the metabolic programs fueling embryo morphogenesis.

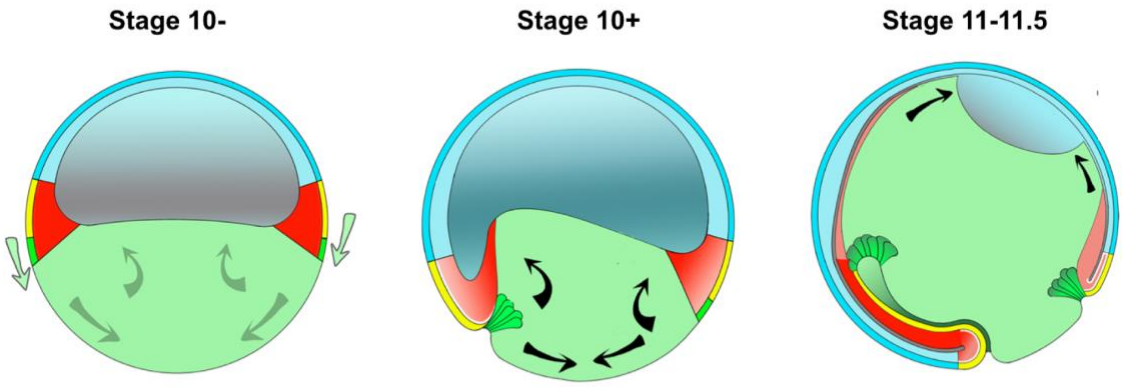
Stage 10-
Stage 10+
Stage 11-11.5

**Figure 1.1: Morphogenetic movements during gastrulation.** Adapted from (Shook et al., 2022). Cartoon diagram of the morphogenetic processes in gastrulation-stage *Xenopus laevis* embryos. The direction of cell movements are denoted by arrows and presented in sagittal sections of the embryo.

Yellow/green = endoderm, pink/red = mesoderm, blue = ectoderm

**Left:** Prior to the onset of gastrulation (Stage 10-), vegetal rotation has not yet occurred (gray arrows).

**Center:** With the onset of gastrulation and convergent thickening (stage 10+), apical constriction of the lower involuting marginal zone epithelium occurs with the start of bottle cell formation (dark green), vegetal rotation, involution and invagination (black arrows). Coinciding with bottle cell formation, the deep mesodermal tissue begins to lose its affinity with the overlying epithelium. However, the the IMZ epithelium is tightly attached at its vegetal edge to the forming bottle cells, which in turn are tightly attached to the adjacent vegetal endodermal tissues. Thus the involuting marginal zone epithelium is pulled along with the bottle cells as they move inside the blastopore. During early involution, as the lower edge of the involuting marginal zone involutes, it transitions from expressing convergent thickening to expressing directed migration. During later involution, the upper involuting marginal zone transitions to expressing convergent extension. In the case of convergent extension, this transition is accompanied by regaining a high deep-epithelial affinity. In the meantime, vegetal rotation (black arrows) has moved the vegetal endoderm inward at the onset of gastrulation such that convergence force generated by convergent thickening cooperates with vegetal rotation to move the involuting marginal zone vegetally and push the vegetal endoderm inside.

**Right:** Vegetal rotation, convergent thickening, and convergent extension also cooperate to stretch the ectodermal region by pulling it vegetally (Stage 11-11.5). When convergent extension begins, it has been positioned by the actions of convergent thickening and vegetal rotation such that it further moves the involuting marginal zone vegetally and pushes the vegetal endoderm inside.

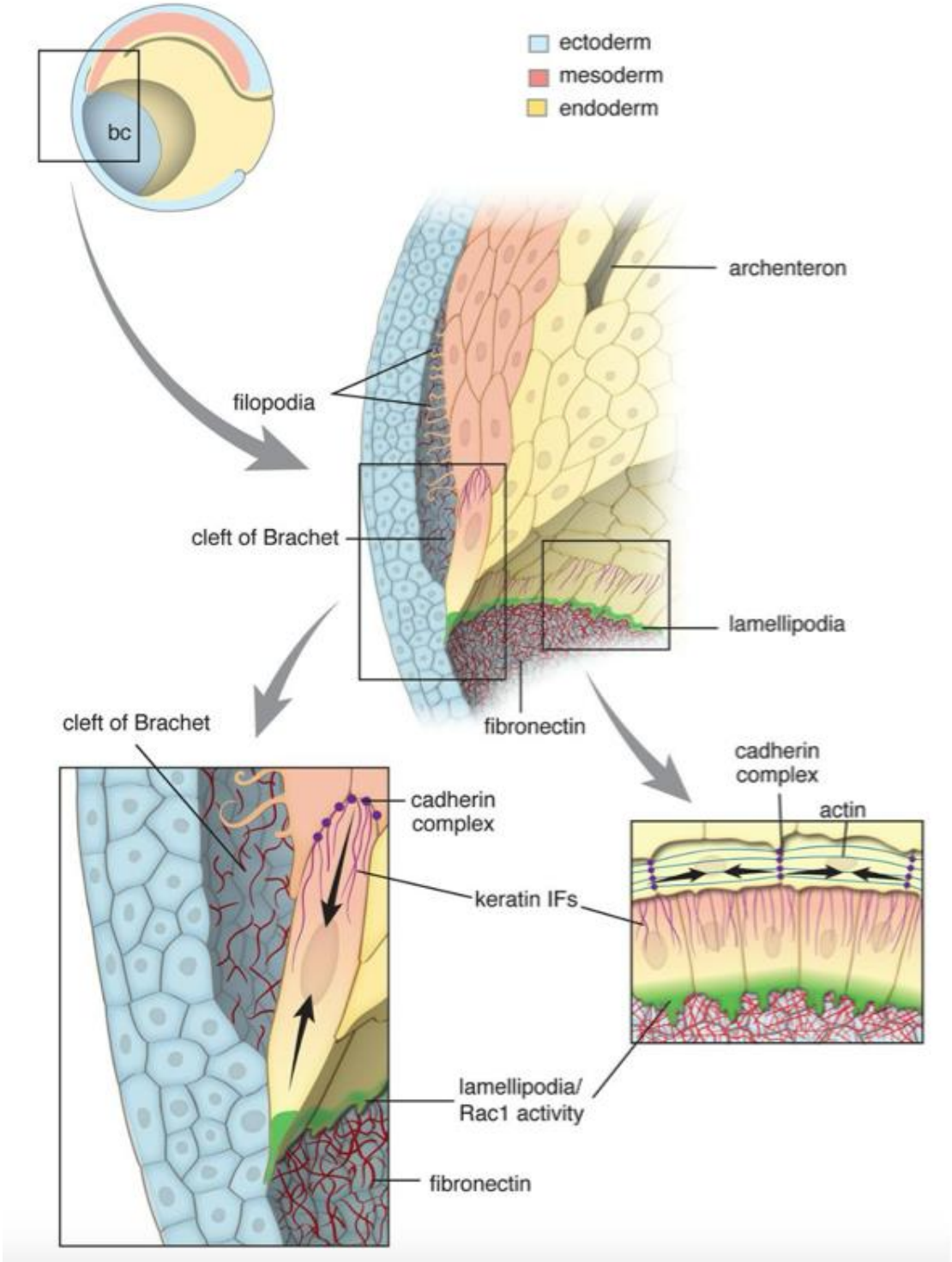
ectoderm
mesoderm
endoderm
bc
archenteron
filopodia
cleft of Brachet
lamellipodia
fibronectin
cleft of Brachet
cadherin complex
keratin IFs
lamellipodia/ Rac1 activity
fibronectin
cadherin complex
actin

**Figure 1.2: Summary of mesendoderm morphogenesis in a mid-gastrula stage *Xenopus* embryo.**

Adapted from (Sonavane et al., 2017).

**Center:** Profile view of the boxed region from a bisected embryo (upper left; blastocoel (bc)), illustrating the forward movement of the mesendoderm and its spatial association with the blastocoel roof, fibronectin fibrillar matrix, and the trailing mesoderm and endoderm.

**Lower left:** A close-up view showcasing a leading-edge mesendoderm cell with a prominent forward protrusion exerting traction on the overlying blastocoel roof. As the leading edge progresses, it remodels the fibronectin matrix beneath it. The rear of the leading-edge cell is connected to follower row cells through a cadherin-based adhesion complex supported by a basket-like arrangement of keratin intermediate filaments (IFs). Arrows indicate the balance between forward traction forces and intercellular stresses at the rear. Follower cells extend long, specialized filopodia (cytonemes) into the cleft of Brachet, which is widened in this region due to the inability of follower row cells to adhere to the blastocoel roof.

**Lower right:** An en face view of the mesendoderm showing the interaction between leading-edge cells, with their broad lamellipodia contacting the blastocoel roof, and the circumferentially arranged upper row cells featuring a stress fiber-like organization of actin filaments. The upper row cells likely assist in closing the mesendoderm mantle by generating tangential stresses (black arrows) perpendicular to the radial stresses exerted by the underlying leading-edge cells. The Rac1 activity gradient (green shading) is most pronounced in the protrusions of the leading-edge cells.

# Chapter 2:

# Spatial regulation of mitochondrial membrane potential by α5β1 integrin engagement in collective cell migration

## Introduction

Cell migration is an energy-intensive process that relies on adenosine triphosphate (ATP) to drive cellular mechanisms underlying movement (Ledderose et al., 2018; Zanotelli et al., 2018). Effective migration also requires physical interactions between the cell surface and the extracellular matrix (ECM), mediated by integrins (Huttenlocher and Horwitz, 2011). These adhesion receptors transmit extracellular mechanical signals, reinforcing cytoskeletal connections and resisting traction forces (Galbraith et al., 2002; Gardel et al., 2010). However, the precise mechanisms linking integrin signaling to cellular bioenergetics during migration remain unclear.

*Xenopus laevis* gastrulation represents a mechanobiologically tractable model of collective cell movements that lends itself to both *in vivo* and *ex vivo* analyses (Bjerke et al., 2014; Comlekoglu et al., 2024; Davidson et al., 2002; Ramos and DeSimone, 1996; Ramos et al., 1996; Rozario et al., 2009; Sonavane et al., 2017; Weber et al., 2012). The mesendoderm, comprised of both mesodermal and endodermal cells, migrates along a fibronectin-rich ECM assembled by the blastocoel roof (BCR) ectoderm (Fig. 2.1A) (Boucaut and Darribere, 1983). Integrin α5β1 engagement with BCR fibronectin is necessary for the forward movement of the tissue (Davidson et al., 2002; Winklbauer and Nagel, 1991) with directed protrusive activity of leading edge cells promoting collective migration and directionality (Weber et al., 2012). Leader row cells also generate oriented integrin □5□1-dependent traction stresses to enable directed movement. In contrast, follower cells exhibit multipolar protrusive activity and randomly directed traction stresses resulting in zero net directional force (Fig. 2.1B) (Sonavane et al., 2017). Integrin adhesions also promote ATP-dependent phosphorylation and activation of signaling

molecules such as Focal Adhesion Kinase (FAK) (Geiger et al., 2009; Parsons, 2003). Consistent with other modes of collective migration, intercellular tension in the mesendoderm is distributed throughout follower rows via cell-cell adhesions (Fig. 2.1B) (Sonavane et al., 2017; Trepat and Fredberg, 2011; Weber et al., 2012). Polarized movements and mechanical behaviors of cells in mesendoderm explants are similar to those in intact embryos where leader row traction stresses result in a localized distortion of the blastocoel roof (Moosmann et al., 2013; Sonavane et al., 2017). These observations point to a unique role for leader row cells in adhesion and traction force generation that "pulls" along follower rows.

The current study reports a spatial increase in mitochondrial activity in the leading row of motile mesendoderm cells where fibronectin-α5β1 integrin substrate traction stresses are greatest. This suggests that integrin engagement and signaling are critical metabolic regulators in collectively migrating cells.

## Results and Discussion

### Mitochondrial activity is highest in leader row cells

Confocal microscopy was used to resolve leader and follower row cells in mesendoderm explanted from gastrula stage embryos (Fig. 2.1B, C). Spatial differences in mitochondrial activity were visualized with tetramethylrhodamine ethyl ester (TMRE), a cell permeant, positively charged molecular probe that fluoresces proportionally to mitochondrial membrane potential (MMP) in live cells (Crowley et al., 2016) and serves as a readout for electron transport chain (ETC) activity (Zorova et al., 2018). TMRE fluorescence was greatest in leader row cells (Fig. 2.2A, B) where high traction stresses

and fibronectin-α5β1 integrin adhesions are located (Sonavane et al., 2017). Symmetrical access of leader and follower rows to TMRE was confirmed by treating live tissue with oligomycin or carbonyl cyanide p-trifluoro-methoxyphenylhydrazone (FCCP) (Fig. 2.3 A,B). Oligomycin is an ATP synthase inhibitor that reduces electron flow through the ETC and hyperpolarizes mitochondria (Suski et al., 2012). The protonophore FCCP inhibits ATP synthesis by collapsing the proton gradient across the inner mitochondrial membrane (Yuan et al., 2013). No difference in MMP was observed between leader and follower rows of explants treated with either oligomycin (i.e., high MMP) or FCCP (i.e., low MMP) (Fig. 2.3 C, D). These results support the conclusion that increased TMRE fluorescence in leader row cells (Fig. 2.2 A, B) reflects a spatially localized energy demand and not simply limited diffusion of TMRE restricting access to follower row cells.

Mesendoderm was fixed and immunostained with an antibody directed against the translocase of outer mitochondrial membrane 20 (TOMM20) in order to establish whether variations in mitochondrial content might contribute to differences in TMRE fluorescence (Liang et al., 2023; Zhao et al., 2014). No significant difference in TOMM20 staining was detected in leader vs follower row cells (Fig. 2.4 A,B). These results were confirmed using embryos from a transgenic line of *Xenopus laevis* that expresses GFP-tagged outer membrane protein 25 (OMP25-EGFP) in live cells (Taguchi et al., 2012) (Fig. 2.5A). As observed with TOMM20, mesendoderm explants from OMP25-EGFP embryos revealed no difference in mitochondrial content between leader and follower rows (Fig. 2.5B).

**Integrin-dependent adhesion supports increased mitochondrial activity**

Integrin involvement in regulating MMP was addressed by comparing mesendoderm cells on fibronectin or poly-l-lysine (PLL; non-specific positively charged control) substrates. Mesendoderm cells express $\alpha 5\beta 1$ (Whittaker and DeSimone, 1993) and will attach and spread on fibronectin coated glass substrates. Cells on PLL attach but fail to spread (Fig. 2.6 A, B) as reported previously (Ramos and DeSimone, 1996). TMRE fluorescence intensity was increased in cells on fibronectin compared to PLL (Fig. 2.6 A-C). In addition, phosphorylation of FAK tyrosine-397 was reduced on PLL (Fig. 2.7 A-C). These data suggest that functional distinctions between fibronectin and PLL in cell attachment, spreading, and MMP are integrin-dependent.

Substrate specific differences in mesendoderm cell oxidative phosphorylation were analyzed using a Seahorse mitochondrial stress test. Oxygen consumption rate (OCR) was determined for cells on fibronectin or PLL following sequential exposure to inhibitors of mitochondrial function (i.e. oligomycin, FCCP, and antimycin A/rotenone) (Ludikhuize et al., 2021). Mesendoderm cells on fibronectin or PLL produced distinct OCR traces (Fig. 2.8 A). A three-fold increase in basal OCR was observed in cells on fibronectin compared to those on PLL (Fig. 2.8B). These results were also generalizable to mammailian cell lines. Baseline OCR was elevated on fibronectin compared to PLL in HeLa cells, immortalized macrophages and myoblasts (Fig 2.9).

Cells on fibronectin showed significant reductions in pre-treatment (Pre-Tx) baseline oxygen consumption in the presence of FAK pharmacologic inhibitors PF-562,271 and PF-573,228 (Slack-Davis et al., 2007; Stokes et al., 2011) (Fig. 2.10 A). In

contrast, no significant change in basal oxygen consumption was detected in cells attached to PLL in the presence of either FAK inhibitor (Figs. 2.9 B, D, F and 2.10B).

Our findings suggest a link between integrin adhesion and signaling, and the activation of FAK pathways that play a critical role in maintaining MMP under stress conditions (Banerjee et al., 2017; Frisch et al., 1996). For example, activation of FAK stimulates pathways (e.g., PI3K/AKT and ERK) that prevent mitochondrial outer membrane permeabilization (Hernández-Corbacho et al., 2015; Zhang et al., 2018), minimize electron leakage that could lead to reactive oxygen species (ROS) production (Raimondi et al., 2020; Visavadiya et al., 2016), and activate adenosine monophosphate-activated protein kinase (AMPK) to enhance mitochondrial biogenesis and activity under energy- demanding conditions (Guo et al., 2020; Lassiter et al., 2018).

**Ligand dependent changes in integrin activation regulate MMP**

Integrins function as bidirectional signaling complexes, undergoing allosteric changes in response to extracellular ligand binding and intracellular interactions with signaling molecules and cytoskeletal proteins (Hynes, 2002). In the case of $\alpha 5\beta 1$ integrin, there are at least three major conformational states: bent-closed (BC), extended-open (EO), and extended-closed (EC) (Li et al., 2021; Schumacher et al., 2021). These conformations reflect high (EO) and low (BC and EC) affinity states for ligand binding. Ligand bound EO conformation is further stabilized by ECM and cytoskeletal derived tensile forces (Li et al., 2024). This prompted us to investigate whether integrin conformational changes and activation are linked to increased mitochondrial activity at the mesendoderm leading edge.

The fibronectin binding site for α5β1 integrin is comprised of both the Arginine-Glycine-Aspartic acid (RGD) sequence located in fibronectin Type III repeat 10 (Ruoslahti and Pierschbacher, 1987) and the "synergy" site sequence Proline-Proline-Serine-Arginine-Asparagine (PPSRN) located in fibronectin Type III repeat 9 (Aota et al., 1991) (Fig. 2.11). While RGD containing fragments of fibronectin can bind with low affinity to the BC conformation of α5β1, recognition of the PPSRN synergy sequence is required for transition to the high affinity EO state (Fig. 2.11) (Benito-Jardón et al., 2017; Danen et al., 1995; Li et al., 2003). Mesendoderm cells are able to attach, spread and migrate on substrates coated with glutathione-s-transferase (GST) fusion proteins containing fibronectin Type III repeats 9-11 (GST-9.11, Figures 2.11 and 2.12A). Cells will attach but spread poorly on fusion proteins containing a mutation (PPSRN>PPS**A**N) in the synergy site (GST-9.11A, Figs. 2.11 and 2.12B). Moreover, integrin-dependent phosphorylation of FAK is decreased on GST-9.11A compared to GST-9.11 (Fig. 2.7A-C). Cells fail altogether to attach to GST-9.11 fusion proteins lacking an intact RGD sequence (Ramos and DeSimone, 1996).

Several lines of evidence suggest that changes in integrin α5β1 conformation affect mitochondrial activity. TMRE fluorescence in cells on GST-9.11A is reduced 50% compared to those on GST-9.11 (Fig. 2.12A-C). Cells on GST-9.11 produce distinct OCR traces compared to cells on GST-9.11A (Fig. 2.13A), with a three-fold increase in basal OCR on GST-9.11 compared to cells on GST-9.11A (Fig. 2.13B). We next addressed whether bioenergetic differences between mesendoderm cells on GST-9.11 and GST-9.11A were dependent on integrin activation state and FAK signaling. Cells adherent to GST-9.11 presented significant reductions in Pre-Tx baseline oxygen consumption when

treated with either FAK inhibitor (Fig. 2.14A). However, cells on GST-9.11A showed no further reductions in baseline oxygen consumption following treatment with FAK inhibitors (Fig. 2.14B).

Explants on GST-9.11 exhibited polarized protrusions oriented in the direction of travel (Fig. 2.15A). Whereas explants on GST-9.11A extended unpolarized protrusions in random directions (Fig. 2.15B) and failed to migrate persistently. TMRE fluorescence was 2.5-fold higher in the leading row of mesendoderm tissue on GST-9.11 compared to GST-9.11A (Fig. 2.15C). In sum, integrin conformational change and activation state are associated with an increase in MMP in single and collectively migrating cells of the mesendoderm explant.

**Cell-stretch on fibronectin increases MMP**

Leader row mesendoderm cells on fibronectin include α5β1 integrins under high traction stress (Sonavane et al., 2017). Ligand binding to integrins such as α5β1 initiates an outside-in switch from BC to EO conformations of the receptor to promote higher affinity ligand binding (Su et al., 2016). Moreover, forces transmitted through ligand-bound α5β1are critical for receptor activation and stabilization in the EO conformation (Li et al., 2024). To address whether tensile forces transmitted through fibronectin-integrin complexes contribute to mitochondrial activity in the mesendoderm, cells were allowed to spread on fibronectin-coated polydimethylsiloxane (PDMS) membranes and changes in TMRE fluorescence in the presence (Fig. 2.16A) or absence (Fig. 2.16B) of cyclical uniaxial stretch quantified. MMP was normalized to total mitochondrial mass by simultaneously labeling mitochondria with the fluorescent dye MitoTracker Green

(MTG). While TMRE and MTG fluorescence of individual cells can be measured, the optical properties of PDMS preclude resolving individual mitochondria. The ratio of TMRE to MTG (TMRE:MTG) fluorescence increased ~3.5-fold in stretched vs unstretched cells suggesting that tensile forces transmitted through fibronectin α5β1 represent a potent enhancer of MMP (Fig. 2.16C). Stretched cells in the presence of FAK inhibitors exhibited a ~50% reduction in TMRE:MTG fluorescence indicating cell stretch-dependent MMP is coupled to integrin and FAK signaling (Fig. 2.16D).

The mesendoderm, like many other collectively motile tissues with sheet-like geometry, maintains a uniaxial anisotropic organization with greatest traction stresses formed along the leading edge (Trepat et al., 2009). Mesendoderm leading row cell polarity is subject to "tugging forces" that result in cytoskeletal rearrangements and directed protrusions, a process we have termed *cohesotaxis* (Comlekoglu et al., 2024; Weber et al., 2012). Therefore, uniaxial stretching of dissociated mesendoderm cells likely mimics cell-ECM dependent mechanical inputs encountered by individual cells within migrating mesendodermal tissues.

**Reduced MMP slows mesendoderm migration velocity *in vivo***

To address the importance of the integrin-dependent enhancement of MMP we imaged live explanted mesendoderm on fibronectin in the presence or absence of FCCP (Fig. 2.17A-D). The consequences of inhibiting MMP in gastrulating embryos was determined by measuring the closure rate of the mesendoderm mantle following injection of FCCP into the blastocoel cavity (Fig. 2.18 A-D). Migration velocity was reduced in both isolated tissue (Fig. 2.17 E) and intact embryos (Figure 2.18 E). Exposure of the

mesendoderm to oligomycin also slowed collective migration (Fig. 2.17F). Therefore, collective migration on fibronectin likely provides an outside-in integrin-dependent feedback signal to increase MMP and ATP production to meet the energetic demands of leader row cells.

The changes in MMP we measure with TMRE do not necessarily reflect changes in ATP production or spatially localized energy demand. That FCCP and oligomycin treatment result in the same reduced migration phenotype (Fig. 2.17E, F), provides support for a model in which increased MMP promotes migration as a result of increased ATP production (Fig. 2.19). These two drugs have opposite effects on MMP but both inhibit ATP production and slow migration. Therefore, it is likely that the reduction in migration is due to a loss in ATP production. If the increased MMP was supporting migration through a process that was independent of ATP demand, these drugs should have opposite effects on migration.

We propose that α5β1 integrin-fibronectin binding permits an "outside-in" change in receptor conformation and signaling through FAK to increase MMP, oxidative phosphorylation and ATP production (Fig. 2.19). Studies of endothelial and epithelial cells have suggested a potential link between bioenergetics and mechanical cellular processes (Bays et al., 2017; Park et al., 2020). While there has been progress in quantifying the specific energetic costs of cell migration events, the coordination of cell migration machinery and energy production remains an active line of investigation (Cunniff et al., 2016; Mosier et al., 2021).

Our findings expand previous studies from the Reinhart-King lab on cell-ECM adhesion and ATP metabolism in cancer cell migration and metastasis (Wu et al., 2021;

Zanotelli et al., 2018). Collective invasion of breast cancer cells is regulated by the energetic statuses of leader and follower rows with leaders exhibiting higher glucose uptake and ATP/ADP ratios, supporting their invasive capabilities (Zhang et al., 2019). As leader cells deplete their energy reserves, they transition roles with followers, highlighting a coordinated energy-dependent mechanism in collective cell migration (Zanotelli et al., 2021).

ECM stiffness is reported to influence metabolic pathways. For example, stiffer conditions enhance dendritic cell activation, cytokine production, and T-cell priming by increasing glycolysis and oxidative phosphorylation, with TAZ and PIEZO1 mediating these effects (Chakraborty et al., 2021). In contrast, soft ECM promotes mitochondrial fission (Romani et al., 2022). ECM stiffening may also promote mitochondrial fusion and suppress mitochondrial fission (Chen et al., 2021; Tharp et al., 2021).

While we observed integrin-dependent increases in MMP, we cannot eliminate the possibility that high MMP may also contribute to ROS production (Suski et al., 2012; Zorova et al., 2018). In fact, it has been previously reported that integrin-Rac signaling can upregulate ROS production and potentially reorganize the surrounding matrix (Kheradmand et al., 1998; Werner and Werb, 2002). NOX2, an NADPH oxidase, responds to Rac1 and PAK1 signaling at the leading edge of motile cells to generate extracellular superoxide to enhance single cell motility (Ikeda et al., 2005; Wu et al., 2005). The contribution of ROS to collective forms of cell migration remains to be explored.

These studies highlight potential links between integrin conformational states, adhesion and signaling, and cellular mechanics and metabolism in migratory cells.

Further elucidation of the mechanisms involved will be important for understanding the regulation of cell and tissue movements in morphogenesis.

## Materials and methods

### Xenopus embryo manipulations

Xenopus embryos were obtained and cultured as described previously (Gerhart and Kirschner, 2020; Sive, 2000). Briefly, *Xenopus* laevis females were super-ovulated by injection of human chorionic gonadotropin (Covetrus). Eggs were obtained on the day following injection. *In vitro* fertilization was performed with a homogenate of harvested testis in 1X Modified Barth's Saline (MBS) and incubated with collected eggs. Thirty minutes after fertilization, embryos were dejellied at the one-cell stage in 3% cysteine (Sigma), pH~7.9. Fertilized embryos were rinsed and cultured in 0.1X MBS solution until stage 10.5 to 11.0. All animal work has been approved by the University of Virginia IACUC.

### Dorsal marginal zone (DMZ) explant preparation

Dorsal marginal zone (DMZ) explants (i.e., the source of mesendoderm tissue used in this study) were prepared as described previously (Comlekoglu et al., 2024; Sonavane et al., 2017). Briefly, stage 10.5 Xenopus gastrulae were placed in 1X MBS and lateral incisions were made to separate dorsal and ventral portions of the embryo. Vegetal cells were removed using an eyebrow knife to obtain the mesendodermal, mesodermal, and bottle cells. Glass-bottom dishes for explant imaging were coated with 500µl of 0.05 mg/ml bovine plasma fibronectin (Corning) overnight at 4°C. Dishes were then rinsed three

times with 1X MBS. To avoid non-specific binding, dishes were subsequently blocked with 500 µL 5% bovine serum albumin (BSA) (Sigma) for ~1 hour at room temperature. Following removal of the blocking solution, the dishes were filled with 3mL of Danilchick's For Amy (DFA) media, which approximates interstitial fluid (Sater et al., 1993). Explants were then placed in the fibronectin coated chamber and gently compressed from above using cover glasses with edges coated in silicone grease. Explants were allowed to attach for approximately 1 hour to allow initial migration before image acquisition. Mitochondrial function inhibitors, such as FCCP and oligomycin, were added following 30 minutes of imaged explant collective migration.

**Mesendoderm cell preparation**

Dorsal mesendoderm tissue from stage 10.5 to 11 Xenopus embryos was dissociated in 1X $Ca^{2+}$/$Mg^{2+}$-free MBS (CMF-MBS). To examine the response of individual mesendoderm cells to distinct adhesive substrates, glass dishes were coated with poly-L-lysine solution (1.0 mg/mL, Sigma), bovine plasma fibronectin (0.05 mg/mL), or equimolar amounts of GST-9.11 (0.01 mg/mL) and GST-9.11A (0.01 mg/mL). All GST fusion protein, fibronectin and PLL coated substrates used in this study were subsequently blocked with 5% bovine serum albumin (BSA) to prevent "non-specific" cell attachment to glass or plastic as previously described (Ramos et al., 1996; Richardson et al., 2018). Mesendoderm cells do not adhere to BSA. Dissociated cells were transferred and allowed to spread on coated glass dishes filled with DFA. Molar equivalents of plasma fibronectin, GST-9.11, and GST-9.11A were kept consistent at 0.23 µM.

**Seahorse mitochondrial stress test**

Mesendoderm cells (1,000 to 2,500 cells) were seeded in a standard 96-well Seahorse culture plate (Agilent) containing 80 µL DFA media per well and placed at room temperature for 1 hour to adhere. Seahorse mitostress media was prepared using DFA containing 10 mM glucose, 2 mM glutamine, and 1 mM sodium pyruvate, pH~7.4. Inhibitors were diluted in assay media using 10X stock solutions. Final concentrations of 10 µM oligomycin, 2 µM FCCP, and 0.5 µM antimycin A/rotenone were produced in each assay well following inhibitor administration. These inhibitors were loaded into a standard 96-well Seahorse flux plate (Agilent) for pressurized dispensing. The media of all the wells with cells was aspirated and replenished with 180 µL Seahorse mitostress media. All mesendoderm cells were seeded at comparable densities. The assay run was completed in approximately two hours and basal mitochondrial oxygen consumption rate (OCR) was calculated by subtracting the final antimycin A/rotenone-treated OCR from the resting OCR (Ludikhuize et al., 2021). Following each assay run cells were lysed and their DNA content was determined using Quant-iT PicoGreen dsDNA assay (Thermo Fisher). The DNA content obtained was compared to a previously established standard curve that was established using the Quant-iT PicoGreen dsDNA assay for predetermined numbers of mesendoderm cells. Such comparisons allowed for an estimation of cells in each well. These readings were then used to normalize the assay findings to 150 cells/well. Each figure legend of Seahorse XF data presents the number of independent fertilizations/experiments or biological replicates (N) and number of wells or technical replicates (n). In other words, egg clutch is represented as a “N” biological replicate.

Embryos from a single clutch were pooled and mesendoderm is collected with cells pooled. Therefore, cells distributed in wells are represented as “n” technical replicates

**Live cell imaging of mitochondrial membrane potential**

To assess MMP, cells or embryo explants were pre-incubated for 30 minutes with the potentiometric dye TMRE (50 nM, Thermo Fisher). Cells or embryos were then washed with 3 changes of DFA to reduce non-specific accumulation of TMRE in yolk platelets.

**Fixed imaging of mitochondria**

Stage 11 embryos were fixed for 10 minutes in 3.7% formaldehyde and 0.1% glutaraldehyde in TBST. The mesendodermal mantle was then removed from the embryos and incubated in TBST containing 1% BSA in TBS and 0.1% tween to block the non-specific binding of antibodies. The tissues were incubated overnight (4$^{o}$C) with rabbit anti-Tom20 (1:100, Cell Signaling) antibodies in TBST. After incubation, the tissue was washed 3X in TBST. To detect TOMM20, preparations were incubated overnight in TBST with Alexafluor 488 anti-rabbit (1:1000). Alexafluor 555 phalloidin (1:100) was used to outline cells.

**Confocal microscopy**

Confocal Z-stack images of mesendoderm were taken on a Nikon AX scanning head confocal microscope with a 60X oil objective at 0.5-1µm intervals. To compare mitochondrial membrane potential of the leading row and follower row of mesendoderm, cell outlines were distinguished via a GFP tag to label plasma membranes via a

myristoylation motif. At least 5 cells were traced for each timepoint and then binned as leaders or followers for statistical analyses of TMRE fluorescence. For individual cell analyses, masks of cell membranes were traced and used for measuring the TMRE fluorescence of a given cell. In comparisons of fluorescence between cells or tissues, the raw integrated density of a collapsed 3-dimensional z-stack was divided by the area of the cell and multiplied by the number of z-sections collected. This allowed us to account for variations in cell or tissue height depending on the substrate examined. Total mitochondrial content was also evaluated in live explants with transgenic expression of GFP tagged outer (mitochondrial) membrane protein 25 (EGFP-OMP25). These mesendoderm explants were derived from fertilized eggs obtained from a transgenic line of *Xenopus laevis* Xla.Tg(CMV:eGFP-OMP25)$^{Wtnbe}$ (Taguchi et al., 2012), provided by the National Xenopus Resource of the Marine Biological Laboratory .

**Mesendoderm migration**

To determine the migratory kinetics of the mesendoderm, time-lapse confocal movies were collected. These movies captured images every three minutes for 60 minutes as indicated for each experiment. We allowed migration for 30 minutes without inhibitors (FCCP and Oligomycin), followed by 30 minutes of migration in the presence of inhibitors. Explant extension tracing for velocity was done by highlighting three positions, one per region (top, middle, bottom) along the leading edge of mesendoderm explants expressing membrane-GFP. In each case the X,Y coordinates were recorded and the movement of the three dots was measured and averaged to determine velocity using FIJI (https://fiji.sc/). As described in Davidson et al., 2002, we determined mesendoderm

mantle closure in animal-pole upright intact albino embryos using brightfield illumination with imaging at 40X on an upright Zeiss AxioZoom microscope. The mesendoderm free area of the blastocoel roof was measured as a circle with subsequent measurements of free areas traced to determine the percent closure from the initial area over 2 hours using FIJI.

**Normalized mitochondrial activity during cell stretching**

Whole mesendoderm tissue from stage 10.5-11.0 embryos was dissected and dissociated in 1X CMF-MBS. Dissociated cells were plated on a polydimethylsiloxane (PDMS) well plate (Cell Scale) previously coated overnight with 0.05 mg/ml fibronectin as described above. Wells were blocked with 5% BSA for ~1 hour at room temperature. Following washing, wells were filled with 100 µl of 1X DFA containing 50 nM TMRE and 50 nM MitoTracker Green FM. Cells were allowed to adhere for 30 minutes before the membranes were cyclically stretched (10% stretch) using the MechanoCulture FX system (Cell Scale). The Mechanoculture FX was programmed as follows: fifteen cycles of 10 seconds stretch, 10 seconds hold, 10 seconds relax and 10 seconds hold to mimic the mechanical stress encountered by the mesendoderm during migration (Sonavane et al., 2017; Weber et al., 2012). Images of TMRE and MitoTracker Green FM fluorescence were captured before and after stretch using a 20X objective on an inverted widefield Zeiss Axio Observer. The ratios of TMRE:MitoTracker Green FM were calculated in FIJI by evaluating the fluorescence intensity in cells of interest and compared in stretched versus unstretched conditions. Resolving individual mitochondria through the PDMS membrane is not possible, therefore our measurements of TMRE and MitoTracker Green

FM were based on their total fluorescent signal. Capturing both TMRE and MitoTracker Green FM allowed for a normalization of mitochondrial activity relative to mitochondrial content.

**pFAK:FAK western blot analysis**

Cells were lysed after 1 hour of adhesion to a given substrate (i.e., fibronectin, PLL, GST-9.11, GST-9.11A) with 100µl lysis buffer [25 mM Tris HCl pH=7.4 containing 100 mM NaCl,1 mM EDTA, 1 mM EGTA, 1 mM beta-glycerophosphate, 2.5 mM $Na_4P_2O_7$, 1% NP40, protease inhibitor cocktail (Sigma) and 1 mM PMSF]. Following cell lysis, lysates were centrifuged for 10 min at 14,000 rpm at 4°C to remove yolk. The supernatants were transferred to new tubes, diluted with 2X reducing Laemmli buffer, and proteins separated by SDS-PAGE (10% or 12%) and transferred onto nitrocellulose membranes. Blots were probed with antibodies directed against pFAK (Cell Signaling Technology; 1:1000 dilution), FAK (Cell Signaling Technology; 1:1000 dilution), and beta-actin (Sigma, 1:25,000 dilution). Signal intensity for each band was quantified using FIJI and ratios of pFAK:FAK to tubulin were calculated in Microsoft Excel. Blot transparency containing raw gels in support of Figure 2.7 is presented in Figure 2.20.

**Statistical analysis**

Prism 10 was used for statistical analyses. For pairwise comparisons, unpaired, two-tailed, Student's t -tests were used to determine P values. For multiple-group comparisons, we used a one-way ANOVA to determine whether multiple groups had a common mean. Data are presented in the SuperPlots format (Lord et al., 2020). Briefly,

each biological replicate (N) is color-coded (i.e. gray, blue, red) with the average from an experimental run being presented as a colored triangle. Each technical replicate (n) is represented as a dot that is color-coded according to the biological replicate it came from.

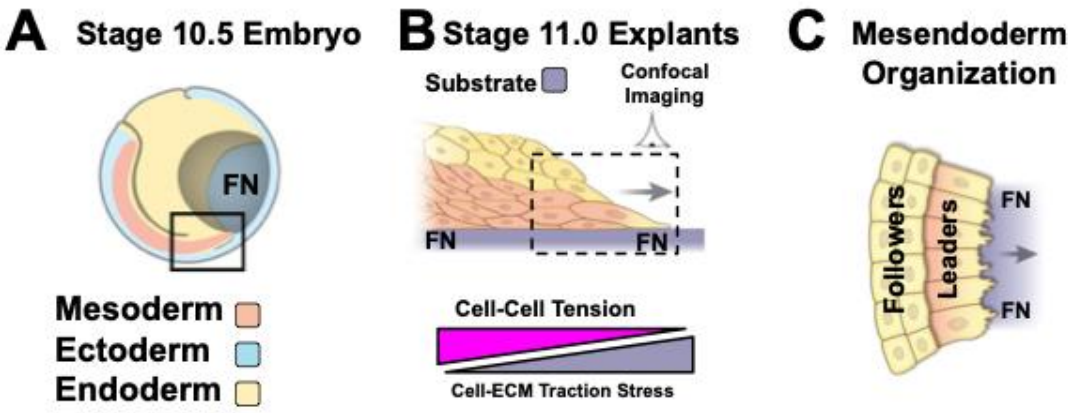
A Stage 10.5 Embryo
FN
Mesoderm
Ectoderm
Endoderm
B Stage 11.0 Explants
Substrate
Confocal Imaging
FN
FN
Cell-Cell Tension
Cell-ECM Traction Stress
C Mesendoderm Organization
Followers
Leaders
FN
FN

**Figure 2.1: Cartoon depicting stage-specific isolation and imaging of mesendoderm during gastrulation.**

(A) Black box over hemisected gastrulation-stage embryo indicates location of migrating dorsal mesendoderm (mesoderm + endoderm) in contact with the blastocoel roof ectoderm.

(B) Dorsal marginal zone explant containing mesendoderm is removed and plated (sagittal view) on a fibronectin substrate (FN, purple). Leader cells (pink-yellow) extend lamellipodia and exert high α5β1 integrin-dependent traction stresses on the fibronectin substrate. Cell-ECM traction stresses (purple wedge) are greatest in leader rows and balanced by increasing cadherin-based cell-cell adhesion stresses (magenta wedge) in follower rows.

(C) Top-down view of explant used for confocal imaging (e.g., panels D and F).

Arrow (B,C) indicates direction of cell movements.

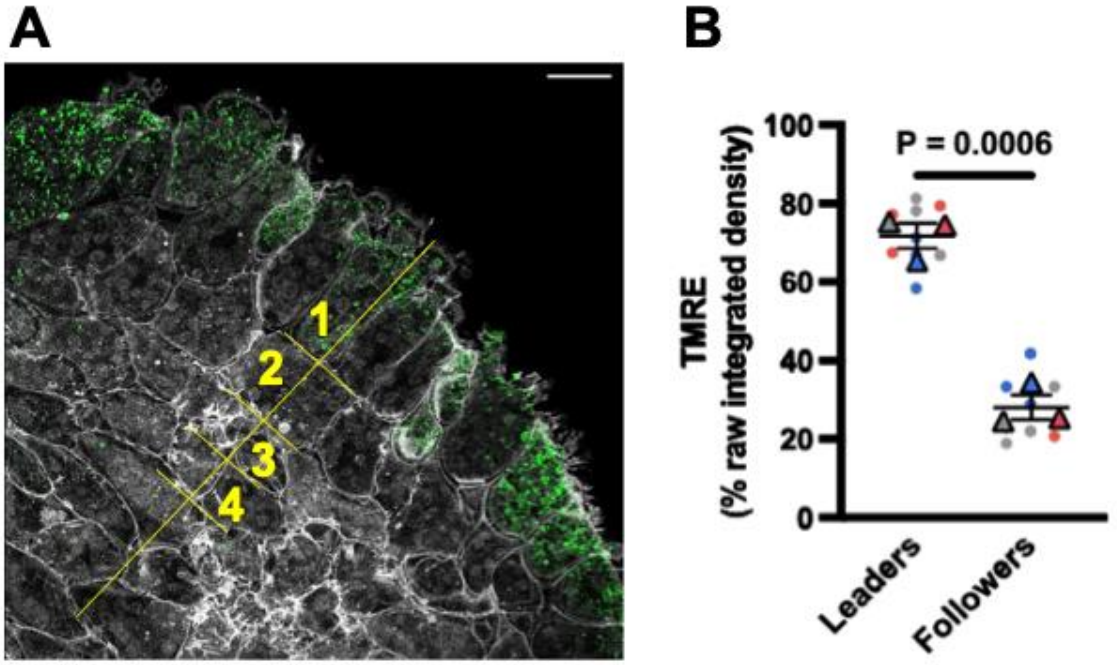
A
1
2
3
4
B
TMRE
(% raw integrated density)
100
80
60
40
20
0
P = 0.0006
Leaders
Followers

**Figure 2.2: Mitochondrial activity is higher in mesendoderm leader row cells than in follower row cells undergoing collective migration.**

(A) Confocal image of mesendoderm explants treated with the potentiometric fluorescent dye tetramethylrhodamine, ethyl ester (TMRE, green pseudocolor) and expressing membrane-GFP to label cell outlines (gray pseudocolor). Locations of cell rows 1, 2, 3, and 4 in (A) are indicated in yellow.

(B) Distribution of TMRE fluorescence between leader and follower row cells of each embryo. Each condition represents the percent of TMRE fluorescence (expressed in raw integrated density) found in leading or following row cells. A minimum of five cells per row were quantified (N=3, n=18).

Conditions were statistically compared using an unpaired two-tailed t-test.

Scale bars = 50 μm.

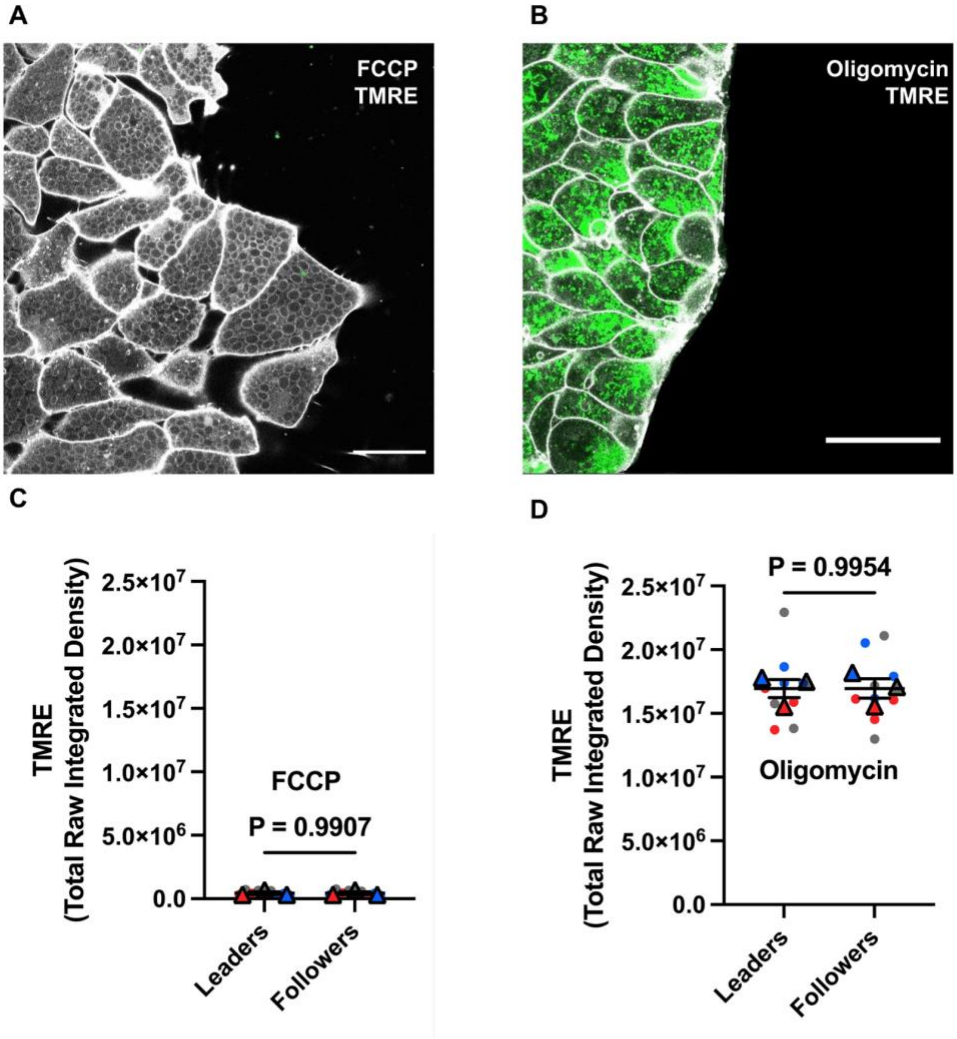
A
FCCP
TMRE
B
Oligomycin
TMRE
C
TMRE
(Total Raw Integrated Density)
2.5×10^7
2.0×10^7
1.5×10^7
1.0×10^7
5.0×10^6
0.0
FCCP
P = 0.9907
Leaders
Followers
D
TMRE
(Total Raw Integrated Density)
2.5×10^7
2.0×10^7
1.5×10^7
1.0×10^7
5.0×10^6
0.0
P = 0.9954
Oligomycin
Leaders
Followers

**Figure 2.3 Oligomycin and FCCP effects on TMRE activity in mesendoderm explants.**

(A,B) Representative low magnification confocal images of mesendoderm explants expressing membrane-GFP for cell outlines (gray pseudocolor) and in presence of the potentiometric dye tetramethylrhodamine, ethyl ester (TMRE, green pseudocolor). Explants treated with (A) FCCP, an uncoupler of mitochondrial membrane potential (MMP) from ETC function, and (B) oligomycin, a MMP hyperpolarizing agent. (C,D) Distribution of TMRE fluorescence in leader and follower row cells of explants treated with (C) FCCP or (D) oligomycin. Each condition represents the total TMRE fluorescence (expressed in raw integrated density) recorded in leading or following row cells. A minimum of five cells per row were quantified (N=3, n=18).

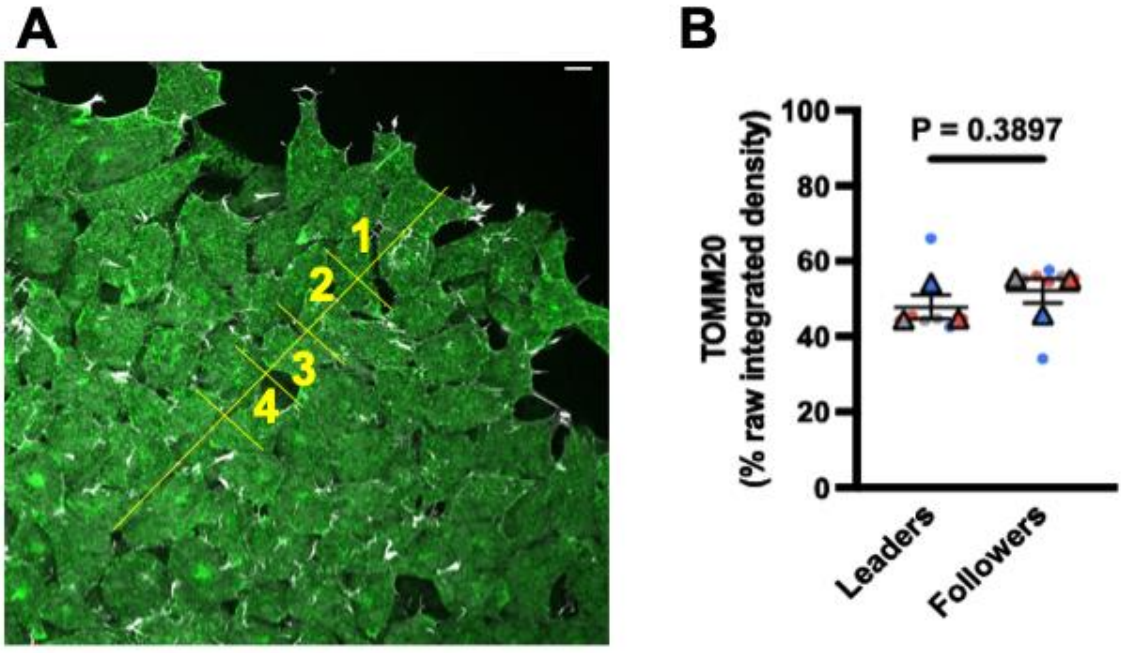
A
1
2
3
4
B
P = 0.3897
TOMM20
(% raw integrated density)
100
80
60
40
20
0
Leaders
Followers

**Figure 2.4: Mitochondrial content is comparable between mesendoderm leader row cells and follower row cells undergoing collective migration.**

(A) Confocal image of mesendoderm explants with TOMM20 antibody staining (green pseudocolor) of total mitochondria and anti-actin antibody staining (gray pseudocolor) in leader and follower row cells of a fixed mesendoderm explant. Locations of cell rows 1, 2, 3, and 4 in (A) are indicated in yellow.

(B) Distribution of TOMM20 fluorescence between leader and follower row cells of each embryo. Each condition represents the percent of TOMM20 fluorescence (expressed in raw integrated density) found in leading or following row cells. A minimum of five cells per row were quantified (N=3, n=14).

Conditions were statistically compared using an unpaired two-tailed t-test.

Scale bars = 50 μm.

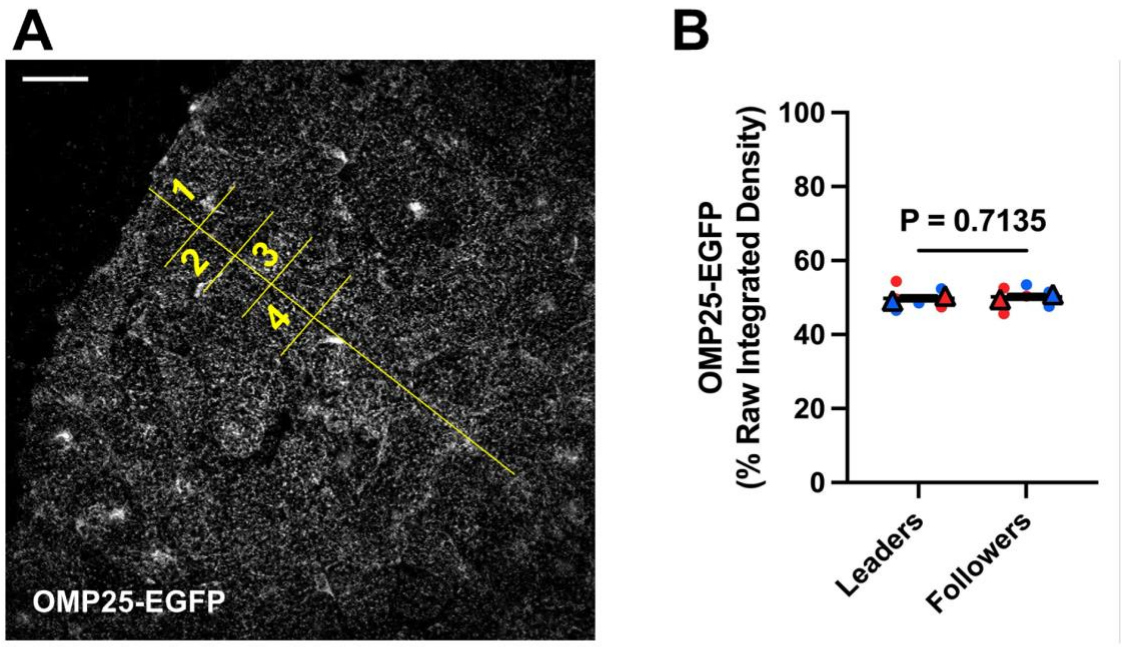
A
1
2
3
4
OMP25-EGFP
B
OMP25-EGFP
(% Raw Integrated Density)
100
80
60
40
20
0
P = 0.7135
Leaders
Followers

**Figure 2.5: Quantification of mitochondrial mass in mesendoderm explants from transgenic *Xenopus laevis* embryos expressing OMP25-EGFP**

(A) Confocal image of a live mesendoderm explant with transgenic expression of the GFP tagged mitochondrial outer membrane protein 25 (OMP25-EGFP, white) to identify total mitochondria. Location of leader row 1 and follower rows 2-4 indicated in yellow. (B) Distribution of OMP25-EGFP fluorescence between leader and follower row cells of each embryo. Each condition represents the percent of OMP25-EGFP fluorescence (expressed in raw integrated density) found in leading or following row cells. A minimum of five cells per row were quantified (N=2, n=6). Conditions were compared using an unpaired two-tailed t-test. Scale bar = 50 μm.

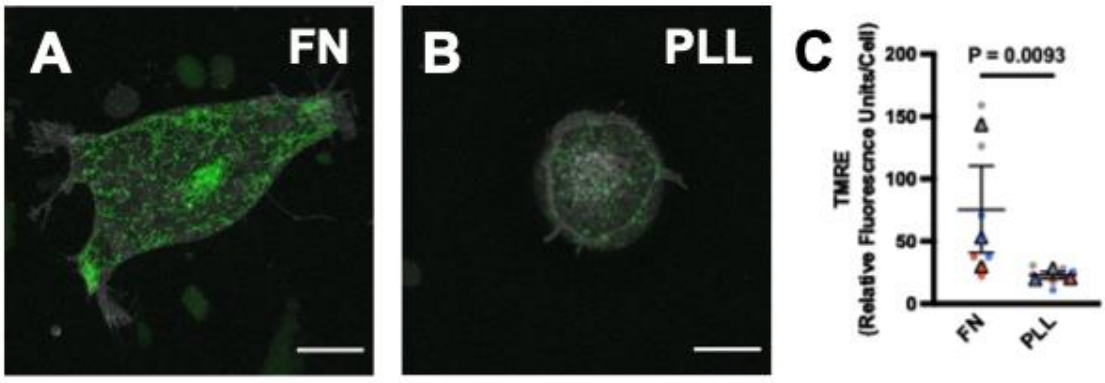
A
FN
B
PLL
C
P = 0.0093
TMRE
(Relative Fluorescnce Units/Cell)
200
150
100
50
0
FN
PLL

**Figure 2.6: Fibronectin adhesion drives high mitochondrial membrane potential in mesendoderm cells.**

(A,B) Spreading of dissociated *Xenopus* mesendoderm cells labeled with Alexa647-dextran (gray pseudocolor) and TMRE (green pseudocolor) on (A) fibronectin (FN) or (B) poly-l-lysine (PLL) substrates. Binding to fibronectin allows for cell spreading in contrast to a spheroidal shape on PLL. Scale bars = 20 μm.

(C) Higher mitochondrial membrane potential is detected in cells bound to FN. Comparison of TMRE fluorescence from dissociated mesendoderm cells on FN and PLL (N=3, n=16). Conditions were statistically compared using an unpaired two-tailed t-test.

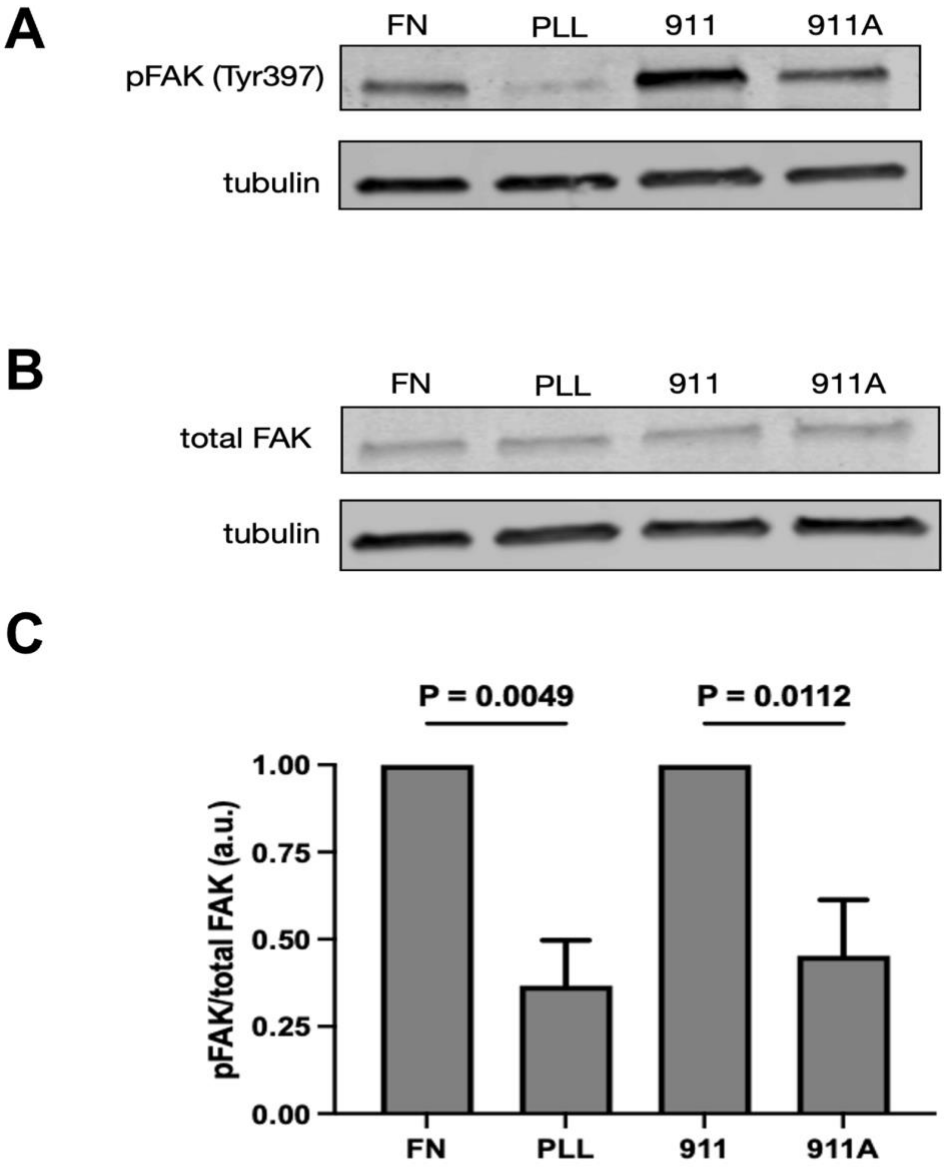
A
FN
PLL
911
911A
pFAK (Tyr397)
tubulin
B
FN
PLL
911
911A
total FAK
tubulin
C
P = 0.0049
P = 0.0112
1.00
0.75
0.50
0.25
0.00
pFAK/total FAK (a.u.)
FN
PLL
911
911A

**Figure 2.7: Western blots for FAK expression and phosphorylation in mesendoderm explants on adhesive substrates.**

(A) pFAK (Tyr397) phosphorylation and (B) total FAK levels in mesendoderm cells on indicated substrates: fibronectin (FN), GST-9.11 (911), GST-9.11A (911A) and poly-l-lysine (PLL). (A,B) Representative western blots. (C) Quantification of pFAK levels normalized to total FAK. Tubulin included as a loading control. Data are mean ± SEM.

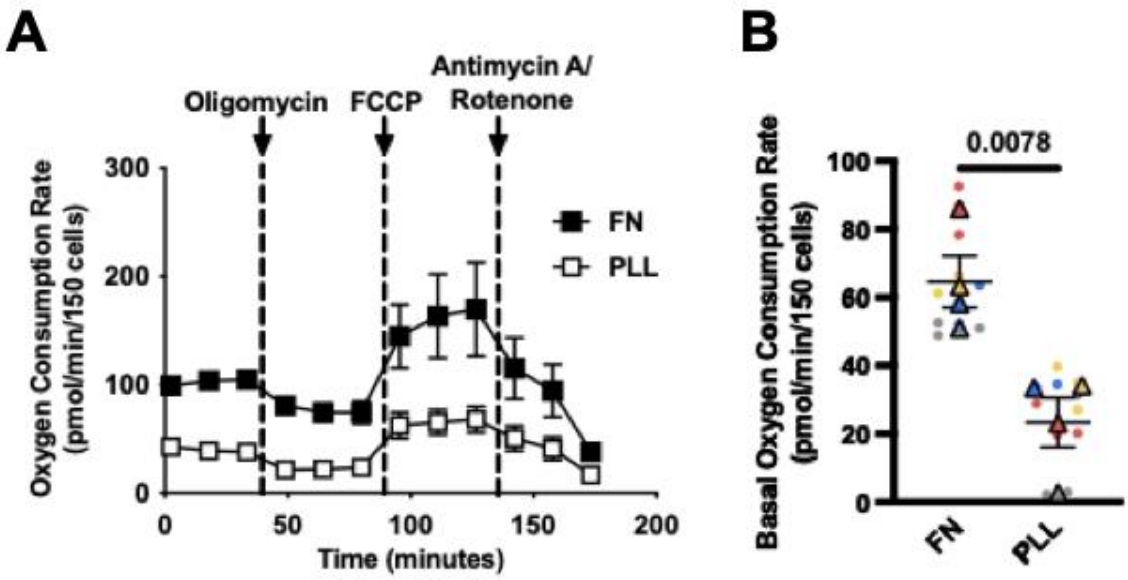
A
Oligomycin
FCCP
Antimycin A/
Rotenone
Oxygen Consumption Rate
(pmol/min/150 cells)
300
200
100
0
0
50
100
150
200
Time (minutes)
FN
PLL
B
Basal Oxygen Consumption Rate
(pmol/min/150 cells)
0.0078
100
80
60
40
20
0
FN
PLL

**Figure 2.8: Fibronectin adhesion drives high oxidative phosphorylation in mesendoderm cells.**

(A) Oxygen Consumption Rate (OCR) of dissociated mesendoderm cells on FN or PLL substrates quantified by Seahorse XFe96 analyzer and normalized to 150 cells per sample. Data are presented as mean ± SEM (N=4, n=12).

(B) Basal OCR of dissociated mesendoderm cells adhered to FN or PLL substrates. (N=4, n=24). Conditions in were statistically compared using an unpaired two-tailed t-test.

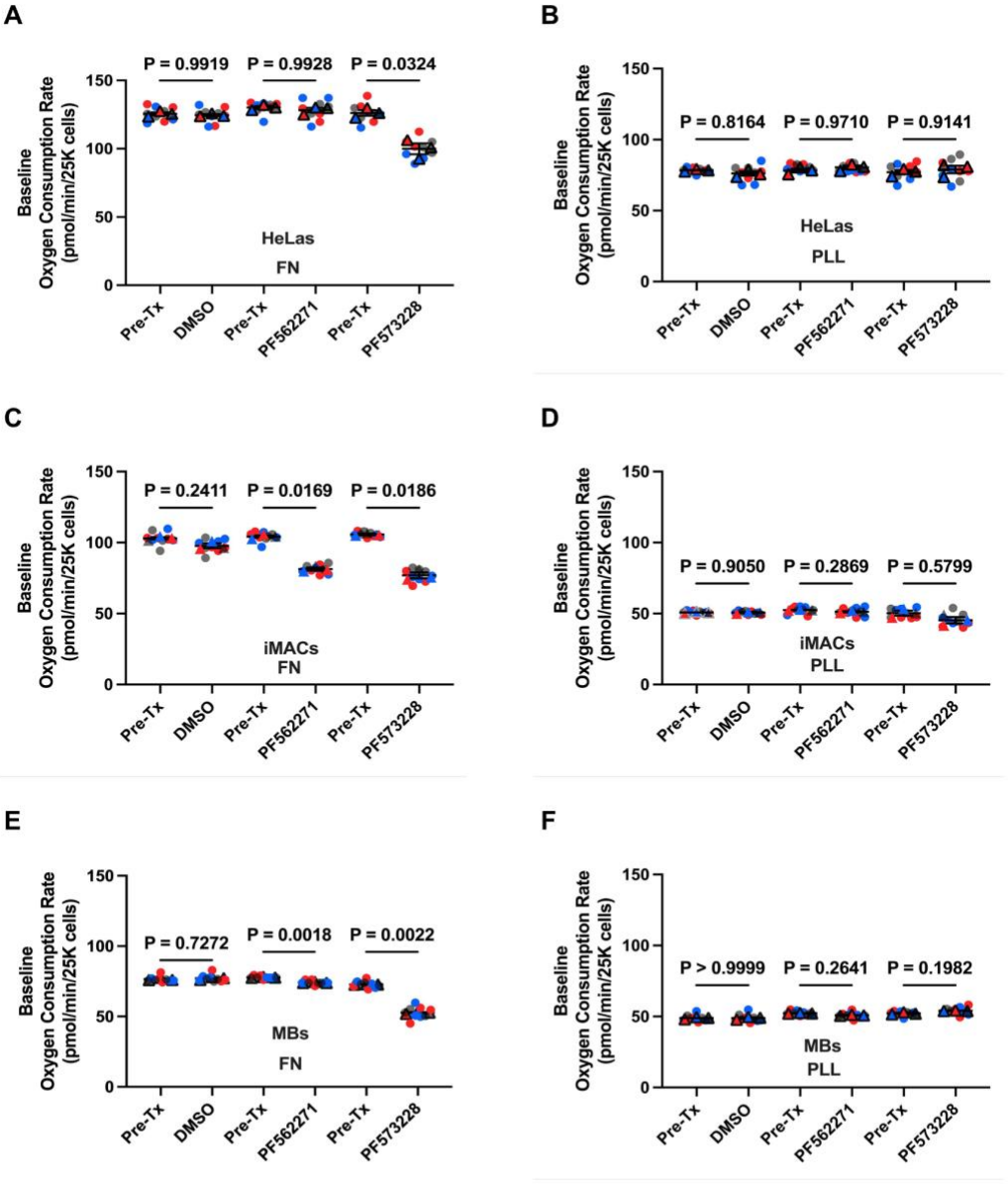
A
P = 0.9919
P = 0.9928
P = 0.0324
Baseline Oxygen Consumption Rate (pmol/min/25K cells)
HeLas
FN
B
P = 0.8164
P = 0.9710
P = 0.9141
HeLas
PLL
C
P = 0.2411
P = 0.0169
P = 0.0186
iMACs
FN
D
P = 0.9050
P = 0.2869
P = 0.5799
iMACs
PLL
E
P = 0.7272
P = 0.0018
P = 0.0022
MBs
FN
F
P > 0.9999
P = 0.2641
P = 0.1982
MBs
PLL
Pre-Tx
DMSO
PF562271
PF573228

**Figure 2.9 Real-time measurements of OCR from mammalian cells.**

(A,B) HeLa cells (HeLas), (C,D) immortalized macrophages (iMACs), and (E,F) myoblasts (MBs) plated on (A,C,E) FN or (B,D,F) pol-l-lysine (PLL). Baseline OCRs collected before drug treatment (Pre-Tx) and in the presence of FAK inhibitors (PF562,271 and PF573,228). DMSO is the vehicle control. Data are representative of wells pooled from three independent experiments. Statistical analyses undertaken using a one-way ANOVA with Šídák's multiple comparisons test (N=3, n=9).

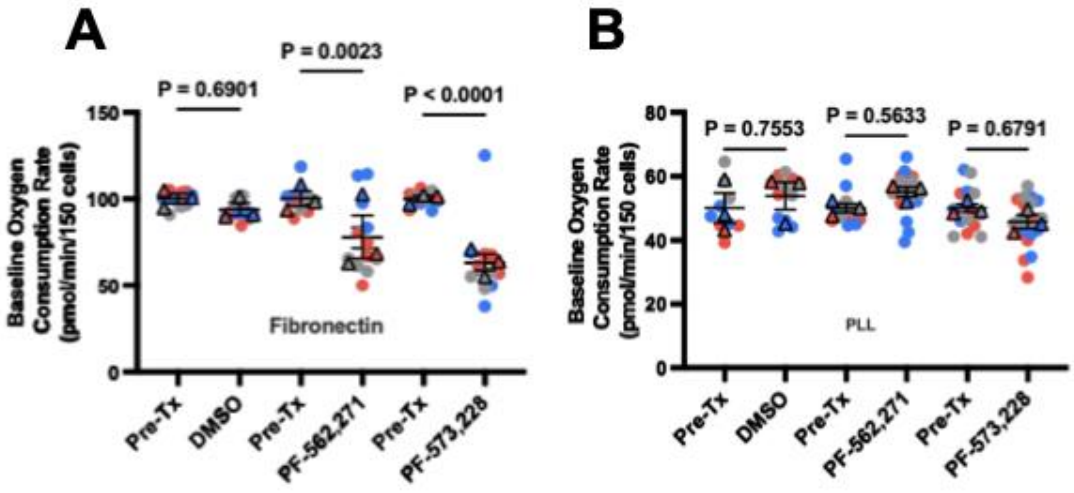
A
P = 0.6901
P = 0.0023
P < 0.0001
Baseline Oxygen Consumption Rate (pmol/min/150 cells)
150
100
50
0
Fibronectin
Pre-Tx
DMSO
Pre-Tx
PF-562,271
Pre-Tx
PF-573,228
B
P = 0.7553
P = 0.5633
P = 0.6791
Baseline Oxygen Consumption Rate (pmol/min/150 cells)
80
60
40
20
0
PLL
Pre-Tx
DMSO
Pre-Tx
PF-562,271
Pre-Tx
PF-573,228

**Figure 2.10: Fibronectin adhesion-dependent mitochondrial activity in mesendoderm cells is through FAK.**

(F,G) Real-time measurements of OCR of mesendoderm cells on FN (F) or PLL (G) before drug treatment (Pre-Tx) and in the presence of FAK inhibitors (PF-562,271 and PF-573,228). Vehicle control (DMSO). Data are representative of wells pooled from three independent experiments. Statistical analyses undertaken using a one-way ANOVA with Šídák's multiple comparisons test (N=3, n=9).

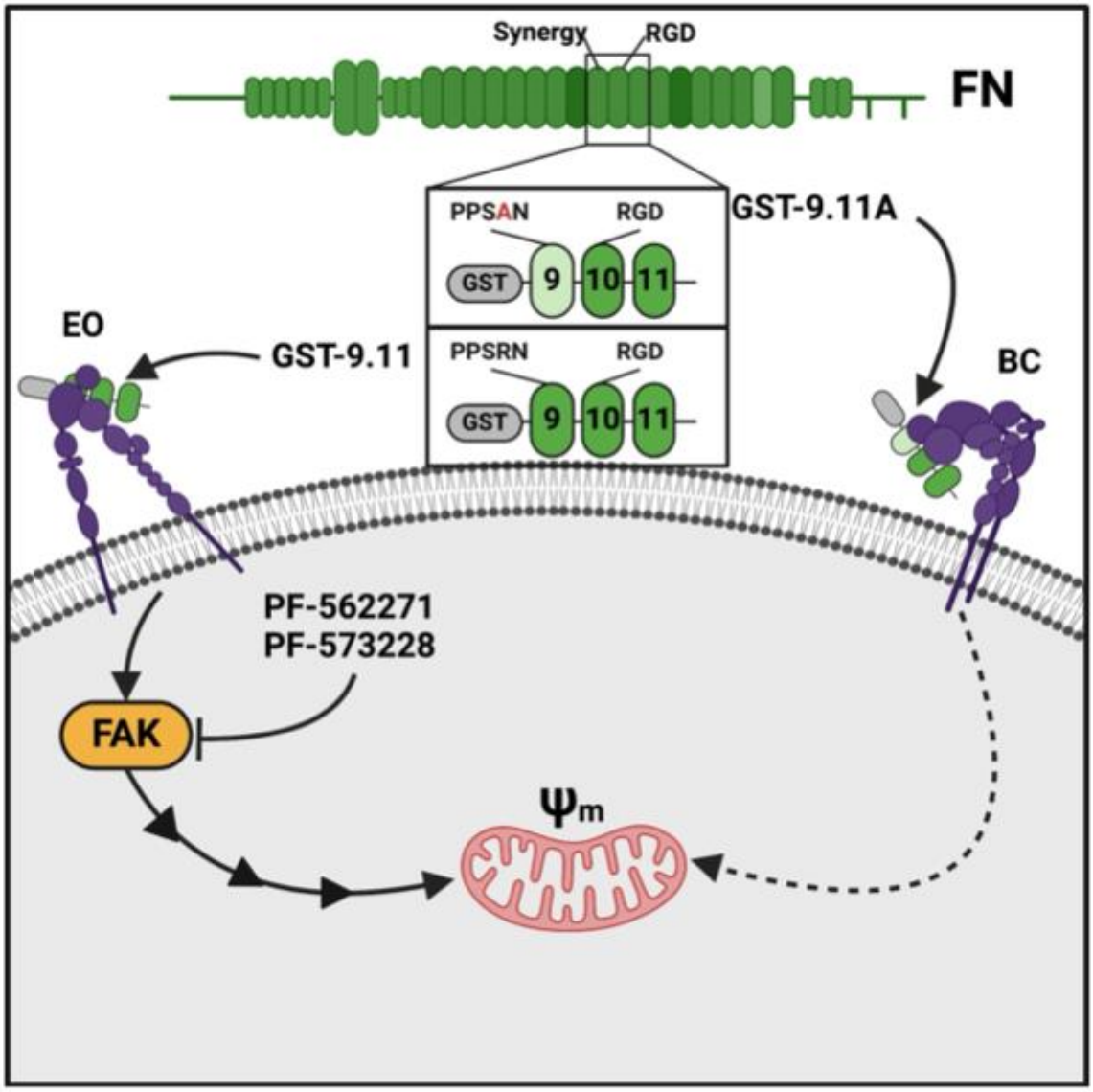
Synergy
RGD
FN
PPSAN
RGD
GST
9
10
11
GST-9.11A
EO
GST-9.11
PPSRN
RGD
GST
9
10
11
BC
PF-562271
PF-573228
FAK
Ψm

**Figure 2.11: Schematic of full-length single subunit of *Xenopus* fibronectin (FN) protein structure and integrin function.**

Glutathione S-transferase (GST) fusion proteins GST-9.11 (Type III repeats 9-11) and GST-9.11A (contains a synergy site mutation (PPS**A**N) in Type III repeat 9). Type III repeat 10 in both proteins contains the Arg-Gly-Asp (RGD) motif critical for binding to α5β1 integrin in its bent-closed (BC) conformation with a low-affinity ligand-binding state. GST-9.11 contains functional RGD and synergy site sequences that support and stabilize the extended-open (EO) active conformation of α5β1 integrin. Full α5β1 integrin engagement and activation allows FN ligand binding with high-affinity and promotes outside-in signaling through FAK to affect mitochondrial membrane potential. FAK inhibitors (PF-562271 and PF-573228) are shown.

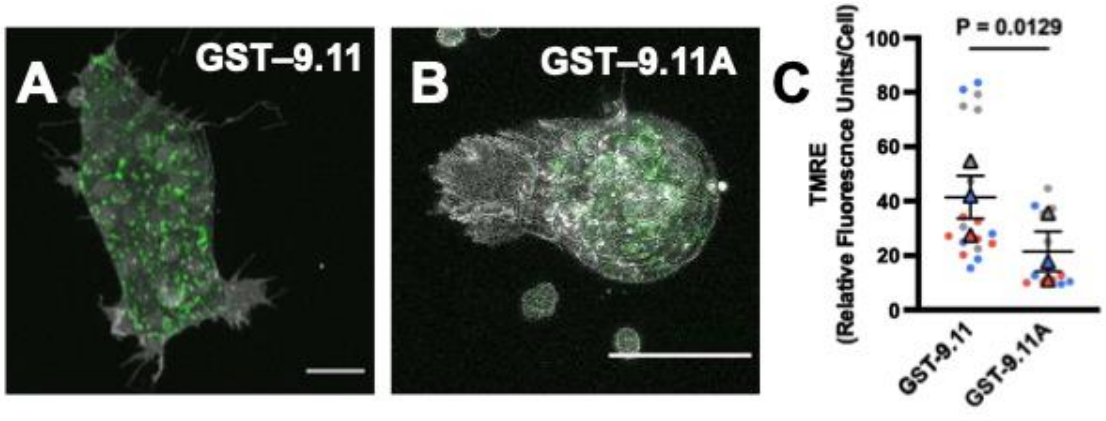
A
GST–9.11
B
GST–9.11A
C
P = 0.0129
TMRE
(Relative Fluorescnce Units/Cell)
100
80
60
40
20
0
GST-9.11
GST-9.11A

**Figure 2.12: Mitochondrial activity in mesendoderm cells is dependent on integrin activation state.**

(A, B) Single cells dissociated from *Xenopus* mesendoderm and adhered to (A) GST-9.11 or (B) GST-9.11A substrates. Cells labelled with membrane-GFP (gray pseudocolor) and mitochondrial membrane potential indicated by TMRE (green pseudocolor). Scale bars = 20 μm.

(C) Comparison of total TMRE fluorescence from dissociated mesendoderm cells on GST-9.11 and GST-9.11A substrates. (N=3, n=30).

Conditions were statistically compared using an unpaired two-tailed t-test.

Scale bars = 20 μm.

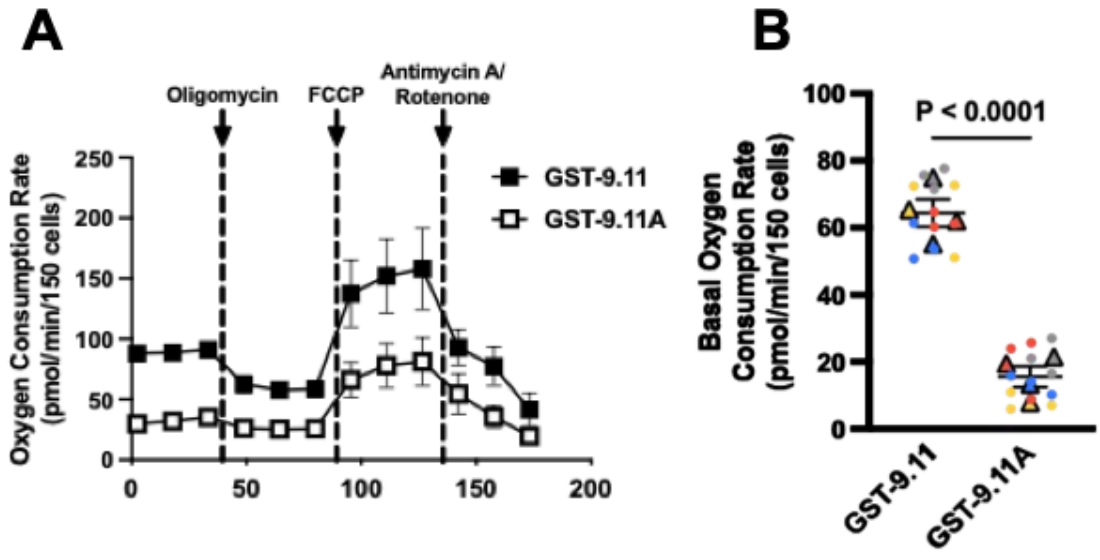
A
Oligomycin
FCCP
Antimycin A/
Rotenone
Oxygen Consumption Rate
(pmol/min/150 cells)
250
200
150
100
50
0
0
50
100
150
200
GST-9.11
GST-9.11A
B
Basal Oxygen
Consumption Rate
(pmol/min/150 cells)
P < 0.0001
100
80
60
40
20
0
GST-9.11
GST-9.11A

**Figure 2.13: Integrin activation supports high oxidative phosphorylation in mesendoderm cells.**

(A) Oxygen consumption rate (OCR) of dissociated mesendoderm cells on GST-9.11 or GST-9.11A substrates measured using the Seahorse XFe96 analyzer and normalized to 150 cells. Data are presented as mean ± SEM (N=4, n=12).

(B) Comparison of basal OCR of dissociated mesendoderm cells on GST-9.11 and GST-9.11A substrates. Data are presented as mean ± SEM (N=4, n=24).

Conditions were statistically compared using an unpaired two-tailed t-test.

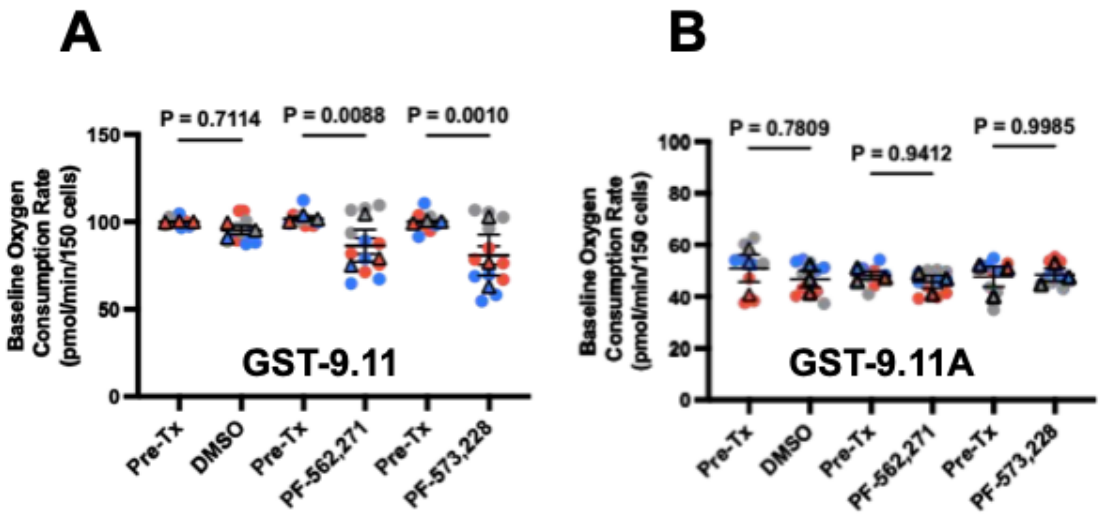
A
P = 0.7114
P = 0.0088
P = 0.0010
Baseline Oxygen Consumption Rate (pmol/min/150 cells)
150
100
50
0
GST-9.11
Pre-Tx
DMSO
Pre-Tx
PF-562,271
Pre-Tx
PF-573,228
B
P = 0.7809
P = 0.9412
P = 0.9985
Baseline Oxygen Consumption Rate (pmol/min/150 cells)
100
80
60
40
20
0
GST-9.11A
Pre-Tx
DMSO
Pre-Tx
PF-562,271
Pre-Tx
PF-573,228

**Figure 2.14: Integrin activation-linked mitochondrial activity in mesendoderm cells depends on FAK signaling.**

(A, B) Real-time measurements of OCR of mesendoderm cells on GST-9.11 (A) or GST-9.11A (B) in the absence (DMSO, control) or presence of FAK inhibitors (PF-562,271 and PF-573,228). OCRs were compared before (Pre-Tx) and after indicated treatments. Statistical analyses undertaken using a one-way ANOVA with
Šídák's multiple comparisons test.

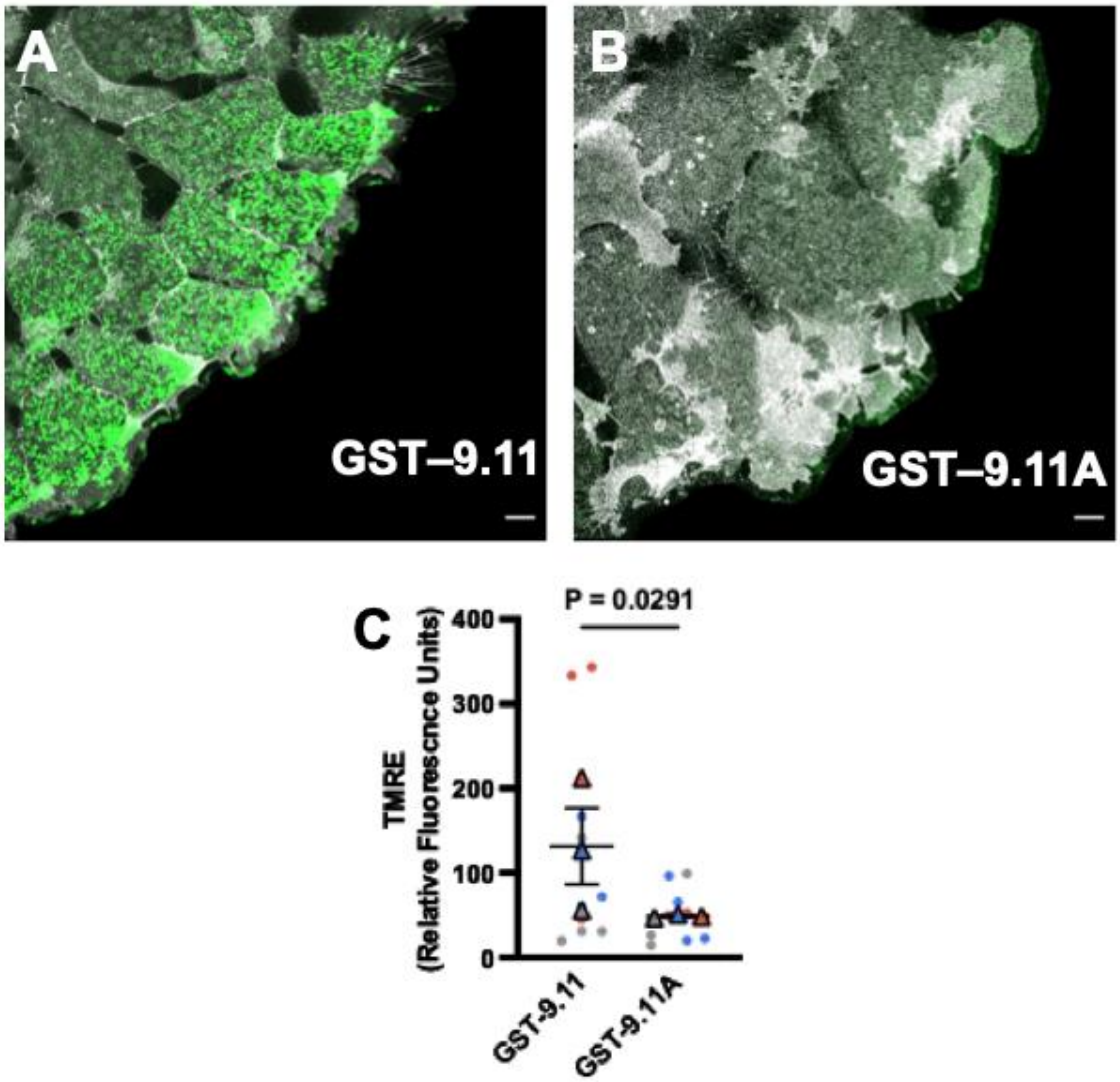
A
GST–9.11
B
GST–9.11A
C
P = 0.0291
TMRE
(Relative Fluorescnce Units)
400
300
200
100
0
GST-9.11
GST-9.11A

**Figure 2.15: Mitochondrial activity in collectively migrating mesendoderm tissue depends on integrin activation state.**

(A, B) TMRE (green pseudocolor) and membrane-GFP labelled (gray pseudocolor) migrating cells in dorsal marginal zone (DMZ) explants on (A) GST-9.11 and (B) GST-9.11A substrates. (A) Protrusive activity of leader row is polarized in forward direction of travel on GST-9.11. (B) Large randomly directed protrusions are apparent on GST-9.11A. Scale bars = 20 μm.

(C) Quantification of TMRE fluorescence from DMZs migrating on GST-9.11 and GST-9.11A substrates. Conditions were statistically compared using an unpaired two-tailed t-test.

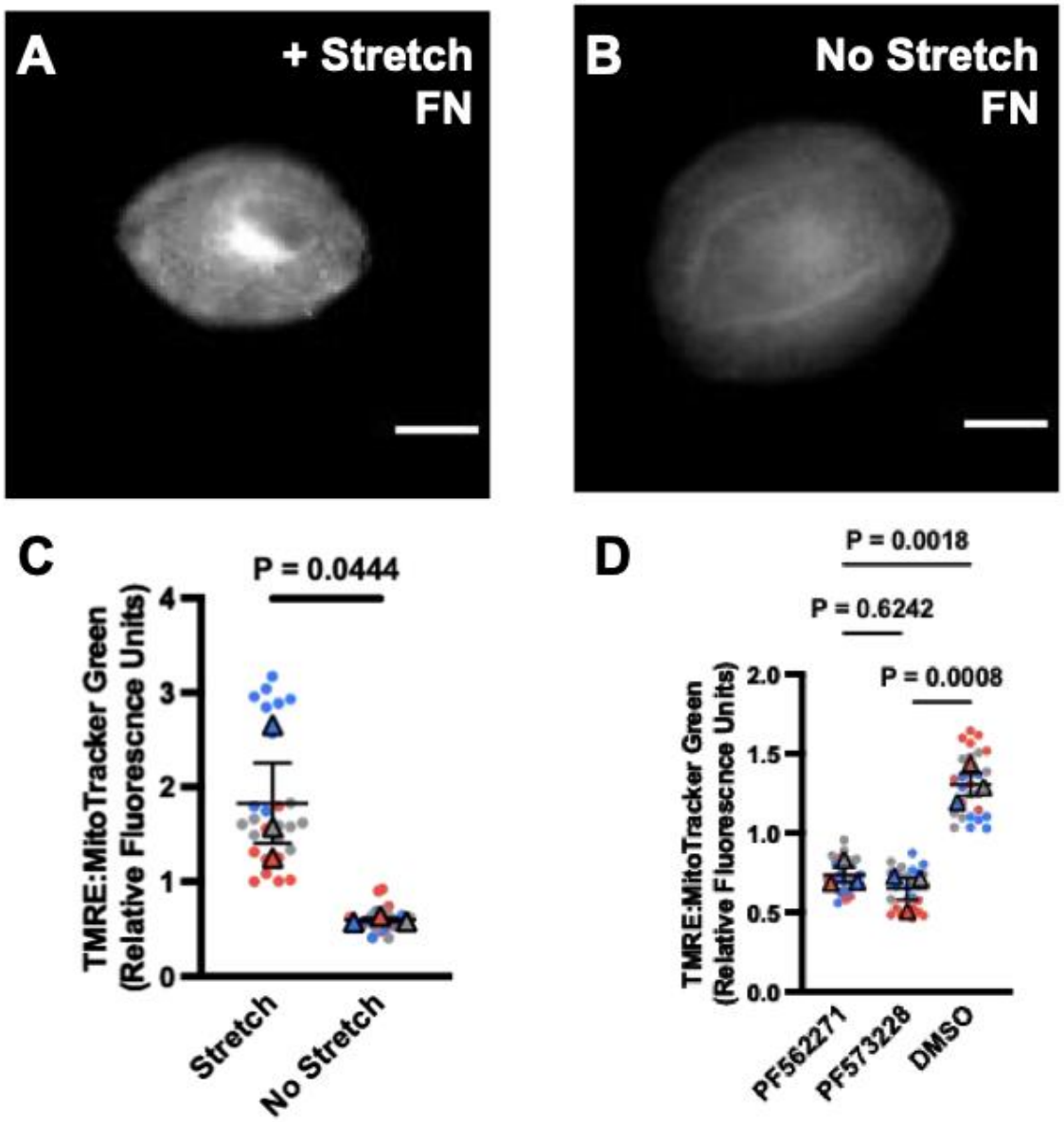
A
+ Stretch
FN
B
No Stretch
FN
C
P = 0.0444
TMRE:MitoTracker Green
(Relative Fluorescnce Units)
0
1
2
3
4
Stretch
No Stretch
D
P = 0.0018
P = 0.6242
P = 0.0008
TMRE:MitoTracker Green
(Relative Fluorescnce Units)
0.0
0.5
1.0
1.5
2.0
PF562271
PF573228
DMSO

**Figure 2.16: Mechanical regulation of mitochondrial membrane potential**

(A,B) Representative TMRE widefield fluorescence (white) of single dissociated mesendoderm cells imaged through FN-coated polydimethylsiloxane (PDMS) membrane. Note, fine cellular detail not resolvable through the PDMS membrane. Cells on PDMS (A) subject to 15 cycles of 10% applied anisotropic stretch or (B) left unstretched. Scale bars = 20 μm.

(C) Ratio of TMRE to MitoTracker Green (MTG) fluorescence intensity from dissociated mesendoderm cells on FN under stretched or unstretched conditions. Data are expressed in relative fluorescence units (RFU). (N=3, n= 55). Conditions were statistically compared using an unpaired two-tailed t-test.

(D) Quantification of TMRE fluorescence relative to MTG fluorescence from dissociated mesendoderm cells on FN following stretching and incubated without (DMS0, control) or with FAK inhibitors (PF-562,271 and PF-573,228). (N=3, n=81). Conditions were statistically compared using a one-way ANOVA with Tukey's multiple comparisons test.

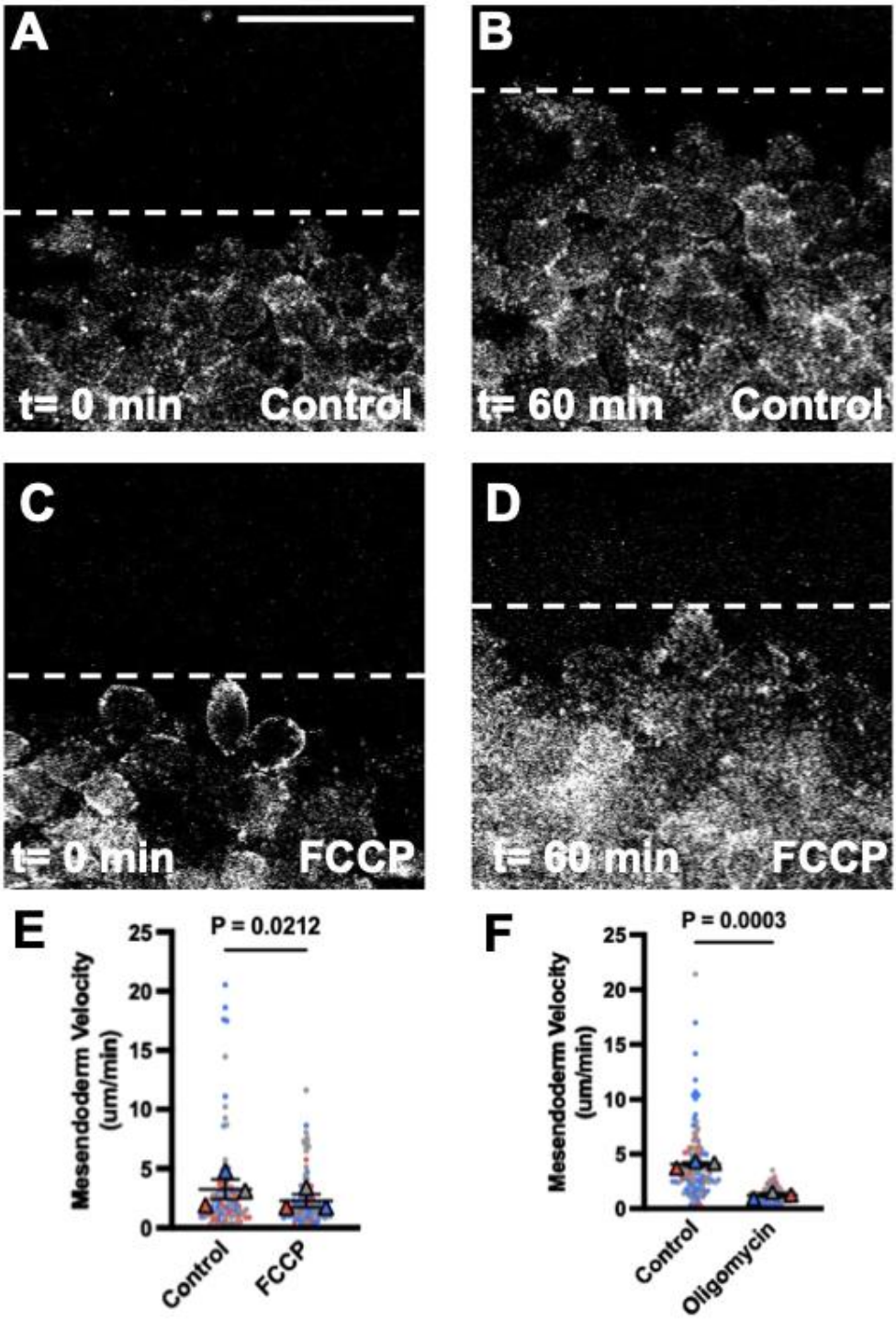
A
t= 0 min
Control
B
t= 60 min
Control
C
t= 0 min
FCCP
D
t= 60 min
FCCP
E
P = 0.0212
Mesendoderm Velocity (um/min)
25
20
15
10
5
0
Control
FCCP
F
P = 0.0003
Mesendoderm Velocity (um/min)
25
20
15
10
5
0
Control
Oligomycin

**Figure 2.17: Mitochondrial membrane potential affects mesendoderm migration velocity in tissue explants.**

(A-D) Mesendoderm cells (white, membrane-GFP) on FN (A and C) at the start of migration and (B and D) after 60 minutes into extension. Dotted white line indicates the leading edge of the tissue. (A) and (B) show cells in presence of DMSO (control). (C) and (D) show cells in the presence of the mitochondrial membrane potential uncoupler, carbonyl cyanide p-trifluoro methoxyphenylhydrazone (FCCP). Scale bar for A-D = 200 μm and shown in (A).

(E) Graph displaying the average instantaneous velocities of mesendoderm explant extension over a one-hour period in the absence (control) or presence of FCCP. (N=3, n=215).

(F) Graph displaying the average instantaneous velocities of mesendoderm explant extension over a one-hour period in the absence (control) or presence of Oligomycin. (N=3, n=216). Conditions in E and F were statistically compared using an unpaired two-tailed t-test.

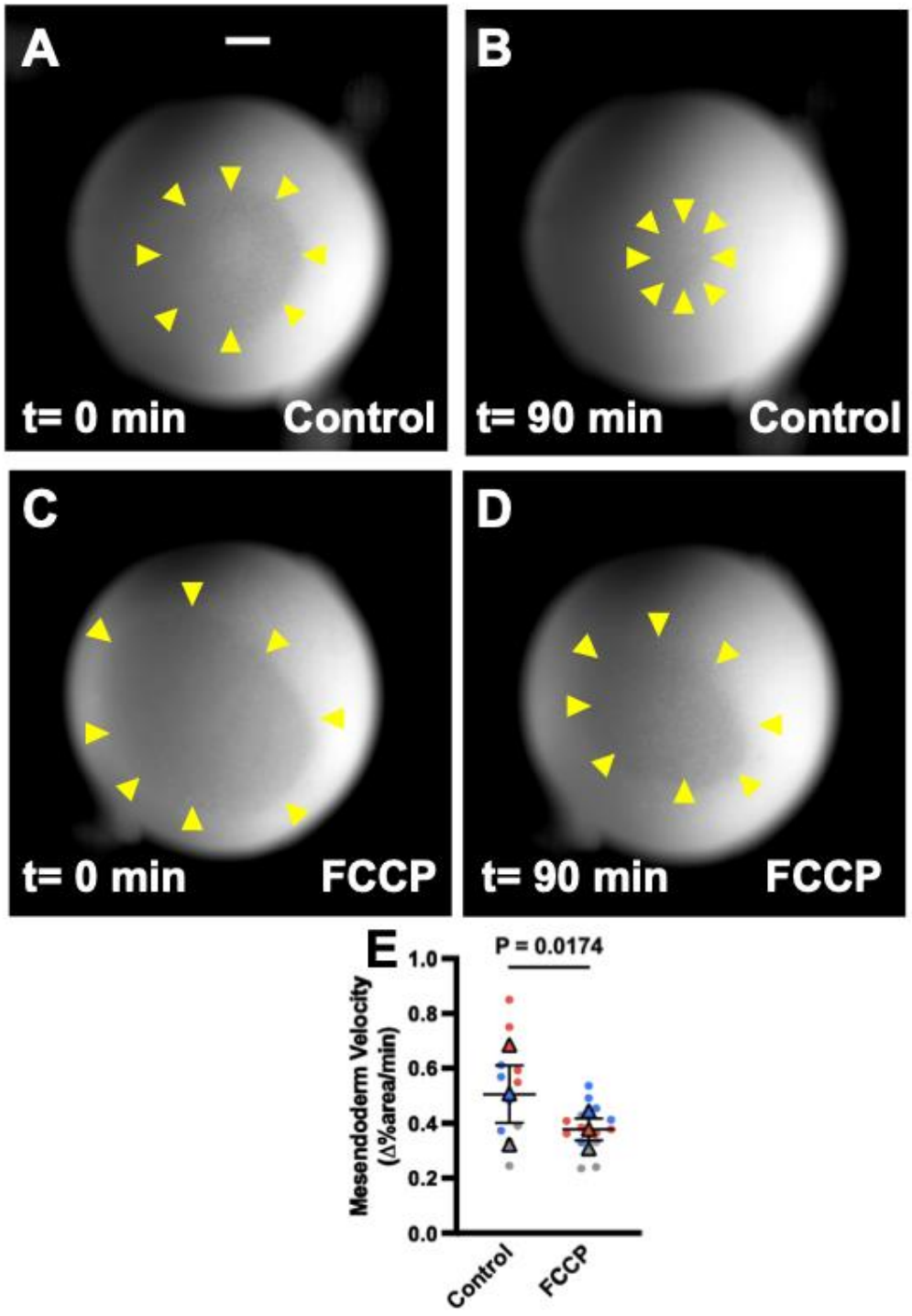
A
t= 0 min
Control
B
t= 90 min
Control
C
t= 0 min
FCCP
D
t= 90 min
FCCP
E
P = 0.0174
Mesendoderm Velocity (Δ%area/min)
1.0
0.8
0.6
0.4
0.2
0.0
Control
FCCP

**Figure 2.18: Mitochondrial membrane potential affects mesendoderm migration velocity in intact embryos.**

(A-D) Gastrulation stage whole albino embryos with blastocoel cavity upright for visualization of mesendoderm closure at stages 10.5 (A and C) and 12.0 (B and D) as imaged through the ectoderm. Yellow arrowheads indicate the direction and extent of mesendoderm closure. (A and B) embryos microinjected with DMSO (control). (C and D) embryos microinjected with FCCP. Scale bar for (A-D) = 200 μm and shown in A. (E) Graph displaying the rate of mesendoderm mantle closure from stage 10.5 to 12.0 in gastrulation stage whole albino embryos microinjected with DMSO (control) or FCCP. (N=3, n=25). Conditions were statistically compared using an unpaired two-tailed t-test.

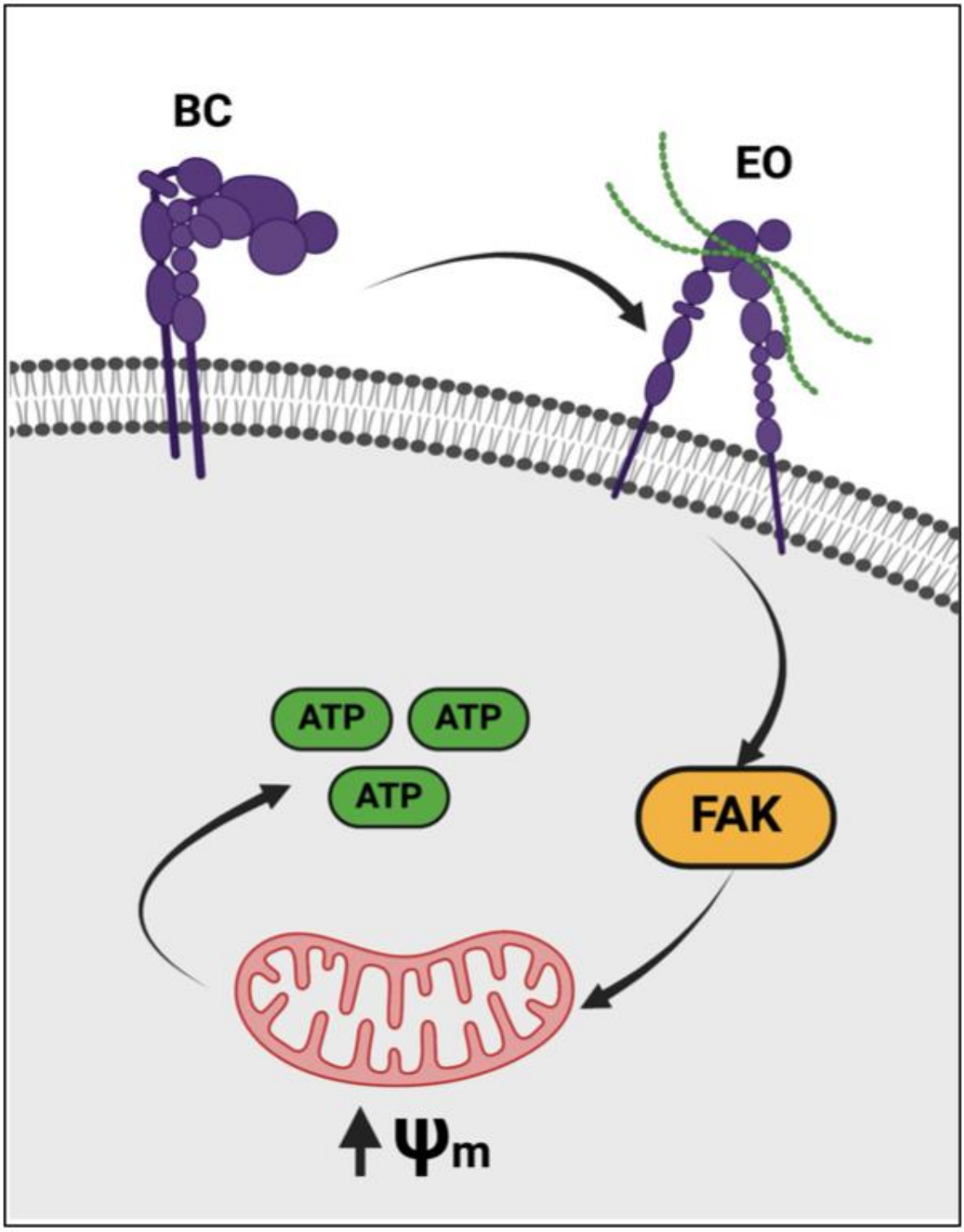
BC
EO
ATP
ATP
ATP
FAK
Ψm

**Figure 2.19: Cartoon of proposed mechanism for integrin-linked mitochondrial activity.**

Low affinity binding of FN ligand to bent-closed (BC) and transitional states of integrin $\alpha5\beta1$ fails to support integrin signaling and activation of mitochondrial respiration. Extended-open (EO) high affinity ligand-bound state leads to FAK activation and signaling and an increase in mitochondrial oxidative phosphorylation.

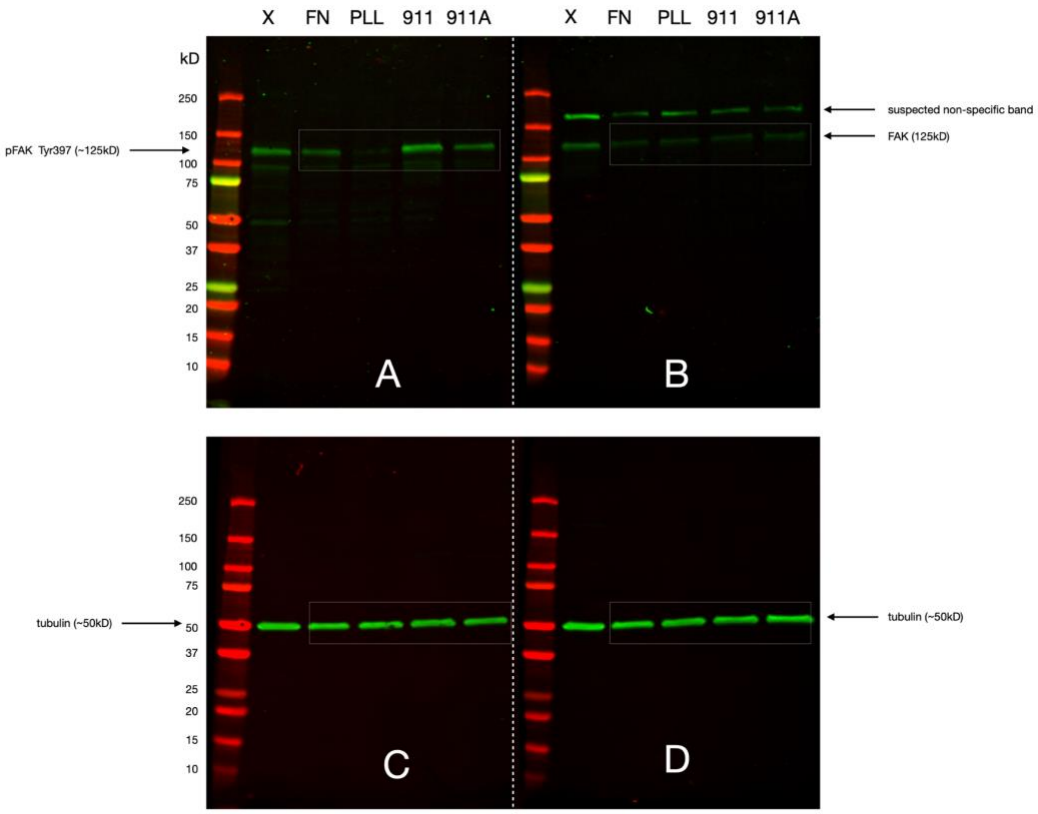
X
FN
PLL
911
911A
X
FN
PLL
911
911A
kD
250
150
100
75
50
37
25
20
15
10
pFAK Tyr397 (~125kD)
suspected non-specific band
FAK (125kD)
A
B
250
150
100
75
50
37
25
20
15
10
tubulin (~50kD)
tubulin (~50kD)
C
D

**Figure 2.20: Raw gel "transparency" blots for FAK and pFAK levels in mesendoderm cells.** Representive raw data supporting the blots presented in Figure 2.7. (A and C) are the same blot and corresponds to Figure 2.7A. (A) is probed with anti-pFAK antibody and then stripped and (C) re-probed for tubulin. (B and D) are the same blot and corresponds to Figure 2.7B. (B) is probed with an anti-FAK antibody and then stripped and (D) re-probed for tubulin. Lanes correspond to substrate conditions: Fibronectin (FN), poly-l-lysine (PLL), GST-9.11 (911), GST-9.11A (911A)
X lanes are whole embryo lysates not included in final Figure S3. Outlined white boxes in A-D correspond to Figures 2.7A and B.

# Chapter 3:

# Mitochondrial processes in cell adhesion and migration

## Introduction

Mechanotransduction is the process by which cells convert physical, mechanical signals into biochemical responses to modulate a variety of cell processes such as migration, proliferation, differentiation, and apoptosis (Ingber, 2006; Jaalouk and Lammerding, 2009). It is proposed that mechanotransduction includes force-induced unfolding and/or relaxation of proteins in response to changing mechanical stimuli (Chen et al., 2005; Gingras et al., 2006; Moore et al., 2010; Smith et al., 2007). (Ha and Loh, 1998; Johnson et al., 2007a). As an extension of this concept, cysteine-shotgun mass spectrometry (CS-MS) enables the identification of proteins that undergo conformational changes in response to physical forces (Johnson et al., 2007b; Krieger et al., 2011). CS-MS is based on the principle that cysteine is a mildly hydrophobic amino acid commonly sequestered from the intracellular milieu by tertiary and quaternary protein structures with changes in protein conformation potentially leading to exposure of some or all of the highly reactive thiol groups of the buried cysteine residues (Ha and Loh, 1998; Johnson et al., 2007a). This can be tested by exposing cells to differing mechanical stresses in the prescence of non-toxic, membrane-permeable, thiol-reactive, fluorescent dyes that bind covalently to exposed thiols, such as monobromobimane (Cotgreave and Moldéus, 1986; Shen et al., 2015). Such approaches identify shear-sensitive sites of spectrin and ankyrin in red blood cells (Krieger et al., 2011) and unique peptides in 27 proteins containing reversibly oxidised cysteines in response to peroxide treatment of Saccharomyces cerevisiae (McDonagh et al., 2009). CS-MS offers a powerful approach for investigating conformational protein changes under a variety of stressors.

In a prior application of CS-MS in the lab, graduate student Maureen Bjerke employed cell stretch to discover proteins that undergo conformational changes in response to mechanical stress at sites of cell-extracellular matrix (ECM) contact (Bjerke, 2014). As summarized in Figure 3.1A, she identified proteins that undergo conformational changes in response to force on the fibronectin-α5β1 integrin adhesion complexes of mesendoderm cells. Briefly, mesendoderm cells on fibronectin were stretched and exposed to monobromobimane (Figure 3.1A). Proteins from labeled cells were then separated by SDS-PAGE to identify changes in monobromobimane fluorescence intensity that normalized to the protein levels by Coomassie staining (Figure 3.1A). Several bands were differentially labeled in repeated experiments. One of these bands was selected for further analysis using liquid chromatography-coupled tandem mass spectrometry (LC-MS/MS) (Figure 3.1A). Analysis of the mass spectrometry data from the selected band yielded three peptides that were differentially labeled by monobromobimane in stretched and unstretched samples (Figure 3.1A). These peptides corresponded to two variants of mitochondrial aconitase (Figure 3.1A) (Bjerke, 2014). Mitochondrial aconitase is a citric acid cycle enzyme responsible for the reversible conversion of citrate to isocitrate (Beinert and Kennedy, 1993; Beinert et al., 1996). While aconitase was labelled as a consequence of stretch it is likely that the links between metabolic enzymes and focal adhesion complex proteins are indirect and may not have any regulatory role, (Romani et al., 2021; Salvi and DeMali, 2018). Furthermore, changes in citric acid cycle metabolic flux present at a slower timescale than the rapid dynamics of mechanotransduction, futher suggesting that metabolic

enzymes are not directly experiencing mechanical deformations in reponse to stretch (Taegtmeyer et al., 1980; Wiskich, 1980).

Regardless, it is important to consider the various processes contributing to the regulation of aconitase enzyme function. Notably, this includes redox regulation of aconitase as it contains a [4Fe-4S] cluster that is highly sensitive to oxidative stress (Gardner, 1997; Gardner and Fridovich, 1992). Oxidation of this cluster converts it to a [3Fe-4S] form, which inactivates the enzyme (Bulteau et al., 2003; Yan et al., 1997). Reactive oxygen species (ROS), such as hydrogen peroxide ($H_2O_2$), can also oxidize the Fe-S cluster, leading to aconitase inactivation thereby linking aconitase activity to cellular redox states to serve as a mechanism for adjusting citric acid cycle flux during oxidative stress (Castro et al., 2019; Murakami and Yoshino, 1997). However, aconitase activity can be restored when antioxidant defenses reduce the Fe-S cluster back to the active [4Fe-4S] form (Gardner, 2002; Lushchak et al., 2014). As our recent studies identified a link between integrin engagement in collective mesendoderm migration and high mitochondrial membrane potential, which can lead to ROS production, it is important to consider the potential interactions between aconitase and ROS in the context of high mitochondrial membrane potential (Lee et al., 2001; Suski et al., 2012).

A variety of interactions linking integrin-associated mechanotransduction and metabolism are reported (Dawson et al., 2023; Romani et al., 2021). In comparing human bronchial epithelial cells spread on stiff versus soft substrates it is found that on stiff substrates F-actin stress fibers sequester the ubiquitin ligase tripartite motif containing 21 (TRIM21) (Park et al., 2020). This sequestration prevents proteasomal degradation of the glycolytic enzyme phosphofructokinase which converts fructose 6-phosphate to fructose

1, 6 bisphosphate thereby resulting in an increase of glycolytic flux (Mor et al., 2011; Park et al., 2020). It is also reported that when lung adenocarcinoma cells are on stiffer substrates a fraction of kindlin-2, a focal adhesion protein critical for integrin activation and cytoskeletal engagement, translocates to the mitochondria (Guo et al., 2019; Montanez et al., 2008). In the mitochodnria it associates with pyrroline-5-carboxylate reductase 1 to promote its stability and activity in proline synthesis which is crtical for protein synthesis, cell proliferation, and collagen synthesis to potentially increase ECM stiffness (Guo et al., 2019). Such studies highlight the potential role of integrin signaling in metabolism.

As highlighted by our recent work (Chapter 2), focal adhesion proteins other than kindlin-2 such as focal adhesion kinase (FAK) play a role in the regulation of metabolism in *Xenopus* mesendoderm (Visavadiya et al., 2016). While the primary fibronectin binding integrin expressed by the *Xenopus* mesendoderm is integrin α5β1, the main fibronectin binding integrin proteins are α5β1, αvβ3, αvβ1, and α4β1 (Hynes, 2002; Leiss et al., 2008; Plow et al., 2000). Integrin α5β1 is the primary and most specific receptor for fibronectin as full adhesion requires engagement of the integrin head with both the arginine-glycine-aspartate (RGD) primary binding site and the Proline-Histidine-Serine-Arginine-Asparagine (PHSRN) synergy sequence (Takagi et al., 2003; Xia and Springer, 2014). The fibronectin synergy site sequence in *Xenopus* is Proline-Proline-Serine-Arginine-Asparagine (PPSRN) (Ramos and DeSimone, 1996). P8D4, a *Xenopus*-specific antibody that targets integrin α5β1, disrupts coordinated cellular movements in the *Xenopus* gastrula (Davidson et al., 2006a; Marsden and DeSimone, 2001). Integrin αvβ3 also recognizes the RGD motif and binds fibronectin, especially in angiogenesis and

wound healing contexts (Kumar, 2003; Xiong et al., 2002). Integrin αvβ1 is another RGD-recognizing integrin that can bind fibronectin, though with lower affinity compared to α5β1 (Reed et al., 2015; Slack et al., 2022). Integrin α4β1 binds to the CS1 region of fibronectin, a sequence outside the RGD domain, and is involved in immune cell trafficking and adhesion (Jackson, 2002; Komoriya et al., 1991).

In the present studies we revisited the identification of proteins that undergo conformational changes in response to fibronectin-integrin stretch and evaluated their contribution to collective mesendoderm migration. We considered the potential contributions of integrin activation to differences in mitochondrial content which are regulated by rates of mitochondrial biogenesis or degradation. We evaluated the spatial distribution of mitochondrial activity and clustering in small groups of mesendoderm cells or motile tissue. We examined the potential for exogenous integrin activation via manganese to support mitochondrial activity. Finally, we observed differences in mitochondrial localization in individual mesendoderm cells depending on the adhesive substrates.

## Results

### Mitochondrial aconitase function in collective mesendoderm migration

As previously demonstrated by an application of CS-MS to mesendoderm cells in the presence or absence of stretch on fibronectin substrates, one of the proteins that was found to be differentially labeled included the citric acid cycle enzyme mitochondrial aconitase (Figure 3.1A). As a result of this finding we sought to evaluate the contribution of this enzyme to collective mesendoderm migration by examining the effect of fluoroacetate, a mitochondrial aconitase inhibitor, on mesndoderm mantle closure in intact albino embryos (Morrison and Peters, 1954). We found a significant reduction in the mesendoderm mantle closure rate of embryos with a blastocoel cavity microinjection of fluoroacetate (Figure 3.1B). Therefore, mitochondrial aconitase function may support the energetic processes involved in collective mesendoderm migration.

### Influence of cell adhesion to the mitochondrial processes of mesendoderm cells

As we identified an association between high mitochondrial activity with $\alpha5\beta1$ integrins in a high affinity, active extended-open (EO) conformation (Chapter 2), we wondered if differences in rates of mitochondrial biogenesis or degradation (mitophagy) could contribute to to this disparity. Therefore, we examined the total mitochondrial content of mesendoderm on the fibronectin fusion proteins glutathione-s-transferase (GST)-9.11 and GST-9.11A which supported a high affinity, active EO conformation and a low-affinity, inactive bent-closed (BC) conformation, respectively. By western blot (Figure 3.2A) against translocase of outer mitochondrial membrane 20 (TOMM20) in mesendoderm cells on GST-9.11 and GST-9.11A we found no difference in total

mitochondrial content (Figure 3.2B). Similarly, when the dye mitotracker green was applied to cells on GST-9.11 (Figure 3.3A) and GST-9.11A (Figure 3.3B), no difference in mitochondrial mass was detected (Figure 3.3C). However, when mitochondrial activity was normalized to mitochondrial content in mesendoderm cells on GST-9.11 (Figure 3.4A) versus GST-9.11A (Figure 3.4B), cells on GST-9.11 showed a higher ratio of active to total mitochondria than cells on GST-9.11A (Figure 3.4C). While integrin activation may not regulate rates of mitochondrial production or mitophagy on the timescale of minutes, the link between integrin activation and mitochondrial activity was independent of the mitochondrial content.

As integrin activation was able to drive mitochondrial activity, we wondered if exogenous integrin activation via chemical methods (i.e. manganese) could impact mitochondrial membrane potential. Therefore, we measured the mitochondrial membrane potential of mesendoderm cells before (Figure 3.5A) and after (Figure 3.5B) treatment with $MnCl_2$ or vehicle control. When mesendoderm cells plated on GST-9.11A were exposed to $MnCl_2$ they showed an increase in TMRE signal relative to Mitotracker Green, but no difference when exposed to the vehicle control (Figure 3.5C). Notably, mesendoderm on GST-9.11 exposed to $MnCl_2$ or vehicle control presented no change in TMRE:MitoTracker Green. Therefore, exogenous activation of integrins via $MnCl_2$ concomitantly increased mitochondrial activity.

While we observed comparable amounts of total mitochondria in the leading and following rows of migrating mesendoderm, we wondered if there was any subcellular pattern to the mitochondrial localization of leading and following rows of mesendoderm. Notably, we found accumulations or clusters of mitochondria near the front of leader

mesendoderm cells (Figure 3.6A). When we segmeneted leader and follower cells into front, cell body, and rear we found a signficant clustering of mitochondria to the front of leading row cells (Figure 3.6B). However, the other regions of leader and follower row cells showed no significant accumulations (Figure 3.6B). This distribution of mitochondrial clustering was recapitulated in cell pairs (Figure 3.7A,B) or clusters with greater accumulations of mitochondria found near polarized protrusions compared to regions of cell-cell contact (Figure 3.7C). Furthermore, in groups of well polarized mesendoderm cells (Figure 3.8 A, B) mitochondria with high mitochondrial membrane potential are found near protrusions with limited localization near cell-cell contacts (Figure 3.8 C). Finally, to evaluate the contributions to mitochondrial localization of adhesive signaling that is encountered by mesendoderm cells, dissociated mesendoderm was plated on fibronectin to engage integrin $\alpha5\beta1$, a C-Cadherin fragment protein (C-Cadherin-FC) to enable cadherin-based adhesion, and PLL as a non-specific adhesive control. We segmented the cells in the Z direction and determined the distance from the substrate at which the greatest accumulation of mitochondria was found. We found that cells on C-Cadherin-FC presented with accumulations of mitochondria closest to the adhesive substrate (Figure 3.9A). However, regardless of the adhesive substrate, cells showed comprable spreads in the distances of mitochondrial clustering (Figure 3.9B). This suggests that the mitochondrial accumulations are shifted closer or further from foci of adhesive signaling, rather than spread or condensed (Figure 3.9C).

Taken together, the cadherin adhesions found in intercellular contacts may play an important role in regulating the localization of mitochondria.

# Discussion

## Fluoroacetate inhibition of mitochondrial aconitase

While our results demonstrated fluoroacetate treatment disrupts collective mesendoderm migration, it is important to consider the possible mechanism of this inhibition. Fluoroacetate itself is not directly toxic, however, once inside the cell, fluoroacetate is converted into fluorocitrate, the active metabolite that interferes with mitochondrial function, by the enzyme acetyl-CoA synthetase (Peters, 1952; Peters and Wakelin, 1953). Fluorocitrate specifically targets and inhibits aconitase by binding to the aconitase iron-sulfur cluster active site and forming a complex that prevents the conversion of citrate to isocitrate (Goncharov et al., 2006; Lauble et al., 1996). With the inhibition of aconitase, citrate accumulates which disrupts the citric acid cycle thereby reducing the efficient production of adenosine triphosphate (ATP) and causing an energy defecit (Buffa et al., 1951; Proudfoot et al., 2006). The citrate accumulation also inhibits other metabolic pathways by feedback mechanisms, including glycolysis (Iacobazzi and Infantino, 2014; Ren et al., 2017). With energy depletion and the disruption of mitochondrial function, cell toxicity and death ensues in cells highly dependent on energy from the citric acid cycle, such as cardiac and neuonal cells (Bosakowski and Levin, 1986; Fonnum et al., 1997). Ultimately, fluoroacetate is a specific and potent inhbitor of aconitase and disruptor of citric acid cycle function.

While not explored in these studies, some alternative methods for modulating aconitase activity should be explored in future studies to define the role of aconitase in mesendoderm migration. For example, fumarate can impair mitochondrial aconitase activity through succination of critical cysteine residues essential for iron-sulfur cluster

binding (Ternette et al., 2013). In addition, supplementary iron levels enhance proper assembly of aconitase's iron-sulfur cluster, which is crucial for its enzymatic activity (Beinert and Kennedy, 1993). Ultimately, expanding the selection of aconitase inhibitors and activators will enable us to control for any non-specific effects from disruption of mitochondrial function.

**Integrin adhesion in mitochondrial biogenesis and mitophagy**

While changes in mitochondrial biogenesis or mitophagy were not detected between cells differing in their integrin activation state, it is critical to consider mechanisms regulating mitochondrial content. The peroxisome proliferator-activated receptor gamma coactivator 1-alpha (PGC-1α) is one of the master regulators of mitochondrial biogenesis through responses to energetic stress (eg. exercise, low energy, and hormonal inputs) as detected by activation of AMP-activated protein kinase (AMPK) and Sirtuin 1 (Sirt1) (Chan and Arany, 2014; Hardie et al., 2012; Tang, 2016). With an increase in PGC-1α function, the key transcription factors Nuclear respiratory factor (NRF)1, NRF2, and mitochondrial transcription factor A (TFAM) are activated for the promotion of mitochondrial DNA replication, transcription of mitochondrial genes, mitochondrial protein synthesis, and mitochondrial fusion or fission dynamics (Fernandez-Marcos and Auwerx, 2011; Ventura-Clapier et al., 2008; Wenz, 2009; Yuan et al., 2019).

In contrast, the PTEN-induced kinase 1 (PINK1)-Parkin pathway is a central regulator of mitophagy, particularly under conditions of mitochondrial damage, with an increase in activation of this pathway enhancing mitophagy rates (Eiyama and Okamoto,

2015; Nguyen et al., 2016a). In cases of mitochondrial damage causing a loss of membrane potential, PINK1 accumulation on the outer mitochondrial membrane will lead to an activation of Parkin ubiquitination of outer mitochondrial proteins, such as mitofusin-1 (Mfn1), Mfn2, and voltage dependent anion channel 1 (Vdac1) (Koyano et al., 2014; Lazarou et al., 2012). In turn this leads to mitochondrial fission which fragments the damaged mitochondria (Chan, 2006a; Knott et al., 2008). At this point, an autophagosome forms via ubiquitination receptors, such as sequestosome 1 (p62), recruiting microtubule-associated proteins 1A/1B light chain 3B (LC3) that can then engulf the damaged mitochondria (Pankiv et al., 2007; Park et al., 2014). Finally, through authophagosome fusion with the lysosome there is degradation of the damaged mitochondria (Audano et al., 2018; Nguyen et al., 2016b).

While mechanotransduction is a rapid process, mitophagy and mitochondrial biogenesis operate on slower timescales. The integrin-containing focal adhesion complexes of a cell respond within seconds to minutes to mechanical stimuli with forces on integrins initiating conformational changes and clustering resulting in the recruitment of talin, paxillin, and vinculin thereby strenghtening cell-ECM adhesion and force transmission across the cell (Galbraith et al., 2002; Plotnikov et al., 2012). The process of mitochondrial biogenesis begins on the timescale of minutes to hours through the rapid upregulation and activation of the transcriptional coactivator PGC-1α and activation of trascription factors that initiate mitochondrial gene expression, such as NRF1 and NRF2 (Popov, 2020; Scarpulla, 2011). However, it is not until days later that mitochondrial expansion and maturation is complete through fusion and fission along with increases in mitochondrial density and optimal respiratory capacity (Palmer et al., 2011; Scarpulla,

2008). Mitophagy operates on the timescale of hours to days with autophagosome formation and mitochondrial engulfment followed by fusion with lysosomes and initial degradation requiring a couple of hours and chronic mitophagy taking place on the order of days in response to sustained low-level stressors, such as hypoxia (Narendra et al., 2008; Youle and Narendra, 2011). As our examination of differences in rates of mitochondrial biogenesis and mitophagy in the context of differential integrin activation showed, the timescale of modulated integrin activation (seconds to minutes) may have been too short of a window for examination of changes in total mitochondrial content.

**Effect of manganese on integrin adhesion**

Manganese is a potent activator of integrins, enhancing their affinity for ligands and promoting cell adhesion, migration, immune cell function, and coagulation (Chen et al., 1994; Zhu et al., 2008). Manganese acts as an allosteric modulator of integrins, specifically by stabilizing the high-affinity conformation of integrins which makes integrins more likely to bind to their ligands, such as fibronectin, collagen, and other ECM proteins (Anderson et al., 2022; Zhang et al., 2008). Unlike calcium and magnesium ions, which support basal integrin function, manganese is particularly potent in enhancing integrin-ligand interactions (Xiong et al., 2003; Zhang and Chen, 2012). $Mn^{2+}$ binds to metal ion-dependent adhesion sites (MIDAS) on the integrin's extracellular domain which induces conformational changes that shift the integrin from a low- to high-affinity state, thus promoting integrin activation and cell adhesion (Bazzoni and Hemler, 1998; Humphries et al., 2003). Notably, excess manganese can cause toxicity as high levels of manganese can lead to oxidative stress and disrupt cellular signaling pathways,

potentially affecting integrin-regulated processes (Dobson et al., 2004; Li and Yang, 2018).

**Cadherin adhesion in mitochondrial processes**

While the basis for integrin regulation of mitochondrial localization and function has been discussed (Chapter 1, 2), the contribution of cadherin signaling found at intercellular contacts to mitochondrial processes must be considered. Cadherin-mediated cell junctions in tissues like epithelia and cardiac muscle have high ATP demands due to the need for constant remodeling of the actin cytoskeleton and maintenance of cell adhesion with mitochondria often localizing near these junctions to provide a readily available supply of ATP (Nieto, 2013; Schwarz, 2013). Cadherins interact with catenin family members including β-catenin, a multifunctional protein that connects cadherins to the actin cytoskeleton and participates in the Wnt signaling pathway (Moon et al., 2004; Yamada et al., 2005). Such Wnt/β-catenin signaling promotes mitochondrial biogenesis and function (Bernkopf et al., 2018; Yoon et al., 2010). Mitochondria are a major source of ROS which can influence cadherin-mediated adhesion by modifying proteins within the cadherin complex or by activating downstream signaling pathways that affect adhesion stability (Lim et al., 2008; van Wetering et al., 2002). Furthermore, in oxidative environments, ROS can impair cadherin function, leading to weaker cell-cell junctions (Parrish et al., 1999; Wang et al., 2021a).) In addition, mitochondria form close associations with other organelles like the endoplasmic reticulum at sites known as mitochondria-associated membranes which are involved in calcium signaling (Patergnani et al., 2011; Raturi and Simmen, 2013). Calcium signaling is a critical process for the

regulation of cell adhesion as calcium is essential for cadherin binding, and mitochondria play a role in buffering cellular calcium levels, which can support cadherin function (Hirano et al., 1987; Nagar et al., 1996).

## Conclusions

In sum, these studies explore how fibronectin-integrin interactions influence mitochondrial metabolism. We found that inhibiton of mitochondrial aconitase, a citric acid cycle enzyme, slows mesendoderm migration. We investigated how integrin activation affects mitochondrial biogenesis and degradation rates. These findings also focused on the spatial distribution of mitochondrial activity and clustering in mesendoderm cells, as well as the effects of external integrin activation via manganese on mitochondrial activity. Finally, we observed variations in mitochondrial localization in individual mesendoderm cells based on the type of adhesive substrate.

## Materials and methods

### Xenopus embryo manipulations

Xenopus embryos are obtained and cultured as described previously (Gerhart and Kirschner, 2020; Sive, 2000).

### Mesendoderm Migration

As previously described (Davidson et al., 2002), we determined mesendoderm mantle closure in animal-pole upright intact albino embryos using brightfield illumination with imaging at 40X on an upright Zeiss AxioZoom microscope. The embryos were micro-injected to produce a final concentration of 100mM sodium fluoroacetate in the blastocoel cavity. Sodium fluoroacetate and the vehicle control (DMSO) were diluted in Danilchick's For Amy (DFA) media, which resembles embryonic interstitial fluid (Sater et al., 1993). The mesendoderm free area of the blastocoel roof was measured as a circle with subsequent measurements of free areas traced to determine the percent closure from the initial area over 2 hours using FIJI.

### TOMM20 western blot analysis

Cells were lysed after 1 hour of adhesion to a given substrate (i.e., GST-9.11 and GST-9.11A) with 100µl lysis buffer [25 mM Tris HCl pH=7.4 containing 100 mM NaCl,1 mM EDTA, 1 mM EGTA, 1 mM beta-glycerophosphate, 2.5 mM $Na_4P_2O_7$, 1% NP40, protease inhibitor cocktail (Sigma) and 1 mM PMSF]. Following cell lysis, lysates were centrifuged for 10 min at 14,000 rpm at 4°C to remove yolk. The supernatants were transferred to new tubes, diluted with 2X reducing Laemmli buffer, and proteins were

separated by SDS-PAGE (10% or 12%) and transferred onto nitrocellulose membranes. Blots were probed with antibodies directed against TOMM20 (Cell Signaling Technology; 1:1000 dilution) and tubulin (Sigma, 1:50,000 dilution). Signal intensity for each band was quantified using FIJI and ratios of TOMM20 to tubulin were calculated in Microsoft Excel.

**Mesendoderm cell preparation**

Dorsal mesendoderm tissue from stage 10.5 to 11 Xenopus embryos was dissociated in 1X $Ca^{2+}$/$Mg^{2+}$-free MBS (CMF-MBS). To examine the response of individual mesendoderm cells to distinct adhesive substrates, glass dishes were coated with poly-L-lysine solution (1.0 mg/mL, Sigma), bovine plasma fibronectin (0.05 mg/mL), C-Cadherin-Fc (0.02 mg/mL) or equimolar amounts of GST-9.11 (0.01 mg/mL) and GST-9.11A (0.01 mg/mL), as previously described (Dzamba et al., 2009; Ramos et al., 1996; Richardson et al., 2018). Dissociated cells were transferred and allowed to spread on the coated glass dishes filled with DFA. Molar equivalents of plasma fibronectin, GST-9.11, and GST-9.11A were kept consistent at 0.23 μM.

**Live imaging of mitochondria**

To assess membrane potential, cells were pre-incubated for 30 minutes with the potentiometric dye TMRE (50 nM, Thermo Fisher). To determine total mitochondrial content, cells were incubated with MitoTracker Green FM (50 nM, Thermo Fisher). Cells

or embryos were washed with 3 changes of DFA prior to imaging to reduce non-specific accumulation of dye in yolk platelets.

**Normalized mitochondrial activity during manganese treatment**

Whole mesendoderm tissue from stage 10.5-11.0 embryos was dissected and dissociated in 1X CMF-MBS. Dissociated cells were spread on a 96-well plate previously coated overnight with GST-9.11 and GST-9.11A as described above. Wells were blocked with 5% BSA for ~1 hour at room temperature. Following washing, wells were filled with 100 µl of 1X DFA containing 50 nM TMRE and 50 nM MitoTracker Green FM. Cells were allowed to adhere for 30 minutes followed by measurement of fluorescence at ~574nm and ~515nm via plate reader. Cells were exposed to 10 mM $MnCl_2$ (or dd$iH_2O$ vehicle control) dissociated in DFA followed by 30 minutes of incubation at room temperature at which point their fluorescence was captured by plate reader. The ratios of TMRE:MitoTracker Green FM were calculated in Excel by evaluating the fluorescence intensity in wells of interest and compared in treated versus control conditions. Resolving individual mitochondria by this method is not possible, therefore our measurements of TMRE and MitoTracker Green FM were based on the total fluorescent signal of a given well. Capturing both TMRE and MitoTracker Green FM allowed for a normalization of mitochondrial activity relative to mitochondrial content.

**Spatial distribution of mitochondria in live mesendoderm**

To assess the distribution of mitochondria in tissue explants and cell pairs or clusters, the GFP-Mitochondria Anchor (GFP-MA) construct was employed by micro-injecting

embryos with 500 pg of GFP-MA RNA per embryo. In evaluating the clustering of mesendoderm between cell-cell contact and protrusion regions polarized cells were divided into 10 segments with 3 segments representing the protrusion proximal region, 4 segments representing the cell body, and 3 segments representing the cell-cell contact region. Using FIJI, the raw integrated density of the GFP-MA fluorescence was divided by the area for the given region to conduct comparisons of mitochondrial density and account for differences in cell size. To assess the distribution of mitochondria in individual cells across different adhesive substrates, the GFP-MA signal from z-stacks of dissociated mesendoderm cells sectioned in 0.25 um z intervals were evaluated. The z-distance of the peak GFP-MA signal from the z-stacks was determined as the location of the greatest mitochondrial density. The spread of the GFP-MA signal for each cell was computed as the standard deviation of the GFP-MA signal across the z-stack.

A

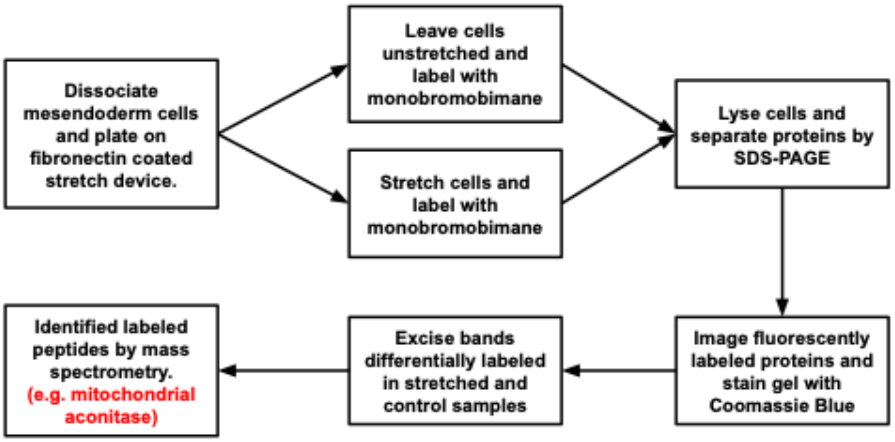
Dissociate mesendoderm cells and plate on fibronectin coated stretch device.
Leave cells unstretched and label with monobromobimane
Stretch cells and label with monobromobimane
Lyse cells and separate proteins by SDS-PAGE
Image fluorescently labeled proteins and stain gel with Coomassie Blue
Excise bands differentially labeled in stretched and control samples
Identified labeled peptides by mass spectrometry. (e.g. mitochondrial aconitase)

B

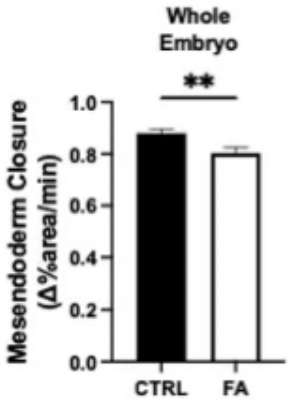
Whole Embryo
**
Mesendoderm Closure (Δ%area/min)
1.0
0.8
0.6
0.4
0.2
0.0
CTRL
FA

**Figure 3.1: In-cell labeling of mesendoderm cells under stretched versus unstretched conditions highlights mitochondrial aconitase**

(A) Flowchart schematic of experimental strategy used for identification of force induced conformational changes. Application of force to the fibronectin-integrin adhesive complexes of mesendoderm cells with labeling of exposed cysteines by monobromobimane identified differentially labeled peptides in proteins such as mitochondrial aconitase. Experiment conducted by Maureen Bjerke.

(B) Graph displaying the rate of mesendoderm mantle closure from stage 10.5 to 12.0 in gastrulation stage whole albino embryos microinjected with DMSO control (CTRL) or fluoroacetate (FA), an inhibitor of mitochondrial aconitase. Each condition represents the average velocity from three independent experiments.

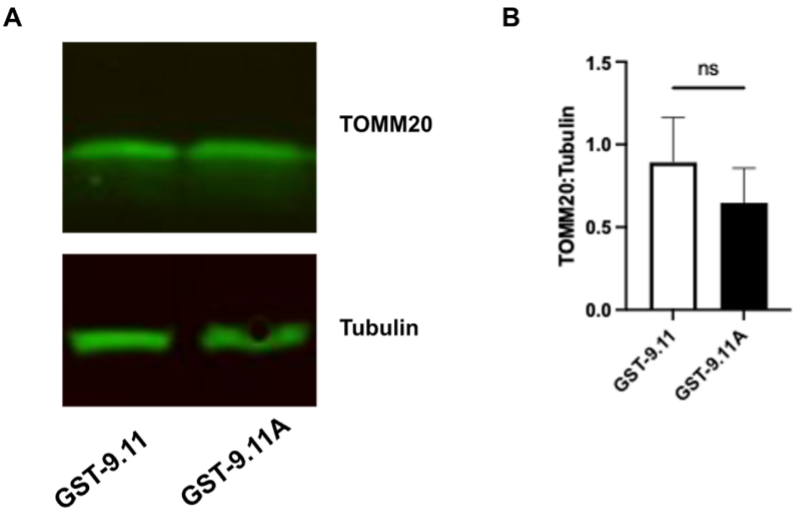
A
TOMM20
Tubulin
GST-9.11
GST-9.11A
B
ns
TOMM20:Tubulin
1.5
1.0
0.5
0.0
GST-9.11
GST-9.11A

**Figure 3.2: Western blot for total mitochondrial content of mesendoderm cells on fibronectin fusion proteins**

(A) Representative western blot of mitochondrial content detected from mesendoderm on distinct substrates (GST-9.11 and GST-9.11A) via antibodies against the translocase of outer mitochondrial membrane 20 (TOMM20) and against tubulin as a loading control. (B) Quantification of TOMM20 levels normalized to tubulin. Data are mean ± SEM. N=4.

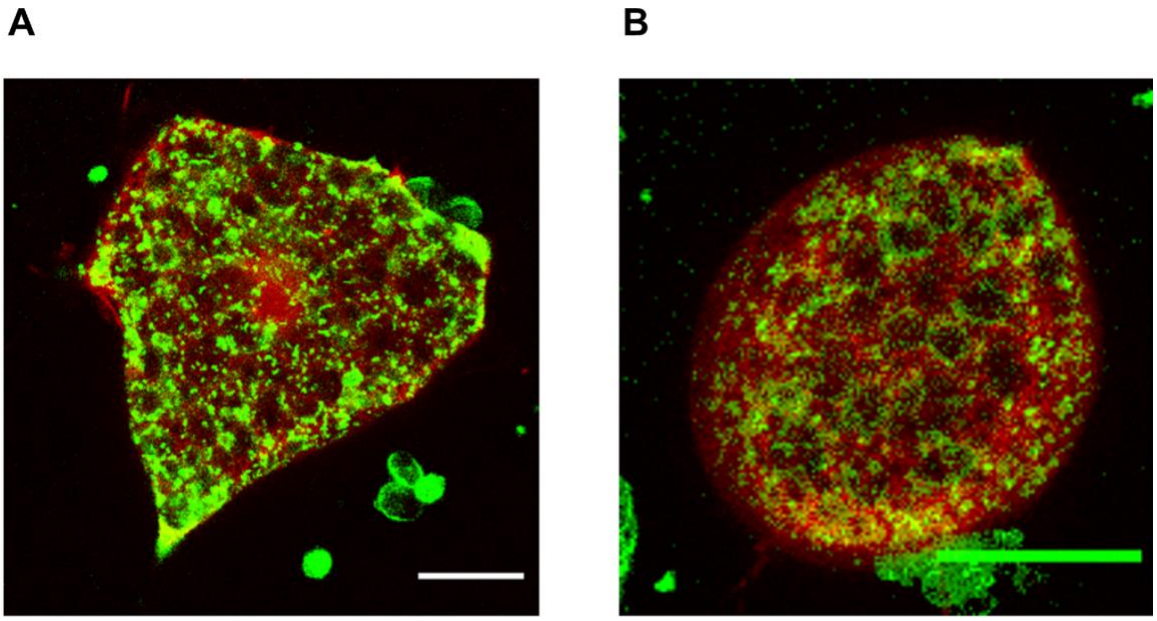
A
B

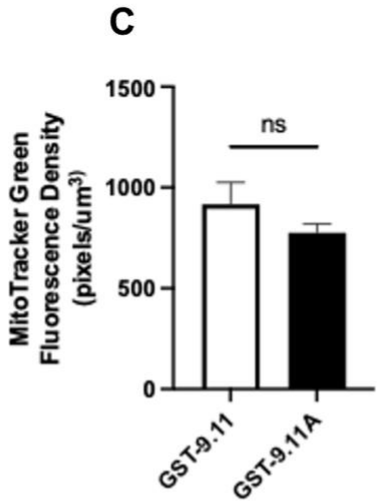
C
MitoTracker Green
Fluorescence Density
(pixels/um3)
1500
1000
500
0
ns
GST-9.11
GST-9.11A

**Figure 3.3: Live imaging of total mitochondrial content in mesendoderm cells on fibronectin fusion proteins**

(A, B) Single cells dissociated from Xenopus mesendoderm and adhered to (A) GST-9.11 or (B) GST-9.11A substrates. Cells labelled with membrane-GFP (red) and mitochondrial content indicated by mitotracker green (green). Scale bars = 20 μm.

(C) Comparison of total mitotracker green fluorescence from dissociated mesendoderm cells on GST-9.11 and GST-9.11A substrates.

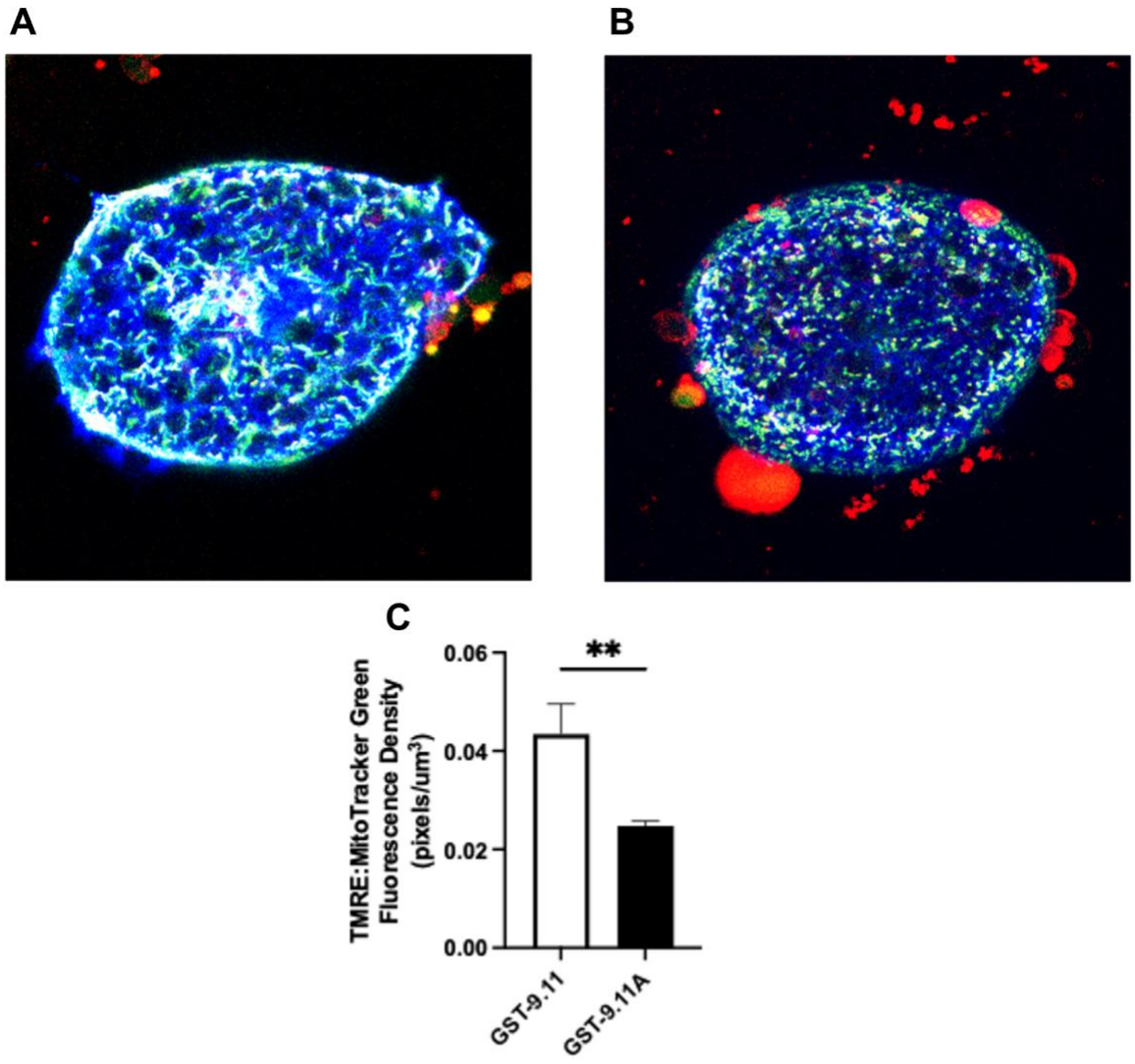
A
B
C
TMRE:MitoTracker Green Fluorescence Density (pixels/um³)
0.06
0.04
0.02
0.00
**
GST-9.11
GST-9.11A

**Figure 3.4: Ratios of active to total mitochondria in mesendoderm cells on fibronectin fusion proteins**

(A, B) Single cells dissociated from Xenopus mesendoderm and adhered to (A) GST-9.11 or (B) GST-9.11A substrates. Cells labelled with dextran (blue), mitochondrial content indicated by mitotracker green (red), and mitochondrial activity indicated by tetramethylrhodamine ethyl ester (TMRE, green).

(C) Ratios of TMRE to mitotracker green fluorescence from dissociated mesendoderm cells on GST-9.11 and GST-9.11A substrates.

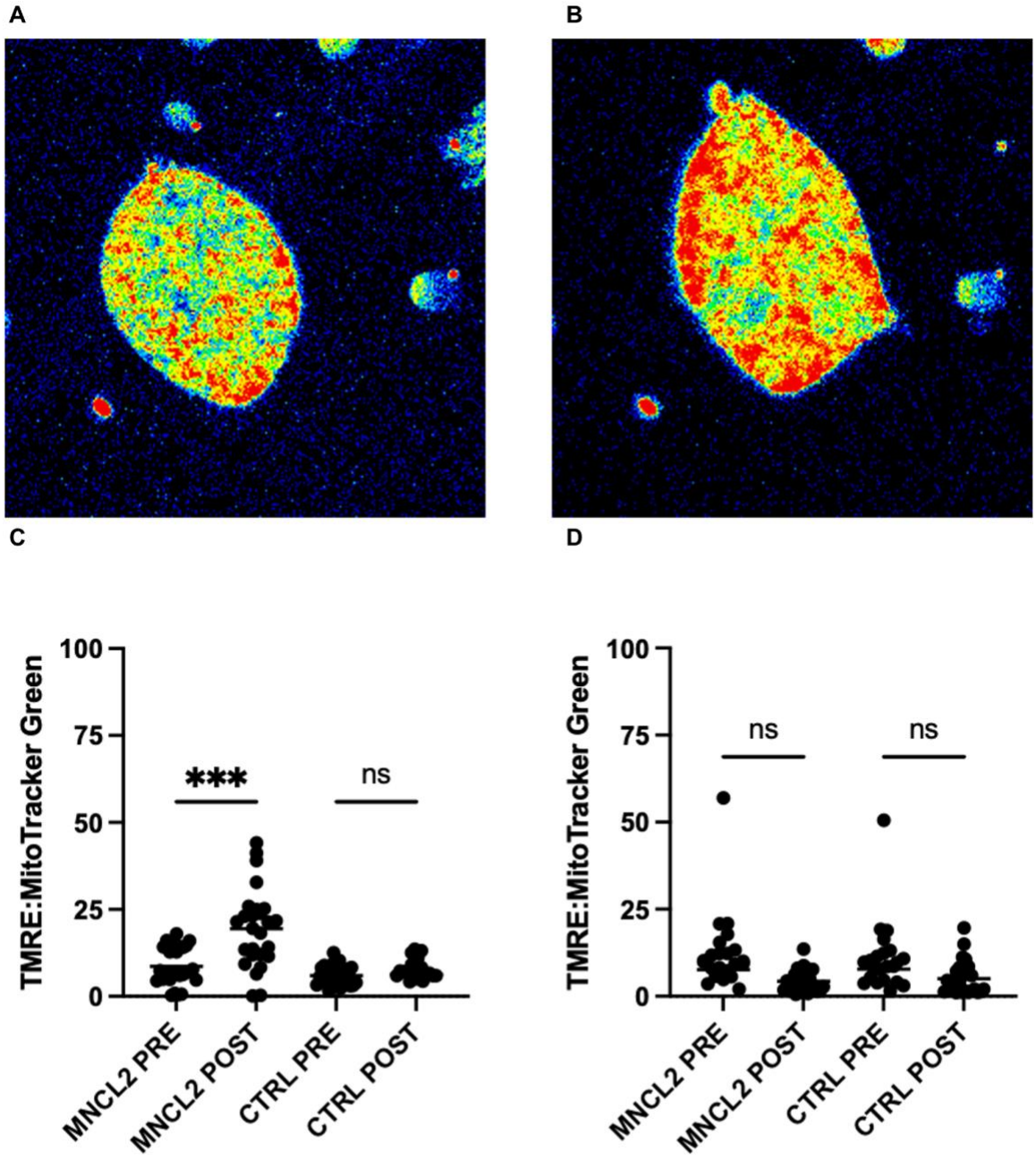
A
B
C
D
TMRE:MitoTracker Green
100
75
50
25
0
***
ns
ns
MNCL2 PRE
MNCL2 POST
CTRL PRE
CTRL POST

**Figure 3.5: Effect of exogenous integrin activation via manganese on mitochondrial activity**

(A, B) TMRE fluorescence intensity (pseudocolor) in mesendoderm cells dissociated and adhered to GST-9.11A before (A) and after (B) the addition of 1mM manganese chloride. (C, D) Ratios of TMRE to mitotracker green fluorescence from dissociated mesendoderm cells on GST-9.11A (C) and GST-9.11 (D) substrates before (PRE) and after (POST) the addition of 1mM manganese chloride (MNCL2) or vehicle (CTRL).

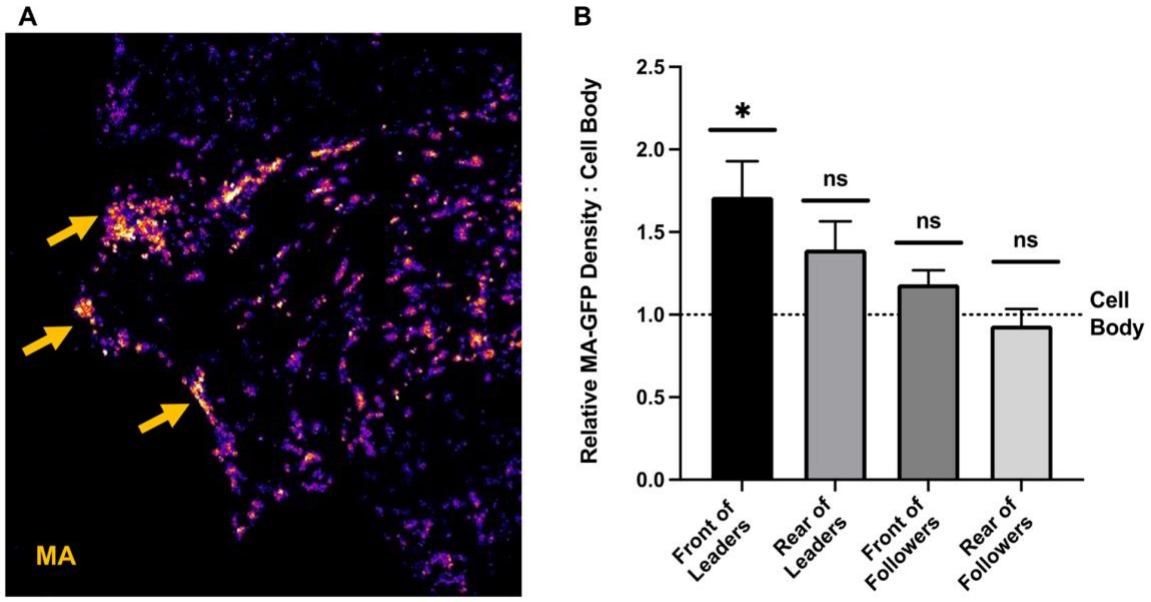
A
MA
B
Relative MA-GFP Density : Cell Body
2.5
2.0
1.5
1.0
0.5
0.0
*
ns
ns
ns
Cell Body
Front of Leaders
Rear of Leaders
Front of Followers
Rear of Followers

**Figure 3.6: Clustering of mitochondria in migrating mesendoderm**

(A) Mesendoderm tissue explant on FN labeled with Mitochondrial Anchor (MA)-GFP to visualize mitochondrial density. Pseudocolors correspond to fluorescence intensity heat map that reflect mitochondria density (yellow: high, purple: low). Mitochondria aggregates along tissue leading edge of polarized mesendoderm (yellow arrows). (B) Quantitation of MA-GFP density in the front and rear of leader or follower mesendoderm cells of explants relative to cell body density (dotted line). Mean ± SEM. Explants analyzed from three independent fertilizations. *$p \leq 0.05$ by ANOVA.

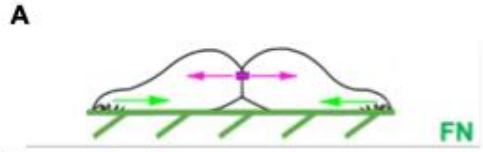
A
FN

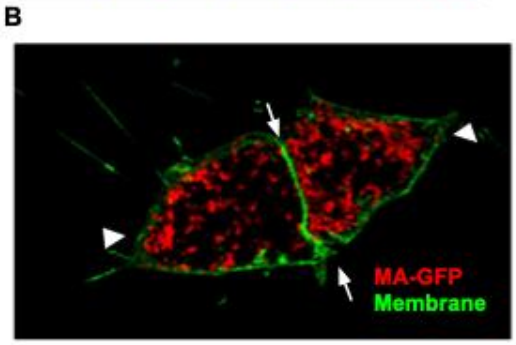
B
MA-GFP
Membrane

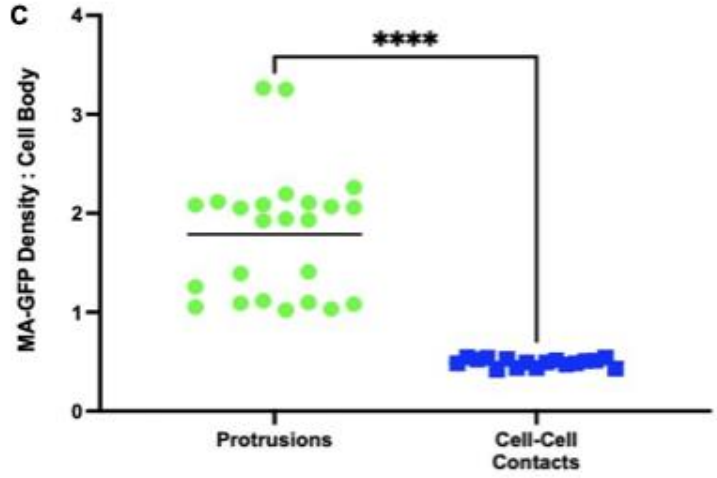
C
MA-GFP Density : Cell Body
4
3
2
1
0
****
Protrusions
Cell-Cell
Contacts

**Figure 3.7: Clustering of mitochondria in mesendoderm cell pairs**

(A) Cartoon of mesendoderm cell pairs producing integrin-fibronectin (FN, green arrow) traction stress and C-cadherin to C-cadherin intercellular tension (pink arrow). (B) Mesendoderm cell outlines labeled with membrane-GFP (green) and mitochondrial density labeled with MA-GFP (red). Arrowheads denote protrusion regions and arrows highlight a region of cell-cell contact. (B) Quantitation of MA-GFP density in the protrusions and the cell-cell contact regions relative to their cell bodies in mesendoderm cell pairs.

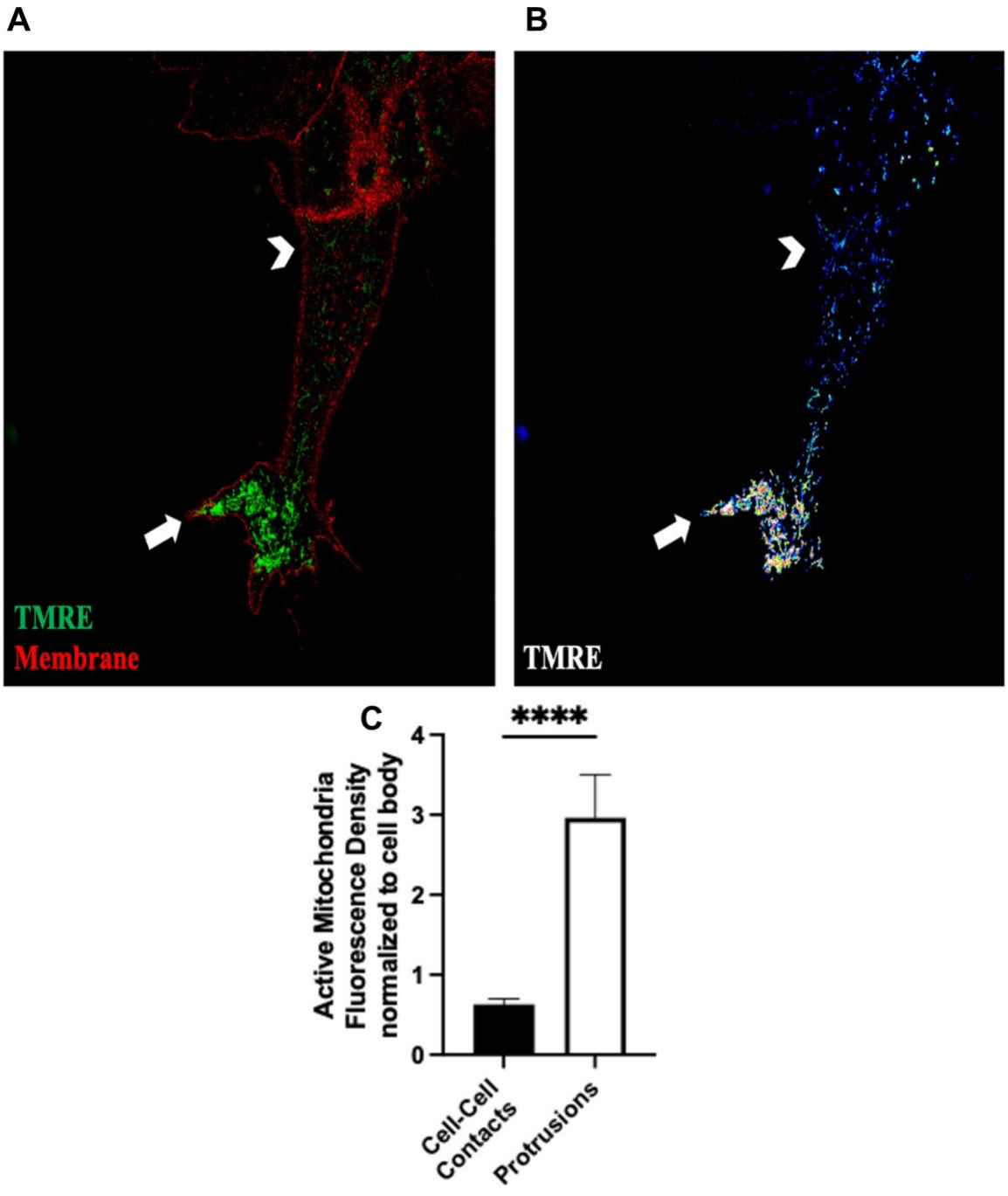
A
B
TMRE
Membrane
TMRE
C
****
Active Mitochondria Fluorescence Density normalized to cell body
0
1
2
3
4
Cell-Cell Contacts
Protrusions

**Figure 3.8: Distribution of mitochondrial activity in mesendoderm cell clusters**

(A, B) Groups of mesendoderm cells dissociated and adhered to fibronectin. Protrusion region indicated by arrow and cell-cell contact indicated by chevron. (A) Cells labelled with membrane-GFP (red) and mitochondrial activity indicated by TMRE (green). (B) TMRE fluorescence intensity (pseudocolor) distributed in cell cluster. Arrow represents protrusion region and chevron indicates region of cell-cell contact. (C) Comparison of the active mitochondrial fluorescence density, as detected by TMRE, in protrusions versus cell-cell contacts of cells in clusters.

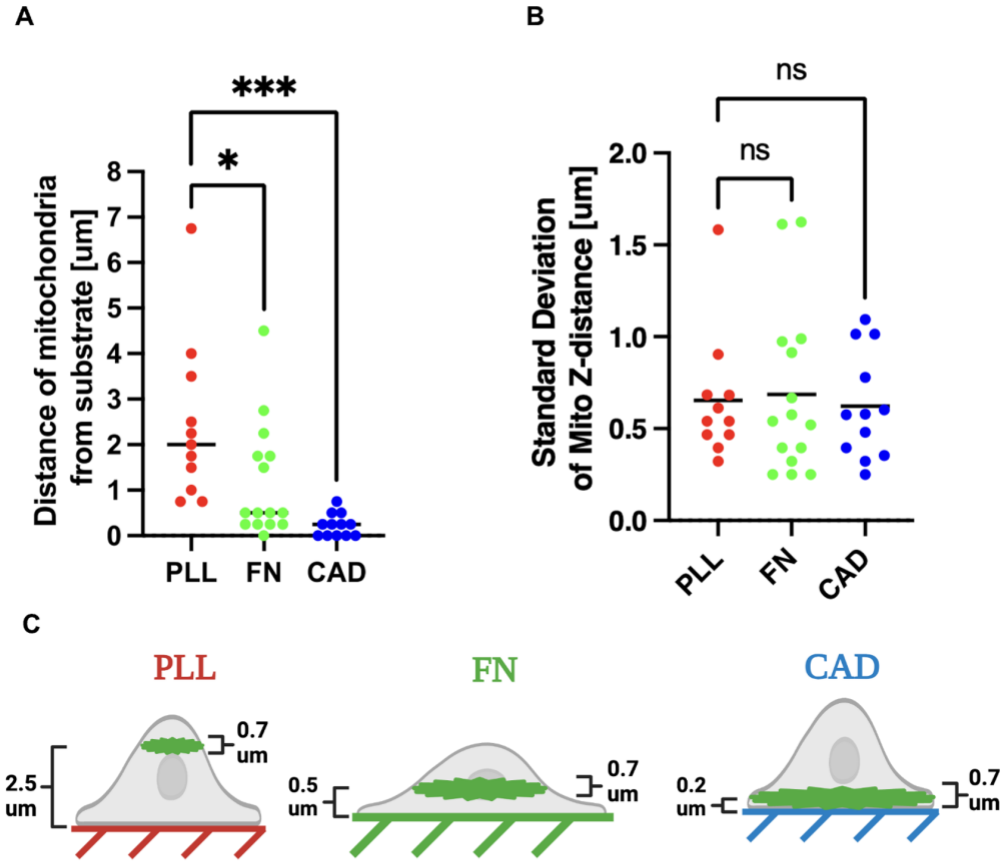
A
***
*
Distance of mitochondria from substrate [um]
0
1
2
3
4
5
6
7
8
PLL
FN
CAD
B
ns
ns
Standard Deviation of Mito Z-distance [um]
0.0
0.5
1.0
1.5
2.0
PLL
FN
CAD
C
PLL
FN
CAD
2.5 um
0.7 um
0.5 um
0.7 um
0.2 um
0.7 um

**Figure 3.9: Relative separation of mitochondrial clusters from adhesive substrates**

(A, B) Distribution of the peak MA-GFP signal z-distances (A) and their standard deviations (B) from mesendoderm cells adhered to poly-l-lysine (PLL), fibronectin (FN), and Fc-Cadherin fragments (CAD). (C) Cartoon of mesendoderm cells adhering to PLL, FN, and CAD substrates depicting their localization and distribution relative to their substrate and relative cell height.

# Chapter 4:

# Conclusions, Future Directions, and Significance

**Summary and major findings**

An overarching goal of this dissertation has been to understand how the adhesive signals intersect with the bioenergetic processes of metabolism. The biochemically and mechanically well-defined collectively migrating *Xenopus* laevis mesendoderm has been a productive model for the pursuit of this goal. This is in addition to useful tools for the specific modulation of integrin signaling. Furthermore, advances in techniques for the evaluation of bioenergetic and mitochondrial function in real time has enabled us to understand the links to metabolic activity. Therefore, the work described in this dissertation is uniquely positioned to expand our understanding of cell adhesion in metabolism.

Chapter 2 uncovers a link between ECM-integrin adhesion and mitochondrial metabolism in collective cell migration. In *Xenopus* laevis mesendoderm cells, increased mitochondrial activity is observed at the leading edge where **α**5β1 integrin traction on fibronectin is strongest. This metabolic boost, driven by oxidative phosphorylation, depends on **α**5β1 integrin and is reduced with inhibition of FAK signaling. Specific fibronectin-integrin interactions and cell stretching further increase mitochondrial membrane potential in a FAK-dependent manner. The regulation of mitochondrial metabolism by integrin-FAK signaling is conserved across different tissues. Inhibiting mitochondrial activity slows migration, suggesting integrin-ECM engagement is key to enhancing ATP production for cell migration. This work highlights the role of ECM-integrin signaling in regulating metabolism during early embryonic cell movements.

In Chapter 3, we examined a variety of aspects related to the intersections between cell adhesion and collective migration with mitochondrial metabolism. We

revisited how changes in citric acid cycle metabolism affect collective mesendoderm migration. We also considered if integrin activation affected mitochondrial content through biogenesis or degradation and assessed the spatial patterns of mitochondrial activity and clustering in mesendoderm cell groups. Finally, we also investigated whether external activation of integrins with $Mn^{2+}$ could enhance mitochondrial activity and noted substrate-dependent variations in mitochondrial localization within individual mesendoderm cells.

While these studies have advanced our understanding of the metabolism of cell adhesion, the specific metabolic pathways and processes involved remain to be defined. Metabolomics offer a path toward addressing these gaps in understanding through an unbiased, comprehensive study of the metabolites, or small molecules involved or produced by metabolic processes that fuel collective mesendoderm migration (Idle and Gonzalez, 2007; Liu and Locasale, 2017). As we look towards future directions for expanding our understanding of adhesive metabolism, I present the preliminary metabolomics results from *Xenopus* laevis gastrulae in the presence of a fibronectin morpholino knockdown (or non-specific control knockdown). Here, we discuss the implications and limitations of these findings and the future for the study of metabolism in adhesive processes.

**Metabolomics: an introduction**

Simply put, metabolomics provide a snapshot of metabolic activity and reveal how biological systems respond to genetic, environmental, or pathological changes (Goodacre, 2007; Zhang et al., 2012). Metabolomics allow for the identification of

metabolites including the detection and characterization of all small molecules present in a biological sample (Guijas et al., 2018; Rinschen et al., 2019). Depending on the approach employed (i.e. targeted vs. untargeted) the quantification strategies available vary (Alseekh et al., 2021; Buchholz et al., 2002). In targeted quantification the analysis is focused on a predefined set of metabolites (e.g. glucose, amino acids, or lipids) using internal and external standards to achieve absolute quantification (Lelli et al., 2021; Zhou and Yin, 2016). It is by using isotopically labeled internal standards for precise measurements that absolute quantification allows for the determination of pathway flux (Wu and Li, 2016; Zhou and Yin, 2016). In contrast, the aim of untargeted profiling is to detect as many metabolites possible and provide a relative quantification of metabolites in the comparison of sample groups (Schrimpe-Rutledge et al., 2016; Zeki et al., 2020). Through relative quantification metabolite levels can be compared between samples without requiring standards (Patti, 2011; Schrimpe-Rutledge et al., 2016). However, untargeted profiling and relative quantification (e.g. the analysis presented in this chapter) only support limited inferences of metabolic pathway flux(Zamboni et al., 2015). Ultimately, through metabolomics we can conduct pathway analyses in which we identify changes in metabolite profiles to map and understand alterations in metabolic pathways (Karnovsky and Li, 2020; Xia and Wishart, 2010).

**Metabolomics Technology**

Methods in chemical analysis are critical in the development of metabolomics. Mass spectrometry (MS) is particularly useful as the mass-to-charge ratio of molecules is measured which enables the analysis of thousands of metabolites simultaneously, often at

very low concentrations (Hoffman et al., 2002; Mann et al., 2001). When analyzing non-volatile metabolites and complex mixtures, Liquid Chromatography (LC)-MS is useful as metabolites are separated via liquid chromatography and then identified via mass spectrometry based on their mass-to-charge ratios (Becker et al., 2012; Fang and Gonzalez, 2014). In the analysis of small, volatile metabolites (e.g. fatty and amino acids) gas chromatography-MS is ideal for the separation of these volatile metabolites (Mastovská and Lehotay, 2003; Santos and Galceran, 2003). During this process a sample is vaporized and injected into a stream of inert carrier gas, usually helium or nitrogen, which transports it through a long, narrow column coated with a stationary phase (Bartle and Myers, 2002; Cramers et al., 1999). As the compounds travel through the column, they interact with the stationary phase based on their chemical properties thereby resulting in separation with each compound exiting the column as an *elute* at a different time (i.e. retention time**)** (Katritzky et al., 1994; Patterson, 1971). Capillary Electrophoresis-MS is also used in metabolomics for the separation of polar and charged compounds (e.g. amino acids and nucleotides) (Cai and Henion, 1995; Schmitt-Kopplin and Frommberger, 2003).

In addition to MS, Nuclear Magnetic Resonance (NMR) spectroscopy is integrated into metabolomics as it provides detailed structural information about metabolites based on the magnetic properties of atomic nuclei (Marion, 2013; NMR Spectroscopy, 2006). As this technique is non-destructive, requires minimal sample preparation, and is highly reproducible it provides quantitative data on known metabolites in studies of living tissues and fluids (Keeler, 2010; Lindon et al., 1999). However, it is less sensitive than MS (Lindon et al., 1999; Pan and Raftery, 2007). To produce a more

comprehensive metabolomic analysis, the rapid and nondestructive technique of Fourier Transform Infrared (FTIR) Spectroscopy is integrated with MS or NMR as FTIR detects metabolites based on their vibrational modes in response to infrared light which provides information about the chemical bonds and functional groups in a sample (Berthomieu and Hienerwadel, 2009; Corte et al., 2015).

**A metabolomics workflow of the *Xenopus* laevis gastrula**

Here, we present the metabolomics workflow prepared to examine the metabolism of the *Xenopus laevis* gastrulae. A variety of biological sample types (e.g. blood, urine, tissue) can be collected and carefully processed to preserve metabolite integrity (Álvarez-Sánchez et al., 2010a; Álvarez-Sánchez et al., 2010b). Processes for quenching, extraction, and filtration are applied to prepare the samples for analysis (Dietmair et al., 2010; Dunn and Winder, 2011). Based on volumetric estimates of the *Xenopus laevis* embryo, each embryo contains the metabolome equivalents of approximately 250,000 mammalian cells (Vastag et al., 2011). Therefore, to obtain about 2 million mammalian cell metabolome equivalents for analysis, we prepared four technical replicates (i.e. samples) of embryos from groupings of eight gastrulation-stage embryos that were microinjected with a fibronectin-targeted morpholino (FNMO) to knockdown fibronectin expression. For comparison, four samples were produced from groupings of eight gastrulation stage embryos microinjected with a control morpholino (COMO) that fails to knock down protein expression.

More specifically for our samples, we prepared an extraction solvent of methanol-water (80%:20%) v/v using at least High-performance liquid chromatography (HPLC)-

grade solvents. The extraction solvent was chilled in a -80ºC freezer for 1 hour. The MO injected embryos were divided into groups of eight and transferred to 1.5 mL microcentrifuge tubes. The 0.1X MBS media was removed as completely as possible via aspiration from the tube which was followed by washing with 1 mL of sterile 1X MBS with flicking of the embryos in the tube to gently wash. The wash solution was then completely aspirated, and the tubes were placed on dry ice. One mL of the pre-chilled extraction solvent was added to each sample (i.e. tube) and flicked to gently mix. The samples were transferred to a -80º freezer for 15 minutes. The samples were removed from the freezer and placed on dry ice. The embryos were then ruptured and resuspended in the extraction solvent using a P1000 micropipette. Next, the embryo lysates were transferred to clean 1.5 mL microcentrifuge tubes for 10 minutes of centrifugation at 4ºC in 14,000 to 20,000 Relative centrifugal force (RCF). This was followed by transferring 900 µL of the supernatant into a clean 1.5 mL microcentrifuge tube, being careful to avoid disrupting the pellet. The cell lysates were then dried completely via centrifugal evaporation using a SpeedVac that maintained the temperature below 40ºC. The tubes were then capped and stored at -80ºC until they were submitted to the Trans-National Institutes of Health (NIH) Metabolomics Core Facility (MCF) (Directed by Alan K. Jarmusch, Ph.D. with chemist support from Kirsten E. Overdahl, Ph.D. at the National Institute of Environmental Health Sciences) on dry ice.

As part of a collaboration (facilitated by Kenneth M Yamada, MD, PhD and Alexander Kiepas, PhD at the National Institute of Dental and Craniofacial Research) with the Trans-NIH MCF, data is acquired as metabolites are detected and quantified using the analytical techniques mentioned (e.g. MS, NMR, FTIR) with software

processing the raw data into readable formats (Chang et al., 2021; Rauh et al., 2022). This then allows for data processing of noise reduction, peak alignment, and normalization to ensure consistency and allow comparison across samples (Vu et al., 2018; Wang et al., 2019). Our samples underwent ultra-high performance liquid chromatography–tandem mass spectrometry (UHPLC-MS/MS) and were normalized across sample group (FNMO versus COMO). Notably, a quality control check eliminated one of the four original FNMO samples. Briefly, in contrast to other forms of LC, UHPLC uses smaller particle sizes in the chromatographic column to allow for faster and higher-resolution separation of complex mixtures into separate compounds based on their polarity, size, or affinity to the stationary phase thereby isolating the compounds before they enter the mass spectrometer (Dong and Zhang, 2014; Fekete et al., 2014). After the UHPLC phase the compounds enter the mass spectrometer for MS/MS, where they are ionized, fragmented, and analyzed in two stages (de Hoffmann, 1996; McLafferty, 1981). In the first stage (MS1) the precursor ions (i.e. intact molecules) are detected, while in the second stage (MS2) product ions (i.e. fragmented molecules) are identified (Gross, 2017; Heiles, 2021). This tandem setup provides detailed structural information, enhancing the identification and quantification of compounds even in trace amounts (Schoeman et al., 2018; Yang et al., 2022).

Statistical analysis, metabolite identification, and biological interpretation followed. The Trans-NIH MCF applies advanced statistical methods, such as principal component analysis (PCA), to identify significant patterns and differences in metabolic profiles (Ren et al., 2015; Worley and Powers, 2013). Software and databases like the Human Metabolome Database help in identifying the metabolites (Wishart et al., 2007;

Wishart et al., 2016). After identifying and quantifying metabolites, I interpret the data in the context of biological pathways with pathway analysis tools like MetaboAnalyst and the Kyoto Encyclopedia of Genes and Genomes (KEGG) to reveal insights into biochemical changes, disease mechanisms, or treatment effects (Chong et al., 2018; Kanehisa and Goto, 2000). In the statistical analyses conducted by the Trans-NIH MCF, compounds are grouped based on the polarity options (positive or negative) of the ionization mode used for MS/MS, thereby reflecting the relative charge of the compound identified (Awad et al., 2015; Nordström et al., 2008). PCA plots of the three FNMO and four COMO samples demonstrated a notable separation of the samples by their treatment (fibronectin knockdown or none) (Figure 4.1) for both positive (Figure 4.1A) and negative (Figure 4.1B) polarity options. The compounds from the positive and negative polarity options were then annotated for known metabolites based on KEGG datasets, fold change differences of metabolites between FNMO and COMO samples were calculated, and p-values from t-test comparisons of the compounds from the FNMO and COMO groupings were produced (Figure 4.2). In my use of Metaboanalyst, annotated metabolites from t-tests that produced a significant p-value<0.05 were submitted for enrichment analysis to identify metabolic processes that showed differences in FNMO and COMO (Figure 4.3).

In sum, we present a metabolomics workflow to analyze the metabolism of *Xenopus* laevis gastrulae. Embryos were divided into two groups: one with fibronectin knockdown (FNMO) and a control group (COMO). After UHPLC-MS/MS analysis at the NIH Metabolomics Core, data processing showed a clear metabolic separation between FNMO and COMO samples. Compounds were categorized by ionization polarity,

annotated using KEGG, and statistically analyzed for fold changes and significance. Significant metabolites ($p < 0.05$) were further examined with MetaboAnalyst for pathway enrichment, highlighting metabolic processes affected by fibronectin knockdown. The metabolic pathways identified and their possible connection to integrin-associated metabolism of gastrulation will be discussed in the sections that follow.

**Pyrimidine metabolism**

Of the metabolite sets identified from our metabolomics analysis, we found pyrimidine metabolism to be notably enriched. Briefly, pyrimidine metabolism refers to the synthesis, degradation, and recycling of pyrimidine nucleotides, which are essential components of DNA and RNA, as well as key players in various cellular processes (Figure 4.4) (Garavito et al., 2015; O'Donovan and Neuhard, 1970). The main pyrimidines in cells are cytosine, thymine (found in DNA), and uracil (found in RNA) (Brown, 2009).

In pyrimidine metabolism there are two main biosynthetic processes: de novo synthesis and the salvage pathway (Figure 4.4) (Berens et al., 1995; Zöllner, 1982). In de novo synthesis pyrimidine nucleotides are synthesized from small, simple molecules such as glutamine, carbon dioxide ($CO_2$), and aspartate (Huang and Graves, 2003; Shambaugh, 1979). This is accomplished through a few key steps beginning with carbamoyl phosphate synthetase II (CPS II) converting glutamine, $CO_2$, and ATP into carbamoyl phosphate (Holden et al., 1999; Tatibana and Shigesada, 1972). Next, carbamoyl phosphate is combined with aspartate to form the pyrimidine precursor, orotate (Löffler et al., 2015; Löffler et al., 2016). It is then through a series of reactions that orotate is

converted to uridine monophosphate (UMP), which is a precursor for other pyrimidine nucleotides (Connolly and Duley, 1999; Dobolyi et al., 2011). From this point, UMP can be converted to a variety of pyrimidine nucleotides. For example, UMP can be phosphorylated to uridine diphosphate (UDP) and uridine triphosphate (UTP) for use in RNA (Anderson and Parkinson, 1997; Chandel, 2021b). UTP can then be converted to cytidine triphosphate (CTP) via CTP synthase for use in RNA and lipid synthesis (Chang and Carman, 2008; Thangadurai et al., 2022). Alternatively, UMP can be used in the formation of thymidine nucleotides as it can be converted to deoxyuridine monophosphate (dUMP) which can then be methylated by thymidylate synthase to form deoxythymidine monophosphate (dTMP) to support DNA synthesis (Carreras and Santi, 1995; Stroud and Finer-Moore, 2003). In contrast, the salvage pathway recycles the free pyrimidine bases of uracil and cytosine from the breakdown of nucleic acids (Poole et al., 2001; Weber et al., 1987). Pyrimidine bases are reattached to ribose-1-phosphate or deoxyribose-1-phosphate to form nucleotides such as UMP and Cytidine monophosphate (CMP) (Ipata et al., 2011; Okesli et al., 2017). Furthermore, this is an energy efficient pathway as it recycles existing pyrimidines instead of synthesizing them from scratch (Walter and Herr, 2022; Zrenner et al., 2006).

Pyrimidines are also degraded by being broken down into smaller, non-toxic products that can be excreted or used in other metabolic pathways (Löffler et al., 2005; van Gennip et al., 1997). For example, uracil and thymine are broken down into β-alanine and β-aminoisobutyric acid, which can be converted to acetyl-CoA or succinyl-CoA, thereby feeding into the citric acid cycle for energy production (Ahmad et al., 1998; Canellakis, 1956). In contrast to purine metabolism, pyrimidine degradation does not

produce uric acid, which avoids the risk of precipitating gout (Dehghan et al., 2008; Martinon et al., 2006).

**Pyrimidine metabolism in gastrulation**

As differences in pyrimidine metabolism were detected in gastrulation-stage embryos, it is critical to consider the contributions of pyrimidine metabolism to gastrulation. During gastrulation, there is rapid cell proliferation, differentiation, and migration which demands an increase in nucleotide synthesis to support associated DNA replication and RNA transcription (Muhr et al., 2024; Solnica-Krezel, 2005). The de novo pyrimidine biosynthesis pathway is likely upregulated to meet these demands through increasing activation of rate limiting enzymes, such as CPS II (Bachvarova et al., 1966; Warner and Finamore, 1962). In addition, mitochondria are likely involved in pyrimidine metabolism during gastrulation as the mitochondrial enzyme dihydroorotate dehydrogenase (DHODH) catalyzes conversion of dihydroorotate to orotate for pyrimidine biosynthesis (Munier-Lehmann et al., 2013; Reis et al., 2017). Notably, DHODH intimately links pyrimidine biosynthesis with mitochondrial oxidative phosphorylation as Coenzyme Q (CoQ) serves as an electron acceptor for electrons from DHODH and those from both electron transport chain complexes I (CI) and CII to then transport them to CIII (Banerjee et al., 2021; Boukalova et al., 2020). Therefore, mitochondrial function is linked to the availability of pyrimidine nucleotides (cytosine, thymine, and uracil) to use in nucleic acids needed for cell proliferation during gastrulation (Allen, 1941; Rice et al., 1965).

The potential contributions of pyrimidine metabolism to cell migration during gastrulation remain poorly defined. Nucleotides have been shown to play chemotactic signaling roles by influencing cell movements via extracellular pyrimidine derivatives, such as UDP and UTP, signaling through P2Y purinergic receptors (Chaulet et al., 2001; Kaczmarek et al., 2005). Preliminary evidence from the *Xenopus* laevis mesendoderm supports the role of adenosine nucleotide signaling contributing to the organization of cellular rearrangements during gastrulation (Hirsh, 2017). Direct connections between ECM components, such as fibronectin, and pyrimidine metabolism are limited. However, there is evidence that integrin signaling may influence pyrimidine metabolism by promoting cell proliferation through engagement of cell cycle progression via Cyclin D1-associated signaling (e.g. Integrin linked kinase (ILK), PI3K, ERK, and Rac signaling) (Cruet-Hennequart et al., 2003; Schwartz and Assoian, 2001). This is in addition to the cell division-independent, pro-migratory role of the pyrimidine metabolism enzyme thymidylate synthase, which converts dUMP to dTMP for incorporation into DNA nucleotides (Siddiqui et al., 2017; Siddiqui et al., 2019).

Metabolic adaptations and environmental cues have also been shown to influence pyrimidine metabolism. Nutrient availability and energy status is critical during early embryogenesis as the energy-intensive process of gastrulation requires adjustments in metabolism to maintain ATP levels (Fujiwara et al., 2016; Zotin et al., 1967). Furthermore, pyrimidine biosynthesis is an energy-demanding process, so cells may regulate pyrimidine production based on nutrient availability (Moffatt and Ashihara, 2002; Reaves et al., 2013). The mechanistic Target Of Rapamycin (mTOR) signaling pathway senses nutrient status and coordinates cell growth in a variety of contexts,

including during gastrulation (Jewell and Guan, 2013; Murakami et al., 2004). Notably, mTOR signaling potently drives pyrimidine synthesis thereby coordinating cell growth with available resources (Ben-Sahra et al., 2013; Robitaille et al., 2013). Purine metabolism must also be coordinated as purine and pyrimidine biosynthesis are closely regulated with both types of nucleotides being required in balanced amounts for nucleic acid synthesis (Gots, 1971; Tatibana, 1978). Coordination between purine and pyrimidine synthesis pathways ensures the availability of nucleotides necessary for the high rates of cell proliferation and RNA transcription present in gastrulation (Gurdon and Brown, 1965; Surrey et al., 1979).

Growth factor signaling present during gastrulation may also present implications for pyrimidine metabolism. The Wnt, Fibroblast growth factor (FGF), and Bone morphogenetic protein (BMP) pathways are among the most critical for helping orchestrate the morphogenetic processes of gastrulation (Roszko et al., 2009; Steventon et al., 2009; Streit et al., 2000). These pathways are regulators of cell division, growth, and differentiation which in turn can affect pyrimidine metabolism (Chen et al., 2012; Dailey et al., 2005). For example, the Wnt pathway is known to influence cellular metabolism and may upregulate nucleotide synthesis pathways, including pyrimidine biosynthesis, to support proliferating cells (Gong et al., 2004; Karner and Long, 2017). The influence of growth factor signaling on transcriptional regulation is also notable with transcription factors such as MYC being activated by growth factor signaling during gastrulation (Adhikary et al., 2003; Kelly et al., 1983). MYC activation can increase the expression of enzymes in the pyrimidine biosynthetic pathway thereby enhancing nucleotide availability during rapid cell proliferation (Liu et al., 2008; Mannava et al.,

2008). In sum, while the ties between pyrimidine metabolism and gastrulation remain poorly defined, our metabolomic findings along with the studies presented herein support a potential role for nucleotide metabolism in enabling the extensive tissue rearrangements and growth required during gastrulation.

**Aromatic amino acid biosynthesis**

Our metabolomic analyses identified enrichment of metabolites related to the biosynthesis of phenylalanine, tyrosine, and tryptophan, which are the aromatic amino acids (AAAs) (Nelson and Cox, 2008). Of the three AAAs, processes related to phenylalanine metabolism followed by tyrosine were most statistically significant. Notably, these are essential amino acids for animals, therefore they must be obtained through diet (Nelson and Cox, 2008). The shikimate pathway found in plants, fungi, and microorganisms is responsible for synthesis of these essential amino acids that contribute to the production of proteins, neurotransmitters, hormones, and other compounds (Figure 4.5) (Bentley, 1990; Herrmann and Weaver, 1999).

Briefly, the shikimate pathway is a seven-step metabolic route that produces the chorismate molecule, a precursor for phenylalanine, tyrosine, and tryptophan (Herrmann, 1995b; Weaver and Herrmann, 1997). In this pathway phosphoenolpyruvate from glycolysis and erythose-4-phosphate from the pentose phosphate pathway combine to form D-arabino-heptulosonate-7-phosphate (DAHP) via DAHP synthase catalysis (Heimhalt et al., 2021; Herrmann, 1995a). DAHP undergoes several steps to convert it to shikimate-3-phosphate and then chorismate (Macheroux et al., 1999; Walsh et al., 1990). From chorismate the AAAs can be produced through branching metabolic pathways with

the production of phenylalanine and tyrosine sharing the common branch of converting chorismate to prephenate (Hur and Bruice, 2003; Kast et al., 1997). For phenylalanine production, prephenate undergoes a decarboxylation reaction that produces phenylpyruvate which can then be converted to phenylalanine (Pascual et al., 2016; Tohge et al., 2013). In the production of tyrosine, prephenate is converted to p-hydroxyphenylpyruvate which can be further processed to form tyrosine (Holland and Jez, 2018; Siehl et al., 1986). For tryptophan synthesis, chorismate is converted to anthranilate in the first committed step (Dosselaere and Vanderleyden, 2001; Poulsen and Verpoorte, 1991). Anthranilate then goes through several enzymatic steps to form tryptophan, including the formation of indole-3-glycerol phosphate, which is an intermediate that cyclizes to yield tryptophan (Ouyang et al., 2000; Weyand and Schlichting, 1999). Ultimately, consumption of plants, fungi, and microorganisms which produce these AAAs allows for the incorporation of essential amino acids into the biochemical processes of animals, such as *Xenopus* laevis and humans.

**Aromatic amino acid metabolism**

Although animals cannot synthesize the AAAs, they are extensively metabolized to produce other critical biomolecules (Han et al., 2019; Strauss and Strauss, 2012). In the case of phenylalanine metabolism, phenylalanine is primarily converted into tyrosine through the action of phenylalanine hydroxylase and its cofactor tetrahydrobiopterin ($BH_4$) in the liver (Figure 4.6) (Flydal and Martinez, 2013; Kobe et al., 1999). Once converted to tyrosine, it can serve as a precursor for catecholamine neurotransmitters through the hydroxylation of tyrosine to L-DOPA, which is a precursor to dopamine, with

further conversion into norepinephrine and epinephrine to support central nervous system signaling and responses to stress (Figure 4.6) (Fernstrom and Fernstrom, 2007; Gnegy, 2012). Tyrosine is also critical for the regulation of metabolism, growth, and development through its conversion to thyroid hormones thyroxine (T4) and triiodothyronine (T3) in the thyroid gland (Hulbert, 2000; Mondal et al., 2016). Tyrosine is converted to melanin in melanocytes thereby influencing pigmentation (Riley, 1997; Slominski et al., 2004). Excess tyrosine can be degraded via the Krebs cycle for energy production (Holme, 2003; Holme and Mitchell, 2014). In the tyrosine degradation pathway tyrosine is catalytically converted into p-hydroxyphenylpyruvate via tyrosine aminotransferase (Granner and Tomkins, 1970; Hayashi et al., 1967). P-hydroxyphenylpyruvate is then converted to homogentisate by p-hydroxyphenylpyruvate dioxygenase (Lee et al., 1997; Ohisalo et al., 1982). Homogentisate is metabolized into maleylacetoacetate by homogentisate 1,2-dioxygenase which is then converted by maleylacetoacetate isomerase to fumarylacetoacetate (Amaya et al., 2004; Fernández-Cañón and Peñalva, 1998). Finally, fumarylacetoacetate is broken down into fumarate and acetoacetate by the enzyme fumarylacetoacetate hydrolase (Stančíková and Rovenský, 2015; St-Louis and Tanguay, 1997). These metabolites are critical for energy production as fumarate can enter the citric acid cycle which supports energy production in the form of ATP and acetoacetate can be converted into acetyl-CoA to be used in ketone body synthesis or energy production in the citric acid cycle (Alabduladhem and Bordoni, 2024; Moffett et al., 2020).

Like phenylalanine and tyrosine, as tryptophan cannot be synthesized in animals, it undergoes extensive metabolism to produce a variety of biomolecules (Figure 4.7)

(Nelson and Cox, 2008; Tymoczko, 2007). Approximately 95% of tryptophan metabolism occurs through the Kynurenine pathway in the liver (Badawy, 2017; Savitz, 2020). To initiate this pathway tryptophan is oxidized to formylkynurenine by either indoleamine 2,3-dioxygenase (IDO), which is found in immune cells and activated under inflammatory conditions, or tryptophan 2,3-dioxygenase (TDO), which is found in the liver and regulated by glucocorticoids and tryptophan levels (Munn and Mellor, 2013; Thackray et al., 2008). In turn, formylkynurenine is converted to kynurenine by formidase (Ala, 2021; Moore and Sullivan, 1975). At this point kynurenine can be converted to 3-hydroxykynurenine for production of 3-hydroxyanthranilic acid which leads to formation of quinolinic acid, a Nicotinamide Adenine Dinucleotide ($NAD^+$) synthesis precursor (Guillemin and Brew, 2002; Heyes et al., 1992). The coenzymes NAD and Nicotinamide Adenine Dinucleotide Phosphate ($NADP^+$) participate in the energy metabolism of glycolysis, the citric acid cycle, and oxidative phosphorylation (VanLinden et al., 2015; Yang and Sauve, 2016). Alternatively, kynurenine can be metabolized through a minor pathway branch into anthranilic acid or metabolized into kynurenic acid, a neuroprotective metabolite that serves as an antagonist at glutamate and N-methyl-D-aspartate receptors (Moroni et al., 2012; Wiklund and Bergman, 2006). Accounting for 1-2% of tryptophan metabolism is the serotonin pathway which occurs predominately in the gut, brain, and pineal gland (O'Mahony et al., 2015; Young and Leyton, 2002). First, tryptophan is hydroxylated by tryptophan hydroxylase to form 5-hydroxytryptophan (McKinney et al., 2005; Walther et al., 2003). Next, 5-hydroxytryptophan is converted to 5-hydroxytryptamine (i.e. serotonin) by aromatic L-amino acid decarboxylase (Brun et al., 2010; Sumi-Ichinose et al., 1992). Serotonin is a

neurotransmitter that regulates mood, appetite, and sleep in addition to modulating gut motility and secretion in the gastrointestinal system (Berger et al., 2009; Mohammad-Zadeh et al., 2008). In the pineal gland through further acetylation and methylation serotonin can form melatonin, an antioxidant and hormone critical for the regulation of circadian rhythm (Huether et al., 2012; Slominski et al., 2002). In addition to these major pathways, gut microbiota can degrade tryptophan into indole, which contributes to intestinal health and signaling through the aryl hydrocarbon receptor (Fiore and Murray, 2021; Hubbard et al., 2015). Alternatively, tryptophan can be decarboxylated into tryptamine, a precursor for serotonin and melatonin (Coppen et al., 1965; Tittarelli et al., 2015). This is in addition to tryptamine's function in the brain as a trace amine that binds to trace amine-associated receptors (TAARs) (Gainetdinov et al., 2018; Zucchi et al., 2006).

**Aromatic amino acid metabolism in gastrulation**

The metabolism of aromatic amino acids serves to support the metabolically demanding processes of gastrulation which include formation of the three germ layers, cell migration, cell proliferation, and cellular differentiation (Gustafson and Hjelte, 1951; Keller et al., 2003). In support of energy metabolism required for these processes, the kynurenine pathway converts tryptophan into energy intermediates like $NAD^+$, a crucial coenzyme for various steps in cellular respiration (Badawy, 2017; Castro-Portuguez and Sutphin, 2020). During glycolysis, $NAD^+$ acts as an electron acceptor in the conversion of glyceraldehyde-3-phosphate (G3P) to 1,3-bisphosphoglycerate (Chandel, 2021a; Chaudhry and Varacallo, 2024). Through this process $NAD^+$ is reduced to NADH which

later contributes to the electron transport chain (ETC) (Nelson and Cox, 2008; Tymoczko, 2007). In pyruvate oxidation taking place in the mitochondrial matrix, $NAD^+$ accepts electrons to form NADH to support the conversion of pyruvate to acetyl-CoA by the pyruvate dehydrogenase complex (Patel and Korotchkina, 2006; Patel et al., 2014). Throughout various steps of the citric acid cycle $NAD^+$ is reduced to NADH which carries high energy electrons to the ETC and supports the oxidation of acetyl-CoA (Wu et al., 2016; Ying, 2006). These citric acid cycle reactions include conversion of isocitrate to α-ketoglutarate via isocitrate dehydrogenase, α-ketoglutarate to succinyl-CoA via α-ketoglutarate dehydrogenase, and malate to oxaloacetate via malate dehydrogenase (Akram, 2014; Williamson and Cooper, 1980). In oxidative phosphorylation NADH donates electrons to Complex I (i.e. NADH dehydrogenase) of the ETC (Walker, 1992; Weiss et al., 1992). This is critical as the donated electrons move through the ETC and generate a protein gradient across the inner mitochondrial membrane which can drive ATP synthesis via ATP synthase (Hinkle and McCarty, 1978; Orgel, 1999). Ultimately, $NAD^+$ is regenerated which allows for its reuse in the earlier steps of cellular respiration (van der Donk and Zhao, 2003; Wu et al., 2013). Aromatic amino acids further support energy metabolism through phenylalanine and tyrosine conversion into fumarate and acetoacetate, which feed into the citric acid cycle for ATP production (Mazelis, 1980; Yanamadala, 2024). More specifically, fumarate is converted into malate by fumarase (i.e. fumarate hydratase) through the addition of a water molecule in the citric acid cycle (Pollard et al., 2003; Schmidt et al., 2020). Acetoacetate can be converted into acetyl-CoA by succinyl-CoA:acetoacetate CoA-transferase (SCOT) in extrahepatic tissues

which can then enter the citric acid cycle (Niezen-Koning et al., 1997; Pérez-Cerdá et al., 1992).

Aromatic amino acids and their metabolites are also notable for their contributions to morphogens and growth factor regulation critical for patterning during gastrulation (Chen, 1956; Gustafson and Hjelte, 1951). While still poorly understood, serotonin, which is derived from tryptophan, acts as a morphogen in early development to establish left-right asymmetry and germ layer specification (Buznikov et al., 2001; Fukumoto et al., 2005). This morphogenesis is accomplished by serotonin influencing the movements of mesodermal and ectodermal cells to help establish the body axis (Colas et al., 1999; Palén et al., 1979). Notably, serotonin regulates the expression of genes like Nodal and Lefty, which are key to the establishment of left-right asymmetry (Kawasumi et al., 2011; Vandenberg et al., 2013). Notably, serotonin acts through concentration gradients to provide positional information, influencing cell fate and tissue organization (Keyes and Rudnick, 1982; Rudnick and Sandtner, 2019). These gradients are established by serotonin synthesis (via tryptophan hydroxylase) and regulated by uptake and release mechanisms involving serotonin transporters (SERT) (Adnot et al., 2013; Hasegawa and Nakamura, 2010). It is also thought that serotonin affects epithelial-to-mesenchymal transition which is a key process in the tissue invagination and migration of gastrulation (Karmakar and Lal, 2021; Li et al., 2024a). Phenylalanine and tyrosine metabolism have also been shown to influence FGF and transforming growth factor-beta (TGF-β) signaling pathways, which are critical for gastrulation (Dolivo et al., 2018; Karamichos et al., 2015).

With a growing appreciation for the importance of reduction-oxidation (redox) homeostasis and antioxidant defense to gastrulation, the participation of aromatic amino acids in these processes have been reconsidered (Harvey et al., 2002; Timme-Laragy et al., 2018). For example, reactive oxygen species (ROS), particularly hydrogen peroxide ($H_2O_2$), act as second messengers in signaling pathways that influence gastrulation processes like cell migration, epithelial-to-mesenchymal transition (EMT), and tissue remodeling (Dunnill et al., 2017; Rhyu et al., 2005; Wang et al., 2011). Spatial and temporal ROS gradients have been shown to be critical for coordinating morphogenetic movements during gastrulation (Baxi et al., 2024; Narayanan et al., 2021). Tryptophan metabolism intersects with these processes as tryptophan generates $NAD^+$, which supports redox balance by facilitating oxidative phosphorylation and protecting cells from ROS (Kushnareva et al., 2002; Li and Sauve, 2015). It is also thought that phenylalanine and tyrosine derivatives, such as dopamine or other catecholamines, may indirectly contribute to cellular redox homeostasis by modulating oxidative stress responses (Costa et al., 2011; Juárez Olguín et al., 2016). In sum, aromatic amino acid metabolism plays a critical role in influencing the energy metabolism, morphogens, and oxidative stress response of gastrulation.

**Mesendoderm metabolism**

As the samples prepared in this chapter were derived from the lysates of whole embryos, the metabolomic results presented in this chapter did not reflect fibronectin-dependent changes in the metabolism of mesendoderm alone. However, some recent studies on mesendoderm differentiation outside of *Xenopus laevis* highlight the potential

role of metabolism on mesendoderm function. As cells transition from pluripotency to mesendoderm, mitochondria undergo structural and functional changes that lead to an increasing reliance on oxidative phosphorylation to meet energy demands (Miyazawa et al., 2022). In further support of a rise in glycolytic flux at gastrulation (Dworkin and Dworkin-Rastl, 1989; Dworkin and Dworkin-Rastl, 1991), mesendoderm cells exhibit Warburg effect-like metabolism with high glycolytic flux even in the presence of oxygen to rapidly generate of ATP and produce metabolic intermediates (Mostafavi et al., 2021).

In addition to Wnt/β-catenin signaling serving as a well-established regulator of mesendoderm differentiation (Rodaway and Patient, 2001; Wang et al., 2017), activation of this pathway enhances glycolysis (Oginuma et al., 2017; Pate et al., 2014). Inhibition of glycolysis can prevent the upregulation of primitive streak markers, resulting in a significant increase in ectodermal cell populations with a reduction of mesodermal and endodermal lineages and downregulation of Wnt, Nodal, and Fgf signaling (Stapornwongkul et al., 2023). Furthermore, during the process of mesendoderm differentiation via Activin/TGF-β activation (Fei et al., 2010; Wang and Chen, 2016), markedly upregulated expression of fatty acid oxidation genes, such as aldehyde dehydrogenase 3 family member A2, is detected (Xu et al., 2018). Vascular Endothelial Growth Factor (VEGF) signaling through the MEK-ERK cascade is critical for mesendoderm differentiation (Na et al., 2010; Xin et al., 2021) and may serve to upregulate glycolytic flux in a variety of tissues (Kivelä et al., 2014; Través et al., 2012). Taken together, these studies on mesendoderm differentiation and their possible connections highlight a possible role for glycolytic activity in mesendoderm function.

**Future directions and limitations**

The metabolomic results presented herein highlight potential links between the metabolism of pyrimidines and aromatic amino acids with fibronectin influenced critical processes in gastrulation like cell migration, differentiation, and division. However, these results remain limited in a few ways. Therefore, we propose some future studies to address these limitations.

While we prepared four samples of FNMO and COMO embryos for analysis, the quality control step eliminated one of the FNMO samples resulting in the analysis of only three FNMO samples. These samples were all prepared from the same clutch, therefore the biological variability encountered between *Xenopus* embryo fertilizations was not present in this experiment (Leibovich et al., 2022; von Dassow and Davidson, 2009). Notably, when the log2 fold change was calculated for the metabolites in COMO relative to FNMO, the adjusted p-value failed to produce any statistically significant results. This suggests that a greater number of samples is required to properly power the analyses and detect differences in metabolites present in the FNMO and COMO groups. Therefore, a future direction for our metabolomic studies would be to increase the number of biological replicates produced for analysis.

While we prepared samples of whole embryos for analyses, regional differences in metabolism of the embryo are lost through our present approach. Preparation of various tissue types will provide a better understanding of the heterogeneous metabolic mechanisms found in the embryo gastrula (Hu and Yu, 2017; Zhao et al., 2021). This would allow for an identification of the metabolic processes that support different tissue movements (e.g. mesendoderm migration, convergent extension, epiboly, etc.). As has

been demonstrated for the mid-blastula transition period in *Xenopus*, the metabolic processes of early embryogenesis are highly dynamic (Vastag et al., 2011). Therefore, we aim to isolate and submit tissues from different germ layers during different timepoints in gastrulation to better understand the metabolic programs employed by different embryonic tissues and how different developmental processes are linked to metabolism.

Assuming subsequent untargeted mesendoderm metabolomic results are consistent with the preliminary result of pyrimidine and aromatic amino acid metabolism being altered by fibronectin-integrin adhesion, it will be critical to employ a more targeted approach for these pathways. Even with expanded biological and technical replicates, the analysis presented in this chapter of untargeted profiling and relative quantification support only limited inferences of metabolic pathway flux. However, in targeted metabolomic quantification the analysis is focused on a specific set of metabolites using internal and external standards to achieve absolute quantification. By using isotopically labeled internal standards for precise measurements, this absolute quantification allows for the determination of pathway flux.

As an initial step it would be helpful to measure the conversion of intermediates at rate-limiting steps of pyrimidine and aromatic amino acid metabolism to identify potential differences in that metabolic enzyme activity due to fibronectin-integrin adhesion. In the case of pyrimidine metabolism, the CPSII reaction serves as a rate limiting step that could be examined using targeted metabolomics (Figure 4.4) (Löffler et al., 2005). To extend the findings to mesendoderm migratory function, the migratory velocity of explanted mesendoderm could be examined in the presence of a CPSII activator, such as phosphoribosyl pyrophosphate, or inhibitor, such as UTP (Wang et al.,

2021b). In aromatic amino acid metabolism, phenylalanine hydroxylase is the rate limiting step of phenylalanine and tyrosine conversion and could also be examined using targeted metabolomics of mesendoderm from FNMO and COMO embryos (Figure 4.6) (Flydal and Martinez, 2013). To examine the role of phenylalanine hydroxylase in mesendoderm function, migratory mesendoderm could be treated with activators or inhibitors of enzymatic activity, such as sapropterin or oudenone, respectively (Burton et al., 2008; Koizumi et al., 1982). As the rate limiting step of tryptophan metabolism is catalyzed by TDO, this enzymatic reaction could be a good initial candidate for targeted evaluation of metabolic flux (Figure 4.7) (Thackray et al., 2008). While small molecule inhibitors of TDO are developed (e.g. 680C91), direct activators of TDO remain limited for potential future use in functional mesendoderm studies (Pilotte et al., 2012; Salter et al., 1995).

Finally, while these initial metabolomics studies did not detect differences between FNMO and COMO samples, there is strong evidence for the role of glycolytic flux in mesendoderm differentiation. One initial step would be to evaluate the spatial distribution of the fluorescent d-glucose analog 2-[N-(7-nitrobenz-2-oxa-1,3-diazol-4-yl) amino]-2-deoxy-D-glucose (2-NBDG) in live mesendoderm (Zou et al., 2005). This would allow us to begin an investigation into the contribution of integrin adhesion and traction stress to glycolytic flux, similar to the studies conducted in Chapter 2. Using targeted metabolomics we can evaluate differences in the enzymatic conversion of Fructose-6-phosphate to Fructose-1,6-bisphosphate by phosphofructokinase-1 (PFK-1), the rate-limiting step of glycolysis (Mor et al., 2011). Furthermore, we can evaluate the

effects of PFK-1 activity on mesendoderm migration through activators and inhibitors of PFK-1, such as Fructose-2,6-bisphosphate and citrate, respectively.

The present metabolomic analyses suggest an examination of pyrimidine and aromatic amino acid metabolism in the processes of gastrulation. Recent work on the role of glycolysis mesendoderm differentiation highlights a possible role for glycolytic flux in mesendoderm function. To accomplish these future studies we propose an expansion in the number and diversity of tissues samples used for untargeted metabolomic analysis. However, these untargeted studies should be paired with targeted studies that examine the metabolic flux of the rate limiting enzymatic steps of the identified metabolic programs. Furthermore, modulation of rate limiting enzymatic function will allow us to better understand the role of these metabolic processes in collective mesendoderm migration. In sum, these proposed studies will allow for a clearer understanding of the connections between metabolism and cell migration.

**Conservation of integrin-FAK function in mammalian cells**

As noted in Chapter 2, we examined the response of the OCR in a variety of mammalian cells to FAK inhibition on fibronectin and pol-l-lysine substrates (Figure 2.9). However, a thorough discussion of these results was excluded from the published work of Chapter 2 due to journal text contraints. Here is a more complete consideration of the results.

The diversity in the integrin expression profiles of the tissues studied is an important consideration. For example, terminally differentiated cells such as macrophages express various integrins that are essential for their roles in adhesion,

migration, phagocytosis, and signaling in response to environmental cues (Berton and Lowell, 1999; Dupuy and Caron, 2008). Some key integrin receptors macrophages express include αMβ2 (CD11b/CD18, also known as Mac-1 or CR3), αXβ2 (CD11c/CD18, also known as CR4), αLβ2 (LFA-1, CD11a/CD18), αDβ2 (CD11d/CD18), α4β1 (VLA-4), α5β1, αVβ3, and αVβ5 (Gordon and Plüddemann, 2017; McWhorter et al., 2015; Rosales and Uribe-Querol, 2017). Poorly differentiated cells from immortalized cancer cell lines, such as HeLa cells, express a range of integrins to support their adhesion to various extracellular matrix components and engage in signaling pathways that regulate growth, survival, and motility which are critical for cancer progression (Hamidi and Ivaska, 2018; Hanahan and Weinberg, 2011). The integrins commonly expressed by HeLa cells include α5β1, αvβ3, α6β1, αvβ5, and α3β1 (Bazzoni and Hemler, 1998; Bergman et al., 1995; Sieg et al., 1999). Precursor cells, such as myoblasts, also express a distinct set of integrin receptors that enable interactions with the extracellular matrix and other cells and guide processes like migration, fusion, and differentiation into mature myofibers that are essential for muscle development and regeneration (Abmayr and Pavlath, 2012; Lehka and Rędowicz, 2020). The key integrins expressed by myoblasts include α7β1, α5β1, αvβ3, α6β1, and α4β1 (Boettiger et al., 1995; Boppart et al., 2006; Gullberg et al., 1998; Rozo et al., 2016)

While mesendoderm, iMAC, and myoblast cells demonstrated an OCR that is responsive to the FAK inhbitors when on fibronectin, HeLa cells show differences in their response to the two FAK inhibitiors tested. Differences in the pharmacology of PF-573,228 and PF-562,271 could explain this disparity. PF-573,228 is a small-molecule ATP-competitive inhibitor of FAK that binds to the ATP-binding site within the kinase

domain of FAK which prevents ATP from accessing the active site (Schaller, 2010; Slack-Davis et al., 2007). This inhibits FAK's kinase activity thereby blocking its ability to phosphrylate itself and other substrates that are critical for downstream signaling (Cohen and Guan, 2005; Hauck et al., 2002). One of the critical phosphorylation sites on FAK is tyrosine 397 (Y397) which is essential in the production of a binding site for Src family kinases and other signaling proteins (Calalb et al., 1995; Hamadi et al., 2005). PF-573, 228 blocks the autophosphorylation of Y397, thereby disrupting further downstream signaling interactions that are dependent on the phosphorylation site (Corsi et al., 2009; Sulzmaier et al., 2014). PF-573, 228 blocks the activation of several downstream pathways that rely on FAK activity, including the PI3K/Akt and Mitogen-activated protein kinase (MAPK)/Extracellular signal-regulated kinase (ERK) pathways (Kallergi et al., 2007; Lin et al., 1997). Finally, PF-573,228 disrupts the assembly and disassembly of focal adhesions, hindering cell migration and potentially reducing cancer cell invasion (Parsons et al., 2007). While PF-562,271 shares many similarities to PF-573,228, it differs in some key ways as a potent, ATP-competitive inhibitor of both FAK and proline-rich tyrosine kinase 2 (Pyk2) (Golubovskaya and Cance, 2011; Roberts et al., 2008). Pyk2 is a FAK-related kinase involved in similar cellular pathways (Murphy et al., 2016; Sieg et al., 1998). Given the dual inhibition of FAK and Pyk2 resulting in a broader disruption of cell signaling by PF-562,271, its efficacy in reducing the tumor growth and metastasis of *in vivo* models has led to its greater success in preclinical and clinical studies for anti-cancer therapy compared to PF-573,228 (Bagi et al., 2009; Stokes et al., 2011). Based on these differences, it is possible that differences in the relative abundance

and activity of FAK to Pyk2 could underlie the differences in OCR response to inhibition by PF-573,228 and PF-562,271.

## Conclusions

Cell migration and adhesion can be adapted or dysregulated in different physiological and pathological contexts, such as wound healing and cancer metastasis. By investigating the process of collective cell migration in the context of embryo morphogenesis we hope to gain a better understanding of diseases that may rely on these same mechanisms. The work in this dissertation focuses on the interplay between adhesive signaling and metabolic processes, using collectively migrating *Xenopu*s laevis mesendoderm as a model. My work demonstrates a connection between ECM-integrin adhesion and mitochondrial metabolism during collective cell migration. Increased mitochondrial activity, driven by oxidative phosphorylation, is observed at the leading edge of mesendoderm where **α**5β1 integrin traction is strongest. This process depends on integrin activation and subsequent integrin-FAK signaling to enhance ATP production needed for migration. My expanded studies reinforce the intersection of mitochondrial metabolism with collective migration. For example, I demonstrate the impact of aconitase, a citric acid cycle enzyme, function on mesendoderm migration. I also show that integrin-FAK signaling is critical for mitochondrial activity across different human tissues. Mesendoderm with ligand activated integrins or mechanically activated integrins near protrusions in cell clusters reveal mitochondria with high membrane potential. We observe clustering of mitochondria near the leading edges of mesendoderm cells in the tissue or in cell clusters. Moreover, integrin activation fails to affect rates of

mitochondrial biogenesis or degradation on the timescale of gastrulation. This is in addition to our observation of accumulations of mitochondria close to C-Cadherin adhesions in dissociated cells. To provide deeper insights into the role of metabolism in adhesive processes I conduct preliminary metabolomics studies on *Xenopus laevis* gastrulae with FNMO (and COMO) knockdown. Using UHPLC-MS/MS for metabolite detection and quantification the PCA plots show clear separation between FNMO and COMO samples. Pathway enrichment analysis identify pyrimidine and aromatic amino acid metabolic processes as the top metabolite sets affected by fibronectin knockdown. This ultimately suggests that the highlighted metabolic processes may be connected to integrin-associated metabolism during gastrulation. Together, the data I present in this thesis helps highlight the role of integrin-linked metabolism in the process of collective cell migration and adhesion. Ultimately, my studies further develop the relationship between bioenergetics and mechanically coupled processes.

**A**

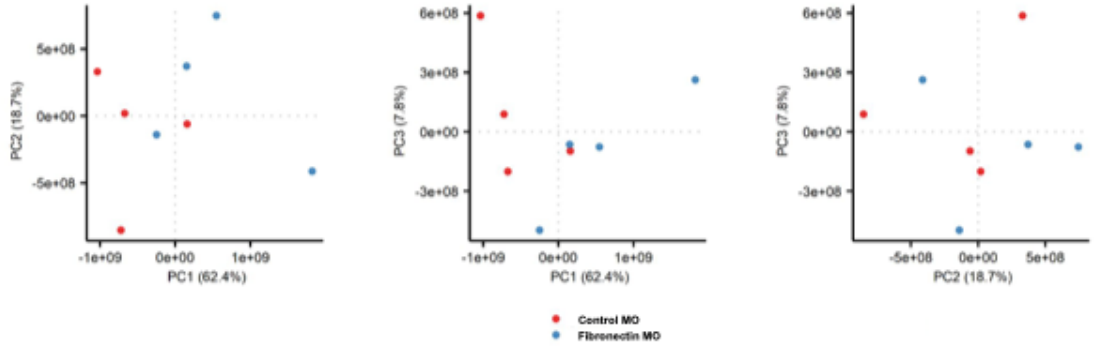
PC2 (18.7%)
PC1 (62.4%)
PC3 (7.8%)
PC1 (62.4%)
PC3 (7.8%)
PC2 (18.7%)
Control MO
Fibronectin MO

**B**

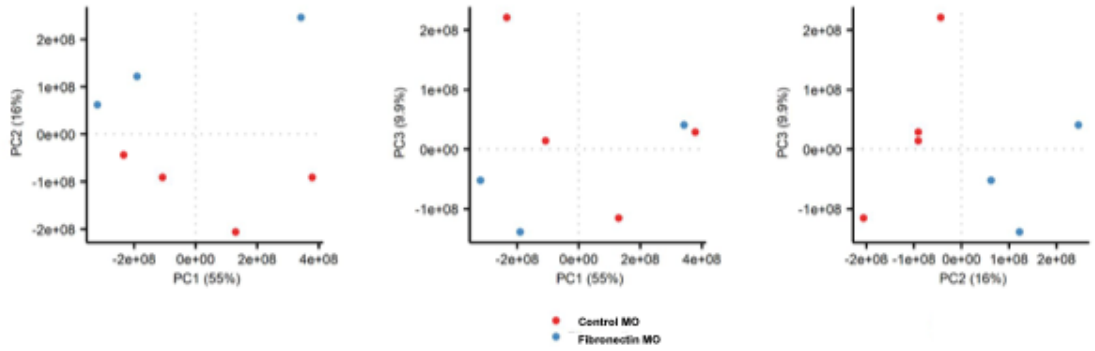
PC2 (16%)
PC1 (55%)
PC3 (9.9%)
PC1 (55%)
PC3 (9.9%)
PC2 (16%)
Control MO
Fibronectin MO

**Figure 4.1: Principal components analysis (PCA) of Fibronectin and Control morpholino (MO) injected *Xenopus* laevis embryos**

PCA plots are segregated based on the polarity option of the ionization mode used in tandem mass spectrometry, positive (A) or negative (B). The PCA plots include three Fibronectin MO injected samples compared to four Control MO injected samples.

A

| Name of metabolite | Fold change COMO:FNMO | P-Value |
|---|---|---|
| 2'-Deoxycytidine | 1.727504878 | 0.00038145 |
| PC-DAG (16:0/18:3) | 0.223934952 | 0.0131042 |
| N-alpha-Acetyl-L-arginine | 0.619879122 | 0.01358898 |
| S-Lactoylglutathione | 13.36239873 | 0.01722484 |
| O-(2-tetradecenoyl)carnitine | 1.341508184 | 0.01791975 |
| 3-Hydroxybutyrylcarnitine | 0.409058279 | 0.0269395 |
| 2-Methylbutyryl-L-carnitine | 1.961840134 | 0.02945384 |
| Acetyl-DL-carnitine | 0.541445693 | 0.03991828 |
| Isobutyryl-L-carnitine | 0.299039676 | 0.04047913 |
| Thymidine-5'-phosphate | 0.291445841 | 0.04526704 |
| 2'-Deoxyadenosine-5'-monophosphate | 0.437778191 | 0.04776869 |

B

| Name of metabolite | Fold change COMO:FNMO | P-Value |
|---|---|---|
| 2'-Deoxycytidine | 1.645499309 | 0.00048728 |
| Tyrosine | 1.403434277 | 0.00722343 |
| N-Acetylleucine | 1.920734569 | 0.00751763 |
| 1,3-Benzothiazole-2-sulfonic acid | 0.505469799 | 0.00810646 |
| 3,3-Dimethyl-2-oxobutanoic acid | 3.151508317 | 0.0291962 |
| 3-methyl-2-oxovalerate | 8.787699618 | 0.03235505 |
| Tyrosine | 1.797480094 | 0.03317818 |
| 2-Hydroxybutyric acid | 1.758464151 | 0.03708766 |
| 3-Oxopentanoic acid | 2.868010935 | 0.03786298 |
| 2'-Deoxyadenosine-5'-monophosphate | 0.437995504 | 0.04282683 |
| 2-Hydroxy-2-methylbutyric acid | 1.967320909 | 0.04432431 |
| Glutathione | 1.209117274 | 0.04945167 |

**Figure 4.2: Metabolites presenting differential abundance in fibronectin and control MO embryos.**

Metabolites are separated by the ionization mode used for identification (i.e. positive (A) or negative (B)). The relative fold change in metabolite abundance between Control MO (COMO) and Fibronectin MO (FNMO) is presented with the respective t-test p-values.

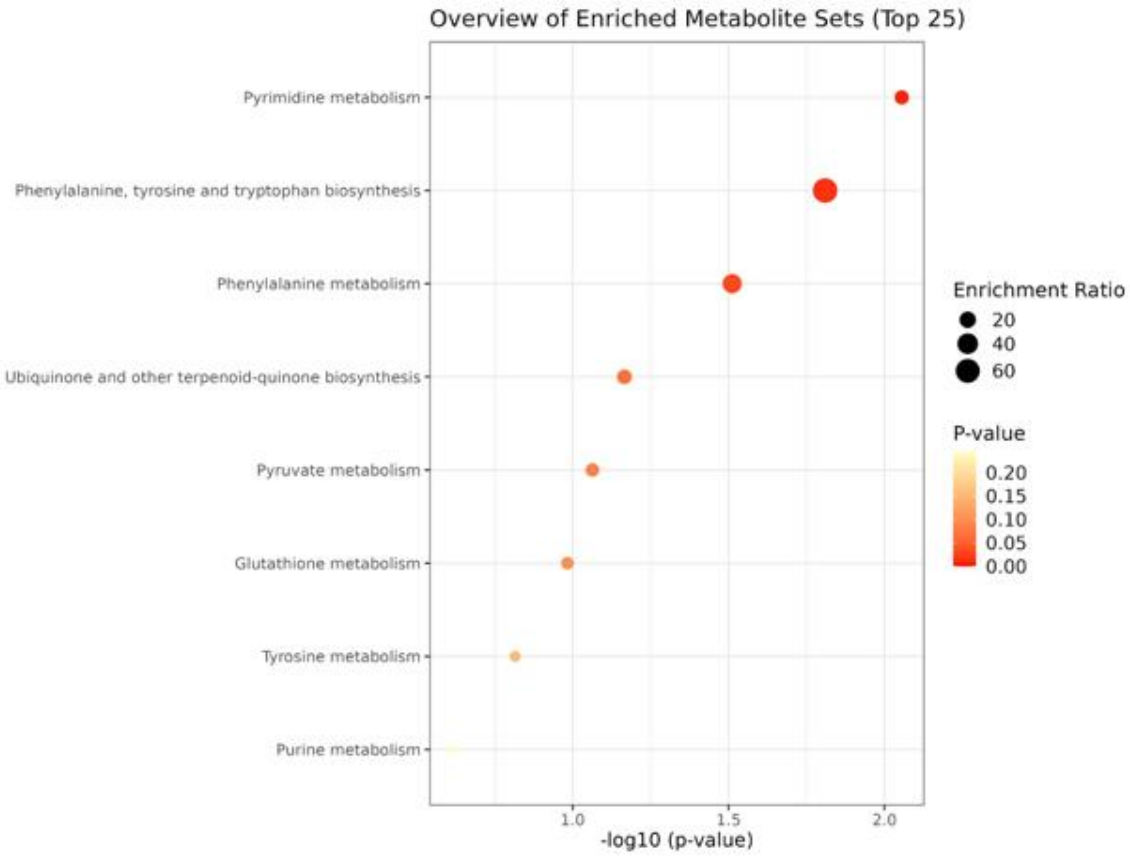
Overview of Enriched Metabolite Sets (Top 25)
Pyrimidine metabolism
Phenylalanine, tyrosine and tryptophan biosynthesis
Phenylalanine metabolism
Ubiquinone and other terpenoid-quinone biosynthesis
Pyruvate metabolism
Glutathione metabolism
Tyrosine metabolism
Purine metabolism
1.0
1.5
2.0
-log10 (p-value)
Enrichment Ratio
20
40
60
P-value
0.20
0.15
0.10
0.05
0.00

**Figure 4.3: Enrichment analysis of annotated metabolites**

Using Metaboanalyst 6.0, the annotated significant metabolites presenting in Figure 4.2 were submitted for enrichment analysis. Enriched metabolite sets related to a variety of metabolic processes. A relative enrichment ratio and p-value were computed for each identified process.

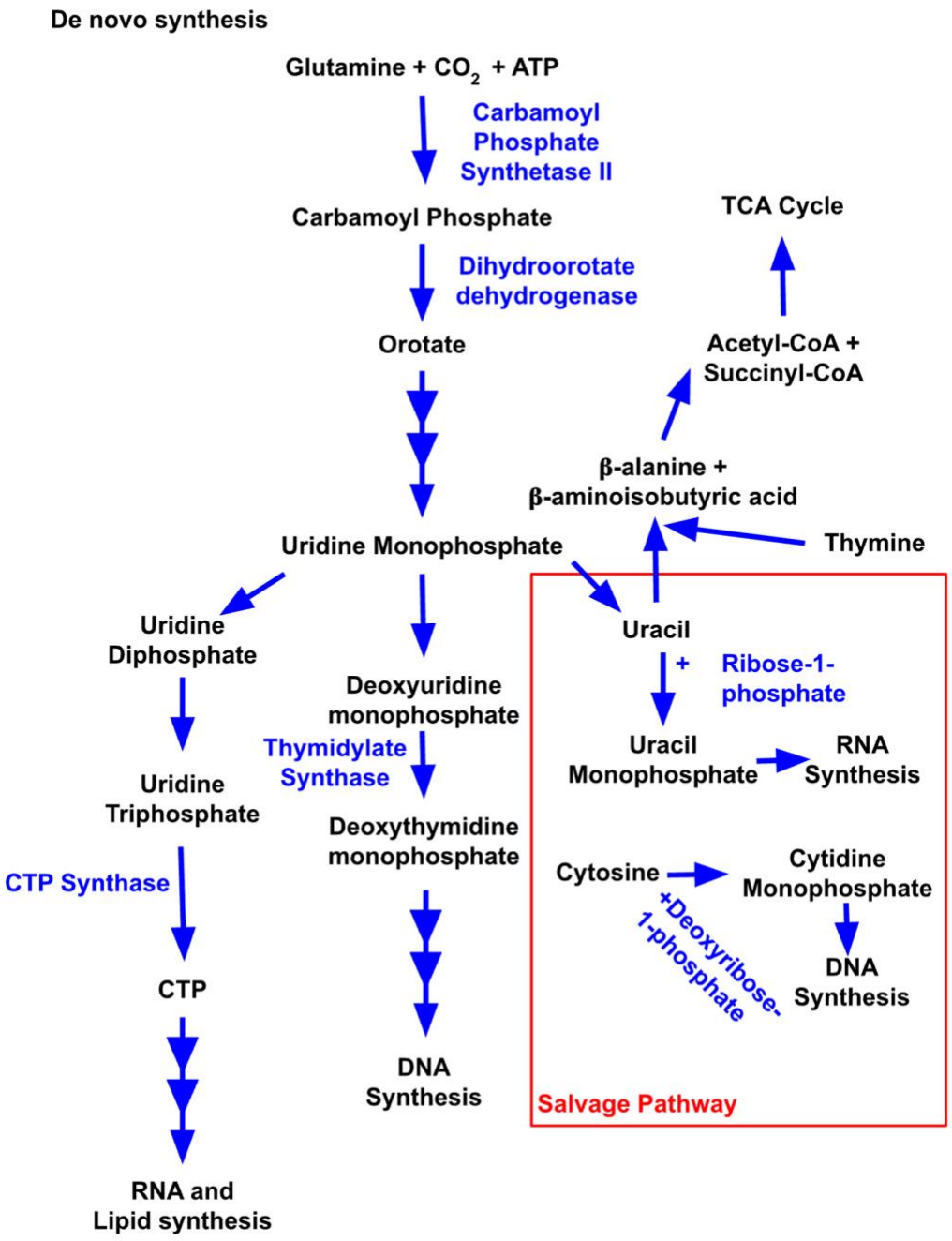
De novo synthesis
Glutamine + $CO_2$ + ATP
Carbamoyl Phosphate Synthetase II
Carbamoyl Phosphate
Dihydroorotate dehydrogenase
Orotate
TCA Cycle
Acetyl-CoA + Succinyl-CoA
β-alanine + β-aminoisobutyric acid
Thymine
Uridine Monophosphate
Uridine Diphosphate
Uridine Triphosphate
CTP Synthase
CTP
RNA and Lipid synthesis
Deoxyuridine monophosphate
Thymidylate Synthase
Deoxythymidine monophosphate
DNA Synthesis
Uracil
+ Ribose-1-phosphate
Uracil Monophosphate
RNA Synthesis
Cytosine
Cytidine Monophosphate
+Deoxyribose-1-phosphate
DNA Synthesis
Salvage Pathway

**Figure 4.4: Summary of pyrimidine metabolism.**

Pyrimidine metabolism is the synthesis, degradation, and recycling of pyrimidine nucleotides for incorporation into DNA and RNA and play critical cell signaling roles. The main pyrimidines in cells are cytosine, thymine (found in DNA), and uracil (found in RNA). The two main biosynthetic processes are de novo synthesis (unboxed reactions) and the salvage pathway (reactions in red box). Abbreviations used: Adenosine triphosphate (ATP), Carbon dioxide ($CO_2$), Cytidine triphosphate (CTP), Coenzyme A (CoA).

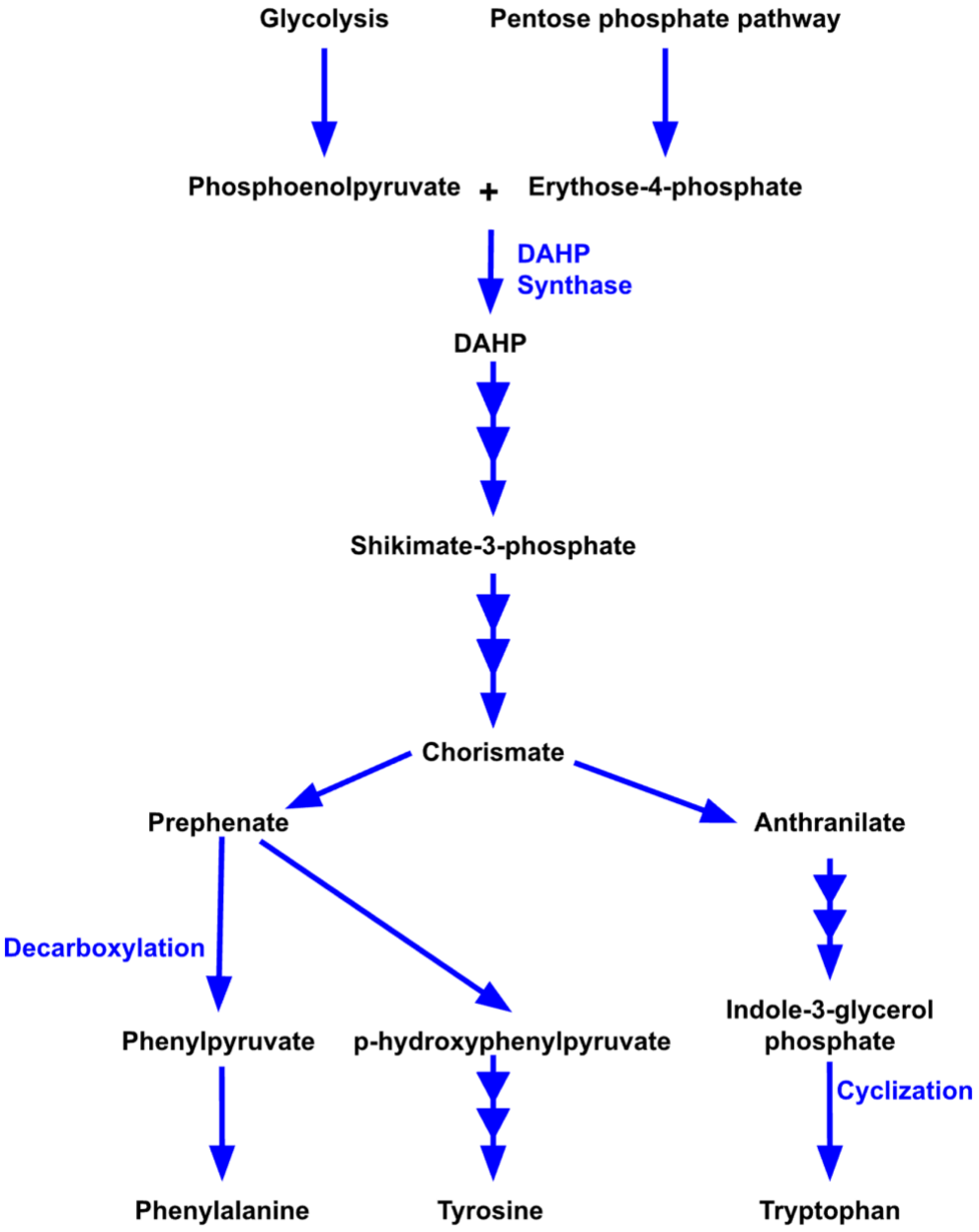
Glycolysis
Pentose phosphate pathway
Phosphoenolpyruvate
+
Erythose-4-phosphate
DAHP
Synthase
DAHP
Shikimate-3-phosphate
Chorismate
Prephenate
Anthranilate
Decarboxylation
Indole-3-glycerol
phosphate
Phenylpyruvate
p-hydroxyphenylpyruvate
Cyclization
Phenylalanine
Tyrosine
Tryptophan

**Figure 4.5: Summary of aromatic amino acid biosynthesis.**

Phenylalanine, tyrosine, and tryptophan are aromatic amino acids (AAAs) (Nelson and Cox, 2008). These are essential amino acids for animals and must be obtained through diet. The shikimate pathway (red box) found in plants, fungi, and microorganisms is responsible for synthesis of these essential amino acids that contribute to the production of proteins, neurotransmitters, hormones, and other compounds. Abbreviations used: 3-Deoxy-D-arabinoheptulosonate 7-phosphate (DAHP).

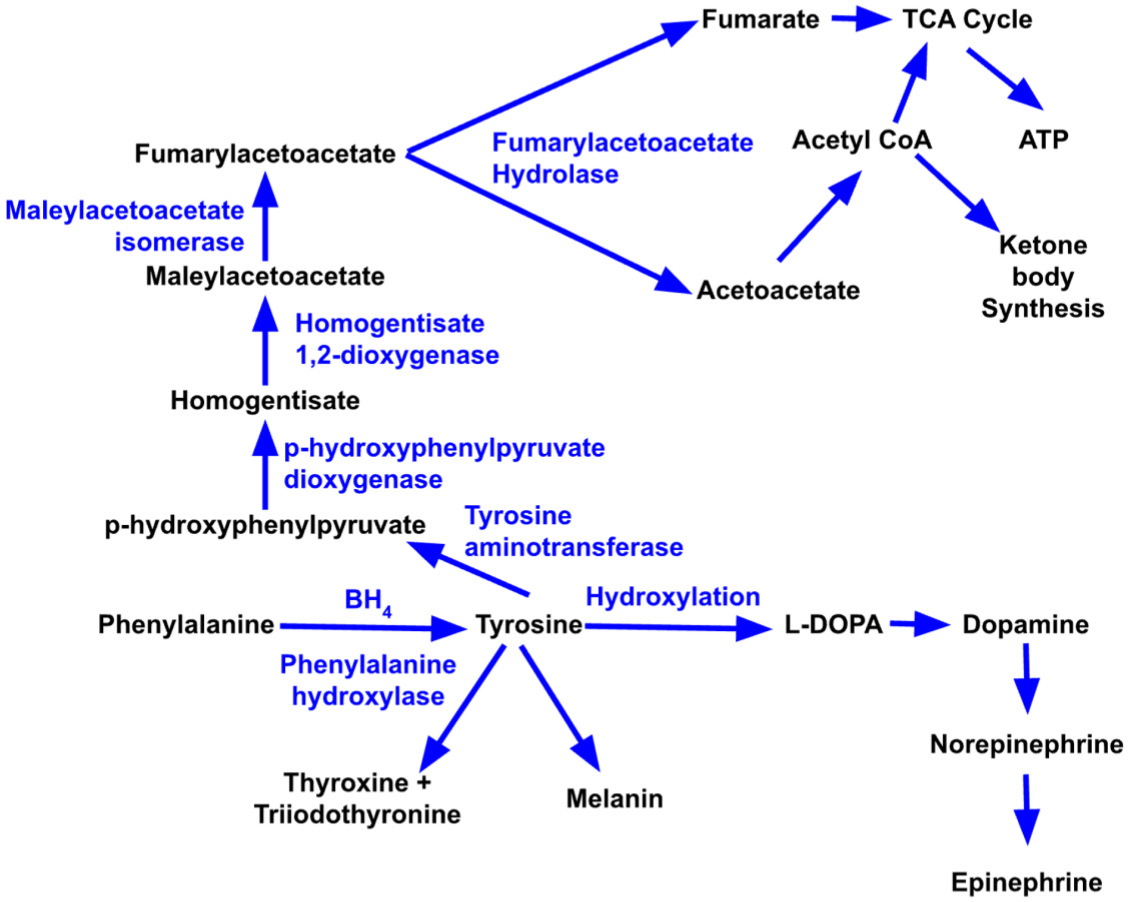
Fumarate
TCA Cycle
ATP
Fumarylacetoacetate
Fumarylacetoacetate Hydrolase
Acetyl CoA
Maleylacetoacetate isomerase
Maleylacetoacetate
Acetoacetate
Ketone body Synthesis
Homogentisate 1,2-dioxygenase
Homogentisate
p-hydroxyphenylpyruvate dioxygenase
p-hydroxyphenylpyruvate
Tyrosine aminotransferase
Hydroxylation
BH4
Phenylalanine
Tyrosine
L-DOPA
Dopamine
Phenylalanine hydroxylase
Norepinephrine
Thyroxine + Triiodothyronine
Melanin
Epinephrine

**Figure 4.6: Summary of phenylalanine and tyrosine metabolism.**

As animals cannot synthesize the phenylalanine and tyrosine, they are extensively metabolized to produce other critical biomolecules. Abbreviations used: Adenosine triphosphate (ATP), Tetrahydrobiopterin ($BH_4$), Coenzyme A, L-3,4-dihydroxyphenylalanine (L-DOPA), Tricarboxylic acid (TCA).

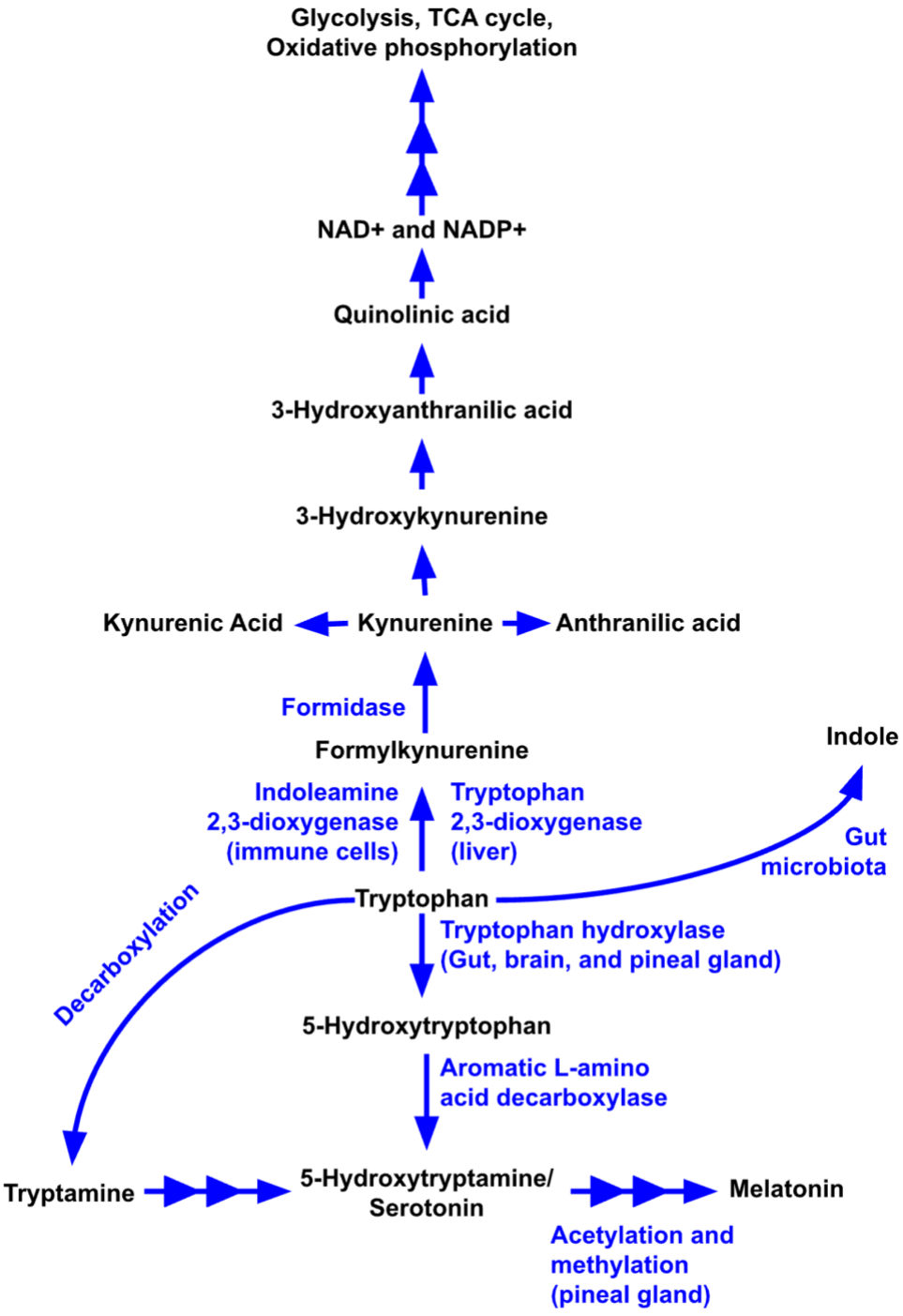
Glycolysis, TCA cycle,
Oxidative phosphorylation
NAD+ and NADP+
Quinolinic acid
3-Hydroxyanthranilic acid
3-Hydroxykynurenine
Kynurenic Acid
Kynurenine
Anthranilic acid
Formidase
Formylkynurenine
Indole
Indoleamine
2,3-dioxygenase
(immune cells)
Tryptophan
2,3-dioxygenase
(liver)
Gut
microbiota
Tryptophan
Decarboxylation
Tryptophan hydroxylase
(Gut, brain, and pineal gland)
5-Hydroxytryptophan
Aromatic L-amino
acid decarboxylase
Tryptamine
5-Hydroxytryptamine/
Serotonin
Melatonin
Acetylation and
methylation
(pineal gland)

**Figure 4.7: Summary of tryptophan metabolism.**

As animals cannot synthesize tryptophan, it is extensively metabolized to produce other critical biomolecules. Abbreviations used: Nicotinamide adenine dinucleotide (NAD+), Nicotinamide adenine dinucleotide phosphate (NADP+), Tricarboxylic acid (TCA).

**References**

**Abmayr, S. M. and Pavlath, G. K.** (2012). Myoblast fusion: lessons from flies and mice. *Development* **139**, 641–656.

**Adhikary, S., Peukert, K., Karsunky, H., Beuger, V., Lutz, W., Elsässer, H.-P., Möröy, T. and Eilers, M.** (2003). Miz1 is required for early embryonic development during gastrulation. *Mol. Cell. Biol.* **23**, 7648–7657.

**Adnot, S., Houssaini, A., Abid, S., Marcos, E. and Amsellem, V.** (2013). Serotonin transporter and serotonin receptors. *Handb Exp Pharmacol* **218**, 365–380.

**Agarwal, E., Altman, B. J., Ho Seo, J., Bertolini, I., Ghosh, J. C., Kaur, A., Kossenkov, A. V., Languino, L. R., Gabrilovich, D. I., Speicher, D. W., et al.** (2019). Myc regulation of a mitochondrial trafficking network mediates tumor cell invasion and metastasis. *Mol. Cell. Biol.* **39**,.

**Ahmad, S. I., Kirk, S. H. and Eisenstark, A.** (1998). Thymine metabolism and thymineless death in prokaryotes and eukaryotes. *Annu. Rev. Microbiol.* **52**, 591–625.

**Akram, M.** (2014). Citric acid cycle and role of its intermediates in metabolism. *Cell Biochem. Biophys.* **68**, 475–478.

**Ala, M.** (2021). The footprint of kynurenine pathway in every cancer: a new target for chemotherapy. *Eur. J. Pharmacol.* **896**, 173921.

**Alabduladhem, T. O. and Bordoni, B.** (2024). Physiology, Krebs Cycle. In *StatPearls*, p. Treasure Island (FL): StatPearls Publishing.

**Alberts, B., Johnson, A., Lewis, J., Raff, M., Roberts, K. and Walter, P.** (2015). *Molecular biology of the cell*. 6th ed. Garland Science.

**Allen, F. W.** (1941). The biochemistry of the nucleic acids, purines, and pyrimidines. *Annu. Rev. Biochem.* **10**, 221–244.

**Alseekh, S., Aharoni, A., Brotman, Y., Contrepois, K., D'Auria, J., Ewald, J., C Ewald, J., Fraser, P. D., Giavalisco, P., Hall, R. D., et al.** (2021). Mass spectrometry-based metabolomics: a guide for annotation, quantification and best reporting practices. *Nat. Methods* **18**, 747–756.

**Álvarez-Sánchez, B., Priego-Capote, F. and Luque de Castro, M. D.** (2010a). Metabolomics analysis I. Selection of biological samples and practical aspects preceding sample preparation. *TrAC Trends in Analytical Chemistry* **29**, 111–119.

**Álvarez-Sánchez, B., Priego-Capote, F. and Castro, M. D. L. de** (2010b). Metabolomics analysis II. Preparation of biological samples prior to detection. *TrAC Trends in Analytical Chemistry* **29**, 120–127.

**Aman, A. and Piotrowski, T.** (2009). Multiple signaling interactions coordinate collective cell migration of the posterior lateral line primordium. *Cell Adh Migr* **3**, 365–368.

**Amaya, A. A., Brzezinski, K. T., Farrington, N. and Moran, G. R.** (2004). Kinetic analysis of human homogentisate 1,2-dioxygenase. *Arch. Biochem. Biophys.* **421**, 135–142.

**Anderson, C. M. and Parkinson, F. E.** (1997). Potential signalling roles for UTP and UDP: sources, regulation and release of uracil nucleotides. *Trends Pharmacol.*

*Sci.* **18**, 387–392.

**Anderson, J. M., Li, J. and Springer, T. A.** (2022). Regulation of integrin α5β1 conformational states and intrinsic affinities by metal ions and the ADMIDAS. *Mol. Biol. Cell* **33**, ar56.

**Aota, S., Nagai, T. and Yamada, K. M.** (1991). Characterization of regions of fibronectin besides the arginine-glycine-aspartic acid sequence required for adhesive function of the cell-binding domain using site-directed mutagenesis. *J. Biol. Chem.* **266**, 15938–15943.

**Apostolova, P. and Pearce, E. L.** (2022). Lactic acid and lactate: revisiting the physiological roles in the tumor microenvironment. *Trends Immunol.*

**Arboleda-Estudillo, Y., Krieg, M., Stühmer, J., Licata, N. A., Muller, D. J. and Heisenberg, C.-P.** (2010). Movement directionality in collective migration of germ layer progenitors. *Curr. Biol.* **20**, 161–169.

**Arendt, D. and Nübler-Jung, K.** (1999). Rearranging gastrulation in the name of yolk: evolution of gastrulation in yolk-rich amniote eggs. *Mech. Dev.* **81**, 3–22.

**Arima, S., Nishiyama, K., Ko, T., Arima, Y., Hakozaki, Y., Sugihara, K., Koseki, H., Uchijima, Y., Kurihara, Y. and Kurihara, H.** (2011). Angiogenic morphogenesis driven by dynamic and heterogeneous collective endothelial cell movement. *Development* **138**, 4763–4776.

**Askari, J. A., Buckley, P. A., Mould, A. P. and Humphries, M. J.** (2009). Linking integrin conformation to function. *J. Cell Sci.* **122**, 165–170.

**Audano, M., Schneider, A. and Mitro, N.** (2018). Mitochondria, lysosomes, and dysfunction: their meaning in neurodegeneration. *J. Neurochem.* **147**, 291–309.

**Awad, H., Khamis, M. M. and El-Aneed, A.** (2015). Mass spectrometry, review of the basics: ionization. *Applied Spectroscopy Reviews* **50**, 158–175.

**Aznavoorian, S., Stracke, M. L., Krutzsch, H., Schiffmann, E. and Liotta, L. A.** (1990). Signal transduction for chemotaxis and haptotaxis by matrix molecules in tumor cells. *J. Cell Biol.* **110**, 1427–1438.

**Bachvarova, R., Davidson, E. H., Allfrey, V. G. and Mirsky, A. E.** (1966). Activation of RNA synthesis associated with gastrulation. *Proc. Natl. Acad. Sci. USA* **55**, 358–365.

**Badawy, A. A.-B.** (2017). Kynurenine pathway of tryptophan metabolism: regulatory and functional aspects. *Int. J. Tryptophan Res.* **10**, 1178646917691938.

**Bagi, C. M., Christensen, J., Cohen, D. P., Roberts, W. G., Wilkie, D., Swanson, T., Tuthill, T. and Andresen, C. J.** (2009). Sunitinib and PF-562,271 (FAK/Pyk2 inhibitor) effectively block growth and recovery of human hepatocellular carcinoma in a rat xenograft model. *Cancer Biol. Ther.* **8**, 856–865.

**Banerjee, K., Keasey, M. P., Razskazovskiy, V., Visavadiya, N. P., Jia, C. and Hagg, T.** (2017). Reduced FAK-STAT3 signaling contributes to ER stress-induced mitochondrial dysfunction and death in endothelial cells. *Cell Signal.* **36**, 154–162.

**Banerjee, R., Purhonen, J. and Kallijärvi, J.** (2021). The mitochondrial coenzyme Q junction and complex III: biochemistry and pathophysiology. *FEBS J.*

**Barczyk, M., Carracedo, S. and Gullberg, D.** (2010). Integrins. *Cell Tissue Res.* **339**, 269–280.

**Barnes, M. R.** (1944). The metabolism of the developing Rana pipiens as revealed by specific inhibitors. *J. Exp. Zool.* **95**, 399–418.

**Barth, L. G.** (1942). Regional differences in oxygen consumption of the amphibian gastrula. *Physiol. Zool.* **15**, 30–47.

**Bartle, K. D. and Myers, P.** (2002). History of gas chromatography. *TrAC Trends in Analytical Chemistry* **21**, 547–557.

**Baxi, A. B., Li, J., Quach, V. M., Pade, L. R., Moody, S. A. and Nemes, P.** (2024). Cell lineage-guided mass spectrometry reveals increased energy metabolism and reactive oxygen species in the vertebrate organizer. *Proc. Natl. Acad. Sci. USA* **121**, e2311625121.

**Bays, J. L., Campbell, H. K., Heidema, C., Sebbagh, M. and DeMali, K. A.** (2017). Linking E-cadherin mechanotransduction to cell metabolism through force-mediated activation of AMPK. *Nat. Cell Biol.* **19**, 724–731.

**Bazzoni, G. and Hemler, M. E.** (1998). Are changes in integrin affinity and conformation overemphasized? *Trends Biochem. Sci.* **23**, 30–34.

**Becker, S., Kortz, L., Helmschrodt, C., Thiery, J. and Ceglarek, U.** (2012). LC-MS-based metabolomics in the clinical laboratory. *J. Chromatogr. B, Analyt. Technol. Biomed. Life Sci.* **883**–**884**, 68–75.

**Beinert, H. and Kennedy, M. C.** (1993). Aconitase, a two-faced protein: enzyme and iron regulatory factor. *FASEB J.* **7**, 1442–1449.

**Beinert, H., Kennedy, M. C. and Stout, C. D.** (1996). Aconitase as Ironminus signSulfur Protein, Enzyme, and Iron-Regulatory Protein. *Chem. Rev.* **96**, 2335–2374.

**Benito-Jardón, M., Klapproth, S., Gimeno-LLuch, I., Petzold, T., Bharadwaj, M., Müller, D. J., Zuchtriegel, G., Reichel, C. A. and Costell, M.** (2017). The fibronectin synergy site re-enforces cell adhesion and mediates a crosstalk between integrin classes. *Elife* **6**,.

**Ben-Sahra, I., Howell, J. J., Asara, J. M. and Manning, B. D.** (2013). Stimulation of de novo pyrimidine synthesis by growth signaling through mTOR and S6K1. *Science* **339**, 1323–1328.

**Bentley, R.** (1990). The shikimate pathway--a metabolic tree with many branches. *Crit Rev Biochem Mol Biol* **25**, 307–384.

**Berens, R. L., Krug, E. C. and Marr, J. J.** (1995). Purine and Pyrimidine Metabolism. In *Biochemistry and Molecular Biology of Parasites*, pp. 89–117. Elsevier.

**Berger, M., Gray, J. A. and Roth, B. L.** (2009). The expanded biology of serotonin. *Annu. Rev. Med.* **60**, s. 355-366.

**Bergink, E. W. and Wallace, R. A.** (1974). Precursor-product relationship between amphibian vitellogenin and the yolk proteins, lipovitellin and phosvitin. *J. Biol. Chem.* **249**, 2897–2903.

**Bergman, M., Joukov, V., Virtanen, I. and Alitalo, K.** (1995). Overexpressed Csk tyrosine kinase is localized in focal adhesions, causes reorganization of alpha v beta 5 integrin, and interferes with HeLa cell spreading. *Mol. Cell. Biol.* **15**, 711–722.

**Bernkopf, D. B., Jalal, K., Brückner, M., Knaup, K. X., Gentzel, M., Schambony, A. and Behrens, J.** (2018). Pgam5 released from damaged mitochondria induces

mitochondrial biogenesis via Wnt signaling. *J. Cell Biol.* **217**, 1383–1394.
**Bernstein, B. W. and Bamburg, J. R.** (2003). Actin-ATP hydrolysis is a major energy drain for neurons. *J. Neurosci.* **23**, 1–6.
**Berthomieu, C. and Hienerwadel, R.** (2009). Fourier transform infrared (FTIR) spectroscopy. *Photosyn Res* **101**, 157–170.
**Berton, G. and Lowell, C. A.** (1999). Integrin signalling in neutrophils and macrophages. *Cell Signal.* **11**, 621–635.
**Bjerke, M. A.** (2014). Mechanosensitive adhesive networks guide collective migration of Xenopus mesendoderm.
**Bjerke, M. A., Dzamba, B. J., Wang, C. and DeSimone, D. W.** (2014). FAK is required for tension-dependent organization of collective cell movements in Xenopus mesendoderm. *Dev. Biol.* **394**, 340–356.
**Blanchoin, L., Boujemaa-Paterski, R., Sykes, C. and Plastino, J.** (2014). Actin dynamics, architecture, and mechanics in cell motility. *Physiol. Rev.* **94**, 235–263.
**Boettiger, D., Enomoto-Iwamoto, M., Yoon, H. Y., Hofer, U., Menko, A. S. and Chiquet-Ehrismann, R.** (1995). Regulation of integrin alpha 5 beta 1 affinity during myogenic differentiation. *Dev. Biol.* **169**, 261–272.
**Boppart, M. D., Burkin, D. J. and Kaufman, S. J.** (2006). Alpha7beta1-integrin regulates mechanotransduction and prevents skeletal muscle injury. *Am. J. Physiol. Cell Physiol.* **290**, C1660-5.
**Bosakowski, T. and Levin, A. A.** (1986). Serum citrate as a peripheral indicator of fluoroacetate and fluorocitrate toxicity in rats and dogs. *Toxicol. Appl. Pharmacol.* **85**, 428–436.
**Boucaut, J. C. and Darribere, T.** (1983). Fibronectin in early amphibian embryos. Migrating mesodermal cells contact fibronectin established prior to gastrulation. *Cell Tissue Res.* **234**, 135–145.
**Boukalova, S., Hubackova, S., Milosevic, M., Ezrova, Z., Neuzil, J. and Rohlena, J.** (2020). Dihydroorotate dehydrogenase in oxidative phosphorylation and cancer. *Biochim. Biophys. Acta Mol. Basis Dis.* 165759.
**Brachet, J.** (1934). Etude du métabolisme de l'oeuf de grenouille (Rana fusca) au cours du développement: 1. La respiration et la glycolyse de la segmentation à l'éclosion. *Arch. Biol. (Liege)* **45**, 611–727.
**Brett, K. E., Ferraro, Z. M., Yockell-Lelievre, J., Gruslin, A. and Adamo, K. B.** (2014). Maternal-fetal nutrient transport in pregnancy pathologies: the role of the placenta. *Int. J. Mol. Sci.* **15**, 16153–16185.
**Britton, C. and Murray, L.** (2004). Cathepsin L protease (CPL-1) is essential for yolk processing during embryogenesis in Caenorhabditis elegans. *J. Cell Sci.* **117**, 5133–5143.
**Brown, D. J.** (2009). *The Pyrimidines, Volume 52*. 1st ed. Wiley.
**Brun, L., Ngu, L. H., Keng, W. T., Ch'ng, G. S., Choy, Y. S., Hwu, W. L., Lee, W. T., Willemsen, M. A. A. P., Verbeek, M. M., Wassenberg, T., et al.** (2010). Clinical and biochemical features of aromatic L-amino acid decarboxylase deficiency. *Neurology* **75**, 64–71.
**Buchholz, A., Hurlebaus, J., Wandrey, C. and Takors, R.** (2002). Metabolomics: quantification of intracellular metabolite dynamics. *Biomol Eng* **19**, 5–15.

**Buffa, P., Peters, R. A. and Wakelin, R. W.** (1951). Biochemistry of fluoroacetate poisoning; isolation of an active tricarboxylic acid fraction from poisoned kidney homogenates. *Biochem. J.* **48**, 467–477.

**Bulteau, A.-L., Ikeda-Saito, M. and Szweda, L. I.** (2003). Redox-dependent modulation of aconitase activity in intact mitochondria. *Biochemistry* **42**, 14846–14855.

**Burton, B. K., Kar, S. and Kirkpatrick, P.** (2008). Sapropterin. *Nat. Rev. Drug Discov.* **7**, 199–200.

**Buznikov, G. A., Lambert, H. W. and Lauder, J. M.** (2001). Serotonin and serotonin-like substances as regulators of early embryogenesis and morphogenesis. *Cell Tissue Res.* **305**, 177–186.

**Cai, J. and Henion, J.** (1995). Capillary electrophoresis-mass spectrometry. *Journal of Chromatography A* **703**, 667–692.

**Cai, Q., Zakaria, H. M., Simone, A. and Sheng, Z.-H.** (2012). Spatial parkin translocation and degradation of damaged mitochondria via mitophagy in live cortical neurons. *Curr. Biol.* **22**, 545–552.

**Caino, M. C., Seo, J. H., Aguinaldo, A., Wait, E., Bryant, K. G., Kossenkov, A. V., Hayden, J. E., Vaira, V., Morotti, A., Ferrero, S., et al.** (2016). A neuronal network of mitochondrial dynamics regulates metastasis. *Nat. Commun.* **7**, 13730.

**Calalb, M. B., Polte, T. R. and Hanks, S. K.** (1995). Tyrosine phosphorylation of focal adhesion kinase at sites in the catalytic domain regulates kinase activity: a role for Src family kinases. *Mol. Cell. Biol.* **15**, 954–963.

**Canellakis, E. S.** (1956). PYRIMIDINE METABOLISM. *J. Bio. Chem.* **221**, 315–322.

**Capuana, L., Boström, A. and Etienne-Manneville, S.** (2020). Multicellular scale front-to-rear polarity in collective migration. *Curr. Opin. Cell Biol.* **62**, 114–122.

**Carreras, C. W. and Santi, D. V.** (1995). The catalytic mechanism and structure of thymidylate synthase. *Annu. Rev. Biochem.* **64**, 721–762.

**Carter, S. B.** (1967). Haptotaxis and the mechanism of cell motility. *Nature* **213**, 256–260.

**Castro, L., Tórtora, V., Mansilla, S. and Radi, R.** (2019). Aconitases: Non-redox Iron-Sulfur Proteins Sensitive to Reactive Species. *Acc. Chem. Res.* **52**, 2609–2619.

**Castro-Portuguez, R. and Sutphin, G. L.** (2020). Kynurenine pathway, NAD+ synthesis, and mitochondrial function: Targeting tryptophan metabolism to promote longevity and healthspan. *Exp. Gerontol.* **132**, 110841.

**Cetin, I. and Alvino, G.** (2009). Intrauterine growth restriction: implications for placental metabolism and transport. A review. *Placenta* **30 Suppl A**, S77-82.

**Chakraborty, M., Chu, K., Shrestha, A., Revelo, X. S., Zhang, X., Gold, M. J., Khan, S., Lee, M., Huang, C., Akbari, M., et al.** (2021). Mechanical stiffness controls dendritic cell metabolism and function. *Cell Rep.* **34**, 108609.

**Chan, D. C.** (2006a). Mitochondrial fusion and fission in mammals. *Annu. Rev. Cell Dev. Biol.* **22**, 79–99.

**Chan, D. C.** (2006b). Mitochondria: dynamic organelles in disease, aging, and development. *Cell* **125**, 1241–1252.

**Chan, M. C. and Arany, Z.** (2014). The many roles of PGC-1α in muscle--recent developments. *Metab. Clin. Exp.* **63**, 441–451.

**Chandel, N. S.** (2021a). Glycolysis. *Cold Spring Harb. Perspect. Biol.* **13**,.
**Chandel, N. S.** (2021b). Nucleotide Metabolism. *Cold Spring Harb. Perspect. Biol.* **13**,.
**Chang, Y.-F. and Carman, G. M.** (2008). CTP synthetase and its role in phospholipid synthesis in the yeast Saccharomyces cerevisiae. *Prog. Lipid Res.* **47**, 333–339.
**Chang, M.-Y., Huang, D.-Y., Ho, F.-M., Huang, K.-C. and Lin, W.-W.** (2012). PKC-dependent human monocyte adhesion requires AMPK and Syk activation. *PLoS One* **7**, e40999.
**Chang, H.-Y., Colby, S. M., Du, X., Gomez, J. D., Helf, M. J., Kechris, K., Kirkpatrick, C. R., Li, S., Patti, G. J., Renslow, R. S., et al.** (2021). A practical guide to metabolomics software development. *Anal. Chem.* **93**, 1912–1923.
**Chaudhry, R. and Varacallo, M.** (2024). Biochemistry, Glycolysis. In *StatPearls*, p. Treasure Island (FL): StatPearls Publishing.
**Chaulet, H., Desgranges, C., Renault, M. A., Dupuch, F., Ezan, G., Peiretti, F., Loirand, G., Pacaud, P. and Gadeau, A. P.** (2001). Extracellular nucleotides induce arterial smooth muscle cell migration via osteopontin. *Circ. Res.* **89**, 772–778.
**Chazotte, B.** (2011). Labeling mitochondria with TMRM or TMRE. *Cold Spring Harb. Protoc.* **2011**, 895–897.
**Chen, P. S.** (1956). Metabolic changes in free amino acids and peptides during urodele development. *Exp. Cell Res.* **10**, 675–686.
**Chen, P. and Parks, W. C.** (2009). Role of matrix metalloproteinases in epithelial migration. *J. Cell Biochem.* **108**, 1233–1243.
**Chen, Y. P., O'Toole, T. E., Shipley, T., Forsyth, J., LaFlamme, S. E., Yamada, K. M., Shattil, S. J. and Ginsberg, M. H.** (1994). "Inside-out" signal transduction inhibited by isolated integrin cytoplasmic domains. *J. Biol. Chem.* **269**, 18307–18310.
**Chen, H., Cohen, D. M., Choudhury, D. M., Kioka, N. and Craig, S. W.** (2005). Spatial distribution and functional significance of activated vinculin in living cells. *J. Cell Biol.* **169**, 459–470.
**Chen, Z., Lu, W., Garcia-Prieto, C. and Huang, P.** (2007). The Warburg effect and its cancer therapeutic implications. *J Bioenerg Biomembr* **39**, 267–274.
**Chen, G., Deng, C. and Li, Y.-P.** (2012). TGF-β and BMP signaling in osteoblast differentiation and bone formation. *Int. J. Biol. Sci.* **8**, 272–288.
**Chien, Y.-H., Srinivasan, S., Keller, R. and Kintner, C.** (2018). Mechanical Strain Determines Cilia Length, Motility, and Planar Position in the Left-Right Organizer. *Dev. Cell* **45**, 316–330.e4.
**Chong, J., Soufan, O., Li, C., Caraus, I., Li, S., Bourque, G., Wishart, D. S. and Xia, J.** (2018). MetaboAnalyst 4.0: towards more transparent and integrative metabolomics analysis. *Nucleic Acids Res.* **46**, W486–W494.
**Cody, V., Davis, P. J. and Davis, F. B.** (2007). Molecular modeling of the thyroid hormone interactions with alpha v beta 3 integrin. *Steroids* **72**, 165–170.
**Cohen, L. A. and Guan, J.-L.** (2005). Mechanisms of focal adhesion kinase regulation. *Curr. Cancer Drug Targets* **5**, 629–643.
**Colas, J. F., Launay, J. M., Vonesch, J. L., Hickel, P. and Maroteaux, L.** (1999). Serotonin synchronises convergent extension of ectoderm with morphogenetic

gastrulation movements in Drosophila. *Mech. Dev.* **87**, 77–91.
**Collins, C. and Nelson, W. J.** (2015). Running with neighbors: coordinating cell migration and cell-cell adhesion. *Curr. Opin. Cell Biol.* **36**, 62–70.
**Comlekoglu, T., Dzamba, B. J., Pacheco, G. G., Shook, D. R., Sego, T. J., Glazier, J. A., Peirce, S. M. and DeSimone, D. W.** (2023). Modeling the roles of cohesotaxis, cell-intercalation, and tissue geometry in collective cell migration of Xenopus mesendoderm. *BioRxiv*.
**Comlekoglu, T., Dzamba, B. J., Pacheco, G. G., Shook, D. R., Sego, T. J., Glazier, J. A., Peirce, S. M. and DeSimone, D. W.** (2024). Modeling the roles of cohesotaxis, cell-intercalation, and tissue geometry in collective cell migration of Xenopus mesendoderm. *Biol. Open* **13**,.
**Connolly, G. P. and Duley, J. A.** (1999). Uridine and its nucleotides: biological actions, therapeutic potentials. *Trends Pharmacol. Sci.* **20**, 218–225.
**Coppen, A., Shaw, D. M., Malleson, A., Eccleston, E. and Gundy, G.** (1965). Tryptamine metabolism in depression. *Br. J. Psychiatry* **111**, 993–998.
**Corsi, J.-M., Houbron, C., Billuart, P., Brunet, I., Bouvrée, K., Eichmann, A., Girault, J.-A. and Enslen, H.** (2009). Autophosphorylation-independent and -dependent functions of focal adhesion kinase during development. *J. Biol. Chem.* **284**, 34769–34776.
**Corte, L., Tiecco, M., Roscini, L., De Vincenzi, S., Colabella, C., Germani, R., Tascini, C. and Cardinali, G.** (2015). FTIR metabolomic fingerprint reveals different modes of action exerted by structural variants of N-alkyltropinium bromide surfactants on Escherichia coli and Listeria innocua cells. *PLoS One* **10**, e0115275.
**Cortese, B., Palamà, I. E., D'Amone, S. and Gigli, G.** (2014). Influence of electrotaxis on cell behaviour. *Integr Biol (Camb)* **6**, 817–830.
**Costa, V. M., Carvalho, F., Bastos, M. L., Carvalho, R. A., Carvalho, M. and Remião, F.** (2011). Contribution of catecholamine reactive intermediates and oxidative stress to the pathologic features of heart diseases. *Curr. Med. Chem.* **18**, 2272–2314.
**Costa, G., Harrington, K. I., Lovegrove, H. E., Page, D. J., Chakravartula, S., Bentley, K. and Herbert, S. P.** (2016). Asymmetric division coordinates collective cell migration in angiogenesis. *Nat. Cell Biol.* **18**, 1292–1301.
**Cotgreave, I. A. and Moldéus, P.** (1986). Methodologies for the application of monobromobimane to the simultaneous analysis of soluble and protein thiol components of biological systems. *J Biochem Biophys Methods* **13**, 231–249.
**Cox, B. D., Natarajan, M., Stettner, M. R. and Gladson, C. L.** (2006). New concepts regarding focal adhesion kinase promotion of cell migration and proliferation. *J. Cell Biochem.* **99**, 35–52.
**Craig, R., Greene, L. E. and Eisenberg, E.** (1985). Structure of the actin-myosin complex in the presence of ATP. *Proc. Natl. Acad. Sci. USA* **82**, 3247–3251.
**Cramer, L. P.** (2013). Mechanism of cell rear retraction in migrating cells. *Curr. Opin. Cell Biol.* **25**, 591–599.
**Cramers, C. A., Janssen, H. G., van Deursen, M. M. and Leclercq, P. A.** (1999). High-speed gas chromatography: an overview of various concepts. *J.*

*Chromatogr. A* **856**, 315–329.

**Crosas-Molist, E., Graziani, V., Maiques, O., Pandya, P., Monger, J., Samain, R., George, S. L., Malik, S., Salise, J., Morales, V., et al.** (2023). AMPK is a mechano-metabolic sensor linking cell adhesion and mitochondrial dynamics to Myosin-dependent cell migration. *Nat. Commun.* **14**, 2740.

**Crowley, L. C., Christensen, M. E. and Waterhouse, N. J.** (2016). Measuring mitochondrial transmembrane potential by TMRE staining. *Cold Spring Harb. Protoc.* **2016**,.

**Cruet-Hennequart, S., Maubant, S., Luis, J., Gauduchon, P., Staedel, C. and Dedhar, S.** (2003). alpha(v) integrins regulate cell proliferation through integrin-linked kinase (ILK) in ovarian cancer cells. *Oncogene* **22**, 1688–1702.

**Cunniff, B., McKenzie, A. J., Heintz, N. H. and Howe, A. K.** (2016). AMPK activity regulates trafficking of mitochondria to the leading edge during cell migration and matrix invasion. *Mol. Biol. Cell* **27**, 2662–2674.

**Dailey, L., Ambrosetti, D., Mansukhani, A. and Basilico, C.** (2005). Mechanisms underlying differential responses to FGF signaling. *Cytokine Growth Factor Rev.* **16**, 233–247.

**Danen, E. H., Aota, S., van Kraats, A. A., Yamada, K. M., Ruiter, D. J. and van Muijen, G. N.** (1995). Requirement for the synergy site for cell adhesion to fibronectin depends on the activation state of integrin alpha 5 beta 1. *J. Biol. Chem.* **270**, 21612–21618.

**Dang, C. V., Lewis, B. C., Dolde, C., Dang, G. and Shim, H.** (1997). Oncogenes in tumor metabolism, tumorigenesis, and apoptosis. *J Bioenerg Biomembr* **29**, 345–354.

**Danhier, P., Bański, P., Payen, V. L., Grasso, D., Ippolito, L., Sonveaux, P. and Porporato, P. E.** (2017). Cancer metabolism in space and time: Beyond the Warburg effect. *Biochim. Biophys. Acta Bioenerg.* **1858**, 556–572.

**Daniel, J. L., Molish, I. R., Robkin, L. and Holmsen, H.** (1986). Nucleotide exchange between cytosolic ATP and F-actin-bound ADP may be a major energy-utilizing process in unstimulated platelets. *Eur. J. Biochem.* **156**, 677–684.

**Danilchik, M. V. and Gerhart, J. C.** (1987). Differention of the animal-vegetal axis in Xenopus laevis oocytes. *Dev. Biol.* **122**, 101–112.

**Davidson, L. A., Hoffstrom, B. G., Keller, R. and DeSimone, D. W.** (2002). Mesendoderm extension and mantle closure in Xenopus laevis gastrulation: combined roles for integrin alpha(5)beta(1), fibronectin, and tissue geometry. *Dev. Biol.* **242**, 109–129.

**Davidson, L. A., Keller, R. and DeSimone, D. W.** (2004). Assembly and remodeling of the fibrillar fibronectin extracellular matrix during gastrulation and neurulation in Xenopus laevis. *Dev. Dyn.* **231**, 888–895.

**Davidson, L. A., Marsden, M., Keller, R. and DeSimone, D. W.** (2006a). Integrin α5β1 and Fibronectin Regulate Polarized Cell Protrusions Required for Xenopus Convergence and Extension. *Curr. Biol.* **16**, 833–844.

**Davidson, L. A., Marsden, M., Keller, R. and Desimone, D. W.** (2006b). Integrin alpha5beta1 and fibronectin regulate polarized cell protrusions required for Xenopus convergence and extension. *Curr. Biol.* **16**, 833–844.

**Davis, P. J., Goglia, F. and Leonard, J. L.** (2016). Nongenomic actions of thyroid hormone. *Nat. Rev. Endocrinol.* **12**, 111–121.

**Dawson, L. W., Cronin, N. M. and DeMali, K. A.** (2023). Mechanotransduction: Forcing a change in metabolism. *Curr. Opin. Cell Biol.* **84**, 102219.

**de Hoffmann, E.** (1996). Tandem mass spectrometry: A primer. *J Mass Spectrom*.

**De Pascalis, C. and Etienne-Manneville, S.** (2017). Single and collective cell migration: the mechanics of adhesions. *Mol. Biol. Cell* **28**, 1833–1846.

**DeBerardinis, R. J. and Chandel, N. S.** (2020). We need to talk about the Warburg effect. *Nat. Metab.* **2**, 127–129.

**Debets, V. E., Janssen, L. M. C. and Storm, C.** (2021). Enhanced persistence and collective migration in cooperatively aligning cell clusters. *Biophys. J.* **120**, 1483–1497.

**Dehghan, A., Köttgen, A., Yang, Q., Hwang, S.-J., Kao, W. L., Rivadeneira, F., Boerwinkle, E., Levy, D., Hofman, A., Astor, B. C., et al.** (2008). Association of three genetic loci with uric acid concentration and risk of gout: a genome-wide association study. *Lancet* **372**, 1953–1961.

**Denko, N. C.** (2008). Hypoxia, HIF1 and glucose metabolism in the solid tumour. *Nat. Rev. Cancer* **8**, 705–713.

**Desai, S. P., Bhatia, S. N., Toner, M. and Irimia, D.** (2013). Mitochondrial localization and the persistent migration of epithelial cancer cells. *Biophys. J.* **104**, 2077–2088.

**DeSimone, D. W., Davidson, L., Marsden, M. and Alfandari, D.** (2005). The Xenopus embryo as a model system for studies of cell migration. *Methods Mol. Biol.* **294**, 235–245.

**Detmer, S. A. and Chan, D. C.** (2007). Functions and dysfunctions of mitochondrial dynamics. *Nat. Rev. Mol. Cell Biol.* **8**, 870–879.

**Dietmair, S., Timmins, N. E., Gray, P. P., Nielsen, L. K. and Krömer, J. O.** (2010). Towards quantitative metabolomics of mammalian cells: development of a metabolite extraction protocol. *Anal. Biochem.* **404**, 155–164.

**Dobolyi, A., Juhász, G., Kovács, Z. and Kardos, J.** (2011). Uridine function in the central nervous system. *Curr. Top. Med. Chem.* **11**, 1058–1067.

**Dobson, A. W., Erikson, K. M. and Aschner, M.** (2004). Manganese neurotoxicity. *Ann. N. Y. Acad. Sci.* **1012**, 115–128.

**Dolivo, D. M., Larson, S. A. and Dominko, T.** (2018). Tryptophan metabolites kynurenine and serotonin regulate fibroblast activation and fibrosis. *Cell Mol. Life Sci.* **75**, 3663–3681.

**Dong, M. W. and Zhang, K.** (2014). Ultra-high-pressure liquid chromatography (UHPLC) in method development. *TrAC Trends in Analytical Chemistry* **63**, 21–30.

**Dong, C., Yuan, T., Wu, Y., Wang, Y., Fan, T. W. M., Miriyala, S., Lin, Y., Yao, J., Shi, J., Kang, T., et al.** (2013). Loss of FBP1 by Snail-mediated repression provides metabolic advantages in basal-like breast cancer. *Cancer Cell* **23**, 316–331.

**Dosselaere, F. and Vanderleyden, J.** (2001). A metabolic node in action: chorismate-utilizing enzymes in microorganisms. *Crit Rev Microbiol* **27**, 75–131.

**Dow, L. E. and Humbert, P. O.** (2007). Polarity Regulators and the Control of Epithelial Architecture, Cell Migration, and Tumorigenesis.pp. 253–302. Elsevier.
**DuChez, B. J., Doyle, A. D., Dimitriadis, E. K. and Yamada, K. M.** (2019). Durotaxis by human cancer cells. *Biophys. J.* **116**, 670–683.
**Dumortier, J. G., Martin, S., Meyer, D., Rosa, F. M. and David, N. B.** (2012). Collective mesendoderm migration relies on an intrinsic directionality signal transmitted through cell contacts. *Proc. Natl. Acad. Sci. USA* **109**, 16945–16950.
**Dunn, W. B. and Winder, C. L.** (2011). Sample preparation related to the intracellular metabolome of yeast methods for quenching, extraction, and metabolite quantitation. *Meth. Enzymol.* **500**, 277–297.
**Dunnill, C., Patton, T., Brennan, J., Barrett, J., Dryden, M., Cooke, J., Leaper, D. and Georgopoulos, N. T.** (2017). Reactive oxygen species (ROS) and wound healing: the functional role of ROS and emerging ROS-modulating technologies for augmentation of the healing process. *Int. Wound J.* **14**, 89–96.
**Dunwoodie, S. L.** (2009). The role of hypoxia in development of the Mammalian embryo. *Dev. Cell* **17**, 755–773.
**Dupuy, A. G. and Caron, E.** (2008). Integrin-dependent phagocytosis: spreading from microadhesion to new concepts. *J. Cell Sci.* **121**, 1773–1783.
**Dworkin, M. B. and Dworkin-Rastl, E.** (1989). Metabolic regulation during early frog development: glycogenic flux in Xenopus oocytes, eggs, and embryos. *Dev. Biol.* **132**, 512–523.
**Dworkin, M. B. and Dworkin-Rastl, E.** (1991). Carbon metabolism in early amphibian embryos. *Trends Biochem. Sci.* **16**, 229–234.
**Dzamba, B. J., Jakab, K. R., Marsden, M., Schwartz, M. A. and DeSimone, D. W.** (2009). Cadherin adhesion, tissue tension, and noncanonical Wnt signaling regulate fibronectin matrix organization. *Dev. Cell* **16**, 421–432.
**Eiyama, A. and Okamoto, K.** (2015). PINK1/Parkin-mediated mitophagy in mammalian cells. *Curr. Opin. Cell Biol.* **33**, 95–101.
**Ely, D. M. and Driscoll, A. K.** (2020). Infant mortality in the united states, 2018: data from the period linked birth/infant death file. *Natl. Vital Stat. Rep.* **69**, 1–18.
**Etienne-Manneville, S.** (2008). Polarity proteins in migration and invasion. *Oncogene* **27**, 6970–6980.
**Etienne-Manneville, S.** (2014). Neighborly relations during collective migration. *Curr. Opin. Cell Biol.* **30**, 51–59.
**Evers, T. M. J., Holt, L. J., Alberti, S. and Mashaghi, A.** (2021). Reciprocal regulation of cellular mechanics and metabolism. *Nat. Metab.* **3**, 456–468.
**Fagerholm, S. C.** (2022). Integrins in health and disease. *N. Engl. J. Med.*
**Fang, Z.-Z. and Gonzalez, F. J.** (2014). LC-MS-based metabolomics: an update. *Arch. Toxicol.* **88**, 1491–1502.
**Fei, T., Zhu, S., Xia, K., Zhang, J., Li, Z., Han, J.-D. J. and Chen, Y.-G.** (2010). Smad2 mediates Activin/Nodal signaling in mesendoderm differentiation of mouse embryonic stem cells. *Cell Res.* **20**, 1306–1318.
**Fekete, S., Schappler, J., Veuthey, J.-L. and Guillarme, D.** (2014). Current and future trends in UHPLC. *TrAC Trends in Analytical Chemistry* **63**, 2–13.
**Fernández-Cañón, J. M. and Peñalva, M. A.** (1998). Characterization of a fungal

maleylacetoacetate isomerase gene and identification of its human homologue. *J. Biol. Chem.* **273**, 329–337.

**Fernandez-Marcos, P. J. and Auwerx, J.** (2011). Regulation of PGC-1α, a nodal regulator of mitochondrial biogenesis. *Am. J. Clin. Nutr.* **93**, 884S–90.

**Fernstrom, J. D. and Fernstrom, M. H.** (2007). Tyrosine, phenylalanine, and catecholamine synthesis and function in the brain. *J. Nutr.* **137**, 1539S–1547S; discussion 1548S.

**Ferrer-Vaquer, A. and Hadjantonakis, A.-K.** (2013). Birth defects associated with perturbations in preimplantation, gastrulation, and axis extension: from conjoined twinning to caudal dysgenesis. *Wiley Interdiscip Rev Dev Biol* **2**, 427–442.

**Finn, R. N.** (2007). Vertebrate yolk complexes and the functional implications of phosvitins and other subdomains in vitellogenins. *Biol. Reprod.* **76**, 926–935.

**Fiore, A. and Murray, P. J.** (2021). Tryptophan and indole metabolism in immune regulation. *Curr. Opin. Immunol.* **70**, 7–14.

**Flydal, M. I. and Martinez, A.** (2013). Phenylalanine hydroxylase: function, structure, and regulation. *IUBMB Life* **65**, 341–349.

**Fonnum, F., Johnsen, A. and Hassel, B.** (1997). Use of fluorocitrate and fluoroacetate in the study of brain metabolism. *Glia*.

**Freeberg, M. A. T., Perelas, A., Rebman, J. K., Phipps, R. P., Thatcher, T. H. and Sime, P. J.** (2020). Mechanical Feed-Forward Loops Contribute to Idiopathic Pulmonary Fibrosis. *Am. J. Pathol.* **191**, 18–25.

**Friedl, P.** (2004). Prespecification and plasticity: shifting mechanisms of cell migration. *Curr. Opin. Cell Biol.* **16**, 14–23.

**Friedl, P. and Gilmour, D.** (2009). Collective cell migration in morphogenesis, regeneration and cancer. *Nat. Rev. Mol. Cell Biol.* **10**, 445–457.

**Friedl, P. and Mayor, R.** (2017). Tuning Collective Cell Migration by Cell-Cell Junction Regulation. *Cold Spring Harb. Perspect. Biol.* **9**,.

**Friedl, P., Borgmann, S. and Bröcker, E. B.** (2001). Amoeboid leukocyte crawling through extracellular matrix: lessons from the Dictyostelium paradigm of cell movement. *J. Leukoc. Biol.* **70**, 491–509.

**Friedl, P., Hegerfeldt, Y. and Tusch, M.** (2004). Collective cell migration in morphogenesis and cancer. *Int. J. Dev. Biol.* **48**, 441–449.

**Fujiwara, S., Ohashi, K., Mashiko, T., Kondo, H. and Mizuno, K.** (2016). Interplay between Solo and keratin filaments is crucial for mechanical force-induced stress fiber reinforcement. *Mol. Biol. Cell* **27**, 954–966.

**Fukumoto, T., Kema, I. P. and Levin, M.** (2005). Serotonin signaling is a very early step in patterning of the left-right axis in chick and frog embryos. *Curr. Biol.* **15**, 794–803.

**Funes, J. M., Quintero, M., Henderson, S., Martinez, D., Qureshi, U., Westwood, C., Clements, M. O., Bourboulia, D., Pedley, R. B., Moncada, S., et al.** (2007). Transformation of human mesenchymal stem cells increases their dependency on oxidative phosphorylation for energy production. *Proc. Natl. Acad. Sci. USA* **104**, 6223–6228.

**Gainetdinov, R. R., Hoener, M. C. and Berry, M. D.** (2018). Trace amines and their receptors. *Pharmacol. Rev.* **70**, 549–620.

**Galbraith, C. G., Yamada, K. M. and Sheetz, M. P.** (2002). The relationship between force and focal complex development. *J. Cell Biol.* **159**, 695–705.

**Garavito, M. F., Narváez-Ortiz, H. Y. and Zimmermann, B. H.** (2015). Pyrimidine metabolism: dynamic and versatile pathways in pathogens and cellular development. *J Genet Genomics* **42**, 195–205.

**Gardel, M. L., Schneider, I. C., Aratyn-Schaus, Y. and Waterman, C. M.** (2010). Mechanical integration of actin and adhesion dynamics in cell migration. *Annu. Rev. Cell Dev. Biol.* **26**, 315–333.

**Gardner, P. R.** (1997). Superoxide-driven aconitase FE-S center cycling. *Biosci. Rep.* **17**, 33–42.

**Gardner, P. R.** (2002). Aconitase: Sensitive target and measure of superoxide. In *Superoxide Dismutase*, pp. 9–23. Elsevier.

**Gardner, P. R. and Fridovich, I.** (1992). Inactivation-reactivation of aconitase in *Escherichia coli*. A sensitive measure of superoxide radical. *J. Biol. Chem.* **267**, 8757–8763.

**Gardner, D. K. and Harvey, A. J.** (2015). Blastocyst metabolism. *Reprod Fertil Dev* **27**, 638–654.

**Gardner, D. K., Pool, T. B. and Lane, M.** (2000). Embryo nutrition and energy metabolism and its relationship to embryo growth, differentiation, and viability. *Semin Reprod Med* **18**, 205–218.

**Garrido-Casado, M., Asensio-Juárez, G. and Vicente-Manzanares, M.** (2021). Nonmuscle myosin II regulation directs its multiple roles in cell migration and division. *Annu. Rev. Cell Dev. Biol.* **37**, 285–310.

**Gatenby, R. A. and Gillies, R. J.** (2004). Why do cancers have high aerobic glycolysis? *Nat. Rev. Cancer* **4**, 891–899.

**Geiger, B., Spatz, J. P. and Bershadsky, A. D.** (2009). Environmental sensing through focal adhesions. *Nat. Rev. Mol. Cell Biol.* **10**, 21–33.

**Gentric, G., Mieulet, V. and Mechta-Grigoriou, F.** (2017). Heterogeneity in cancer metabolism: new concepts in an old field. *Antioxid. Redox Signal.* **26**, 462–485.

**Gerhart, J. and Kirschner, M.** (2020). *Normal Table of Xenopus Laevis (Daudin) A Systematical and Chronological Survey of the Development from the Fertilized Egg Till the End of Metamorphosis*. (ed. Nieuwkoop, P. D.) and Faber, J.) Garland Science.

**Gilbert, S. F.** (2013). *Developmental Biology (Looseleaf), Tenth Edition*. 10th ed. Sinauer Associates, Inc.

**Gimeno-LLuch, I., Benito-Jardón, M., Guerrero-Barberà, G., Burday, N. and Costell, M.** (2022). The role of the fibronectin synergy site for skin wound healing. *Cells* **11**,.

**Gingras, A. R., Vogel, K.-P., Steinhoff, H.-J., Ziegler, W. H., Patel, B., Emsley, J., Critchley, D. R., Roberts, G. C. K. and Barsukov, I. L.** (2006). Structural and dynamic characterization of a vinculin binding site in the talin rod. *Biochemistry* **45**, 1805–1817.

**Gnegy, M. E.** (2012). Catecholamines. In *Basic Neurochemistry*, pp. 283–299. Elsevier.

**Gobin, A. S. and West, J. L.** (2002). Cell migration through defined, synthetic ECM analogs. *FASEB J.* **16**, 751–753.

**Godfrey, K. M.** (2002). The role of the placenta in fetal programming-a review. *Placenta* **23 Suppl A**, S20-7.

**Goglia, F., Lanni, A., Horst, C., Moreno, M. and Thoma, R.** (1994). In vitro binding of 3,5-di-iodo-L-thyronine to rat liver mitochondria. *J. Mol. Endocrinol.* **13**, 275–282.

**Golubovskaya, V. M. and Cance, W. G.** (2011). FAK and p53 protein interactions. *Anticancer Agents Med. Chem.* **11**, 617–619.

**Goncharov, N. V., Jenkins, R. O. and Radilov, A. S.** (2006). Toxicology of fluoroacetate: a review, with possible directions for therapy research. *J Appl Toxicol* **26**, 148–161.

**Gong, Y., Mo, C. and Fraser, S. E.** (2004). Planar cell polarity signalling controls cell division orientation during zebrafish gastrulation. *Nature* **430**, 689–693.

**Goodacre, R.** (2007). Metabolomics of a superorganism. *J. Nutr.* **137**, 259S–266S.

**Gordon, S. and Plüddemann, A.** (2017). Tissue macrophages: heterogeneity and functions. *BMC Biol.* **15**, 53.

**Gots, J. S.** (1971). Regulation of purine and pyrimidine metabolism. In *Metabolic Regulation*, pp. 225–255. Elsevier.

**Granner, D. K. and Tomkins, G. M.** (1970). [80] Tyrosine aminotransferase (rat liver). In *Metabolism of amino acids and amines part A*, pp. 633–637. Elsevier.

**Green, K. J., Getsios, S., Troyanovsky, S. and Godsel, L. M.** (2010). Intercellular junction assembly, dynamics, and homeostasis. *Cold Spring Harb. Perspect. Biol.* **2**, a000125.

**Gross, J. H.** (2017). Tandem Mass Spectrometry. In *Mass Spectrometry*, pp. 539–612. Cham: Springer International Publishing.

**Gu, W., Gaeta, X., Sahakyan, A., Chan, A. B., Hong, C. S., Kim, R., Braas, D., Plath, K., Lowry, W. E. and Christofk, H. R.** (2016). Glycolytic metabolism plays a functional role in regulating human pluripotent stem cell state. *Cell Stem Cell* **19**, 476–490.

**Guijas, C., Montenegro-Burke, J. R., Warth, B., Spilker, M. E. and Siuzdak, G.** (2018). Metabolomics activity screening for identifying metabolites that modulate phenotype. *Nat. Biotechnol.* **36**, 316–320.

**Guillemin, G. J. and Brew, B. J.** (2002). Implications of the kynurenine pathway and quinolinic acid in Alzheimer's disease. *Redox Rep* **7**, 199–206.

**Gullberg, D., Velling, T., Lohikangas, L. and Tiger, C.-F.** (1998). Integrins during muscle development and in muscular dystrophies. *Pediatr Pathol Mol Med* **18**, 303–327.

**Gumbiner, B. M.** (1996). Cell adhesion: the molecular basis of tissue architecture and morphogenesis. *Cell* **84**, 345–357.

**Guo, L., Cui, C., Zhang, K., Wang, J., Wang, Y., Lu, Y., Chen, K., Yuan, J., Xiao, G., Tang, B., et al.** (2019). Kindlin-2 links mechano-environment to proline synthesis and tumor growth. *Nat. Commun.* **10**, 845.

**Gurdon, J. B. and Brown, D. D.** (1965). Cytoplasmic regulation of RNA synthesis and nucleolus formation in developing embryos of Xenopus laevis. *J. Mol. Biol.* **12**, 27-IN4.

**Gustafson, T. and Hjelte, M.-B.** (1951). The amino acid metabolism of the developing

sea urchin egg. *Exp. Cell Res.* **2**, 474–490.

**Ha, J. H. and Loh, S. N.** (1998). Changes in side chain packing during apomyoglobin folding characterized by pulsed thiol-disulfide exchange. *Nat. Struct. Biol.* **5**, 730–737.

**Halbleib, J. M. and Nelson, W. J.** (2006). Cadherins in development: cell adhesion, sorting, and tissue morphogenesis. *Genes Dev.* **20**, 3199–3214.

**Hamadi, A., Bouali, M., Dontenwill, M., Stoeckel, H., Takeda, K. and Rondé, P.** (2005). Regulation of focal adhesion dynamics and disassembly by phosphorylation of FAK at tyrosine 397. *J. Cell Sci.* **118**, 4415–4425.

**Hamidi, H. and Ivaska, J.** (2018). Every step of the way: integrins in cancer progression and metastasis. *Nat. Rev. Cancer* **18**, 533–548.

**Han, Q., Phillips, R. S. and Li, J.** (2019). Editorial: aromatic amino acid metabolism. *Front. Mol. Biosci.* **6**, 22.

**Hanahan, D. and Weinberg, R. A.** (2011). Hallmarks of cancer: the next generation. *Cell* **144**, 646–674.

**Harburger, D. S. and Calderwood, D. A.** (2009). Integrin signalling at a glance. *J. Cell Sci.* **122**, 159–163.

**Hardie, D. G., Ross, F. A. and Hawley, S. A.** (2012). AMPK: a nutrient and energy sensor that maintains energy homeostasis. *Nat. Rev. Mol. Cell Biol.* **13**, 251–262.

**Harland, R. M.** (2018). A new view of embryo development and regeneration. *Science* **360**, 967–968.

**Harrison, O. J., Jin, X., Hong, S., Bahna, F., Ahlsen, G., Brasch, J., Wu, Y., Vendome, J., Felsovalyi, K., Hampton, C. M., et al.** (2011). The extracellular architecture of adherens junctions revealed by crystal structures of type I cadherins. *Structure* **19**, 244–256.

**Harvey, A. J., Kind, K. L. and Thompson, J. G.** (2002). REDOX regulation of early embryo development. *Reproduction* **123**, 479–486.

**Hasegawa, H. and Nakamura, K.** (2010). Tryptophan hydroxylase and serotonin synthesis regulation. In *Handbook of the behavioral neurobiology of serotonin*, pp. 183–202. Elsevier.

**Hauck, C. R., Hsia, D. A. and Schlaepfer, D. D.** (2002). The focal adhesion kinase--a regulator of cell migration and invasion. *IUBMB Life* **53**, 115–119.

**Häussinger, D., Ahrens, T., Sass, H.-J., Pertz, O., Engel, J. and Grzesiek, S.** (2002). Calcium-dependent homoassociation of E-cadherin by NMR spectroscopy: changes in mobility, conformation and mapping of contact regions. *J. Mol. Biol.* **324**, 823–839.

**Hayashi, S. I., Granner, D. K. and Tomkins, G. M.** (1967). Tyrosine aminotransferase. Purificaton and characterization. *J. Biol. Chem.* **242**, 3998–4006.

**Heiles, S.** (2021). Advanced tandem mass spectrometry in metabolomics and lipidomics-methods and applications. *Anal. Bioanal. Chem.* **413**, 5927–5948.

**Heimhalt, M., Mukherjee, P., Grainger, R. A., Szabla, R., Brown, C., Turner, R., Junop, M. S. and Berti, P. J.** (2021). An Inhibitor-in-Pieces Approach to DAHP Synthase Inhibition: Potent Enzyme and Bacterial Growth Inhibition. *ACS Infect. Dis.*

**Herrmann, K. M.** (1995a). The shikimate pathway as an entry to aromatic secondary

metabolism. *Plant Physiol.* **107**, 7–12.
**Herrmann, K. M.** (1995b). The shikimate pathway: early steps in the biosynthesis of aromatic compounds. *Plant Cell* **7**, 907–919.
**Herrmann, K. M. and Weaver, L. M.** (1999). The shikimate pathway. *Annu. Rev. Plant Physiol. Plant Mol. Biol.* **50**, 473–503.
**Herzig, S. and Shaw, R. J.** (2018). AMPK: guardian of metabolism and mitochondrial homeostasis. *Nat. Rev. Mol. Cell Biol.* **19**, 121–135.
**Hetmanski, J. H. R., de Belly, H., Busnelli, I., Waring, T., Nair, R. V., Sokleva, V., Dobre, O., Cameron, A., Gauthier, N., Lamaze, C., et al.** (2019). Membrane Tension Orchestrates Rear Retraction in Matrix-Directed Cell Migration. *Dev. Cell* **51**, 460–475.e10.
**Hewitson, L. C. and Leese, H. J.** (1993). Energy metabolism of the trophectoderm and inner cell mass of the mouse blastocyst. *J. Exp. Zool.* **267**, 337–343.
**Heyes, M. P., Saito, K., Crowley, J. S., Davis, L. E., Demitrack, M. A., Der, M., Dilling, L. A., Elia, J., Kruesi, M. J. and Lackner, A.** (1992). Quinolinic acid and kynurenine pathway metabolism in inflammatory and non-inflammatory neurological disease. *Brain* **115 ( Pt 5)**, 1249–1273.
**Hinkle, P. C. and McCarty, R. E.** (1978). How cells make ATP. *Sci. Am.* **238**, 104–17, 121.
**Hirano, S., Nose, A., Hatta, K., Kawakami, A. and Takeichi, M.** (1987). Calcium-dependent cell-cell adhesion molecules (cadherins): subclass specificities and possible involvement of actin bundles. *J. Cell Biol.* **105**, 2501–2510.
**Hirsh, G. D.** (2017). Mechanisms of Morphogenetic Regulation During Gastrulation .
**Hockel, M.** (2001). Biological consequences of tumor hypoxia. *Semin. Oncol.* **28**, 36–41.
**Höckel, M. and Vaupel, P.** (2001). Tumor hypoxia: definitions and current clinical, biologic, and molecular aspects. *J. Natl. Cancer Inst.* **93**, 266–276.
**Hoffman, S. J., Vasko-Moser, J., Miller, W. H., Lark, M. W., Gowen, M. and Stroup, G.** (2002). Rapid inhibition of thyroxine-induced bone resorption in the rat by an orally active vitronectin receptor antagonist. *J. Pharmacol. Exp. Ther.* **302**, 205–211.
**Hogan, B. L.** (1999). Morphogenesis. *Cell* **96**, 225–233.
**Holden, H. M., Thoden, J. B. and Raushel, F. M.** (1999). Carbamoyl phosphate synthetase: an amazing biochemical odyssey from substrate to product. *Cellular and Molecular Life Sciences (CMLS)* **56**, 507–522.
**Holland, C. K. and Jez, J. M.** (2018). Reaction mechanism of prephenate dehydrogenase from the alternate tyrosine biosynthesis pathway in plants. *Chembiochem* **19**, 1132–1136.
**Hollenbeck, P. J. and Saxton, W. M.** (2005). The axonal transport of mitochondria. *J. Cell Sci.* **118**, 5411–5419.
**Holme, E.** (2003). Disorders of tyrosine degradation. In *Physician's guide to the laboratory diagnosis of metabolic diseases* (ed. Blau, N.), Duran, M.), Blaskovics, M. E.), and Gibson, K. M.), pp. 141–153. Berlin, Heidelberg: Springer Berlin Heidelberg.
**Holme, E. and Mitchell, G. A.** (2014). Tyrosine Metabolism. In *Physician's Guide to*

*the Diagnosis, Treatment, and Follow-Up of Inherited Metabolic Diseases* (ed. Blau, N.), Duran, M.), Gibson, K. M.), and Dionisi Vici, C.), pp. 23–31. Berlin, Heidelberg: Springer Berlin Heidelberg.

**Horwitz, A. R. and Parsons, J. T.** (1999). Cell migration--movin' on. *Science* **286**, 1102–1103.

**Horwitz, R. and Webb, D.** (2003). Cell migration. *Curr. Biol.* **13**, R756-9.

**Hosios, A. M., Hecht, V. C., Danai, L. V., Johnson, M. O., Rathmell, J. C., Steinhauser, M. L., Manalis, S. R. and Vander Heiden, M. G.** (2016). Amino Acids Rather than Glucose Account for the Majority of Cell Mass in Proliferating Mammalian Cells. *Dev. Cell* **36**, 540–549.

**Houghton, F. D.** (2006). Energy metabolism of the inner cell mass and trophectoderm of the mouse blastocyst. *Differentiation.* **74**, 11–18.

**Hu, K. and Yu, Y.** (2017). Metabolite availability as a window to view the early embryo microenvironment in vivo. *Mol. Reprod. Dev.* **84**, 1027–1038.

**Huang, M. and Graves, L. M.** (2003). De novo synthesis of pyrimidine nucleotides; emerging interfaces with signal transduction pathways. *Cell Mol. Life Sci.* **60**, 321–336.

**Huang, Y. and Winklbauer, R.** (2018). Cell migration in the Xenopus gastrula. *Wiley Interdiscip Rev Dev Biol* **7**, e325.

**Hubbard, T. D., Murray, I. A. and Perdew, G. H.** (2015). Indole and tryptophan metabolism: endogenous and dietary routes to ah receptor activation. *Drug Metab. Dispos.* **43**, 1522–1535.

**Huether, G., Kochen, Walter and Simat, Thomas J.** (2012). *Tryptophan, Serotonin, and Melatonin*. 1st ed. Springer Nature.

**Hulbert, A. J.** (2000). Thyroid hormones and their effects: a new perspective. *Biol. Rev. Camb. Philos. Soc.* **75**, 519–631.

**Humphries, M. J., McEwan, P. A., Barton, S. J., Buckley, P. A., Bella, J. and Mould, A. P.** (2003). Integrin structure: heady advances in ligand binding, but activation still makes the knees wobble. *Trends Biochem. Sci.* **28**, 313–320.

**Hur, S. and Bruice, T. C.** (2003). The near attack conformation approach to the study of the chorismate to prephenate reaction. *Proc. Natl. Acad. Sci. USA* **100**, 12015–12020.

**Huttenlocher, A. and Horwitz, A. R.** (2011). Integrins in cell migration. *Cold Spring Harb. Perspect. Biol.* **3**, a005074.

**Hynes, R. O.** (2002). Integrins: bidirectional, allosteric signaling machines. *Cell* **110**, 673–687.

**Iacobazzi, V. and Infantino, V.** (2014). Citrate--new functions for an old metabolite. *Biol. Chem.* **395**, 387–399.

**Ichikawa, T., Stuckenholz, C. and Davidson, L. A.** (2020). Non-junctional role of Cadherin3 in cell migration and contact inhibition of locomotion via domain-dependent, opposing regulation of Rac1. *Sci. Rep.* **10**, 17326.

**Idle, J. R. and Gonzalez, F. J.** (2007). Metabolomics. *Cell Metab.* **6**, 348–351.

**Ikeda, S., Yamaoka-Tojo, M., Hilenski, L., Patrushev, N. A., Anwar, G. M., Quinn, M. T. and Ushio-Fukai, M.** (2005). IQGAP1 regulates reactive oxygen species-dependent endothelial cell migration through interacting with Nox2. *Arterioscler.*

*Thromb. Vasc. Biol.* **25**, 2295–2300.

**Ilina, O. and Friedl, P.** (2009). Mechanisms of collective cell migration at a glance. *J. Cell Sci.* **122**, 3203–3208.

**Ingber, D. E.** (2006). Cellular mechanotransduction: putting all the pieces together again. *FASEB J.* **20**, 811–827.

**Innocenti, M.** (2018). New insights into the formation and the function of lamellipodia and ruffles in mesenchymal cell migration. *Cell Adh Migr* **12**, 401–416.

**Inoue, M., Williams, K. L., Gunn, M. D. and Shinohara, M. L.** (2012). NLRP3 inflammasome induces chemotactic immune cell migration to the CNS in experimental autoimmune encephalomyelitis. *Proc. Natl. Acad. Sci. USA* **109**, 10480–10485.

**Intlekofer, A. M. and Finley, L. W. S.** (2019). Metabolic signatures of cancer cells and stem cells. *Nat. Metab.* **1**, 177–188.

**Ipata, P. L., Camici, M., Micheli, V. and Tozz, M. G.** (2011). Metabolic network of nucleosides in the brain. *Curr. Top. Med. Chem.* **11**, 909–922.

**Ishihara, N., Nomura, M., Jofuku, A., Kato, H., Suzuki, S. O., Masuda, K., Otera, H., Nakanishi, Y., Nonaka, I., Goto, Y.-I., et al.** (2009). Mitochondrial fission factor Drp1 is essential for embryonic development and synapse formation in mice. *Nat. Cell Biol.* **11**, 958–966.

**Jaalouk, D. E. and Lammerding, J.** (2009). Mechanotransduction gone awry. *Nat. Rev. Mol. Cell Biol.* **10**, 63–73.

**Jackson, D. Y.** (2002). Alpha 4 integrin antagonists. *Curr. Pharm. Des.* **8**, 1229–1253.

**Jacob, M., Lopata, A. L., Dasouki, M. and Abdel Rahman, A. M.** (2019). Metabolomics toward personalized medicine. *Mass Spectrom Rev* **38**, 221–238.

**Jaeger, L.** (1945). Glycogen utilization by the amphibian gastrula in relation to invagination and induction. *J Cell Comp Physiol* **25**, 97–120.

**Jewell, J. L. and Guan, K.-L.** (2013). Nutrient signaling to mTOR and cell growth. *Trends Biochem. Sci.* **38**, 233–242.

**Johnson, C. P., Gaetani, M., Ortiz, V., Bhasin, N., Harper, S., Gallagher, P. G., Speicher, D. W. and Discher, D. E.** (2007a). Pathogenic proline mutation in the linker between spectrin repeats: disease caused by spectrin unfolding. *Blood* **109**, 3538–3543.

**Johnson, C. P., Tang, H.-Y., Carag, C., Speicher, D. W. and Discher, D. E.** (2007b). Forced unfolding of proteins within cells. *Science* **317**, 663–666.

**Jorgensen, P.** (2008). Yolk. *Curr. Biol.* **18**, R103-4.

**Jorgensen, P., Steen, J. A. J., Steen, H. and Kirschner, M. W.** (2009). The mechanism and pattern of yolk consumption provide insight into embryonic nutrition in Xenopus. *Development* **136**, 1539–1548.

**Juárez Olguín, H., Calderón Guzmán, D., Hernández García, E. and Barragán Mejía, G.** (2016). The role of dopamine and its dysfunction as a consequence of oxidative stress. *Oxid. Med. Cell. Longev.* **2016**, 9730467.

**Juneja, L. R. and Kim, M.** (2018). Egg Yolk Proteins. In *Hen eggs: their basic and applied science* (ed. Yamamoto, T.), Juneja, L. R.), Hatta, H.), and Kim, M.), pp. 57–71. CRC Press.

**Kabashima, K., Shiraishi, N., Sugita, K., Mori, T., Onoue, A., Kobayashi, M.,**

**Sakabe, J.-I., Yoshiki, R., Tamamura, H., Fujii, N., et al.** (2007). CXCL12-CXCR4 engagement is required for migration of cutaneous dendritic cells. *Am. J. Pathol.* **171**, 1249–1257.

**Kabla, A. J.** (2012). Collective cell migration: leadership, invasion and segregation. *J. R. Soc. Interface* **9**, 3268–3278.

**Kaczmarek, E., Erb, L., Koziak, K., Jarzyna, R., Wink, M. R., Guckelberger, O., Blusztajn, J. K., Trinkaus-Randall, V., Weisman, G. A. and Robson, S. C.** (2005). Modulation of endothelial cell migration by extracellular nucleotides: involvement of focal adhesion kinase and phosphatidylinositol 3-kinase-mediated pathways. *Thromb. Haemost.* **93**, 735–742.

**Kallergi, G., Agelaki, S., Markomanolaki, H., Georgoulias, V. and Stournaras, C.** (2007). Activation of FAK/PI3K/Rac1 signaling controls actin reorganization and inhibits cell motility in human cancer cells. *Cell Physiol. Biochem.* **20**, 977–986.

**Kanehisa, M. and Goto, S.** (2000). KEGG: Kyoto encyclopedia of genes and genomes. *Nucleic Acids Res.* **28**, 27–30.

**Karamichos, D., Asara, J. M. and Zieske, J. D.** (2015). Transforming growth factor: β3 regulates cell metabolism in corneal keratocytes and fibroblasts. In *Studies on the cornea and lens* (ed. Babizhayev, M. A.), Li, D. W.-C.), Kasus-Jacobi, A.), Žorić, L.), and Alió, J. L.), pp. 83–97. New York, NY: Springer New York.

**Karmakar, S. and Lal, G.** (2021). Role of serotonin receptor signaling in cancer cells and anti-tumor immunity. *Theranostics* **11**, 5296–5312.

**Karner, C. M. and Long, F.** (2017). Wnt signaling and cellular metabolism in osteoblasts. *Cell Mol. Life Sci.* **74**, 1649–1657.

**Karnovsky, A. and Li, S.** (2020). Pathway analysis for targeted and untargeted metabolomics. *Methods Mol. Biol.* **2104**, 387–400.

**Kast, P., Tewari, Y. B., Wiest, O., Hilvert, D., Houk, K. N. and Goldberg, R. N.** (1997). Thermodynamics of the conversion of chorismate to prephenate: experimental results and theoretical predictions. *J. Phys. Chem. B* **101**, 10976–10982.

**Katritzky, A. R., Ignatchenko, E. S., Barcock, R. A., Lobanov, V. S. and Karelson, M.** (1994). Prediction of Gas Chromatographic Retention Times and Response Factors Using a General Qualitative Structure-Property Relationships Treatment. *Anal. Chem.* **66**, 1799–1807.

**Kawasumi, A., Nakamura, T., Iwai, N., Yashiro, K., Saijoh, Y., Belo, J. A., Shiratori, H. and Hamada, H.** (2011). Left-right asymmetry in the level of active Nodal protein produced in the node is translated into left-right asymmetry in the lateral plate of mouse embryos. *Dev. Biol.* **353**, 321–330.

**Keeler, J.** (2010). *Understanding NMR Spectroscopy, Second Edition*. 1st ed. Chichester, U.K: Wiley.

**Keller, R. E.** (1975). Vital dye mapping of the gastrula and neurula of Xenopus laevis. I. Prospective areas and morphogenetic movements of the superficial layer. *Dev. Biol.* **42**, 222–241.

**Keller, R. E.** (1976). Vital dye mapping of the gastrula and neurula of Xenopus laevis. *Dev. Biol.* **51**, 118–137.

**Keller, R.** (2002). Shaping the vertebrate body plan by polarized embryonic cell

movements. *Science* **298**, 1950–1954.
**Keller, E. F. and Segel, L. A.** (1971). Model for chemotaxis. *J. Theor. Biol.* **30**, 225–234.
**Keller, R., Davidson, L. A. and Shook, D. R.** (2003). How we are shaped: the biomechanics of gastrulation. *Differentiation.* **71**, 171–205.
**Kelley, L. C., Chi, Q., Cáceres, R., Hastie, E., Schindler, A. J., Jiang, Y., Matus, D. Q., Plastino, J. and Sherwood, D. R.** (2019). Adaptive F-Actin Polymerization and Localized ATP Production Drive Basement Membrane Invasion in the Absence of MMPs. *Dev. Cell* **48**, 313–328.e8.
**Kelly, K., Cochran, B. H., Stiles, C. D. and Leder, P.** (1983). Cell-specific regulation of the c-myc gene by lymphocyte mitogens and platelet-derived growth factor. *Cell* **35**, 603–610.
**Kery, M. and Papandreou, I.** (2020). Emerging strategies to target cancer metabolism and improve radiation therapy outcomes. *Br. J. Radiol.* **93**, 20200067.
**Keyes, S. R. and Rudnick, G.** (1982). Coupling of transmembrane proton gradients to platelet serotonin transport. *J. Biol. Chem.* **257**, 1172–1176.
**Kheradmand, F., Werner, E., Tremble, P., Symons, M. and Werb, Z.** (1998). Role of Rac1 and oxygen radicals in collagenase-1 expression induced by cell shape change. *Science* **280**, 898–902.
**Kiani, F. A. and Fischer, S.** (2014). Catalytic strategy used by the myosin motor to hydrolyze ATP. *Proc. Natl. Acad. Sci. USA* **111**, E2947-56.
**Kierans, S. J. and Taylor, C. T.** (2021). Regulation of glycolysis by the hypoxia-inducible factor (HIF): implications for cellular physiology. *J. Physiol. (Lond.)* **599**, 23–37.
**Kim, S. A., Tai, C.-Y., Mok, L.-P., Mosser, E. A. and Schuman, E. M.** (2011). Calcium-dependent dynamics of cadherin interactions at cell-cell junctions. *Proc. Natl. Acad. Sci. USA* **108**, 9857–9862.
**Kivelä, R., Bry, M., Robciuc, M. R., Räsänen, M., Taavitsainen, M., Silvola, J. M. U., Saraste, A., Hulmi, J. J., Anisimov, A., Mäyränpää, M. I., et al.** (2014). VEGF-B-induced vascular growth leads to metabolic reprogramming and ischemia resistance in the heart. *EMBO Mol. Med.* **6**, 307–321.
**Knott, A. B., Perkins, G., Schwarzenbacher, R. and Bossy-Wetzel, E.** (2008). Mitochondrial fragmentation in neurodegeneration. *Nat. Rev. Neurosci.* **9**, 505–518.
**Kobe, B., Jennings, I. G., House, C. M., Michell, B. J., Goodwill, K. E., Santarsiero, B. D., Stevens, R. C., Cotton, R. G. and Kemp, B. E.** (1999). Structural basis of autoregulation of phenylalanine hydroxylase. *Nat. Struct. Biol.* **6**, 442–448.
**Koizumi, S., Nagatsu, T., Iinuma, H., Ohno, M., Takeuchi, T. and Umezawa, H.** (1982). Inhibition of phenylalanine hydroxylase, a pterin-requiring monooxygenase, by oudenone and its derivatives. *J Antibiot* **35**, 458–462.
**Komazaki, S., Tanaka, N. and Nakamura, H.** (2002). Regional differences in yolk platelet degradation activity and in types of yolk platelets degraded during early amphibian embryogenesis. *Cells Tissues Organs (Print)* **172**, 13–20.
**Komoriya, A., Green, L. J., Mervic, M., Yamada, S. S., Yamada, K. M. and Humphries, M. J.** (1991). The minimal essential sequence for a major cell type-

specific adhesion site (CS1) within the alternatively spliced type III connecting segment domain of fibronectin is leucine-aspartic acid-valine. *J. Biol. Chem.* **266**, 15075–15079.

**Korn, E. D., Carlier, M. F. and Pantaloni, D.** (1987). Actin polymerization and ATP hydrolysis. *Science* **238**, 638–644.

**Koshikawa, N., Giannelli, G., Cirulli, V., Miyazaki, K. and Quaranta, V.** (2000). Role of cell surface metalloprotease MT1-MMP in epithelial cell migration over laminin-5. *J. Cell Biol.* **148**, 615–624.

**Kostakoglu, L., Agress, H. and Goldsmith, S. J.** (2003). Clinical role of FDG PET in evaluation of cancer patients. *Radiographics* **23**, 315–40; quiz 533.

**Koyano, F., Okatsu, K., Kosako, H., Tamura, Y., Go, E., Kimura, M., Kimura, Y., Tsuchiya, H., Yoshihara, H., Hirokawa, T., et al.** (2014). Ubiquitin is phosphorylated by PINK1 to activate parkin. *Nature* **510**, 162–166.

**Krieger, C. C., An, X., Tang, H.-Y., Mohandas, N., Speicher, D. W. and Discher, D. E.** (2011). Cysteine shotgun-mass spectrometry (CS-MS) reveals dynamic sequence of protein structure changes within mutant and stressed cells. *Proc. Natl. Acad. Sci. USA* **108**, 8269–8274.

**Krisher, R. L. and Prather, R. S.** (2012). A role for the Warburg effect in preimplantation embryo development: metabolic modification to support rapid cell proliferation. *Mol. Reprod. Dev.* **79**, 311–320.

**Kuksis, A.** (1992). Yolk lipids. *Biochimica et Biophysica Acta (BBA) - Lipids and Lipid Metabolism* **1124**, 205–222.

**Kumar, C. C.** (2003). Integrin alpha v beta 3 as a therapeutic target for blocking tumor-induced angiogenesis. *Curr Drug Targets* **4**, 123–131.

**Kushnareva, Y., Murphy, A. N. and Andreyev, A.** (2002). Complex I-mediated reactive oxygen species generation: modulation by cytochrome c and NAD(P)+ oxidation-reduction state. *Biochem. J.* **368**, 545–553.

**Lager, S. and Powell, T. L.** (2012). Regulation of nutrient transport across the placenta. *J. Pregnancy* **2012**, 179827.

**Lane, A. N. and Fan, T. W.-M.** (2015). Regulation of mammalian nucleotide metabolism and biosynthesis. *Nucleic Acids Res.* **43**, 2466–2485.

**Lansdown, A. B. G.** (2002). Calcium: a potential central regulator in wound healing in the skin. *Wound Repair Regen.* **10**, 271–285.

**Lauble, H., Kennedy, M. C., Emptage, M. H., Beinert, H. and Stout, C. D.** (1996). The reaction of fluorocitrate with aconitase and the crystal structure of the enzyme-inhibitor complex. *Proc. Natl. Acad. Sci. USA* **93**, 13699–13703.

**Lawson, C. D. and Burridge, K.** (2014). The on-off relationship of Rho and Rac during integrin-mediated adhesion and cell migration. *Small GTPases* **5**, e27958.

**Lazarou, M., Jin, S. M., Kane, L. A. and Youle, R. J.** (2012). Role of PINK1 binding to the TOM complex and alternate intracellular membranes in recruitment and activation of the E3 ligase Parkin. *Dev. Cell* **22**, 320–333.

**Le Clainche, C. and Carlier, M.-F.** (2008). Regulation of actin assembly associated with protrusion and adhesion in cell migration. *Physiol. Rev.* **88**, 489–513.

**Leahy, D. J., Aukhil, I. and Erickson, H. P.** (1996). 2.0 A crystal structure of a four-domain segment of human fibronectin encompassing the RGD loop and synergy

region. *Cell* **84**, 155–164.

**Lecuit, T. and Lenne, P.-F.** (2007). Cell surface mechanics and the control of cell shape, tissue patterns and morphogenesis. *Nat. Rev. Mol. Cell Biol.* **8**, 633–644.

**Ledderose, C., Liu, K., Kondo, Y., Slubowski, C. J., Dertnig, T., Denicoló, S., Arbab, M., Hubner, J., Konrad, K., Fakhari, M., et al.** (2018). Purinergic P2X4 receptors and mitochondrial ATP production regulate T cell migration. *J. Clin. Invest.* **128**, 3583–3594.

**Lee, D. L., Prisbylla, M. P., Cromartie, T. H., Dagarin, D. P., Howard, S. W., Provan, W. M., Ellis, M. K., Fraser, T. and Mutter, L. C.** (1997). The discovery and structural requirements of inhibitors of *p* -hydroxyphenylpyruvate dioxygenase. *Weed Sci.* **45**, 601–609.

**Lee, I., Bender, E., Arnold, S. and Kadenbach, B.** (2001). New control of mitochondrial membrane potential and ROS formation--a hypothesis. *Biol. Chem.* **382**, 1629–1636.

**Lees, J. G., Gardner, D. K. and Harvey, A. J.** (2018). Mitochondrial and glycolytic remodeling during nascent neural differentiation of human pluripotent stem cells. *Development*.

**Legrand, C., Gilles, C., Zahm, J. M., Polette, M., Buisson, A. C., Kaplan, H., Birembaut, P. and Tournier, J. M.** (1999). Airway epithelial cell migration dynamics. MMP-9 role in cell-extracellular matrix remodeling. *J. Cell Biol.* **146**, 517–529.

**Lehka, L. and Rędowicz, M. J.** (2020). Mechanisms regulating myoblast fusion: A multilevel interplay. *Semin. Cell Dev. Biol.* **104**, 81–92.

**Leibovich, A., Moody, S. A., Klein, S. L. and Fainsod, A.** (2022). Xenopus: A Model to Study Natural Genetic Variation and its Disease Implications. In *Xenopus: from basic biology to disease models in the genomic era* (ed. Fainsod, A.) and Moody, S. A.), pp. 313–324. Boca Raton: CRC Press.

**Leiss, M., Beckmann, K., Girós, A., Costell, M. and Fässler, R.** (2008). The role of integrin binding sites in fibronectin matrix assembly in vivo. *Curr. Opin. Cell Biol.* **20**, 502–507.

**Lelli, V., Belardo, A. and Maria Timperio, A.** (2021). From targeted quantification to untargeted metabolomics. In *Metabolomics - Methodology and Applications in Medical Sciences and Life Sciences* (ed. Zhan, X.), p. IntechOpen.

**Leptin, M.** (2005). Gastrulation movements: the logic and the nuts and bolts. *Dev. Cell* **8**, 305–320.

**Levin, L. A. and Bridges, T. S.** (2020). Pattern and diversity in reproduction and development. In *Ecology of marine invertebrate larvae* (ed. McEdward, L.), pp. 1–48. CRC Press.

**Levine, A. J. and Puzio-Kuter, A. M.** (2010). The control of the metabolic switch in cancers by oncogenes and tumor suppressor genes. *Science* **330**, 1340–1344.

**Levraut, J., Iwase, H., Shao, Z. H., Vanden Hoek, T. L. and Schumacker, P. T.** (2003). Cell death during ischemia: relationship to mitochondrial depolarization and ROS generation. *Am. J. Physiol. Heart Circ. Physiol.* **284**, H549-58.

**Li, W. and Sauve, A. A.** (2015). $NAD^+$ content and its role in mitochondria. *Methods Mol. Biol.* **1241**, 39–48.

**Li, L. and Yang, X.** (2018). The essential element manganese, oxidative stress, and metabolic diseases: links and interactions. *Oxid. Med. Cell. Longev.* **2018**, 7580707.

**Li, H. and Zhang, S.** (2017). Functions of vitellogenin in eggs. *Results Probl Cell Differ* **63**, 389–401.

**Li, F., Redick, S. D., Erickson, H. P. and Moy, V. T.** (2003). Force measurements of the alpha5beta1 integrin-fibronectin interaction. *Biophys. J.* **84**, 1252–1262.

**Li, L., He, Y., Zhao, M. and Jiang, J.** (2013). Collective cell migration: Implications for wound healing and cancer invasion. *Burns Trauma* **1**, 21–26.

**Li, T., Wei, L., Zhang, X., Fu, B., Zhou, Y., Yang, M., Cao, M., Chen, Y., Tan, Y., Shi, Y., et al.** (2024a). Serotonin Receptor HTR2B Facilitates Colorectal Cancer Metastasis via CREB1-ZEB1 Axis-Mediated Epithelial-Mesenchymal Transition. *Mol. Cancer Res.* **22**, 538–554.

**Li, J., Jo, M. H., Yan, J., Hall, T., Lee, J., López-Sánchez, U., Yan, S., Ha, T. and Springer, T. A.** (2024b). Ligand binding initiates single-molecule integrin conformational activation. *Cell* **187**, 2990–3005.e17.

**Liang, W., Huang, L., Whelchel, A., Yuan, T., Ma, X., Cheng, R., Takahashi, Y., Karamichos, D. and Ma, J.-X.** (2023). Peroxisome proliferator-activated receptor-α (PPARα) regulates wound healing and mitochondrial metabolism in the cornea. *Proc. Natl. Acad. Sci. USA* **120**, e2217576120.

**Liberti, M. V. and Locasale, J. W.** (2016). The warburg effect: how does it benefit cancer cells? *Trends Biochem. Sci.* **41**, 211–218.

**Liesa, M. and Shirihai, O. S.** (2013). Mitochondrial dynamics in the regulation of nutrient utilization and energy expenditure. *Cell Metab.* **17**, 491–506.

**Lim, S.-O., Gu, J.-M., Kim, M. S., Kim, H.-S., Park, Y. N., Park, C. K., Cho, J. W., Park, Y. M. and Jung, G.** (2008). Epigenetic changes induced by reactive oxygen species in hepatocellular carcinoma: methylation of the E-cadherin promoter. *Gastroenterology* **135**, 2128–40, 2140.e1.

**Lin, T. H., Aplin, A. E., Shen, Y., Chen, Q., Schaller, M., Romer, L., Aukhil, I. and Juliano, R. L.** (1997). Integrin-mediated activation of MAP kinase is independent of FAK: evidence for dual integrin signaling pathways in fibroblasts. *J. Cell Biol.* **136**, 1385–1395.

**Lin, H.-Y., Landersdorfer, C. B., London, D., Meng, R., Lim, C.-U., Lin, C., Lin, S., Tang, H.-Y., Brown, D., Van Scoy, B., et al.** (2011a). Pharmacodynamic modeling of anti-cancer activity of tetraiodothyroacetic acid in a perfused cell culture system. *PLoS Comput. Biol.* **7**, e1001073.

**Lin, H.-Y., Cody, V., Davis, F. B., Hercbergs, A. A., Luidens, M. K., Mousa, S. A. and Davis, P. J.** (2011b). Identification and functions of the plasma membrane receptor for thyroid hormone analogues. *Discov Med* **11**, 337–347.

**Lindon, J. C., Nicholson, J. K. and Everett, J. R.** (1999). NMR spectroscopy of biofluids. In *Annual reports on NMR spectroscopy volume 38*, pp. 1–88. Elsevier.

**Liu, X. and Locasale, J. W.** (2017). Metabolomics: A Primer. *Trends Biochem. Sci.* **42**, 274–284.

**Liu, Y.-C., Li, F., Handler, J., Huang, C. R. L., Xiang, Y., Neretti, N., Sedivy, J. M., Zeller, K. I. and Dang, C. V.** (2008). Global regulation of nucleotide

biosynthetic genes by c-Myc. *PLoS One* **3**, e2722.

**Löffler, M., Fairbanks, L. D., Zameitat, E., Marinaki, A. M. and Simmonds, H. A.** (2005). Pyrimidine pathways in health and disease. *Trends Mol. Med.* **11**, 430–437.

**Löffler, M., Carrey, E. A. and Zameitat, E.** (2015). Orotic Acid, More Than Just an Intermediate of Pyrimidine de novo Synthesis. *J Genet Genomics* **42**, 207–219.

**Löffler, M., Carrey, E. A. and Zameitat, E.** (2016). Orotate (orotic acid): An essential and versatile molecule. *Nucleosides Nucleotides Nucleic Acids* **35**, 566–577.

**Loose, M. and Patient, R.** (2004). A genetic regulatory network for Xenopus mesendoderm formation. *Dev. Biol.* **271**, 467–478.

**Løvtrup-Rein, H. and Nelson, L.** (1982). Changes in energy metabolism during the early development of Xenopus laevis. *Exp. Cell Biol.* **50**, 162–168.

**Lucas, E. P., Khanal, I., Gaspar, P., Fletcher, G. C., Polesello, C., Tapon, N. and Thompson, B. J.** (2013). The Hippo pathway polarizes the actin cytoskeleton during collective migration of Drosophila border cells. *J. Cell Biol.* **201**, 875–885.

**Ludikhuize, M. C., Meerlo, M., Burgering, B. M. T. and Rodríguez Colman, M. J.** (2021). Protocol to profile the bioenergetics of organoids using Seahorse. *STAR Protocols* **2**, 100386.

**Lunt, S. Y. and Vander Heiden, M. G.** (2011). Aerobic glycolysis: meeting the metabolic requirements of cell proliferation. *Annu. Rev. Cell Dev. Biol.* **27**, 441–464.

**Luo, Z., Eichinger, K. M., Zhang, A. and Li, S.** (2023). Targeting cancer metabolic pathways for improving chemotherapy and immunotherapy. *Cancer Lett.* **575**, 216396.

**Lushchak, O. V., Piroddi, M., Galli, F. and Lushchak, V. I.** (2014). Aconitase post-translational modification as a key in linkage between Krebs cycle, iron homeostasis, redox signaling, and metabolism of reactive oxygen species. *Redox Rep* **19**, 8–15.

**Ma, Y., Zhang, P., Wang, F., Yang, J., Yang, Z. and Qin, H.** (2010). The relationship between early embryo development and tumourigenesis. *J. Cell Mol. Med.* **14**, 2697–2701.

**MacColl Garfinkel, A., Mnatsakanyan, N., Patel, J. H., Wills, A. E., Shteyman, A., Smith, P. J. S., Alavian, K. N., Jonas, E. A. and Khokha, M. K.** (2023). Mitochondrial leak metabolism induces the Spemann-Mangold Organizer via Hif-1α in Xenopus. *Dev. Cell* **58**, 2597–2613.e4.

**Macheroux, P., Schmid, J., Amrhein, N. and Schaller, A.** (1999). A unique reaction in a common pathway: mechanism and function of chorismate synthase in the shikimate pathway. *Planta* **207**, 325–334.

**Mai, C. T., Isenburg, J. L., Canfield, M. A., Meyer, R. E., Correa, A., Alverson, C. J., Lupo, P. J., Riehle-Colarusso, T., Cho, S. J., Aggarwal, D., et al.** (2019). National population-based estimates for major birth defects, 2010-2014. *Birth Defects Res.* **111**, 1420–1435.

**Majumdar, R., Steen, K., Coulombe, P. A. and Parent, C. A.** (2019). Non-canonical processes that shape the cell migration landscape. *Curr. Opin. Cell Biol.* **57**, 123–134.

**Mallya, S. K., Partin, J. S., Valdizan, M. C. and Lennarz, W. J.** (1992). Proteolysis of the major yolk glycoproteins is regulated by acidification of the yolk platelets in sea urchin embryos. *J. Cell Biol.* **117**, 1211–1221.

**Mandal, S., Lindgren, A. G., Srivastava, A. S., Clark, A. T. and Banerjee, U.** (2011). Mitochondrial function controls proliferation and early differentiation potential of embryonic stem cells. *Stem Cells* **29**, 486–495.

**Mañes, S., Gómez-Moutón, C., Lacalle, R. A., Jiménez-Baranda, S., Mira, E. and Martínez-A, C.** (2005). Mastering time and space: immune cell polarization and chemotaxis. *Semin. Immunol.* **17**, 77–86.

**Mann, M., Hendrickson, R. C. and Pandey, A.** (2001). Analysis of proteins and proteomes by mass spectrometry. *Annu. Rev. Biochem.* **70**, 437–473.

**Mannava, S., Grachtchouk, V., Wheeler, L. J., Im, M., Zhuang, D., Slavina, E. G., Mathews, C. K., Shewach, D. S. and Nikiforov, M. A.** (2008). Direct role of nucleotide metabolism in C-MYC-dependent proliferation of melanoma cells. *Cell Cycle* **7**, 2392–2400.

**Marin-Hernandez, A., Gallardo-Perez, J., Ralph, S., Rodriguez-Enriquez, S. and Moreno-Sanchez, R.** (2009). HIF-1α Modulates Energy Metabolism in Cancer Cells by Inducing Over-Expression of Specific Glycolytic Isoforms. *MRMC* **9**, 1084–1101.

**Marion, D.** (2013). An introduction to biological NMR spectroscopy. *Mol. Cell Proteomics* **12**, 3006–3025.

**Marsden, M. and DeSimone, D. W.** (2001). Regulation of cell polarity, radial intercalation and epiboly in Xenopus: novel roles for integrin and fibronectin. *Development* **128**, 3635–3647.

**Martinon, F., Pétrilli, V., Mayor, A., Tardivel, A. and Tschopp, J.** (2006). Gout-associated uric acid crystals activate the NALP3 inflammasome. *Nature* **440**, 237–241.

**Mastovská, K. and Lehotay, S. J.** (2003). Practical approaches to fast gas chromatography-mass spectrometry. *J. Chromatogr. A* **1000**, 153–180.

**Mazelis, M.** (1980). Amino Acid Catabolism. In *Amino acids and derivatives*, pp. 541–567. Elsevier.

**McCullagh, M., Saunders, M. G. and Voth, G. A.** (2014). Unraveling the mystery of ATP hydrolysis in actin filaments. *J. Am. Chem. Soc.* **136**, 13053–13058.

**McDonagh, B., Ogueta, S., Lasarte, G., Padilla, C. A. and Bárcena, J. A.** (2009). Shotgun redox proteomics identifies specifically modified cysteines in key metabolic enzymes under oxidative stress in Saccharomyces cerevisiae. *J. Proteomics* **72**, 677–689.

**McKinney, J., Knappskog, P. M. and Haavik, J.** (2005). Different properties of the central and peripheral forms of human tryptophan hydroxylase. *J. Neurochem.* **92**, 311–320.

**McLafferty, F. W.** (1981). Tandem mass spectrometry. *Science* **214**, 280–287.

**McWhorter, F. Y., Davis, C. T. and Liu, W. F.** (2015). Physical and mechanical regulation of macrophage phenotype and function. *Cell Mol. Life Sci.* **72**, 1303–1316.

**Méhes, E. and Vicsek, T.** (2014). Collective motion of cells: from experiments to

models. *Integr Biol (Camb)* **6**, 831–854.
**Meng, W. and Takeichi, M.** (2009). Adherens junction: molecular architecture and regulation. *Cold Spring Harb. Perspect. Biol.* **1**, a002899.
**Miles, K. A. and Williams, R. E.** (2008). Warburg revisited: imaging tumour blood flow and metabolism. *Cancer Imaging* **8**, 81–86.
**Milman, L. S. and Yurowitzki, Y. G.** (1967). The control of glycolysis in early embryogenesis. *Biochimica et Biophysica Acta (BBA) - General Subjects* **148**, 362–371.
**Mitchison, T. J. and Cramer, L. P.** (1996). Actin-based cell motility and cell locomotion. *Cell* **84**, 371–379.
**Mitra, K., Rikhy, R., Lilly, M. and Lippincott-Schwartz, J.** (2012). DRP1-dependent mitochondrial fission initiates follicle cell differentiation during Drosophila oogenesis. *J. Cell Biol.* **197**, 487–497.
**Miyazawa, H., Snaebjornsson, M. T., Prior, N., Kafkia, E., Hammarén, H. M., Tsuchida-Straeten, N., Patil, K. R., Beck, M. and Aulehla, A.** (2022). Glycolytic flux-signaling controls mouse embryo mesoderm development. *Elife* **11**,.
**Moffatt, B. A. and Ashihara, H.** (2002). Purine and pyrimidine nucleotide synthesis and metabolism. *Arabidopsis Book* **1**, e0018.
**Moffett, J. R., Puthillathu, N., Vengilote, R., Jaworski, D. M. and Namboodiri, A. M.** (2020). Acetate Revisited: A Key Biomolecule at the Nexus of Metabolism, Epigenetics and Oncogenesis-Part 1: Acetyl-CoA, Acetogenesis and Acyl-CoA Short-Chain Synthetases. *Front. Physiol.* **11**, 580167.
**Mohammad-Zadeh, L. F., Moses, L. and Gwaltney-Brant, S. M.** (2008). Serotonin: a review. *J Vet Pharmacol Ther* **31**, 187–199.
**Mondal, S., Raja, K., Schweizer, U. and Mugesh, G.** (2016). Chemistry and biology in the biosynthesis and action of thyroid hormones. *Angew. Chem. Int. Ed.* **55**, 7606–7630.
**Montanez, E., Ussar, S., Schifferer, M., Bösl, M., Zent, R., Moser, M. and Fässler, R.** (2008). Kindlin-2 controls bidirectional signaling of integrins. *Genes Dev.* **22**, 1325–1330.
**Montell, D. J.** (2003). Border-cell migration: the race is on. *Nat. Rev. Mol. Cell Biol.* **4**, 13–24.
**Moon, R. T., Kohn, A. D., De Ferrari, G. V. and Kaykas, A.** (2004). WNT and beta-catenin signalling: diseases and therapies. *Nat. Rev. Genet.* **5**, 691–701.
**Moore, G. P. and Sullivan, D. T.** (1975). The characterization of multiple forms of kynurenine formidase in Drosophila melanogaster. *Biochimica et Biophysica Acta (BBA) - Enzymology* **397**, 468–477.
**Moore, S. W., Roca-Cusachs, P. and Sheetz, M. P.** (2010). Stretchy proteins on stretchy substrates: the important elements of integrin-mediated rigidity sensing. *Dev. Cell* **19**, 194–206.
**Mor, I., Cheung, E. C. and Vousden, K. H.** (2011). Control of glycolysis through regulation of PFK1: old friends and recent additions. *Cold Spring Harb. Symp. Quant. Biol.* **76**, 211–216.
**Moris, N., Alev, C., Pera, M. and Martinez Arias, A.** (2021). Biomedical and societal

impacts of in vitro embryo models of mammalian development. *Stem Cell Rep.* **16**, 1021–1030.

**Morlino, G., Barreiro, O., Baixauli, F., Robles-Valero, J., González-Granado, J. M., Villa-Bellosta, R., Cuenca, J., Sánchez-Sorzano, C. O., Veiga, E., Martín-Cófreces, N. B., et al.** (2014). Miro-1 links mitochondria and microtubule Dynein motors to control lymphocyte migration and polarity. *Mol. Cell. Biol.* **34**, 1412–1426.

**Moroni, F., Cozzi, A., Sili, M. and Mannaioni, G.** (2012). Kynurenic acid: a metabolite with multiple actions and multiple targets in brain and periphery. *J. Neural Transm.* **119**, 133–139.

**Morris, R. L. and Hollenbeck, P. J.** (1993). The regulation of bidirectional mitochondrial transport is coordinated with axonal outgrowth. *J. Cell Sci.* **104 ( Pt 3)**, 917–927.

**Morrison, J. F. and Peters, R. A.** (1954). Biochemistry of fluoroacetate poisoning: the effect of fluorocitrate on purified aconitase. *Biochem. J.* **58**, 473–479.

**Mosier, J. A., Wu, Y. and Reinhart-King, C. A.** (2021). Recent advances in understanding the role of metabolic heterogeneities in cell migration. *Fac. Rev.* **10**, 8.

**Mostafavi, S., Balafkan, N., Pettersen, I. K. N., Nido, G. S., Siller, R., Tzoulis, C., Sullivan, G. J. and Bindoff, L. A.** (2021). Distinct Mitochondrial Remodeling During Mesoderm Differentiation in a Human-Based Stem Cell Model. *Front. Cell Dev. Biol.* **9**, 744777.

**Mostafavi-Pour, Z., Askari, J. A., Parkinson, S. J., Parker, P. J., Ng, T. T. C. and Humphries, M. J.** (2003). Integrin-specific signaling pathways controlling focal adhesion formation and cell migration. *J. Cell Biol.* **161**, 155–167.

**Moussaieff, A., Rouleau, M., Kitsberg, D., Cohen, M., Levy, G., Barasch, D., Nemirovski, A., Shen-Orr, S., Laevsky, I., Amit, M., et al.** (2015). Glycolysis-mediated changes in acetyl-CoA and histone acetylation control the early differentiation of embryonic stem cells. *Cell Metab.* **21**, 392–402.

**Mozdy, A. D., McCaffery, J. M. and Shaw, J. M.** (2000). Dnm1p GTPase-mediated mitochondrial fission is a multi-step process requiring the novel integral membrane component Fis1p. *J. Cell Biol.* **151**, 367–380.

**Muhr, J., Arbor, T. C. and Ackerman, K. M.** (2024). Embryology, Gastrulation. In *StatPearls*, p. Treasure Island (FL): StatPearls Publishing.

**Munier-Lehmann, H., Vidalain, P.-O., Tangy, F. and Janin, Y. L.** (2013). On dihydroorotate dehydrogenases and their inhibitors and uses. *J. Med. Chem.* **56**, 3148–3167.

**Munn, D. H. and Mellor, A. L.** (2013). Indoleamine 2,3 dioxygenase and metabolic control of immune responses. *Trends Immunol.* **34**, 137–143.

**Murakami, K. and Yoshino, M.** (1997). Inactivation of aconitase in yeast exposed to oxidative stress. *Biochem Mol Biol Int* **41**, 481–486.

**Murakami, M., Ichisaka, T., Maeda, M., Oshiro, N., Hara, K., Edenhofer, F., Kiyama, H., Yonezawa, K. and Yamanaka, S.** (2004). mTOR is essential for growth and proliferation in early mouse embryos and embryonic stem cells. *Mol. Cell. Biol.* **24**, 6710–6718.

**Murphy, J. M., Park, H. and Lim, S.-T. S.** (2016). FAK and Pyk2 in disease. *Front Biol (Beijing)* **11**, 1–9.

**Murphy, S. L., Kochanek, K. D., Xu, J. and Arias, E.** (2021). Mortality in the United States, 2020. *NCHS Data Brief* 1–8.

**Na, J., Furue, M. K. and Andrews, P. W.** (2010). Inhibition of ERK1/2 prevents neural and mesendodermal differentiation and promotes human embryonic stem cell self-renewal. *Stem Cell Res.* **5**, 157–169.

**Nabeshima, K., Inoue, T., Shimao, Y. and Sameshima, T.** (2002). Matrix metalloproteinases in tumor invasion: role for cell migration. *Pathol Int* **52**, 255–264.

**Nagano, M., Hoshino, D., Koshikawa, N., Akizawa, T. and Seiki, M.** (2012). Turnover of focal adhesions and cancer cell migration. *Int. J. Cell Biol.* **2012**, 310616.

**Nagar, B., Overduin, M., Ikura, M. and Rini, J. M.** (1996). Structural basis of calcium-induced E-cadherin rigidification and dimerization. *Nature* **380**, 360–364.

**Narayanan, R., Mendieta-Serrano, M. A. and Saunders, T. E.** (2021). The role of cellular active stresses in shaping the zebrafish body axis. *Curr. Opin. Cell Biol.* **73**, 69–77.

**Narendra, D., Tanaka, A., Suen, D.-F. and Youle, R. J.** (2008). Parkin is recruited selectively to impaired mitochondria and promotes their autophagy. *J. Cell Biol.* **183**, 795–803.

**Nelson, D. L. and Cox, M. M.** (2008). *Lehninger Principles of Biochemistry*. 5th ed. New York: W. H. Freeman.

**Nguyen, T. N., Padman, B. S. and Lazarou, M.** (2016a). Deciphering the molecular signals of pink1/parkin mitophagy. *Trends Cell Biol.* **26**, 733–744.

**Nguyen, T. N., Padman, B. S., Usher, J., Oorschot, V., Ramm, G. and Lazarou, M.** (2016b). Atg8 family LC3/GABARAP proteins are crucial for autophagosome-lysosome fusion but not autophagosome formation during PINK1/Parkin mitophagy and starvation. *J. Cell Biol.* **215**, 857–874.

**Nielsen, J.** (2017). Systems biology of metabolism: A driver for developing personalized and precision medicine. *Cell Metab.* **25**, 572–579.

**Niessen, C. M., Leckband, D. and Yap, A. S.** (2011). Tissue organization by cadherin adhesion molecules: dynamic molecular and cellular mechanisms of morphogenetic regulation. *Physiol. Rev.* **91**, 691–731.

**Nieto, M. A.** (2013). Epithelial plasticity: a common theme in embryonic and cancer cells. *Science* **342**, 1234850.

**Niezen-Koning, K. E., Wanders, R. J., Ruiter, J. P., Ijlst, L., Visser, G., Reitsma-Bierens, W. C., Heymans, H. S., Reijngoud, D. J. and Smit, G. P.** (1997). Succinyl-CoA:acetoacetate transferase deficiency: identification of a new patient with a neonatal onset and review of the literature. *Eur. J. Pediatr.* **156**, 870–873.

**NMR Spectroscopy** (2006). In *Fundamentals of protein NMR spectroscopy*, pp. 1–27. Berlin/Heidelberg: Springer-Verlag.

**Nordström, A., Want, E., Northen, T., Lehtiö, J. and Siuzdak, G.** (2008). Multiple ionization mass spectrometry strategy used to reveal the complexity of metabolomics. *Anal. Chem.* **80**, 421–429.

**Oda, H. and Takeichi, M.** (2011). Evolution: structural and functional diversity of cadherin at the adherens junction. *J. Cell Biol.* **193**, 1137–1146.

**O'Donovan, G. A. and Neuhard, J.** (1970). Pyrimidine metabolism in microorganisms. *Bacteriol Rev* **34**, 278–343.

**Oginuma, M., Moncuquet, P., Xiong, F., Karoly, E., Chal, J., Guevorkian, K. and Pourquié, O.** (2017). A Gradient of Glycolytic Activity Coordinates FGF and Wnt Signaling during Elongation of the Body Axis in Amniote Embryos. *Dev. Cell* **40**, 342–353.e10.

**Ohisalo, J. J., Laskowska-Klita, T. and Andersson, S. M.** (1982). Development of tyrosine aminotransferase and para-hydroxyphenylpyruvate dioxygenase activities in fetal and neonatal human liver. *J. Clin. Invest.* **70**, 198–200.

**O'Keefe, E. J., Briggaman, R. A. and Herman, B.** (1987). Calcium-induced assembly of adherens junctions in keratinocytes. *J. Cell Biol.* **105**, 807–817.

**Okesli, A., Khosla, C. and Bassik, M. C.** (2017). Human pyrimidine nucleotide biosynthesis as a target for antiviral chemotherapy. *Curr. Opin. Biotechnol.* **48**, 127–134.

**O'Mahony, S. M., Clarke, G., Borre, Y. E., Dinan, T. G. and Cryan, J. F.** (2015). Serotonin, tryptophan metabolism and the brain-gut-microbiome axis. *Behav. Brain Res.* **277**, 32–48.

**Orgel, L. E.** (1999). Are you serious, Dr Mitchell? *Nature* **402**, 17.

**Ouyang, J., Shao, X. and Li, J.** (2000). Indole-3-glycerol phosphate, a branchpoint of indole-3-acetic acid biosynthesis from the tryptophan biosynthetic pathway in Arabidopsis thaliana. *The Plant Journal* **24**, 327–333.

**Padron, A. S., Neto, R. A. L., Pantaleão, T. U., de Souza dos Santos, M. C., Araujo, R. L., de Andrade, B. M., da Silva Leandro, M., de Castro, J. P. S. W., Ferreira, A. C. F. and de Carvalho, D. P.** (2014). Administration of 3,5-diiodothyronine (3,5-T2) causes central hypothyroidism and stimulates thyroid-sensitive tissues. *J. Endocrinol.* **221**, 415–427.

**Painter, K. J.** (2009). Modelling cell migration strategies in the extracellular matrix. *J Math Biol* **58**, 511–543.

**Palén, K., Thörneby, L. and Emanuelsson, H.** (1979). Effects of serotonin and serotonin antagonists on chick embryogenesis. *Wilhelm Roux'. Archiv.* **187**, 89–103.

**Palmer, C. S., Osellame, L. D., Laine, D., Koutsopoulos, O. S., Frazier, A. E. and Ryan, M. T.** (2011). MiD49 and MiD51, new components of the mitochondrial fission machinery. *EMBO Rep.* **12**, 565–573.

**Pan, Z. and Raftery, D.** (2007). Comparing and combining NMR spectroscopy and mass spectrometry in metabolomics. *Anal. Bioanal. Chem.* **387**, 525–527.

**Pandya, P., Orgaz, J. L. and Sanz-Moreno, V.** (2017). Actomyosin contractility and collective migration: may the force be with you. *Curr. Opin. Cell Biol.* **48**, 87–96.

**Pankiv, S., Clausen, T. H., Lamark, T., Brech, A., Bruun, J.-A., Outzen, H., Øvervatn, A., Bjørkøy, G. and Johansen, T.** (2007). p62/SQSTM1 binds directly to Atg8/LC3 to facilitate degradation of ubiquitinated protein aggregates by autophagy. *J. Biol. Chem.* **282**, 24131–24145.

**Pankov, R., Endo, Y., Even-Ram, S., Araki, M., Clark, K., Cukierman, E.,**

**Matsumoto, K. and Yamada, K. M.** (2005). A Rac switch regulates random versus directionally persistent cell migration. *J. Cell Biol.* **170**, 793–802.

**Park, S., Choi, S.-G., Yoo, S.-M., Son, J. H. and Jung, Y.-K.** (2014). Choline dehydrogenase interacts with SQSTM1/p62 to recruit LC3 and stimulate mitophagy. *Autophagy* **10**, 1906–1920.

**Park, J. S., Burckhardt, C. J., Lazcano, R., Solis, L. M., Isogai, T., Li, L., Chen, C. S., Gao, B., Minna, J. D., Bachoo, R., et al.** (2020). Mechanical regulation of glycolysis via cytoskeleton architecture. *Nature* **578**, 621–626.

**Parks, S. K., Mueller-Klieser, W. and Pouysségur, J.** (2020). Lactate and acidity in the cancer microenvironment. *Annu. Rev. Cancer Biol.* **4**, 141–158.

**Parrish, A. R., Catania, J. M., Orozco, J. and Gandolfi, A. J.** (1999). Chemically induced oxidative stress disrupts the E-cadherin/catenin cell adhesion complex. *Toxicol. Sci.* **51**, 80–86.

**Parsons, J. T.** (2003). Focal adhesion kinase: the first ten years. *J. Cell Sci.* **116**, 1409–1416.

**Parsons, J., Slack-Davis, J., Tilghman, R., Iwanicki, M., Ung, E., Autry, C., Luzzio, M., Fingert, H. and Roberts, G.** (2007). Focal Adhesion Kinase: Targeting Adhesions Signals in Normal and Cancer Cells | Clinical Cancer Research | American Association for Cancer Research. *Clin. Cancer Res.*

**Pascual, M. B., El-Azaz, J., de la Torre, F. N., Cañas, R. A., Avila, C. and Cánovas, F. M.** (2016). Biosynthesis and metabolic fate of phenylalanine in conifers. *Front. Plant Sci.* **7**, 1030.

**Pate, K. T., Stringari, C., Sprowl-Tanio, S., Wang, K., TeSlaa, T., Hoverter, N. P., McQuade, M. M., Garner, C., Digman, M. A., Teitell, M. A., et al.** (2014). Wnt signaling directs a metabolic program of glycolysis and angiogenesis in colon cancer. *EMBO J.* **33**, 1454–1473.

**Patel, M. S. and Korotchkina, L. G.** (2006). Regulation of the pyruvate dehydrogenase complex. *Biochem. Soc. Trans.* **34**, 217–222.

**Patel, M. S., Nemeria, N. S., Furey, W. and Jordan, F.** (2014). The pyruvate dehydrogenase complexes: structure-based function and regulation. *J. Biol. Chem.* **289**, 16615–16623.

**Patergnani, S., Suski, J. M., Agnoletto, C., Bononi, A., Bonora, M., De Marchi, E., Giorgi, C., Marchi, S., Missiroli, S., Poletti, F., et al.** (2011). Calcium signaling around Mitochondria Associated Membranes (MAMs). *Cell Commun. Signal.* **9**, 19.

**Patterson, G. W.** (1971). Relation between structure and retention time of sterols in gas chromatograpphy. *Anal. Chem.* **43**, 1165–1170.

**Patti, G. J.** (2011). Separation strategies for untargeted metabolomics. *J Sep Sci* **34**, 3460–3469.

**Peglion, F., Llense, F. and Etienne-Manneville, S.** (2014). Adherens junction treadmilling during collective migration. *Nat. Cell Biol.* **16**, 639–651.

**Pelicano, H., Martin, D. S., Xu, R. H. and Huang, P.** (2006). Glycolysis inhibition for anticancer treatment. *Oncogene* **25**, 4633–4646.

**Pérez-Cerdá, C., Merinero, B., Sanz, P., Jiménez, A., Hernández, C., García, M. J. and Ugarte, M.** (1992). A new case of succinyl-CoA: acetoacetate transferase

deficiency. *J. Inherit. Metab. Dis.* **15**, 371–373.

**Peters, R. A.** (1952). Lethal synthesis. *Proc R Soc Lond, B, Biol Sci* **139**, 143–170.

**Peters, R. and Wakelin, R. W.** (1953). Biochemistry of fluoroacetate poisoning; the isolation and some properties of the fluorotricarboxylic acid inhibitor of citrate metabolism. *Proc R Soc Lond, B, Biol Sci* **140**, 497–507.

**Petrie, R. J., Koo, H. and Yamada, K. M.** (2014). Generation of compartmentalized pressure by a nuclear piston governs cell motility in a 3D matrix. *Science* **345**, 1062–1065.

**Pilotte, L., Larrieu, P., Stroobant, V., Colau, D., Dolusic, E., Frédérick, R., De Plaen, E., Uyttenhove, C., Wouters, J., Masereel, B., et al.** (2012). Reversal of tumoral immune resistance by inhibition of tryptophan 2,3-dioxygenase. *Proc. Natl. Acad. Sci. USA* **109**, 2497–2502.

**Plotnikov, S. V., Pasapera, A. M., Sabass, B. and Waterman, C. M.** (2012). Force fluctuations within focal adhesions mediate ECM-rigidity sensing to guide directed cell migration. *Cell* **151**, 1513–1527.

**Plow, E. F., Haas, T. A., Zhang, L., Loftus, J. and Smith, J. W.** (2000). Ligand binding to integrins. *J. Biol. Chem.* **275**, 21785–21788.

**Pollard, P. J., Wortham, N. C. and Tomlinson, I. P. M.** (2003). The TCA cycle and tumorigenesis: the examples of fumarate hydratase and succinate dehydrogenase. *Ann. Med.* **35**, 632–639.

**Poole, A., Penny, D. and Sjöberg, B. M.** (2001). Confounded cytosine! Tinkering and the evolution of DNA. *Nat. Rev. Mol. Cell Biol.* **2**, 147–151.

**Popov, L.-D.** (2020). Mitochondrial biogenesis: An update. *J. Cell Mol. Med.* **24**, 4892–4899.

**Potter, M., Newport, E. and Morten, K. J.** (2016). The Warburg effect: 80 years on. *Biochem. Soc. Trans.* **44**, 1499–1505.

**Poulsen, C. and Verpoorte, R.** (1991). Roles of chorismate mutase, isochorismate synthase and anthranilate synthase in plants. *Phytochemistry* **30**, 377–386.

**Proudfoot, A. T., Bradberry, S. M. and Vale, J. A.** (2006). Sodium fluoroacetate poisoning. *Toxicol. Rev.* **25**, 213–219.

**Qin, L., Yang, D., Yi, W., Cao, H. and Xiao, G.** (2021). Roles of leader and follower cells in collective cell migration. *Mol. Biol. Cell* **32**, 1267–1272.

**Raftopoulou, M. and Hall, A.** (2004). Cell migration: Rho GTPases lead the way. *Dev. Biol.* **265**, 23–32.

**Ramos, J. W. and DeSimone, D. W.** (1996). Xenopus embryonic cell adhesion to fibronectin: position-specific activation of RGD/synergy site-dependent migratory behavior at gastrulation. *J. Cell Biol.* **134**, 227–240.

**Ramos, J. W., Whittaker, C. A. and DeSimone, D. W.** (1996). Integrin-dependent adhesive activity is spatially controlled by inductive signals at gastrulation. *Development* **122**, 2873–2883.

**Raturi, A. and Simmen, T.** (2013). Where the endoplasmic reticulum and the mitochondrion tie the knot: the mitochondria-associated membrane (MAM). *Biochim. Biophys. Acta* **1833**, 213–224.

**Rauh, D., Blankenburg, C., Fischer, T. G., Jung, N., Kuhn, S., Schatzschneider, U., Schulze, T. and Neumann, S.** (2022). Data format standards in analytical

chemistry. *Pure Appl. Chem.* **94**, 725–736.

**Reaves, M. L., Young, B. D., Hosios, A. M., Xu, Y.-F. and Rabinowitz, J. D.** (2013). Pyrimidine homeostasis is accomplished by directed overflow metabolism. *Nature* **500**, 237–241.

**Redel, B. K., Brown, A. N., Spate, L. D., Whitworth, K. M., Green, J. A. and Prather, R. S.** (2012). Glycolysis in preimplantation development is partially controlled by the Warburg Effect. *Mol. Reprod. Dev.* **79**, 262–271.

**Reed, N. I., Jo, H., Chen, C., Tsujino, K., Arnold, T. D., DeGrado, W. F. and Sheppard, D.** (2015). The αvβ1 integrin plays a critical in vivo role in tissue fibrosis. *Sci. Transl. Med.* **7**, 288ra79.

**Reffay, M., Petitjean, L., Coscoy, S., Grasland-Mongrain, E., Amblard, F., Buguin, A. and Silberzan, P.** (2011). Orientation and polarity in collectively migrating cell structures: statics and dynamics. *Biophys. J.* **100**, 2566–2575.

**Reintsch, W. E. and Hausen, P.** (2001). Dorsoventral differences in cell-cell interactions modulate the motile behaviour of cells from the Xenopus gastrula. *Dev. Biol.* **240**, 387–403.

**Reis, R. A. G., Calil, F. A., Feliciano, P. R., Pinheiro, M. P. and Nonato, M. C.** (2017). The dihydroorotate dehydrogenases: Past and present. *Arch. Biochem. Biophys.* **632**, 175–191.

**Ren, S., Hinzman, A. A., Kang, E. L., Szczesniak, R. D. and Lu, L. J.** (2015). Computational and statistical analysis of metabolomics data. *Metabolomics* **11**, 1492–1513.

**Ren, J.-G., Seth, P., Ye, H., Guo, K., Hanai, J.-I., Husain, Z. and Sukhatme, V. P.** (2017). Citrate Suppresses Tumor Growth in Multiple Models through Inhibition of Glycolysis, the Tricarboxylic Acid Cycle and the IGF-1R Pathway. *Sci. Rep.* **7**, 4537.

**Reynolds, L. P., McLean, K. J., McCarthy, K. L., Diniz, W. J. S., Menezes, A. C. B., Forcherio, J. C., Scott, R. R., Borowicz, P. P., Ward, A. K., Dahlen, C. R., et al.** (2022). Nutritional regulation of embryonic survival, growth, and development. *Adv. Exp. Med. Biol.* **1354**, 63–76.

**Rhyu, D. Y., Yang, Y., Ha, H., Lee, G. T., Song, J. S., Uh, S. and Lee, H. B.** (2005). Role of reactive oxygen species in TGF-beta1-induced mitogen-activated protein kinase activation and epithelial-mesenchymal transition in renal tubular epithelial cells. *J. Am. Soc. Nephrol.* **16**, 667–675.

**Rice, J. M., Dudek, G. O. and Barber, M.** (1965). Mass spectra of nucleic acid derivatives. Pyrimidines. *J. Am. Chem. Soc.* **87**, 4569–4576.

**Richardson, C. M., Dzamba, B. J., Sonavane, P. R. and DeSimone, D. W.** (2018). Integrin and ligand-independent PDGFr signaling synergistically contribute to directional migration of Xenopus mesendoderm. *BioRxiv*.

**Ridley, A. J.** (2001). Rho GTPases and cell migration. *J. Cell Sci.* **114**, 2713–2722.

**Ridley, A. J., Schwartz, M. A., Burridge, K., Firtel, R. A., Ginsberg, M. H., Borisy, G., Parsons, J. T. and Horwitz, A. R.** (2003). Cell migration: integrating signals from front to back. *Science* **302**, 1704–1709.

**Riley, P. A.** (1997). Melanin. *Int. J. Biochem. Cell Biol.* **29**, 1235–1239.

**Rinschen, M. M., Ivanisevic, J., Giera, M. and Siuzdak, G.** (2019). Identification of

bioactive metabolites using activity metabolomics. *Nat. Rev. Mol. Cell Biol.* **20**, 353–367.

**Roberts, W. G., Ung, E., Whalen, P., Cooper, B., Hulford, C., Autry, C., Richter, D., Emerson, E., Lin, J., Kath, J., et al.** (2008). Antitumor activity and pharmacology of a selective focal adhesion kinase inhibitor, PF-562,271. *Cancer Res.* **68**, 1935–1944.

**Robertson, N.** (1979). The carbohydrate content of isolated yolk platelets from early developmental stages of Xenopus laevis. *Cell Differ.* **8**, 173–185.

**Robitaille, A. M., Christen, S., Shimobayashi, M., Cornu, M., Fava, L. L., Moes, S., Prescianotto-Baschong, C., Sauer, U., Jenoe, P. and Hall, M. N.** (2013). Quantitative phosphoproteomics reveal mTORC1 activates de novo pyrimidine synthesis. *Science* **339**, 1320–1323.

**Rodaway, A. and Patient, R.** (2001). Mesendoderm. an ancient germ layer? *Cell* **105**, 169–172.

**Rogers, C. D., Saxena, A. and Bronner, M. E.** (2013). Sip1 mediates an E-cadherin-to-N-cadherin switch during cranial neural crest EMT. *J. Cell Biol.* **203**, 835–847.

**Romani, P., Valcarcel-Jimenez, L., Frezza, C. and Dupont, S.** (2021). Crosstalk between mechanotransduction and metabolism. *Nat. Rev. Mol. Cell Biol.* **22**, 22–38.

**Romani, P., Nirchio, N., Arboit, M., Barbieri, V., Tosi, A., Michielin, F., Shibuya, S., Benoist, T., Wu, D., Hindmarch, C. C. T., et al.** (2022). Mitochondrial fission links ECM mechanotransduction to metabolic redox homeostasis and metastatic chemotherapy resistance. *Nat. Cell Biol.* **24**, 168–180.

**Romano, M., Rosanova, P., Anteo, C. and Limatola, E.** (2004). Vertebrate yolk proteins: a review. *Mol. Reprod. Dev.* **69**, 109–116.

**Rørth, P.** (2007). Collective guidance of collective cell migration. *Trends Cell Biol.* **17**, 575–579.

**Rørth, P.** (2009). Collective cell migration. *Annu. Rev. Cell Dev. Biol.* **25**, 407–429.

**Rosales, C. and Uribe-Querol, E.** (2017). Phagocytosis: A fundamental process in immunity. *Biomed Res. Int.* **2017**, 9042851.

**Roszko, I., Sawada, A. and Solnica-Krezel, L.** (2009). Regulation of convergence and extension movements during vertebrate gastrulation by the Wnt/PCP pathway. *Semin. Cell Dev. Biol.* **20**, 986–997.

**Roussos, E. T., Condeelis, J. S. and Patsialou, A.** (2011). Chemotaxis in cancer. *Nat. Rev. Cancer* **11**, 573–587.

**Rozo, M., Li, L. and Fan, C.-M.** (2016). Targeting β1-integrin signaling enhances regeneration in aged and dystrophic muscle in mice. *Nat. Med.* **22**, 889–896.

**Rudnick, G. and Sandtner, W.** (2019). Serotonin transport in the 21st century. *J. Gen. Physiol.* **151**, 1248–1264.

**Ruoslahti, E.** (1991). Integrins. *J. Clin. Invest.* **87**, 1–5.

**Ruoslahti, E. and Pierschbacher, M. D.** (1987). New perspectives in cell adhesion: RGD and integrins. *Science* **238**, 491–497.

**Salter, M., Hazelwood, R., Pogson, C. I., Iyer, R. and Madge, D. J.** (1995). The effects of a novel and selective inhibitor of tryptophan 2,3-dioxygenase on tryptophan and serotonin metabolism in the rat. *Biochem. Pharmacol.* **49**, 1435–

1442.

**Salvi, A. M. and DeMali, K. A.** (2018). Mechanisms linking mechanotransduction and cell metabolism. *Curr. Opin. Cell Biol.* **54**, 114–120.

**Santos, F. J. and Galceran, M. T.** (2003). Modern developments in gas chromatography-mass spectrometry-based environmental analysis. *J. Chromatogr. A* **1000**, 125–151.

**Sater, A. K., Steinhardt, R. A. and Keller, R.** (1993). Induction of neuronal differentiation by planar signals in Xenopus embryos. *Dev. Dyn.* **197**, 268–280.

**Sattler, U. G. A. and Mueller-Klieser, W.** (2009). The anti-oxidant capacity of tumour glycolysis. *Int J Radiat Biol* **85**, 963–971.

**Savitz, J.** (2020). The kynurenine pathway: a finger in every pie. *Mol. Psychiatry* **25**, 131–147.

**Scarpa, E. and Mayor, R.** (2016). Collective cell migration in development. *J. Cell Biol.* **212**, 143–155.

**Scarpulla, R. C.** (2008). Transcriptional paradigms in mammalian mitochondrial biogenesis and function. *Physiol. Rev.* **88**, 611–638.

**Scarpulla, R. C.** (2011). Metabolic control of mitochondrial biogenesis through the PGC-1 family regulatory network. *Biochim. Biophys. Acta* **1813**, 1269–1278.

**Schaller, M. D.** (2010). Cellular functions of FAK kinases: insight into molecular mechanisms and novel functions. *J. Cell Sci.* **123**, 1007–1013.

**Scheid, A. D., Beadnell, T. C. and Welch, D. R.** (2021). Roles of mitochondria in the hallmarks of metastasis. *Br. J. Cancer* **124**, 124–135.

**Schmidt, C., Sciacovelli, M. and Frezza, C.** (2020). Fumarate hydratase in cancer: A multifaceted tumour suppressor. *Semin. Cell Dev. Biol.* **98**, 15–25.

**Schmitt-Kopplin, P. and Frommberger, M.** (2003). Capillary electrophoresis-mass spectrometry: 15 years of developments and applications. *Electrophoresis* **24**, 3837–3867.

**Schoeman, J. C., Harms, A. C., van Weeghel, M., Berger, R., Vreeken, R. J. and Hankemeier, T.** (2018). Development and application of a UHPLC-MS/MS metabolomics based comprehensive systemic and tissue-specific screening method for inflammatory, oxidative and nitrosative stress. *Anal. Bioanal. Chem.* **410**, 2551–2568.

**Schrimpe-Rutledge, A. C., Codreanu, S. G., Sherrod, S. D. and McLean, J. A.** (2016). Untargeted Metabolomics Strategies-Challenges and Emerging Directions. *J Am Soc Mass Spectrom* **27**, 1897–1905.

**Schuler, M.-H., Lewandowska, A., Caprio, G. D., Skillern, W., Upadhyayula, S., Kirchhausen, T., Shaw, J. M. and Cunniff, B.** (2017). Miro1-mediated mitochondrial positioning shapes intracellular energy gradients required for cell migration. *Mol. Biol. Cell* **28**, 2159–2169.

**Schumacher, S., Dedden, D., Nunez, R. V., Matoba, K., Takagi, J., Biertümpfel, C. and Mizuno, N.** (2021). Structural insights into integrin α5β1 opening by fibronectin ligand. *Sci. Adv.* **7**,.

**Schwager, S. C., Mosier, J. A., Padmanabhan, R. S., White, A., Xing, Q., Hapach, L. A., Taufalele, P. V., Ortiz, I. and Reinhart-King, C. A.** (2022). Link between glucose metabolism and epithelial-to-mesenchymal transition drives triple-

negative breast cancer migratory heterogeneity. *iScience* **25**, 105190.
**Schwartz, M. A. and Assoian, R. K.** (2001). Integrins and cell proliferation: regulation of cyclin-dependent kinases via cytoplasmic signaling pathways. *J. Cell Sci.* **114**, 2553–2560.
**Schwarz, T. L.** (2013). Mitochondrial trafficking in neurons. *Cold Spring Harb. Perspect. Biol.* **5**,.
**Seetharaman, S. and Etienne-Manneville, S.** (2020). Cytoskeletal crosstalk in cell migration. *Trends Cell Biol.* **30**, 720–735.
**Seo, J. H., Agarwal, E., Bryant, K. G., Caino, M. C., Kim, E. T., Kossenkov, A. V., Tang, H.-Y., Languino, L. R., Gabrilovich, D. I., Cohen, A. R., et al.** (2018). Syntaphilin ubiquitination regulates mitochondrial dynamics and tumor cell movements. *Cancer Res.* **78**, 4215–4228.
**Sessions, D. T. and Kashatus, D. F.** (2021). Mitochondrial dynamics in cancer stem cells. *Cell Mol. Life Sci.*
**Sessions, D. T., Kim, K.-B., Kashatus, J. A., Churchill, N., Park, K.-S., Mayo, M. W., Sesaki, H. and Kashatus, D. F.** (2022). Opa1 and Drp1 reciprocally regulate cristae morphology, ETC function, and NAD+ regeneration in KRas-mutant lung adenocarcinoma. *Cell Rep.* **41**, 111818.
**Sferruzzi-Perri, A. N. and Camm, E. J.** (2016). The programming power of the placenta. *Front. Physiol.* **7**, 33.
**Shambaugh, G. E.** (1979). Pyrimidine biosynthesis. *Am. J. Clin. Nutr.* **32**, 1290–1297.
**Sharpley, M. S., Chi, F., Hoeve, J. T. and Banerjee, U.** (2021). Metabolic plasticity drives development during mammalian embryogenesis. *Dev. Cell* **56**, 2329–2347.e6.
**Sheetz, M. P.** (1994). Cell migration by graded attachment to substrates and contraction. *Semin. Cell Biol.* **5**, 149–155.
**Shen, X., Kolluru, G. K., Yuan, S. and Kevil, C. G.** (2015). Measurement of H2S in vivo and in vitro by the monobromobimane method. *Meth. Enzymol.* **554**, 31–45.
**Shimaoka, M., Takagi, J. and Springer, T. A.** (2002). Conformational regulation of integrin structure and function. *Annu. Rev. Biophys. Biomol. Struct.* **31**, 485–516.
**Shimogama, S., Iwao, Y. and Hara, Y.** (2021). Yolk platelets impede nuclear expansion in Xenopus embryos. *Dev. Biol.*
**Sholl-Franco, A., Fragel-Madeira, L., Macama, A. da C. C., Linden, R. and Ventura, A. L. M.** (2010). ATP controls cell cycle and induces proliferation in the mouse developing retina. *Int. J. Dev. Neurosci.* **28**, 63–73.
**Shook, D. R., Wen, J. W. H., Rolo, A., O'Hanlon, M., Francica, B., Dobbins, D., Skoglund, P., DeSimone, D. W., Winklbauer, R. and Keller, R. E.** (2022). Characterization of convergent thickening, a major convergence force producing morphogenic movement in amphibians. *Elife* **11**,.
**Shyh-Chang, N., Daley, G. Q. and Cantley, L. C.** (2013). Stem cell metabolism in tissue development and aging. *Development* **140**, 2535–2547.
**Sica, V., Bravo-San Pedro, J. M., Stoll, G. and Kroemer, G.** (2020). Oxidative phosphorylation as a potential therapeutic target for cancer therapy. *Int. J. Cancer* **146**, 10–17.
**Siddiqui, A., Vazakidou, M. E., Schwab, A., Napoli, F., Fernandez-Molina, C.,**

**Rapa, I., Stemmler, M. P., Volante, M., Brabletz, T. and Ceppi, P.** (2017). Thymidylate synthase is functionally associated with ZEB1 and contributes to the epithelial-to-mesenchymal transition of cancer cells. *J. Pathol.* **242**, 221–233.

**Siddiqui, A., Gollavilli, P. N., Schwab, A., Vazakidou, M. E., Ersan, P. G., Ramakrishnan, M., Pluim, D., Coggins, S., Saatci, O., Annaratone, L., et al.** (2019). Thymidylate synthase maintains the de-differentiated state of triple negative breast cancers. *Cell Death Differ.* **26**, 2223–2236.

**Sieg, D. J., Ilić, D., Jones, K. C., Damsky, C. H., Hunter, T. and Schlaepfer, D. D.** (1998). Pyk2 and Src-family protein-tyrosine kinases compensate for the loss of FAK in fibronectin-stimulated signaling events but Pyk2 does not fully function to enhance FAK- cell migration. *EMBO J.* **17**, 5933–5947.

**Sieg, D. J., Hauck, C. R. and Schlaepfer, D. D.** (1999). Required role of focal adhesion kinase (FAK) for integrin-stimulated cell migration. *J. Cell Sci.* **112 ( Pt 16)**, 2677–2691.

**Siehl, D. L., Connelly, J. A. and Conn, E. E.** (1986). Tyrosine biosynthesis in Sorghum bicolor: characteristics of prephenate aminotransferase. *Z Naturforsch, C, J Biosci* **41**, 79–86.

**Sive, H. L.** (2000). *Early development of Xenopus laevis : a laboratory manual*. Cold Spring Harbor Laboratory Press,.

**Slack, R. J., Macdonald, S. J. F., Roper, J. A., Jenkins, R. G. and Hatley, R. J. D.** (2022). Emerging therapeutic opportunities for integrin inhibitors. *Nat. Rev. Drug Discov.* **21**, 60–78.

**Slack-Davis, J. K., Martin, K. H., Tilghman, R. W., Iwanicki, M., Ung, E. J., Autry, C., Luzzio, M. J., Cooper, B., Kath, J. C., Roberts, W. G., et al.** (2007). Cellular characterization of a novel focal adhesion kinase inhibitor. *J. Biol. Chem.* **282**, 14845–14852.

**Slominski, A., Semak, I., Pisarchik, A., Sweatman, T., Szczesniewski, A. and Wortsman, J.** (2002). Conversion ofL -tryptophan to serotonin and melatonin in human melanoma cells. *FEBS Lett.* **511**, 102–106.

**Slominski, A., Tobin, D. J., Shibahara, S. and Wortsman, J.** (2004). Melanin pigmentation in mammalian skin and its hormonal regulation. *Physiol. Rev.* **84**, 1155–1228.

**Smith, M. L., Gourdon, D., Little, W. C., Kubow, K. E., Eguiluz, R. A., Luna-Morris, S. and Vogel, V.** (2007). Force-induced unfolding of fibronectin in the extracellular matrix of living cells. *PLoS Biol.* **5**, e268.

**Solaini, G., Sgarbi, G., Lenaz, G. and Baracca, A.** (2007). Evaluating mitochondrial membrane potential in cells. *Biosci. Rep.* **27**, 11–21.

**Solnica-Krezel, L.** (2005). Conserved patterns of cell movements during vertebrate gastrulation. *Curr. Biol.* **15**, R213-28.

**Sonavane, P. R., Wang, C., Dzamba, B., Weber, G. F., Periasamy, A. and DeSimone, D. W.** (2017). Mechanical and signaling roles for keratin intermediate filaments in the assembly and morphogenesis of Xenopus mesendoderm tissue at gastrulation. *Development* **144**, 4363–4376.

**Sousa, B., Pereira, J. and Paredes, J.** (2019). The crosstalk between cell adhesion and cancer metabolism. *Int. J. Mol. Sci.* **20**,.

**Speake, B. K., Murray, A. M. and Noble, R. C.** (1998). Transport and transformations of yolk lipids during development of the avian embryo. *Prog. Lipid Res.* **37**, 1–32.

**Srinivas, U. S., Tan, B. W. Q., Vellayappan, B. A. and Jeyasekharan, A. D.** (2019). ROS and the DNA damage response in cancer. *Redox Biol* **25**, 101084.

**Stančíková, M. and Rovenský, J.** (2015). Metabolism of aromatic amino acids. In *Alkaptonuria and Ochronosis* (ed. Rovenský, J.), Urbánek, T.), Oľga, B.), and Gallagher, J. A.), pp. 9–12. Cham: Springer International Publishing.

**Stapornwongkul, K. S., Hahn, E. M., Palau, L. S., Arato, K., Gritti, N., Anlas, K., Polinski, P., Lopez, M., Ebisuya, M. and Trivedi, V.** (2023). Metabolic control of germ layer proportions through regulation of Nodal and Wnt signalling. *BioRxiv*.

**Stark, G.** (2005). Functional consequences of oxidative membrane damage. *J. Membr. Biol.* **205**, 1–16.

**Stemmler, M. P.** (2008). Cadherins in development and cancer. *Mol. Biosyst.* **4**, 835–850.

**Steventon, B., Araya, C., Linker, C., Kuriyama, S. and Mayor, R.** (2009). Differential requirements of BMP and Wnt signalling during gastrulation and neurulation define two steps in neural crest induction. *Development* **136**, 771–779.

**St-Louis, M. and Tanguay, R. M.** (1997). Mutations in the fumarylacetoacetate hydrolase gene causing hereditary tyrosinemia type I: overview. *Hum. Mutat.* **9**, 291–299.

**Stokes, J. B., Adair, S. J., Slack-Davis, J. K., Walters, D. M., Tilghman, R. W., Hershey, E. D., Lowrey, B., Thomas, K. S., Bouton, A. H., Hwang, R. F., et al.** (2011). Inhibition of focal adhesion kinase by PF-562,271 inhibits the growth and metastasis of pancreatic cancer concomitant with altering the tumor microenvironment. *Mol. Cancer Ther.* **10**, 2135–2145.

**Strahl, H. and Hamoen, L. W.** (2010). Membrane potential is important for bacterial cell division. *Proc. Natl. Acad. Sci. USA* **107**, 12281–12286.

**Strauss, E. G. and Strauss, J. H.** (2012). *Comparative Biochemistry V4*. 2nd ed. Elsevier S & T.

**Streit, A., Berliner, A. J., Papanayotou, C., Sirulnik, A. and Stern, C. D.** (2000). Initiation of neural induction by FGF signalling before gastrulation. *Nature* **406**, 74–78.

**Stroud, R. M. and Finer-Moore, J. S.** (2003). Conformational dynamics along an enzymatic reaction pathway: thymidylate synthase, “the movie”. *Biochemistry* **42**, 239–247.

**Su, Y., Xia, W., Li, J., Walz, T., Humphries, M. J., Vestweber, D., Cabañas, C., Lu, C. and Springer, T. A.** (2016). Relating conformation to function in integrin α5β1. *Proc. Natl. Acad. Sci. USA* **113**, E3872-81.

**Sulzmaier, F. J., Jean, C. and Schlaepfer, D. D.** (2014). FAK in cancer: mechanistic findings and clinical applications. *Nat. Rev. Cancer* **14**, 598–610.

**Sumi-Ichinose, C., Ichinose, H., Takahashi, E., Hori, T. and Nagatsu, T.** (1992). Molecular cloning of genomic DNA and chromosomal assignment of the gene for human aromatic L-amino acid decarboxylase, the enzyme for catecholamine and serotonin biosynthesis. *Biochemistry* **31**, 2229–2238.

**Sunyer, R. and Trepat, X.** (2020). Durotaxis. *Curr. Biol.* **30**, R383–R387.
**Sunyer, R., Conte, V., Escribano, J., Elosegui-Artola, A., Labernadie, A., Valon, L., Navajas, D., García-Aznar, J. M., Muñoz, J. J., Roca-Cusachs, P., et al.** (2016). Collective cell durotaxis emerges from long-range intercellular force transmission. *Science* **353**, 1157–1161.
**Surrey, S., Ginzburg, I. and Nemer, M.** (1979). Ribosomal RNA synthesis in pre- and post-gastrula-stage sea urchin embryos. *Dev. Biol.* **71**, 83–99.
**Suski, J. M., Lebiedzinska, M., Bonora, M., Pinton, P., Duszynski, J. and Wieckowski, M. R.** (2012). Relation between mitochondrial membrane potential and ROS formation. *Methods Mol. Biol.* **810**, 183–205.
**Symes, K. and Smith, J. C.** (1987). Gastrulation movements provide an early marker of mesoderm induction in *Xenopus laevis*. *Development* **101**, 339–349.
**Taegtmeyer, H., Hems, R. and Krebs, H. A.** (1980). Utilization of energy-providing substrates in the isolated working rat heart. *Biochem. J.* **186**, 701–711.
**Takagi, J., Petre, B. M., Walz, T. and Springer, T. A.** (2002). Global conformational rearrangements in integrin extracellular domains in outside-in and inside-out signaling. *Cell* **110**, 599–511.
**Takagi, J., Strokovich, K., Springer, T. A. and Walz, T.** (2003). Structure of integrin alpha5beta1 in complex with fibronectin. *EMBO J.* **22**, 4607–4615.
**Takeichi, M.** (1988). The cadherins: cell-cell adhesion molecules controlling animal morphogenesis. *Development* **102**, 639–655.
**Takeichi, M.** (1991). Cadherin cell adhesion receptors as a morphogenetic regulator. *Science* **251**, 1451–1455.
**Tang, B. L.** (2016). Sirt1 and the mitochondria. *Mol. Cells* **39**, 87–95.
**Tatibana, M.** (1978). Interrelationship of purine and pyrimidine metabolism. In *Uric Acid* (ed. Kelley, W. N.) and Weiner, I. M.), pp. 125–154. Berlin, Heidelberg: Springer Berlin Heidelberg.
**Tatibana, M. and Shigesada, K.** (1972). Two carbamyl phosphate synthetases of mammals: Specific roles in control of pyrimidine and urea biosynthesis. *Adv. Enzyme Regul.* **10**, 249–271.
**Tennessen, J. M., Bertagnolli, N. M., Evans, J., Sieber, M. H., Cox, J. and Thummel, C. S.** (2014). Coordinated metabolic transitions during Drosophila embryogenesis and the onset of aerobic glycolysis. *G3 (Bethesda)* **4**, 839–850.
**Ternette, N., Yang, M., Laroyia, M., Kitagawa, M., O'Flaherty, L., Wolhulter, K., Igarashi, K., Saito, K., Kato, K., Fischer, R., et al.** (2013). Inhibition of mitochondrial aconitase by succination in fumarate hydratase deficiency. *Cell Rep.* **3**, 689–700.
**Thackray, S. J., Mowat, C. G. and Chapman, S. K.** (2008). Exploring the mechanism of tryptophan 2,3-dioxygenase. *Biochem. Soc. Trans.* **36**, 1120–1123.
**Thangadurai, S., Bajgiran, M., Manickam, S., Mohana-Kumaran, N. and Azzam, G.** (2022). CTP synthase: the hissing of the cellular serpent. *Histochem. Cell Biol.* **158**, 517–534.
**Théry, M. and Piel, M.** (2009). Adhesive micropatterns for cells: a microcontact printing protocol. *Cold Spring Harb. Protoc.* **2009**, pdb.prot5255.
**Theveneau, E. and Linker, C.** (2017). Leaders in collective migration: are front cells

really endowed with a particular set of skills? [version 1; peer review: 2 approved]. *F1000Res.* **6**, 1899.

**Theveneau, E. and Mayor, R.** (2012). Cadherins in collective cell migration of mesenchymal cells. *Curr. Opin. Cell Biol.* **24**, 677–684.

**Thiery, J. P., Acloque, H., Huang, R. Y. J. and Nieto, M. A.** (2009). Epithelial-mesenchymal transitions in development and disease. *Cell* **139**, 871–890.

**Thomas, K. J. and Jacobson, M. R.** (2012). Defects in mitochondrial fission protein dynamin-related protein 1 are linked to apoptotic resistance and autophagy in a lung cancer model. *PLoS One* **7**, e45319.

**Tilekar, K., Upadhyay, N., Iancu, C. V., Pokrovsky, V., Choe, J.-Y. and Ramaa, C. S.** (2020). Power of two: Combination of therapeutic approaches involving glucose transporter (GLUT) inhibitors to combat cancer. *Biochim. Biophys. Acta Rev. Cancer* 188457.

**Timme-Laragy, A. R., Hahn, M. E., Hansen, J. M., Rastogi, A. and Roy, M. A.** (2018). Redox stress and signaling during vertebrate embryonic development: Regulation and responses. *Semin. Cell Dev. Biol.* **80**, 17–28.

**Tittarelli, R., Mannocchi, G., Pantano, F. and Romolo, F. S.** (2015). Recreational use, analysis and toxicity of tryptamines. *Curr Neuropharmacol* **13**, 26–46.

**Tohge, T., Watanabe, M., Hoefgen, R. and Fernie, A. R.** (2013). Shikimate and phenylalanine biosynthesis in the green lineage. *Front. Plant Sci.* **4**, 62.

**Través, P. G., de Atauri, P., Marín, S., Pimentel-Santillana, M., Rodríguez-Prados, J.-C., Marín de Mas, I., Selivanov, V. A., Martín-Sanz, P., Boscá, L. and Cascante, M.** (2012). Relevance of the MEK/ERK signaling pathway in the metabolism of activated macrophages: a metabolomic approach. *J. Immunol.* **188**, 1402–1410.

**Trepat, X. and Fredberg, J. J.** (2011). Plithotaxis and emergent dynamics in collective cellular migration. *Trends Cell Biol.* **21**, 638–646.

**Trepat, X., Wasserman, M. R., Angelini, T. E., Millet, E., Weitz, D. A., Butler, J. P. and Fredberg, J. J.** (2009). Physical forces during collective cell migration. *Nat. Phys.* **5**, 426–430.

**Trepat, X., Chen, Z. and Jacobson, K.** (2012). Cell migration. *Compr. Physiol.* **2**, 2369–2392.

**Trexler, J. C. and DeAngelis, D. L.** (2003). Resource allocation in offspring provisioning: an evaluation of the conditions favoring the evolution of matrotrophy. *Am. Nat.* **162**, 574–585.

**Turing, A. M.** (1990). The chemical basis of morphogenesis. *Bull Math Biol* **52**, 153–97; discussion 119.

**Tymoczko, S. B.** (2007). *Biochemistry*. 6th ed. New York: W. H. Freeman and Company.

**US Centers for Disease Control** (2020). *Web-based Injury Statistics Query and Reporting System (WISQARS)*. Atlanta, GA: CDC, National Center for Injury Prevention and Control.

**van der Donk, W. A. and Zhao, H.** (2003). Recent developments in pyridine nucleotide regeneration. *Curr. Opin. Biotechnol.* **14**, 421–426.

**van Gennip, A. H., Abeling, N. G., Vreken, P. and van Kuilenburg, A. B.** (1997).

Inborn errors of pyrimidine degradation: clinical, biochemical and molecular aspects. *J. Inherit. Metab. Dis.* **20**, 203–213.

**van Wetering, S., van Buul, J. D., Quik, S., Mul, F. P. J., Anthony, E. C., ten Klooster, J.-P., Collard, J. G. and Hordijk, P. L.** (2002). Reactive oxygen species mediate Rac-induced loss of cell-cell adhesion in primary human endothelial cells. *J. Cell Sci.* **115**, 1837–1846.

**Vandenberg, L. N., Lemire, J. M. and Levin, M.** (2013). Serotonin has early, cilia-independent roles in Xenopus left-right patterning. *Dis. Model. Mech.* **6**, 261–268.

**Vander Heiden, M. G., Cantley, L. C. and Thompson, C. B.** (2009). Understanding the Warburg effect: the metabolic requirements of cell proliferation. *Science* **324**, 1029–1033.

**VanderVorst, K., Dreyer, C. A., Konopelski, S. E., Lee, H., Ho, H.-Y. H. and Carraway, K. L.** (2019). Wnt/pcp signaling contribution to carcinoma collective cell migration and metastasis. *Cancer Res.* **79**, 1719–1729.

**VanLinden, M. R., Skoge, R. H. and Ziegler, M.** (2015). Discovery, metabolism and functions of NAD and NADP. *Biochem (Lond)* **37**, 9–13.

**Vastag, L., Jorgensen, P., Peshkin, L., Wei, R., Rabinowitz, J. D. and Kirschner, M. W.** (2011). Remodeling of the metabolome during early frog development. *PLoS One* **6**, e16881.

**Vaupel, P. and Multhoff, G.** (2021). Revisiting the Warburg effect: historical dogma versus current understanding. *J. Physiol. (Lond.)* **599**, 1745–1757.

**Vazquez, A., Liu, J., Zhou, Y. and Oltvai, Z. N.** (2010). Catabolic efficiency of aerobic glycolysis: the Warburg effect revisited. *BMC Syst. Biol.* **4**, 58.

**Ventura-Clapier, R., Garnier, A. and Veksler, V.** (2008). Transcriptional control of mitochondrial biogenesis: the central role of PGC-1alpha. *Cardiovasc. Res.* **79**, 208–217.

**Vicente-Manzanares, M. and Horwitz, A. R.** (2011). Cell migration: an overview. *Methods Mol. Biol.* **769**, 1–24.

**Vicente-Manzanares, M., Ma, X., Adelstein, R. S. and Horwitz, A. R.** (2009). Non-muscle myosin II takes centre stage in cell adhesion and migration. *Nat. Rev. Mol. Cell Biol.* **10**, 778–790.

**Visavadiya, N. P., Keasey, M. P., Razskazovskiy, V., Banerjee, K., Jia, C., Lovins, C., Wright, G. L. and Hagg, T.** (2016). Integrin-FAK signaling rapidly and potently promotes mitochondrial function through STAT3. *Cell Commun. Signal.* **14**, 32.

**Vitorino, P., Hammer, M., Kim, J. and Meyer, T.** (2011). A steering model of endothelial sheet migration recapitulates monolayer integrity and directed collective migration. *Mol. Cell. Biol.* **31**, 342–350.

**von Dassow, M. and Davidson, L. A.** (2009). Natural variation in embryo mechanics: gastrulation in Xenopus laevis is highly robust to variation in tissue stiffness. *Dev. Dyn.* **238**, 2–18.

**Vu, T., Riekeberg, E., Qiu, Y. and Powers, R.** (2018). Comparing normalization methods and the impact of noise. *Metabolomics* **14**, 108.

**Wacker, S., Grimm, K., Joos, T. and Winklbauer, R.** (2000). Development and control of tissue separation at gastrulation in Xenopus. *Dev. Biol.* **224**, 428–439.

**Walker, J. E.** (1992). The NADH:ubiquinone oxidoreductase (complex I) of respiratory chains. *Q Rev Biophys* **25**, 253–324.

**Wallingford, J. B.** (2019). We are all developmental biologists. *Dev. Cell* **50**, 132–137.

**Walsh, C. T., Liu, J., Rusnak, F. and Sakaitani, M.** (1990). Molecular studies on enzymes in chorismate metabolism and the enterobactin biosynthetic pathway. *Chem. Rev.* **90**, 1105–1129.

**Walter, M. and Herr, P.** (2022). Re-Discovery of Pyrimidine Salvage as Target in Cancer Therapy. *Cells* **11**,.

**Walther, D. J., Peter, J.-U., Bashammakh, S., Hörtnagl, H., Voits, M., Fink, H. and Bader, M.** (2003). Synthesis of serotonin by a second tryptophan hydroxylase isoform. *Science* **299**, 76.

**Wang, L. and Chen, Y.-G.** (2016). Signaling Control of Differentiation of Embryonic Stem Cells toward Mesendoderm. *J. Mol. Biol.* **428**, 1409–1422.

**Wang, Y., Zang, Q. S., Liu, Z., Wu, Q., Maass, D., Dulan, G., Shaul, P. W., Melito, L., Frantz, D. E., Kilgore, J. A., et al.** (2011). Regulation of VEGF-induced endothelial cell migration by mitochondrial reactive oxygen species. *Am. J. Physiol. Cell Physiol.* **301**, C695-704.

**Wang, Q., Zou, Y., Nowotschin, S., Kim, S. Y., Li, Q. V., Soh, C.-L., Su, J., Zhang, C., Shu, W., Xi, Q., et al.** (2017). The p53 family coordinates wnt and nodal inputs in mesendodermal differentiation of embryonic stem cells. *Cell Stem Cell* **20**, 70–86.

**Wang, Y., Ma, L., Zhang, M., Chen, M., Li, P., He, C., Yan, C. and Wan, J.-B.** (2019). A Simple Method for Peak Alignment Using Relative Retention Time Related to an Inherent Peak in Liquid Chromatography-Mass Spectrometry-Based Metabolomics. *J Chromatogr Sci* **57**, 9–16.

**Wang, Y., Tang, B., Long, L., Luo, P., Xiang, W., Li, X., Wang, H., Jiang, Q., Tan, X., Luo, S., et al.** (2021a). Improvement of obesity-associated disorders by a small-molecule drug targeting mitochondria of adipose tissue macrophages. *Nat. Commun.* **12**, 102.

**Wang, W., Cui, J., Ma, H., Lu, W. and Huang, J.** (2021b). Targeting pyrimidine metabolism in the era of precision cancer medicine. *Front. Oncol.* **11**, 684961.

**Warner, A. H. and Finamore, F. J.** (1962). Nucleotide and nucleic acid metabolism in developing amphibian embryos—III. Metabolism of acid-soluble nucleotides. *Comp. Biochem. Physiol.* **5**, 233–240.

**Watson, A. J. and Barcroft, L. C.** (2001). Regulation of blastocyst formation. *Front. Biosci.* **6**, D708-30.

**Weaver, L. M. and Herrmann, K. M.** (1997). Dynamics of the shikimate pathway in plants. *Trends Plant Sci.* **2**, 346–351.

**Weber, G., Jayaram, H. N., Pillwein, K., Natsumeda, Y., Reardon, M. A. and Zhen, Y. S.** (1987). Salvage pathways as targets of chemotherapy. *Adv. Enzyme Regul.* **26**, 335–352.

**Weber, G. F., Bjerke, M. A. and DeSimone, D. W.** (2011). Integrins and cadherins join forces to form adhesive networks. *J. Cell Sci.* **124**, 1183–1193.

**Weber, G. F., Bjerke, M. A. and DeSimone, D. W.** (2012). A mechanoresponsive cadherin-keratin complex directs polarized protrusive behavior and collective cell

migration. *Dev. Cell* **22**, 104–115.
**Webster, W. S. and Abela, D.** (2007). The effect of hypoxia in development. *Birth Defects Res C Embryo Today* **81**, 215–228.
**Weijer, C. J.** (2009). Collective cell migration in development. *J. Cell Sci.* **122**, 3215–3223.
**Weiss, H., Friedrich, T., Hofhaus, G. and Preis, D.** (1992). The respiratory-chain NADH dehydrogenase (complex I) of mitochondria. In *EJB Reviews 1991* (ed. Christen, P.) and Hofmann, E.), pp. 55–68. Berlin, Heidelberg: Springer Berlin Heidelberg.
**Wells, C. M. and Parsons, M. eds.** (2011). *Cell Migration*. Totowa, NJ: Humana Press.
**Wenz, T.** (2009). PGC-1alpha activation as a therapeutic approach in mitochondrial disease. *IUBMB Life* **61**, 1051–1062.
**Werner, E. and Werb, Z.** (2002). Integrins engage mitochondrial function for signal transduction by a mechanism dependent on Rho GTPases. *J. Cell Biol.* **158**, 357–368.
**Weyand, M. and Schlichting, I.** (1999). Crystal structure of wild-type tryptophan synthase complexed with the natural substrate indole-3-glycerol phosphate. *Biochemistry* **38**, 16469–16480.
**Whittaker, C. A. and DeSimone, D. W.** (1993). Integrin alpha subunit mRNAs are differentially expressed in early Xenopus embryos. *Development* **117**, 1239–1249.
**Wiklund, P. and Bergman, J.** (2006). The chemistry of anthranilic acid. *Curr. Org. Synth.* **3**, 379–402.
**Wiley, H. S. and Wallace, R. A.** (1981). The structure of vitellogenin. Multiple vitellogenins in Xenopus laevis give rise to multiple forms of the yolk proteins. *J. Biol. Chem.* **256**, 8626–8634.
**Williamson, J. R. and Cooper, R. H.** (1980). Regulation of the citric acid cycle in mammalian systems. *FEBS Lett.* **117 Suppl**, K73-85.
**Winklbauer, R. and Nagel, M.** (1991). Directional mesoderm cell migration in the Xenopus gastrula. *Dev. Biol.* **148**, 573–589.
**Wishart, D. S., Tzur, D., Knox, C., Eisner, R., Guo, A. C., Young, N., Cheng, D., Jewell, K., Arndt, D., Sawhney, S., et al.** (2007). HMDB: the human metabolome database. *Nucleic Acids Res.* **35**, D521-6.
**Wishart, D. S., Mandal, R., Stanislaus, A. and Ramirez-Gaona, M.** (2016). Cancer metabolomics and the human metabolome database. *Metabolites* **6**,.
**Wiskich, J. T.** (1980). Control of the Krebs Cycle**Abbreviations F1-ATPase; the mitochondrial ATP-synthesizing complex; NAD, nicotinamide adenine dinucleotide (oxidized form-NAD+; reduced form-NADH); NADP, nicotinamide adenine dinucleotide phosphate. In *Metabolism and Respiration*, pp. 243–278. Elsevier.
**Wolf, K., Mazo, I., Leung, H., Engelke, K., von Andrian, U. H., Deryugina, E. I., Strongin, A. Y., Bröcker, E.-B. and Friedl, P.** (2003). Compensation mechanism in tumor cell migration: mesenchymal-amoeboid transition after blocking of pericellular proteolysis. *J. Cell Biol.* **160**, 267–277.
**Wolpert, L. and Vicente, C.** (2015). An interview with Lewis Wolpert. *Development* **142**, 2547–2548.

**Wolpert, L., Tickle, C., Arias, A. M., Lawrence, P. A. and (Cytogeneticist), J. L.** (2023). *Principles Of Development*.

**Worley, B. and Powers, R.** (2013). Multivariate analysis in metabolomics. *Curr. Metabolomics* **1**, 92–107.

**Wu, Y. and Li, L.** (2016). Sample normalization methods in quantitative metabolomics. *J. Chromatogr. A* **1430**, 80–95.

**Wu, R. F., Gu, Y., Xu, Y. C., Nwariaku, F. E. and Terada, L. S.** (2003). Vascular endothelial growth factor causes translocation of p47phox to membrane ruffles through WAVE1. *J. Biol. Chem.* **278**, 36830–36840.

**Wu, R. F., Xu, Y. C., Ma, Z., Nwariaku, F. E., Sarosi, G. A. and Terada, L. S.** (2005). Subcellular targeting of oxidants during endothelial cell migration. *J. Cell Biol.* **171**, 893–904.

**Wu, H., Tian, C., Song, X., Liu, C., Yang, D. and Jiang, Z.** (2013). Methods for the regeneration of nicotinamide coenzymes. *Green Chem.* **15**, 1773.

**Wu, J., Jin, Z., Zheng, H. and Yan, L.-J.** (2016). Sources and implications of NADH/NAD(+) redox imbalance in diabetes and its complications. *Diabetes. Metab. Syndr. Obes.* **9**, 145–153.

**Xia, W. and Springer, T. A.** (2014). Metal ion and ligand binding of integrin α5β1. *Proc. Natl. Acad. Sci. USA* **111**, 17863–17868.

**Xia, J. and Wishart, D. S.** (2010). MetPA: a web-based metabolomics tool for pathway analysis and visualization. *Bioinformatics* **26**, 2342–2344.

**Xin, C., Zhu, C., Jin, Y. and Li, H.** (2021). Discovering the role of VEGF signaling pathway in mesendodermal induction of human embryonic stem cells. *Biochem. Biophys. Res. Commun.* **553**, 58–64.

**Xiong, J.-P., Stehle, T., Zhang, R., Joachimiak, A., Frech, M., Goodman, S. L. and Arnaout, M. A.** (2002). Crystal structure of the extracellular segment of integrin alpha Vbeta3 in complex with an Arg-Gly-Asp ligand. *Science* **296**, 151–155.

**Xiong, J. P., Stehle, T., Goodman, S. L. and Arnaout, M. A.** (2003). Integrins, cations and ligands: making the connection. *J. Thromb. Haemost.* **1**, 1642–1654.

**Xu, X., Wang, L., Liu, B., Xie, W. and Chen, Y.-G.** (2018). Activin/Smad2 and Wnt/β-catenin up-regulate HAS2 and ALDH3A2 to facilitate mesendoderm differentiation of human embryonic stem cells. *J. Biol. Chem.* **293**, 18444–18453.

**Xue, F., Janzen, D. M. and Knecht, D. A.** (2010). Contribution of Filopodia to Cell Migration: A Mechanical Link between Protrusion and Contraction. *Int. J. Cell Biol.* **2010**, 507821.

**Yamada, K. M. and Sixt, M.** (2019). Mechanisms of 3D cell migration. *Nat. Rev. Mol. Cell Biol.* **20**, 738–752.

**Yamada, S., Pokutta, S., Drees, F., Weis, W. I. and Nelson, W. J.** (2005). Deconstructing the cadherin-catenin-actin complex. *Cell* **123**, 889–901.

**Yamaguchi, N., Mizutani, T., Kawabata, K. and Haga, H.** (2015). Leader cells regulate collective cell migration via Rac activation in the downstream signaling of integrin β1 and PI3K. *Sci. Rep.* **5**, 7656.

**Yamamoto, A., Doak, A. E. and Cheung, K. J.** (2023). Orchestration of collective migration and metastasis by tumor cell clusters. *Annu. Rev. Pathol.* **18**, 231–256.

**Yan, L. J., Levine, R. L. and Sohal, R. S.** (1997). Oxidative damage during aging

targets mitochondrial aconitase. *Proc. Natl. Acad. Sci. USA* **94**, 11168–11172.
**Yanamadala, V.** (2024). Amino Acid Metabolism. In *Essential medical biochemistry and metabolic disease: A pocket guide for medical students and residents*, pp. 91–123. Cham: Springer Nature Switzerland.
**Yang, Y. and Sauve, A. A.** (2016). NAD(+) metabolism: Bioenergetics, signaling and manipulation for therapy. *Biochim. Biophys. Acta* **1864**, 1787–1800.
**Yang, Z., Dan Wang, Li, Y., Zhou, X., Liu, T., Shi, C., Li, R., Zhang, Y., Zhang, J., Yan, J., et al.** (2022). Untargeted metabolomics analysis of the anti-diabetic effect of Red ginseng extract in Type 2 diabetes Mellitus rats based on UHPLC-MS/MS. *Biomed. Pharmacother.* **146**, 112495.
**Yap, A. S., Brieher, W. M. and Gumbiner, B. M.** (1997). Molecular and functional analysis of cadherin-based adherens junctions. *Annu. Rev. Cell Dev. Biol.* **13**, 119–146.
**Yehuda-Shnaidman, E., Kalderon, B. and Bar-Tana, J.** (2014). Thyroid hormone, thyromimetics, and metabolic efficiency. *Endocr. Rev.* **35**, 35–58.
**Yeung, S. J., Pan, J. and Lee, M. H.** (2008). Roles of p53, MYC and HIF-1 in regulating glycolysis - the seventh hallmark of cancer. *Cell Mol. Life Sci.* **65**, 3981–3999.
**Ying, W.** (2006). NAD+ and NADH in cellular functions and cell death. *Front. Biosci.* **11**, 3129.
**Yoon, J. C., Ng, A., Kim, B. H., Bianco, A., Xavier, R. J. and Elledge, S. J.** (2010). Wnt signaling regulates mitochondrial physiology and insulin sensitivity. *Genes Dev.* **24**, 1507–1518.
**Youle, R. J. and Narendra, D. P.** (2011). Mechanisms of mitophagy. *Nat. Rev. Mol. Cell Biol.* **12**, 9–14.
**Young, S. N. and Leyton, M.** (2002). The role of serotonin in human mood and social interaction. *Pharmacology Biochemistry and Behavior* **71**, 857–865.
**Yuan, H., Cho, H., Chen, H. H., Panagia, M., Sosnovik, D. E. and Josephson, L.** (2013). Fluorescent and radiolabeled triphenylphosphonium probes for imaging mitochondria. *Chem. Commun.* **49**, 10361–10363.
**Yuan, D., Xiao, D., Gao, Q. and Zeng, L.** (2019). PGC-1α activation: a therapeutic target for type 2 diabetes? *Eat Weight Disord* **24**, 385–395.
**Zamboni, N., Saghatelian, A. and Patti, G. J.** (2015). Defining the metabolome: size, flux, and regulation. *Mol. Cell* **58**, 699–706.
**Zanotelli, M. R., Goldblatt, Z. E., Miller, J. P., Bordeleau, F., Li, J., VanderBurgh, J. A., Lampi, M. C., King, M. R. and Reinhart-King, C. A.** (2018). Regulation of ATP utilization during metastatic cell migration by collagen architecture. *Mol. Biol. Cell* **29**, 1–9.
**Zanotelli, M. R., Zhang, J. and Reinhart-King, C. A.** (2021). Mechanoresponsive metabolism in cancer cell migration and metastasis. *Cell Metab.* **33**, 1307–1321.
**Zanotelli, M. R., Zhang, J., Ortiz, I., Wang, W., Chada, N. C. and Reinhart-King, C. A.** (2022). Highly motile cells are metabolically responsive to collagen density. *Proc. Natl. Acad. Sci. USA* **119**, e2114672119.
**Zegers, M. M. and Friedl, P.** (2014). Rho GTPases in collective cell migration. *Small GTPases* **5**, e28997.

**Zeki, Ö. C., Eylem, C. C., Reçber, T., Kır, S. and Nemutlu, E.** (2020). Integration of GC-MS and LC-MS for untargeted metabolomics profiling. *J. Pharm. Biomed. Anal.* **190**, 113509.

**Zhang, K. and Chen, J.** (2012). The regulation of integrin function by divalent cations. *Cell Adh Migr* **6**, 20–29.

**Zhang, Y., Hayenga, H. N., Sarantos, M. R., Simon, S. I. and Neelamegham, S.** (2008). Differential regulation of neutrophil CD18 integrin function by di- and tri-valent cations: manganese vs. gadolinium. *Ann. Biomed. Eng.* **36**, 647–660.

**Zhang, J., Kamdar, O., Le, W., Rosen, G. D. and Upadhyay, D.** (2009). Nicotine induces resistance to chemotherapy by modulating mitochondrial signaling in lung cancer. *Am. J. Respir. Cell Mol. Biol.* **40**, 135–146.

**Zhang, A., Sun, H., Wang, P., Han, Y. and Wang, X.** (2012). Modern analytical techniques in metabolomics analysis. *Analyst* **137**, 293–300.

**Zhang, Z., Li, T.-E., Chen, M., Xu, D., Zhu, Y., Hu, B.-Y., Lin, Z.-F., Pan, J.-J., Wang, X., Wu, C., et al.** (2020). MFN1-dependent alteration of mitochondrial dynamics drives hepatocellular carcinoma metastasis by glucose metabolic reprogramming. *Br. J. Cancer* **122**, 209–220.

**Zhao, M.** (2009). Electrical fields in wound healing-An overriding signal that directs cell migration. *Semin. Cell Dev. Biol.* **20**, 674–682.

**Zhao, J., Zhang, J., Yu, M., Xie, Y., Huang, Y., Wolff, D. W., Abel, P. W. and Tu, Y.** (2013). Mitochondrial dynamics regulates migration and invasion of breast cancer cells. *Oncogene* **32**, 4814–4824.

**Zhao, Z., Han, F., He, Y., Yang, S., Hua, L., Wu, J. and Zhan, W.** (2014). Stromal-epithelial metabolic coupling in gastric cancer: stromal MCT4 and mitochondrial TOMM20 as poor prognostic factors. *Eur J Surg Oncol* **40**, 1361–1368.

**Zhao, J., Yao, K., Yu, H., Zhang, L., Xu, Y., Chen, L., Sun, Z., Zhu, Y., Zhang, C., Qian, Y., et al.** (2021). Metabolic remodelling during early mouse embryo development. *Nat. Metab.* **3**, 1372–1384.

**Zheng, J.** (2012). Energy metabolism of cancer: Glycolysis versus oxidative phosphorylation (Review). *Oncol. Lett.* **4**, 1151–1157.

**Zheng, X., Boyer, L., Jin, M., Mertens, J., Kim, Y., Ma, L., Ma, L., Hamm, M., Gage, F. H. and Hunter, T.** (2016). Metabolic reprogramming during neuronal differentiation from aerobic glycolysis to neuronal oxidative phosphorylation. *Elife* **5**,.

**Zhou, J. and Yin, Y.** (2016). Strategies for large-scale targeted metabolomics quantification by liquid chromatography-mass spectrometry. *Analyst* **141**, 6362–6373.

**Zhu, J., Luo, B.-H., Xiao, T., Zhang, C., Nishida, N. and Springer, T. A.** (2008). Structure of a complete integrin ectodomain in a physiologic resting state and activation and deactivation by applied forces. *Mol. Cell* **32**, 849–861.

**Zöllner, N.** (1982). Purine and pyrimidine metabolism. *Proc Nutr Soc* **41**, 329–342.

**Zorova, L. D., Popkov, V. A., Plotnikov, E. Y., Silachev, D. N., Pevzner, I. B., Jankauskas, S. S., Babenko, V. A., Zorov, S. D., Balakireva, A. V., Juhaszova, M., et al.** (2018). Mitochondrial membrane potential. *Anal. Biochem.* **552**, 50–59.

**Zotin, A. I., Faustov, V. S., Radzinskaja, L. I. and Ozernyuk, N. D.** (1967). ATP level and respiration of embryos. *Development* **18**, 1–12.

**Zou, C., Wang, Y. and Shen, Z.** (2005). 2-NBDG as a fluorescent indicator for direct glucose uptake measurement. *J Biochem Biophys Methods* **64**, 207–215.

**Zrenner, R., Stitt, M., Sonnewald, U. and Boldt, R.** (2006). Pyrimidine and purine biosynthesis and degradation in plants. *Annu. Rev. Plant Biol.* **57**, 805–836.

**Zucchi, R., Chiellini, G., Scanlan, T. S. and Grandy, D. K.** (2006). Trace amine-associated receptors and their ligands. *Br. J. Pharmacol.* **149**, 967–978.